Brake Wear Particle Emission Rates and Characterization

United States Environmental Protection Agency

Brake Wear Particle Emission Rates and Characterization

Assessment and Standards Division
Office of Transportation and Air Quality
U.S. Environmental Protection Agency

Prepared for EPA by
ERG, Eastern Research Group, Inc.
EPA Contract No. 68HE0C18C0001
Work Assignment No. 1-04

NOTICE

This technical report does not necessarily represent final EPA decisions or positions. It is intended to present technical analysis of issues using data that are currently available. The purpose in the release of such reports is to facilitate the exchange of technical information and to inform the public of technical developments.

United States Environmental Protection Agency

EPA-420-R-21-009
December 2021

Acknowledgment

ERG would like to thank the participating staff members from EPA National Fuel, Vehicle, and Emissions Laboratory (NVFEL) and California Air Resources Board (CARB) for their joint cooperation and contributions to this work.

ERG would like to acknowledge the work performed by Caltrans on the 2010-2012 California Household Travel Survey. The results of that survey are hosted and presented for public use by the National Renewable Energy Laboratory (NREL), and ERG would like to acknowledge the benefit to researchers by NREL maintaining and hosting the data. ERG would also like to thank the project subcontractor LINK Engineering, Inc. staff for their efforts and dedication to this project.

ERG and LINK wish to acknowledge the significant contributions of Dan Berletchick from RAYLOC providing business intelligence and detailed vehicle and brake information; of Gregory Vyletel from Federal Mogul for review of the vehicle selection to validate it against common industry practices; of Jerry Forystek from Brake Parts International for the proper use of the replacement rate index.

Table of Contents

Appendices

List of Figures

List of Tables

Executive Summary

Background

As tailpipe emissions of PM from the light-duty fleet have decreased significantly, non-tailpipe PM emissions, such as brake and tire wear have become more relevant and may be significantly impacting air quality near roadways. This research project was jointly funded by EPA and CARB to measure and analyze particulate matter (PM) emitted during light-duty vehicle braking to allow for updating inventory model emission factors as well as to better understand the vehicle operational conditions associated with varying levels of brake PM emissions. This study utilized a LINK Engineering (LINK) brake dynamometer (in which the brake components of a single wheel are mounted and operated electronically) for the measurement of PM emissions over a prescribed driving cycle.

Objectives and Methods

Based on literature search, Eastern Research Group (ERG) and LINK determined that 4 parameters of a test cycle would be most likely to affect braking PM emissions: vehicle speed, deceleration rate, brake component temperature, and the duration of a given brake event. These four parameters formed the basis of the development of a new test cycle and procedure to test vehicle brake assemblies on the brake dynamometer.

Six test vehicles (with common cross-platform brake components) were selected to represent the range of vehicle types in the light-duty fleet. These vehicles were subject to track tests in which brake system temperatures were measured during standardized driving cycles. This temperature data was used to both inform a light-duty brake temperature model that ERG developed (temperature as a function of vehicle speed) and to select the cooling level used during brake dynamometer tests.

A new test cycle was developed to represent the operation of real-world vehicles in California based on the 2010-2012 Caltrans Household Travel Survey. This survey included speed data logged from over 2,000 vehicles operating throughout the state. ERG used the developed temperature model to estimate the distribution of brake temperatures encountered by these actual California trips. ERG developed a new test cycle to be as similar as possible to the speeds, deceleration rates, temperatures, and braking durations encountered by real vehicles. This new cycle is composed of three distinctive operation patterns characterized with 3 speed bins such that emission rates could be resolved across different trip average speed ranges.

The LINK lab site included a constant volume sampling (CVS) system with an integrated brake dynamometer. The airflow through the CVS provides the medium for transferring brake particles to the point of sampling and brake cooling. Cooling flowrates were selected for the front and rear brake for each model to match temperatures encountered during track testing. Measurements were made in batch and continuously by a variety of instruments including gravimetric sampling in parallel on coated aluminum impactors (TSI 100S4) as well as on 47mm Teflon filters. Instrumentation was also installed to

measure particle size distributions, particle counts, and continuous particle mass. A test matrix was developed consisting of 85 single-day tests of different test parameters: brake friction materials, vehicle test weights, and the 6 selected vehicles. All test parameter combinations were replicated in at least two different tests. One of the vehicles was equipped with regenerative braking and the dynamometer was programmed to simulate that regenerative braking function during testing of that model.

Results

Figure ES-1 presents the vehicle-level results for each of the 6 tested models by three different pad materials: Original Equipment Service non-asbestos organic (OES-NAO), aftermarket NAO, and aftermarket Low-Metallic (LM). Vehicle-level emissions for each pad type are calculated by doubling the average front and rear single-wheel emission rates and summing.

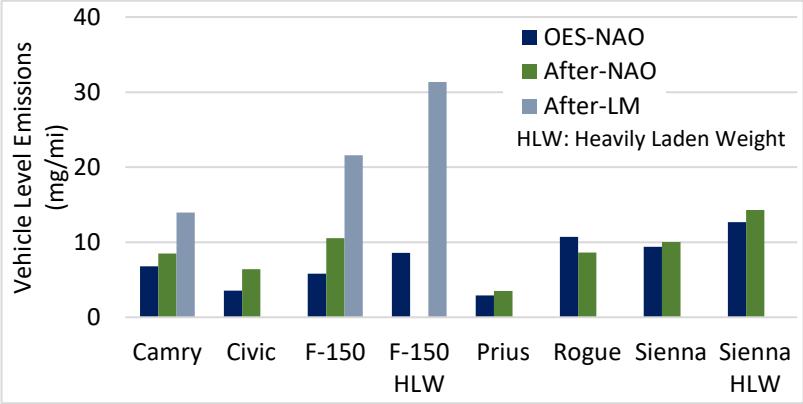

Figure ES-1. Vehicle level braking emissions by model and friction material

Correlations were also found between PM emissions and other test parameters. In general, for a given friction material type, emission rates increased linearly with vehicle tested weight. Particle count emissions generally trended with overall mass, however the observed range from the lowest to highest emitter was reduced as compared to the range of measured masses.

ERG also analyzed emissions measurements for the purposes of comparison to existing emissions factors in EPA's Motor Vehicle Emissions Simulator (MOVES), which includes an operating mode (Opmode) bin specifically for braking. In MOVES2014, this bin includes an emission rate of 0.558 g/hr during braking. The test results from this program, when averaged (and not weighted by model prevalence in-use), had an average of 0.35 g/hr during braking. This value is likely lower because the vehicles in the program are lighter than the average light-duty vehicle, and also because vehicles tend to have lower brake wear levels due to technology developments over time.

Conclusions

The test results were sensitive to the various parameters in the test matrix. When in-use pad material rates are accounted for, the estimated vehicle-level PM emission rates vary from 3.3 mg/mi to 13.6 mg/mi depending on model. Metallic pad materials tended to emit higher PM masses and tended to have larger particles in their emitted size distributions.

Main Report

Introduction

This report presents the findings of a research study to measure and analyze particulate matter (PM) emitted during light-duty vehicle braking. Research was conducted by Eastern Research Group, Inc. (ERG) and subcontractor LINK Engineering (LINK) and funded in cooperation between the US Environmental Protection Agency (EPA) and the California Air Resources Board (CARB). The project was initiated by CARB Project 17RD016 for the purposes of updating the emission factors in the Emission Factor inventory model (EMFAC). EPA contributed additional funding to broaden the types of measurements made during this work with the aim of potentially updating the emissions factors used in the Motor Vehicle Emissions Simulator (MOVES). This report covers all aspects of the project and, where appropriate, presents results in a manner comparable to MOVES emission factors.

EPA provided additional funding to this project to expand the types of measurements planned in the original CARB study. These additions involved the parallel gravimetric measurement of PM emissions using Teflon (PTFE) filters in a manner consistent with the requirements for PM sampling described in 40 CFR 1065. Additionally, the project funding allowed for the use of the sampling of PM onto transmission electron microscope (TEM) grids during many of the tests.

As tailpipe emissions of PM from the light-duty fleet have decreased significantly, non-tailpipe PM emissions, such as brake and tire wear have become more relevant and may be significantly impacting air quality near roadways. This research was conducted to inform the relative level of PM emissions from braking in the light-duty fleet, characterize PM emission factors to potentially allow for emissions model updates, and generally better understand the variables most significant in affecting brake emissions.

Light-Duty Vehicle Braking Systems

Typical light-duty vehicle braking systems rely on hydraulically activated friction between two component surfaces, one that is generally stationary with respect to the vehicle’s suspension, and the other that rotates with the vehicle’s wheel. During braking, the friction generated between brake components generates heat and abrades the components at their frictional interface resulting in particles being released into the atmosphere.

Most modern vehicles rely on pad and rotor combinations for braking; the rotor rotates with the wheel, and the pads are mounted in a caliper stationary to the suspension. The driver’s application of force to the brake pedal provides hydraulic pressure within the caliper to squeeze the pads against opposite sides of the rotor and the resulting frictional torque slows the vehicle. Less common in modern light-duty vehicles are drum brakes, in which a cylindrical drum rotates with the wheel and hydraulic force presses stationary shoes against the inside of the rotating drum to provide deceleration torque.

Hybrid and modern electric vehicles also employ a relatively new method of slowing the vehicle, regenerative braking, that operates in parallel with the hydraulic brake system and uses the electric drive motor to slow the vehicle and provide energy back to the vehicle's electric storage. These vehicles use complex blending strategies to manage the amount of braking between the regenerative system and the hydraulic system such that driver perceives the system as operating like a conventional vehicle.

LINK Brake Dynamometer Experience and Capabilities

ERG partnered with LINK at the proposal stage of CARB project 17RD016. LINK has been designing, manufacturing, and performing testing with brake dynamometers for decades. Their organization is a part of the Particle Matter Program (PMP) overseen by the EU's Joint Research Centre (JRC). They have been involved in recent years with the development of the state of the art for the measurement of PM emissions from braking. LINK has the capability to:

- conduct particulate matter emissions sampling of different brake configurations using a brake dynamometer and representative drive cycle.
- sample particulate matter emissions between 6 nm and 20 µm in size,
- collect particle characterization measurements of the particles, including particle number, particle mass, and size distribution
- collect continuous particulate matter measurements (g/sec), with the ability to correlate the continuous measurements to gravimetric filter measurements

LINK operates in accordance with all sections of the ISO 17025:2017 standard, titled General Requirements for the Competence of Testing and Calibration Laboratories[1], and management is committed to continually improving the quality of all operations. A familiarity with, implementation of and compliance with the ISO 17025:2017 standard is a mandatory requirement for individuals at all levels of the LINK organization.

ERG initiated the program by reviewing two existing test cycles relevant to this work, the EMFAC Unified Cycle (UC) and its associated Speed Correction Cycles (SCCs), as well as the World-Harmonized WLTP-Brake cycle, developed in Europe in cooperation with the JRC.[2] The UC/SCCs were designed for exhaust emissions testing, while the WLTP-Brake was designed specifically for use on brake dynamometers. ERG also reviewed available literature to begin developing a list of vehicle operational parameters most relevant to brake emissions. ERG selected the following four parameters as the initial assumption of the operational parameters with the most relevance to brake PM emissions:

- Vehicle speed during braking event
- Deceleration rate
- Brake component temperature

[1] International Standards Organization "General requirements for the competence of testing and calibration laboratories". https://www.iso.org/standard/66912.html

[2] Mathissen, M. et. al., A novel real-world braking cycle for studying brake wear particle emissions, Wear, Volumes 414–415, 2018

- Brake event duration

The test program was designed to evaluate the PM emission responses to the above parameters as well as to perform testing over a representative range of values for each.

Materials and Methods

Representative Test Vehicle and Friction Material Selection

ERG and LINK first determined the list of representative test vehicle models that would be used to develop an understanding of brake thermal regimes during in-use vehicle operation. Brake system components from these vehicle models would then be used during PM emissions tests on the brake dynamometer. The on-track vehicle testing involved operating each vehicle over the WLTP-Brake cycle (adapted for track testing) followed by a heating and cooling matrix cycle of standardized stops and cruises. By measuring brake temperatures during these on track operations, the laboratory testing could be designed to replicate actual vehicle temperatures within reason and provide relevant measurement and characterization of brake emissions. Also, the temperature ranges encountered during track testing informed a new ERG-developed model of operational temperatures of the driving in an in-use vehicle speed dataset. The measurement of brake emissions using repeatable and reproducible systems and isokinetic constant volume sampling will further improve the estimation of emissions inventories for light duty vehicles.

To guide the selection of vehicle models, LINK adapted the concept of the brake wear index (BWI), which is a representation of the total material present in the in-use fleet that can be emitted as particulate. There are several assumptions used to determine a BWI to guide the vehicle selection. First, the ranking assumes proportionality between the number of registered vehicles and the amount of PM becoming airborne during and after braking. Second, the larger the wearable mass of the foundation brakes, the larger the potential for contribution of PM. The wearable mass is assumed to be a direct function of the friction material volume before reaching the service thickness. In addition to the friction material, the wearable mass includes the volume of the mating disc or drum with its volume up to its service thickness. To estimate the mass, the method uses nominal and typical material density for the predominant compositions (non-asbestos organic/ceramic versus semi-metallic or low-metallic for the friction material) with the estimated market share as a function of the vehicle age range. The wearable mass uses grey cast iron for the disc and drums. The third assumption to complete the computation of a BWI, combines the number of registered vehicles with the total wearable mass as well as the replacement rate of the friction material and the disc or drum. The main sources of information used by LINK in this analysis were: a) registration counts by make, model, and year of manufacture provided by CARB for 2016; b) brake dimensions obtained from the yearly publication and the online catalog from the Friction Materials Standards Institute (FMSI®) and from consulting with aftermarket friction manufacturers; c) material densities from consulting with friction

materials formulators, and d) replacement rates as the fraction of vehicles that have had brake materials replaced during a given year for vehicles in a given age range.
The selection of six vehicles to characterize brake emissions representative of the light-duty vehicle market in California was completed in multiple steps. The first step was to review the statistics for vehicles registered in California for the year 2017. The top-25 vehicles based on registration counts included 'make' and 'series' of different 'model year' and 'model'. Therefore, LINK prescreened vehicles of different series from the original statistics. The column "Top-25 Reg" in Table 1 illustrates an extract of this pre-screening step. The approach is to treat all models of Toyota Corolla as a single entry in the development of the top-25 vehicles list. The next vehicle with a series different than Corolla is Toyota Camry. Camry was selected as the second vehicle in the top-25 vehicles list. Only the first few vehicles are included here for brevity, but the complete list is presented later in this section.

Table 1. Counts of Make, Series, Model, and Model Year

Entry #	Model Year	Make	Series	Model	Count	Top-25 Reg
1	2016	Toyota	Corolla	L	58637	1
2	2015	Toyota	Corolla	L	55315	1
3	2010	Toyota	Corolla	BASE	54362	1
4	2014	Toyota	Camry	L	53570	2
5	2015	Toyota	Prius		53318	3

Next, the friction material and backing plate identification codes ('FMSI' codes) of front and rear axle friction materials were determined for more than 100 different entries of different model years, make, series, and models. The number of vehicles having the same FMSI codes were then summed together and this new count was taken for each model, grouped together by all series and model years having the same FMSI codes. The FMSI database and industry surveys were used to determine the dimensions of disc or drum and friction material. These dimensions, along with representative material density values were used to estimate the wearable mass of the brake parts using the following equation. The actual values used during this process for each of the top-25 vehicles are included in Appendix A.

Estimated wearable mass =
(Wearable volume of friction material) · (Density of friction material)
+ (Wearable volume of front axle disc) · (Density of disc)
+ (Wearable volume of rear axle disc/drum) · (Density of disc/drum)

Density of friction material depends on the type of friction material used in the vehicle of interest. For example, density of non-asbestos organic (NAO) material is 2.9 g/cm^3 and density of semi- or low-metallic (LM) material is 3.75 g/cm^3. Thus, a brake lining made of semi-metallic material contains higher wearable mass than an equivalent lining made of NAO material.

Interviews and surveys with technical specialists resulted in percent population of friction material formulations as a factor of vehicle age. Figure 1 illustrates the overall general trend regarding the relative presence of NAO and Semi-metallic/Low-metallic (SM/LM) friction materials for light-duty vehicles in use. Except for special applications, most street service passenger car and light truck Original Equipment Manufacturer (OEM) and Original Equipment Service (OES) pads in North America use NAO friction materials. As vehicles age, SM/LM pads become more common as they tend to cost less than NAO pads and are therefore more likely to be selected as vehicles depreciate.

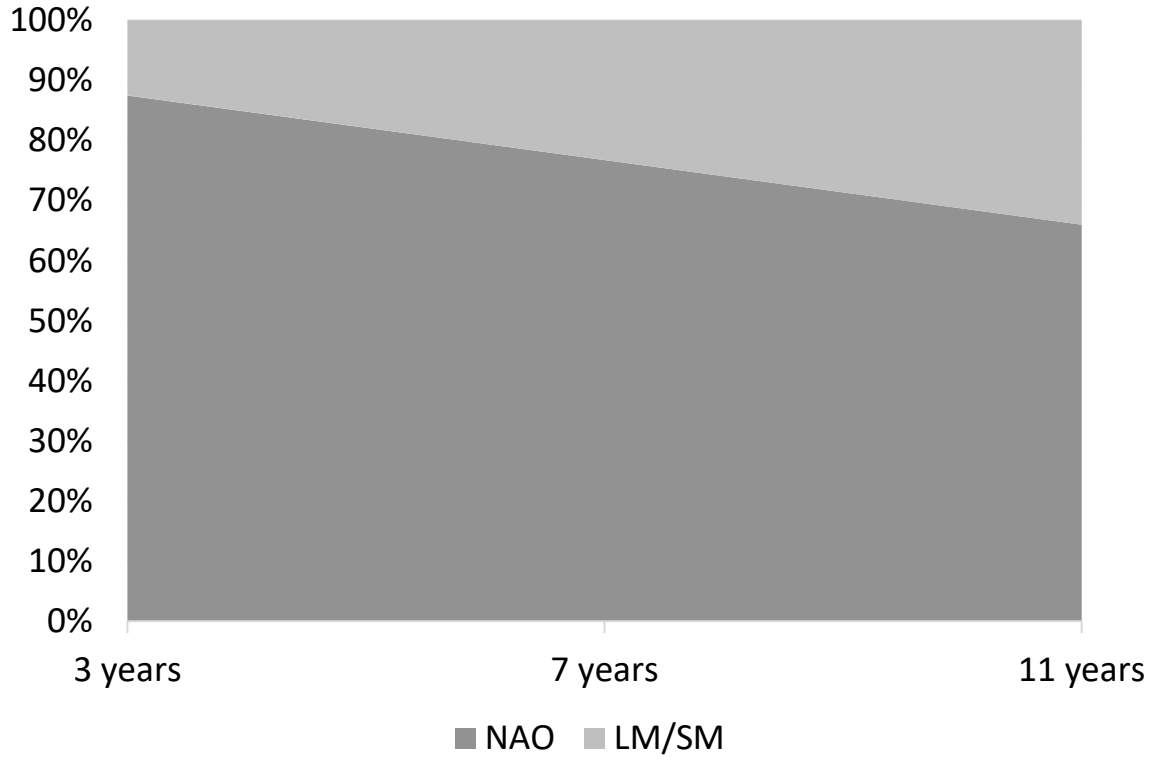

Figure 1. General trend in pad material mix by vehicle age

Using these market statistics based on vehicle age, LINK generated Table 2, which indicates the estimated mix of metallic versus NAO for the six vehicles selected. The wearable mass for the friction material prorates the density of the friction material (NAO v. Semi- or Low-Metallic) and the estimated market share. Note that the estimates presented are based on vehicle age range and general vehicle type only and are not adjusted for specific vehicle characteristics (as that level of detail was not available from industry surveys). For example, the Prius may have a different level of low/semi-metallic market share as a result of its regenerative braking systems.

Table 2. Estimated Pad Material Breakdowns by Combined Models

Make	Model	MY	Production Years	Est. % NAO	Est. % Metallic
HONDA	CIVIC LX	2012-2015	3-6	77%	23%
TOYOTA	PRIUS REGULAR	2010-2016	2-8	82%	18%
NISSAN	ROGUE S	2014-2016	2-4	88%	12%
TOYOTA	CAMRY (BASE, L, LE)	2009-2016	2-9	82%	18%
TOYOTA	SIENNA LE	2011-2015	3-7	77%	23%
FORD	F150 SUPERCREW	2015-2016	2-3	87%	13%

In addition, it is important to note the fact that, in aftermarket supplier parlance, there are three broad commonly-used categories of aftermarket friction materials of “good, better, and best.” Good friction materials provide a good performance and relatively quiet braking at a reasonable price in NAO and semi-metallic formulations. Better friction materials are the most extensive line of aftermarket friction materials and also come in NAO and semi-metallic formulations. They are designed to last longer and wear better and perform well at the mid-price range. Better friction materials feature chamfers, slots, and anti-noise shims in many applications, and provide smooth pedal feel and proper fit. Best aftermarket friction materials are the closest to the OEM/OES friction material in terms of dimensional quality, hardware kits, performance, comfort, and product life. Figure 2 illustrates the general mix of friction material quality in relation to the vehicle age. In the chart, the total percentages for NAO and SM sum to 100% within each vehicle age group.

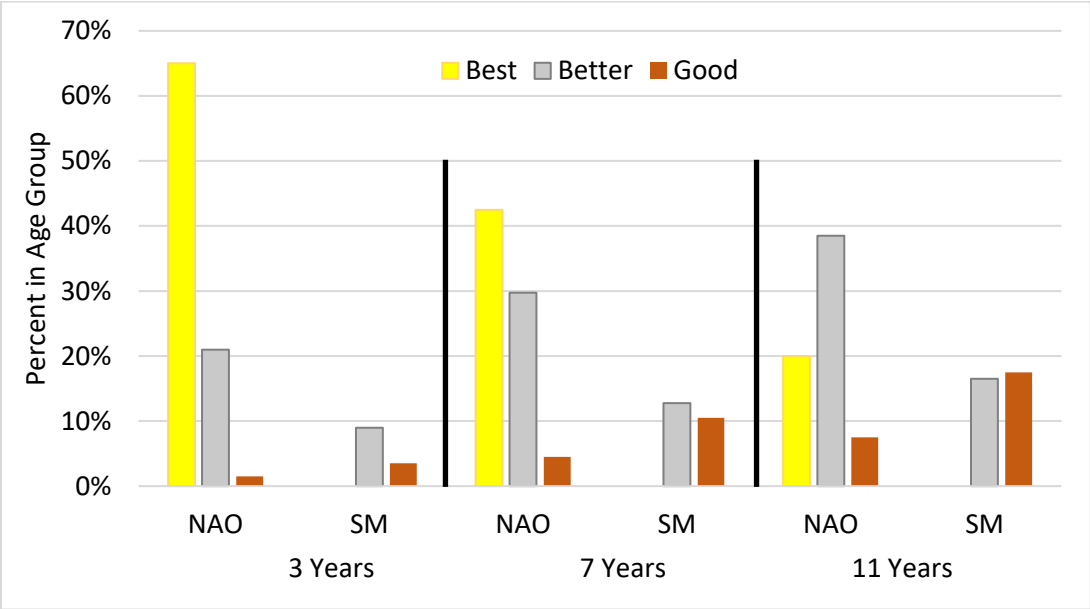

Figure 2. Overall mix of friction material quality by age

When all the above factors are combined in one graph, it becomes apparent how wide the range of friction materials is that can be applied to a given vehicle during a given brake job. Figure 3 illustrates the combined effect of vehicle age on friction material type and formulation equipped on in-use vehicles. The figure is based on combining the data presented in Figure 1 and Figure 2.

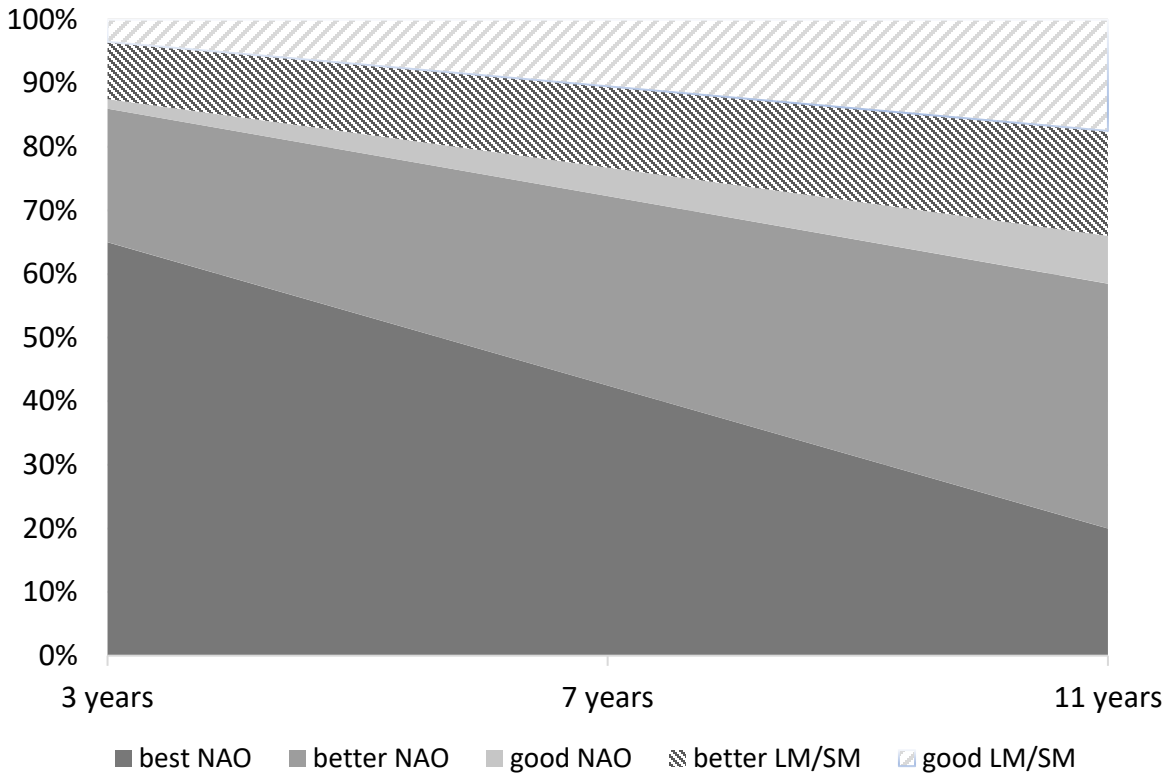

Figure 3. Overall Mix of Friction Materials, Quality Grade, and Vehicle Age

Other factors which influence the ultimate friction material used for the specific vehicle include vehicle aging behavior, demographics, market dynamics among dealers, large retailers, and private branding, etc.

Based on aforementioned steps to determine registration count as well as the wearable mass (including pad material type), a first iteration index, BWI_1 was determined for the top-registered vehicles as follows.

$$BWI_1 = (\text{Registration Count}) \cdot (\text{Wearable mass})$$

To complete the numerical assessment of which vehicles were relevant, representative, and available for rental to conduct the proving ground test track measurements, LINK conducted a technical survey to determine the replacement rates of brakes. The survey provided by the brake suppliers and manufacturers resulted in replacement rates as a function of vehicle age. A second BWI index (BWI_2) was then determined as follows:

$$BWI_2 = (BWI_1) \cdot (\text{Replacement rate by vehicle age})$$

In the end, three levels of ranking were established among the top 25 vehicles. The total registration count of vehicles for a given make, series, and model resulted in the first phase of ranking. The BWI_1, with the total wearable mass resulted in a second phase of ranking. The BWI_2, includes an additional factor (replacement rate), to generate the third phase for the vehicle ranking. The BWI_2 allows the adjustment of the BWI_1 index to reflect the relative wear rate of different vehicles having a similar registration count, and a similar wearable mass. Low replacement rates will demote the total ranking for the vehicle as it wears (releases debris and PM) at a lower rate, compared to another vehicle with similar registration count and wearable mass but with a higher wear rate (reflected indirectly by the replacement rate).

Vehicle models were grouped by all series and model years within a model that had the same FMSI codes. Table 3 lists an excerpt of the top vehicles of various make, series, model year, and models. Shaded rows indicate vehicles that are 10 years old or newer from the publication date of registration statistics. This age range is considered to avoid uncertainties of working condition, availability and procurement of specific vehicles for track testing with older vehicles. The last column in Table 3 'FMSI FRONT AXLE' shows the friction material identifier for brake lining on front axle. The first four digits represent the friction formulation and the digits after the letter represent the geometrical features and dimensions of backing plate. As seen, the same FMSI identifiers apply for various entries (vehicle make, series, model year, and model).

Table 3. Series, Model, Model Year, and FMSI Code for Most Common Vehicles

MAKE	SERIES	MY	MODEL	COUNT	FMSI FRONT AXLE
TOYOTA	COROLLA	2016	LX	58637	8969-D1210
TOYOTA	COROLLA	2015	LX	55315	8969-D1210
TOYOTA	COROLLA	2014	LX	45202	8969-D1210
TOYOTA	COROLLA	2013	BASE	45180	8330-D1210
TOYOTA	COROLLA	2012	BASE	27327	8330-D1210
TOYOTA	COROLLA	2011	BASE	26460	8330-D1210
TOYOTA	COROLLA	2010	BASE	54362	8330-D1210
TOYOTA	COROLLA	2009	BASE	38783	8330-D1210
TOYOTA	COROLLA	2007	CE	36541	7824-D923
TOYOTA	COROLLA	2006	CE	38106	7824-D923
TOYOTA	COROLLA	2005	CE	39963	7824-D923
TOYOTA	COROLLA	2004	CE	30255	7824-D923
TOYOTA	COROLLA	2003	CE	34015	7824-D923
TOYOTA	COROLLA	2001	CE	20481	7611-D741
TOYOTA	COROLLA	1999	VE	20106	7611-D741
TOYOTA	CAMRY	2016	LE	45855	8331-D1293
TOYOTA	CAMRY	2015	LE	46855	8331-D1293
TOYOTA	CAMRY	2014	L	53570	8331-D1293
TOYOTA	CAMRY	2013	L	30383	8331-D1293

Table 4 shows the revised list that shows the combination of all rows in Table 3 with a same FMSI # into a single entry that covers a model year range and all model identifiers.

Table 4. Consolidating Top Series by Model Year and FMSI

MAKE	SERIES	MY	COUNT	AXLE	FMSI FA
TOYOTA	COROLLA	2014-2016	159154	FA	8330-D1210
TOYOTA	COROLLA	2014-2016	159154	RA	1635-S945
TOYOTA	COROLLA	2009-2013	192112	FA	8330-D1210
TOYOTA	COROLLA	2009-2013	192112	RA	1635-S945
TOYOTA	COROLLA	2003-2007	178880	FA	7824-D923
TOYOTA	COROLLA	2003-2007	178880	RA	1515-S801
TOYOTA	COROLLA	1999-2001	40587	FA	7611-D741
TOYOTA	COROLLA	1999-2001	40587	RA	1515-S750
TOYOTA	CAMRY	2009-2016	342992	FA	8331-D1293
TOYOTA	CAMRY	2009-2016	342992	RA	8332-D1212
TOYOTA	CAMRY	2007	50693	FA	8331-D1222
TOYOTA	CAMRY	2007	50693	RA	8332-D1212
TOYOTA	CAMRY	2002-2006	185766	FA	7787-D908
TOYOTA	CAMRY	2005-2006	67612	RA	1617-S911
TOYOTA	CAMRY	2002-2004	118154	FA	7787-D908
TOYOTA	CAMRY	1998-2004	198316	RA	1447-587
TOYOTA	CAMRY	2001	25651	FA	7357-D697

Table 5 lists the top 25 light-duty vehicles registered in the state of California, as grouped according to the above process. It should be noted that the column labeled ‘weight class’ is defined according to CFR 45, Part 565 VIN (Class A = GVWR less than or equal to 3000 lbs., B for (3001 to 4000) lbs., C for (4001-5000 lbs., etc., up to GVWR of 10 000 lbs.). The top 25 vehicles list includes a mix of a variety of vehicle weight classes spanning from class B thru F. The goal in vehicle selection was to select representative models from a range of vehicle types including compacts, sedans, SUVs, minivans, full-size trucks, as well as at least one vehicle with regenerative braking. These corresponded in some cases to the weight classes, but the priority in diversifying vehicle selection was on vehicle type, not weight. Based on the registration count ranking only, the vehicles selected would have been: Camry, Prius, Corolla, Altima, Civic, and Sentra. These vehicles fall under two vehicle weight classes and one vehicle type (4-door sedan), and alone do not provide enough representation of the vehicle population in California to suit the needs of this program. The top 25 vehicles were selected to ensure multiple models would remain for each of the following desired vehicle groups: compacts, sedans, pickups, minivans, SUVs, and hybrids.

Table 5. Counts of the Top 25 FMSI-Grouped Vehicles in California

MAKE	SERIES/MODEL	MY	WEIGHT CLASS	GVWR	Reg #	RANK BY Reg
			/ A-to-H	/ kg	#	
TOYOTA	CAMRY (BASE, L, LE)	2009-2016	C	2073	342992	1
TOYOTA	PRIUS REGULAR	2010-2016	B	1800	241055	2
TOYOTA	COROLLA L	2014-2016	B	1732	159154	3
NISSAN	ALTIMA (BASE, 2.5)	2012-2016	C	1910	149096	4
HONDA	CIVIC LX	2012-2015	B	1595	140733	5
NISSAN	SENTRA S	2013-2016	B	1687	110629	6
HONDA	ACCORD LX	2014-2016	C	1934	52193	7
TOYOTA	SIENNA LE	2011-2015	D	2715	44921	8
LEXUS	RX 350	2014-2015	D	2527	43306	9
NISSAN	ROGUE S	2014-2016	C	1968	41213	9
HYUNDAI	SONATA (GLS, SE, SPORT)	2013-2015	C	2074	40117	11
HONDA	ACCORD EX	2014-2016	C	1904	39344	12
HONDA	ACCORD SPORT	2014-2015	C	2107	37332	13
TOYOTA	RAV4 XLE	2014-2016	C	2035	36803	14
TOYOTA	TACOMA DOUBLE CAB	2015-2016	D	2540	36052	15
FORD	F150 SUPERCREW	2013-2014	F	3239	33721	16
FORD	F150 SUPERCREW	2015-2016	E	3000	32921	17
HYUNDAI	ELANTRA GLS	2013	B	1720	30566	18
CHEVROLET	SILVERADO 1500	2014-2015	E	3085	27578	19
HONDA	CIVIC LX	2016	B	1695	25782	20
HONDA	ACCORD SPORT	2016	C	1964	22978	21
DODGE	RAM 1500 ST	2004	E	2989	19739	22
CHEVROLET	TAHOE C1500	2007	F	3266	19517	23
LEXUS	RX 350	2016	D	2562	12540	24
HYUNDAI	SONATA SE	2016	C	2074	11363	25

Table 6 shows the revised and re-ordered ranking based on the brake wear index BWI_1. The index BWI_1 is a product of registration count and the total wearable mass of pads/shoes and discs/drums at all four brake corners of a given vehicle. On comparing the registration counts with the BWI_1 rankings, the influence of wearable mass on BWI_1 ranking was more evident for SUVs and trucks such as the Nissan Rogue, Toyota Tacoma, and F150 trucks. Based on the BWI_1 ranking, the vehicles selected would have been: Camry, Corolla, Prius, Civic, Altima, and Tacoma. These vehicles fall under three vehicle weight classes and two vehicle types (4-door sedan and pick-up truck). The selection of the Tacoma would overemphasize this vehicle due to its wearable mass (over two times the average of the other five vehicles selected with the BWI_1 ranking). In addition, this selection limits the selection of vehicle types, makes, and models present in California.

Table 6. Top FMSI-Grouped Series, with BWI_1

MAKE	SERIES/MODEL	MY	Reg #	RANK BY Reg	TOTAL WEARABLE MASS / gm	BWI_1 / ton	RANK BY BWI_1
TOYOTA	CAMRY (BASE, L, LE)	2009-2016	342992	1	2133	732	1
TOYOTA	COROLLA L	2014-2016	159154	3	3028	482	2
TOYOTA	PRIUS REGULAR	2010-2016	241055	2	1749	422	3
HONDA	CIVIC LX	2012-2015	140733	5	2322	327	4
NISSAN	ALTIMA (BASE, 2.5)	2012-2016	149096	4	1510	225	5
TOYOTA	TACOMA DOUBLE CAB	2015-2016	36052	15	5256	189	6
NISSAN	SENTRA S	2013-2016	110629	6	1436	159	7
TOYOTA	SIENNA LE	2011-2015	44921	8	2717	122	8
LEXUS	RX 350	2014-2015	43306	9	2707	117	9
FORD	F150 SUPERCREW	2013-2014	33721	16	2878	97	10
FORD	F150 SUPERCREW	2015-2016	32921	17	2895	95	11
TOYOTA	RAV4 XLE	2014-2016	36803	14	2462	91	12
HONDA	ACCORD LX	2014-2016	52193	7	1598	83	13
NISSAN	ROGUE S	2014-2016	41213	10	1845	76	14
HYUNDAI	SONATA (GLS, SE, SPORT)	2013-2015	40117	11	1678	67	15
CHEVROLET	SILVERADO 1500	2014-2015	27578	19	2431	67	16
HYUNDAI	ELANTRA GLS	2013	30566	18	1649	50	17
CHEVROLET	TAHOE C1500	2007	19517	23	2521	49	18
DODGE	RAM 1500 ST	2004	19739	22	2180	43	19
HONDA	CIVIC LX	2016	25782	20	1666	43	20
HONDA	ACCORD EX	2014-2016	39344	12	993	39	21
LEXUS	RX 350	2016	12540	24	2668	33	22
HONDA	ACCORD SPORT	2014-2015	37332	13	803	30	23
HYUNDAI	SONATA SE	2016	11363	25	1803	20	24
HONDA	ACCORD SPORT	2016	22978	21	803	18	25

The total wearable mass may or may not indicate the actual amount of wear debris seen during a typical year of driving activity because different models' brake components do not all wear out after the same amount of driving. The annual estimates of the brake replacement rates were acquired through a business intelligence survey. Table 7 presents the continued analysis by including the replacement rates by vehicle age. A newer vehicle is expected to have low value of replacement rate and vice versa. A value of 16% in the first row of Table 7 implies that 16% of all vehicle population with year of manufacture between 2009 and 2016 are estimated to have had a brake service. The prevailing brake service job at the time of this survey was to replace friction couple i.e. pad and rotor or shoes and drum at any given service. A second wear index is formulated which assumes that a brake service would include replacement of brake parts. The wear index BWI_2 is a product of BWI_1 and the brake replacement rate. Table 7 includes vehicles in the order determined by BWI_2. This ranking still leaves the Sentra, Altima, and Corolla near the top of the list, though they are in the same vehicle class.

Table 7. Top FSMI-Grouped Series, with BWI_2

MAKE	SERIES/MODEL	MY	RANK BY BWI_1	REPLACEMENT RATE PER VEHICLE AGE	BWI_2	RANK BY BWI_2
				/ %	/ ton	
TOYOTA	CAMRY (BASE, L, LE)	2009-2016	1	16	117	1
TOYOTA	COROLLA L	2014-2016	2	11	53	2
HONDA	CIVIC LX	2012-2015	4	14	46	3
NISSAN	ALTIMA (BASE, 2.5)	2012-2016	5	14	32	4
NISSAN	SENTRA S	2013-2016	7	11	17	5
TOYOTA	SIENNA LE	2011-2015	8	14	17	6
FORD	F150 SUPERCREW	2013-2014	10	16	16	7
LEXUS	RX 350	2014-2015	9	11	13	8
CHEVROLET	TAHOE C1500	2007	18	23	11	9
FORD	F150 SUPERCREW	2015-2016	11	11	10	10
TOYOTA	RAV4 XLE	2014-2016	12	11	10	11
TOYOTA	TACOMA DOUBLE CAB	2015-2016	6	5	9	12
HONDA	ACCORD LX	2014-2016	13	11	9	13
DODGE	RAM 1500 ST	2004	19	21	9	14
TOYOTA	PRIUS REGULAR	2010-2016	3	2	8	15
NISSAN	ROGUE S	2014-2016	14	11	8	16
HYUNDAI	ELANTRA GLS	2013	17	16	8	17
HYUNDAI	SONATA (GLS, SE, SPORT)	2013-2015	15	11	7	18
CHEVROLET	SILVERADO 1500	2014-2015	16	11	7	19
HONDA	ACCORD EX	2014-2016	21	11	4	20
HONDA	ACCORD SPORT	2014-2015	23	11	3	21
HONDA	CIVIC LX	2016	20	5	2	22
LEXUS	RX 350	2016	22	5	2	23
HYUNDAI	SONATA SE	2016	24	5	1	24
HONDA	ACCORD SPORT	2016	25	5	1	25

Table 8 indicates the final vehicle selection after a joint engineering review with CARB, ERG, and LINK. The first update was to include an SUV, and the team selected the Nissan Rogue. Note that the Lexus RX 350 was higher ranked among SUV's than the Nissan Rogue, however the RX 350 was excluded due to it being a luxury vehicle and being likely to have a significantly higher cost for brake components than the Rogue which was not accounted for in the project budget estimate. The second update was to include a pick-up truck, with the F-150 being selected for being the most common pick-up truck in California (and the United States). The model year range for the F-150 was selected to be 2015-2016 (instead of the previous FMSI model year range of 2013-2014) because interviews with industry experts suggested that this year range was a very common benchmarking and development candidate. After confirming the availability for rental and availability of brake parts, the project moved on to its next phase, to prepare the logistics and technical documentation for track testing.

Table 8. The 6 Specific Makes, Series, and Model Years Selected for Testing

Selected Vehicle Model	Reg RANK	BWI_1 RANK	BWI_2 RANK	COMMENTS
2009-2016 Toyota Camry	1	1	1	Top rank by all three metrics
2012-2015 Honda Civic	5	4	3	Rear drum brakes
2011-2015 Toyota Sienna	8	8	6	Top in the list of class 'D' Reg #, Minivan
2015-2016 Ford F-150	17	11	10	Top in the list of class 'E' Reg #, Large Pickup, Very common vehicle for friction material formulation evaluations
2010-2016 Toyota Prius	2	3	15	Regenerative braking
2014-2016 Nissan Rogue	10	14	16	Top in the list of non-luxury SUVs Medium level ranking based on BWI_1 and BWI_2

The processes followed during this phase of the project allowed the evaluation of a significant list of vehicles in terms of make, model, and trim level, with the goal of selecting a subset for track and dynamometer testing. The final list of six vehicles given in Table 8 provides a good cross section of vehicle weight class/type and powertrain systems while representing common light-duty vehicles used for brake development and brake testing. The range of vehicle weights and disc brake dimensions allow the proper characterization of the thermal regimes of a wide variety of light-duty vehicles during the planned measurements of brake emissions on the brake inertia dynamometer. This task also introduced the concept of BWI as a predictor for the total potential contribution of a given vehicle to PM (fallout, airborne, and resuspension). The inclusion of BWI_2 as a metric for evaluation did not significantly alter the vehicle selection as compared to selecting based on registration counts when also accounting for selecting from a variety of vehicle types, however.

At the conclusion of this task, LINK procured one of each of the following vehicle models for track testing. These vehicle models were also used as the basis for acquiring brake assemblies for testing on the brake dynamometer. The selected FMSI numbers are also included.

- **2011 Toyota Camry LE**
  - Front axle FMSI# 8331-D1293
  - Rear axle FMSI# 8332-D1212
- **2013 Honda Civic LX**
  - Front axle FMSI# 8791-D1578
  - Rear axle FMSI# 1618-S913
- **2013 Toyota Sienna LE**
  - Front axle FMSI# 8436-D1324

    - Rear axle FMSI# 8500-D1391
- **2015 Ford F-150 Supercrew**
    - Front axle FMSI# 8528-D1770
    - Rear axle FMSI# 9018-D1790
- **2016 Toyota Prius Two Eco**
    - Front axle FMSI# 8538-D1184
    - Rear axle FMSI# 8463-D1423
- **2016 Nissan Rogue S**
    - Front axle FMSI# 8449-D1737
    - Rear axle FMSI# 8501-D1393

In addition to representing the vehicles registered in California, the listing provides the appropriate representation of vehicle weight classes from 1700 kg to 3200 kg of gross vehicle weight; vehicle types with sedans, pickup trucks, and sport utility vehicles; brake systems with disc brakes all around and with drum brakes on the rear axle; and vehicles with conventional gasoline powertrains and with regenerative braking systems. Note that specific model years are given from the ranges of model years with the same FMSI values provided in previous tables. The model years given above represent the actual model years of test vehicles sourced by LINK for track testing.

Track Testing and the Brake Temperature Model

Existing literature regarding PM emissions from braking indicates that brake temperature has a significant effect on emission rates.[3,4] To account for this, ERG selected brake temperature as a parameter for use in cycle development. Because brake temperature was not measured during the Caltrans survey, ERG developed a model of brake temperature based on track testing data. This temperature model was used to determine the distribution of in-use brake temperatures associated with vehicle speed data from the Caltrans household travel study and to estimate the brake temperature profile during operation on the dynamometer for the new test cycle.

ERG and LINK conducted track testing to gather data about operational brake temperatures. LINK acquired the test vehicles and replaced their wearable brake components with new components. Test vehicles were instrumented for temperature measurement of various brake system components and the vehicles were subject to controlled driving in three different phases. A photograph of the type of temperature measurement equipment installed by LINK is presented in Figure 4, which depicts a brake mounted thermocouple installed on the Camry test vehicle. The thermocouple

[3] Garg, Bhagwan D. et. al. “Brake Wear Particulate Matter Emissions.” Environmental Science & Technology 34.21 (2000): 4463–4469

[4] Sanders, Paul G. et. al. “Airborne Brake Wear Debris: Size Distributions, Composition, and a Comparison of Dynamometer and Vehicle Tests.” Environmental Science & Technology 37 (2003): 4060–4069

wires are routed through the wheels to a wireless transmitter that rotates with the vehicle's wheel and transmits measured data to a receiver mounted inside the vehicle.

Figure 4. Brake Thermocouples and wireless hub transmitter installed on the Camry test vehicle

After installing the instrumentation, LINK then burnished the new friction materials of each vehicle on-track over five repeats of Trips 2 and 4 of the WLTP-Brake cycle. Then, brake temperatures were logged while driving the complete WLTP-Brake cycle followed by an ERG-defined **Heating and Cooling Matrix**. The Heating and Cooling Matrix consisted of a series of standardized stops and steady-speed cruises to help separately analyze brake heating and cooling patterns. The events making up the Matrix are tabulated in Appendix B. The WLTP-Brake and Heating and Cooling Matrix temperature measurements were used in the development of ERG's brake temperature model. Historgrams of rotor/drum temperatures measured over the WLTP-Brake cycle on the test track are presented in Figure 5. In the figure, the temperature range is presented as the temperature difference above the ambient temperature in the wheel well (which was approximately 25°C during most of the testing.

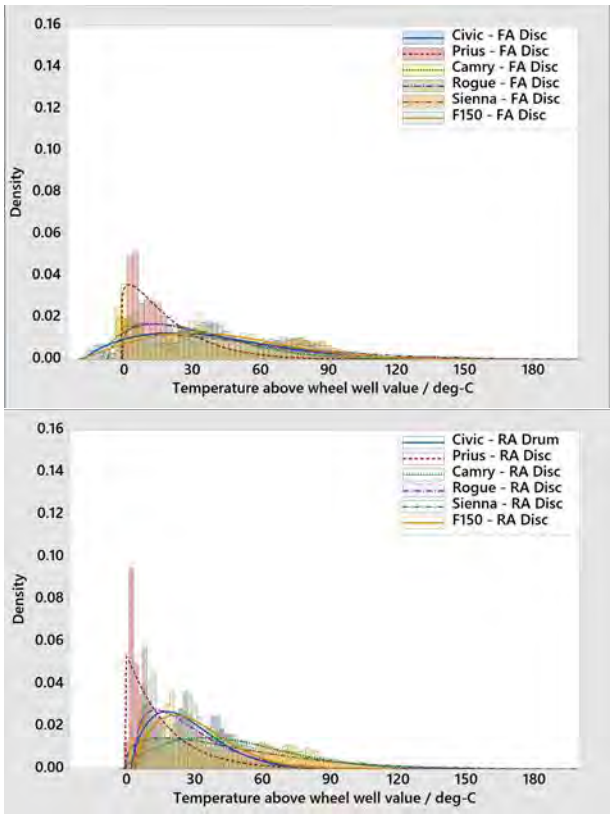

Figure 5. Histograms of temperatures of front rotors (top) and rear rotors/drums (bottom) over the WLTP-Brake cycle operated on the test track.

ERG developed a generalized form of an equation to describe brake heating and cooling rates based on an energy balance of the energy flow into the brakes during deceleration and the energy flow from the brakes due to convective cooling. The equation for change in temperature, ΔT, is of the form:

$$\Delta T = (A + B \cdot V_0 + C \cdot V_0^2) \cdot (T_0 - T_{amb}) \cdot \Delta time + D \cdot (V_0^2 - V_1^2) \cdot \Delta time$$

In the equation, A, B, C, and D are heating/cooling coefficients specific to a given vehicle. V_0 is the vehicle speed (kph) at the prior instant and V_1 is the speed (kph) at the next instant. T_0 is the brake temperature at the given instant (°C), and T_{amb} is the air temperature around the brake system. Track testing was conducted for six vehicles to determine brake temperature trends over the two measured driving cycles, the WLTP-Brake cycle (adapted for track driving) and the Heating and Cooling Matrix consisting of standardized stops of various intensities to determine brake heating rates as well as steady-speed cruises to determine cooling rates. The temperature measurements during track testing were used to determine the coefficients A, B, C, and D for the different vehicles. Note that D is set to zero if braking is not taking place (i.e. the vehicle is not decelerating more rapidly than would occur during a coastdown).

Track data excerpts containing only the cooling periods from the Heating/Cooling matrix were initially extracted to determine cooling coefficients A, B, and C. The cooling periods were extracted first because the cooling is a relatively slow process that follows

a readily-modeled exponential decay, and any time delays in the data for this operational regime would not have much effect on measured temperature and thereby confound the modeling. Cooling coefficients were modeled by first using the nonlinear regression procedure (Proc NLIN) in SAS on each of the 13 steady-speed cooling segments of the Heating and Cooling Matrix to fit e^(A+Bv). Then, a polynomial fit to speed was applied to the results of the NLIN procedure for the 13 different segments using Excel. The coefficients of this polynomial model became the cooling coefficients. Using these, ERG then determined the best single heating coefficient by determining the best least-squares fit between the entire modeled and measured temperatures by means of iteration using the already-determined cooling coefficients. For the units given in the previous paragraph, the coefficients for the Toyota Camry are given in Table 9Table 9. The Toyota Camry was selected for use in modeling the Caltrans data (and for cycle development) due to its representativeness of the vehicle fleet as well as having a good fit between the modeled and measured temperatures of the test vehicles. ERG determined that the decision to use the results of a single vehicle was acceptable because the temperature model used for the complete Caltrans dataset was the same as that used for cycle-building. The form of the equation is the key aspect, not the specific coefficients; the temperature model was used only as a bridge between the relative amounts of heating energy and cooling time in the in-use dataset and in the new cycle.

Table 9. Temperature Model Coefficients (based on the Toyota Camry)

A, 1/s	B, 1/(s·kph)	C, 1/(s·kph^2)	D, °C/(s·kph^2)
-0.001264	-0.000053926	0.0000001431	0.0088

The level of agreement between the model and the measured data is presented in Figure 6. Note that there were 10 instances in the following graph in which the test vehicle's braking system was allowed to return to at or near ambient (and in some cases datalogging was stopped during those intervals to allow for driver rest). At these times, the model was also set back to match the measured temperature (which was near ambient at the end of these intervals). The plot presents approximately 8 hours of operation.

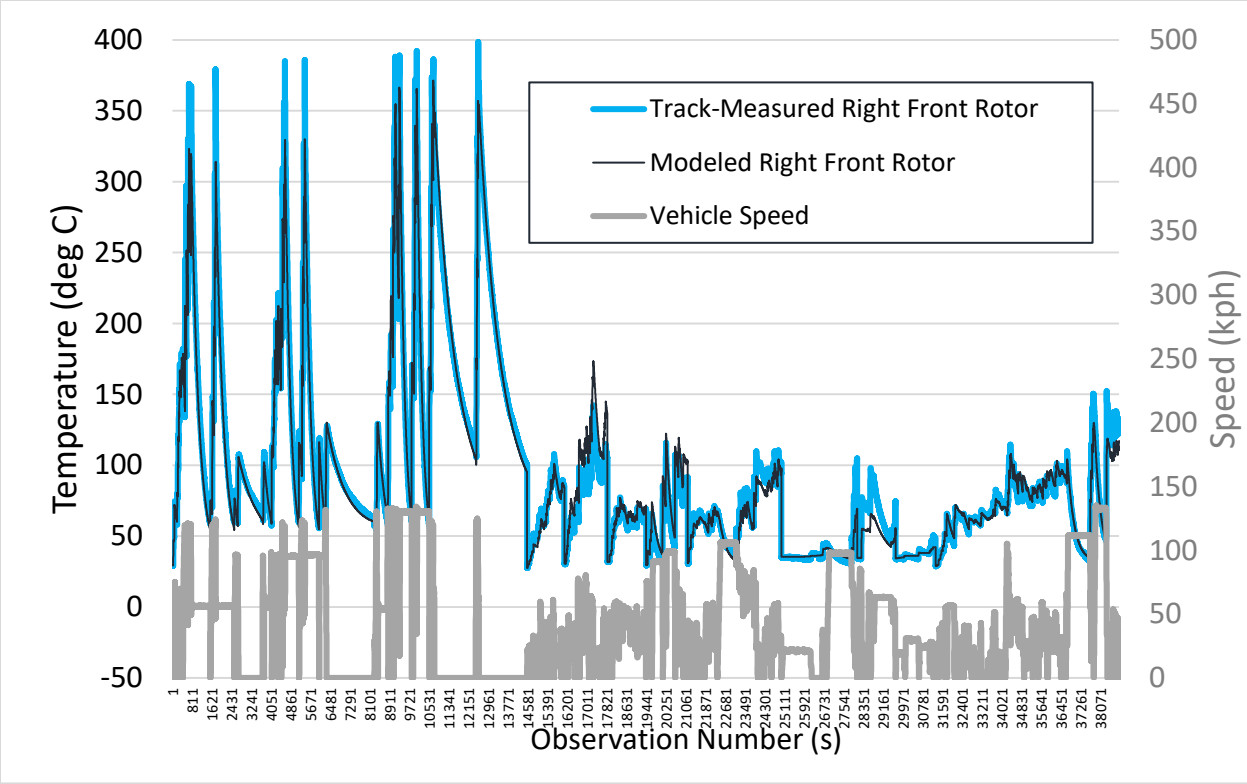

Figure 6. The modeled right front outer rotor temperature and the corresponding track-test measured temperature.

Test Cycle Development

After completing the temperature model, ERG proceeded to the selection of a test cycle to be followed on a brake dynamometer during PM emissions testing. The goal for the project was to utilize a cycle that is representative of California driving and practical for brake dynamometer operation. In this project, ERG developed a completely new cycle as a candidate for use during testing under this project. Consideration was also given to two existing test cycles, the EMFAC UC and its associated SCCs, as well as the World-Harmonized WLTP-Brake cycle, developed in Europe specifically for use on brake dynamometers. The UC was designed for exhaust emissions testing on a chassis dynamometer, so this report will describe its potential application as a braking test. The WLTP-Brake cycle is an "engineered" cycle, meaning it is not intended to be directly based on actual driving traces, but rather consists of engineered braking events at various deceleration thresholds.[5] The engineered aspects were constructed from vehicle activity data from Europe, the US, India, Japan, and South Korea. ERG evaluated all three cycles with various measures of their representativeness of real-world California driving. ERG presented the results of the evaluation to CARB and collaborated to select the cycle that would be used during the PM testing during this program. The driving cycle was developed prior to EPA involvement in the program.

Data Sources

This section describes the data sources used in this work including the two existing candidate test cycles that were evaluated. The data sources included in-use on-road vehicle survey data, temperature measurements performed on test vehicles operating on the track, and data from EPA's new vehicle emissions certification results. The existing cycles were either sourced from public information (for the WLTP-Brake cycle and the UC) or provided by CARB (for the EMFAC SCCs). This section also describes the methods that ERG followed to prepare and use these data sources in the selection of the test cycle for use on the brake dynamometer in this project.

The key material gathered for cycle selection was the Caltrans 2010-2012 California Household Survey data. This data includes actual in-use second-by-second operational data (vehicle speed over time is of primary interest for this work) from a variety of vehicle types operating across the state. ERG analyzed logged data from the operation of over 2,000 vehicles including over 14,000 hours of operation. This data served as the basis for evaluating the representativeness of both existing cycles (WLTP-Brake cycle and the EMFAC UC/SCCs) as well as for the creation of a new ERG-developed brake dynamometer test cycle.

[5] Marcel Mathissen, Jaroslaw Grochowicz, Christian Schmidt, Rainer Vogt, Ferdinand H. Farwick zum Hagen, Tomasz Grabiec, Heinz Steven and Theodoros Grigoratos, A novel real-world braking cycle for studying brake wear particle emissions, Wear, https://doi.org/10.1016/j.wear.2018.07.020e

Caltrans Survey Data

The Caltrans Survey included instrumentation of vehicles using either On-board Diagnostic (OBD) dataloggers, GPS dataloggers, or both OBD and GPS dataloggers. The survey was designed to be as random as possible and included participants from each county in California making it an excellent data source to represent typical California driving. The quantity of vehicles and logged data for each logger type is presented in Table 10. It can be seen that the vast majority of the data was collected using OBD-only dataloggers.

Table 10. Statistics on data logged with the 3 different logger types in the Caltrans Survey Data

	OBD-Only	OBD+GPS	GPS Only
Number of Vehicles	2130	365	677
Hours of Data	14,001	1,819	3,162
Time gaps of 2s in data	1.6%	0.1%	0.1%

The survey data included over 60 million seconds of data. Because of the large (and, therefore computationally-intensive) amount of data, ERG elected to use only the cleanest subset of data. After reviewing samples of each data type, ERG determined that the OBD-only dataloggers appeared to generate the highest quality data. This decision was based on reviews of the amount of clipping of trip starts and ends, the data resolution, and the steadiness of the zero measurement when vehicles were at idle. ERG also looked for time lags in the data (which would be of particular concern for braking analysis). Calculated mean and median deceleration rates during braking events were higher for the OBD-measured data than for the GPS data. This was consistent with ERG's previous experience that GPS data tended to have speed lag in time during acceleration or deceleration (which would likely result in a lower reported deceleration rate for a given braking event). For all reasons given, ERG selected only the OBD-only survey data for use in this work.

ERG applied further adjustments/corrections to the relatively clean OBD-only Caltrans data. Most notably, OBD speed data is reported to the nearest whole kph value, with no decimal places given. As a result, the speed traces were digitized, which challenged the ability to discern braking events from cruising events in the speed-trace data on a 1-second basis. This is because, due to digitization, an actual gradual reduction in speed by a vehicle would be represented as a constant value with a single 1 kph/s jump, followed by further constant values. Using a formula to assign braking would assign braking to that one second even though the vehicle was actually coasting for the whole period of time. To address this, ERG numerically smoothed all OBD data using the local weighted regression procedure (Proc LOESS) in Statistical Analysis Software (SAS). This procedure included a feature in which the optimum smoothing parameter can be automatically detected. ERG found the average optimum smoothing parameter for each vehicle and applied the average to all vehicles. The goal in the regression was to address the digitization without over-smoothing and reducing the measured deceleration rates of all braking events. Finally, some vehicles that had various speed

discrepancies were dropped from analysis. Less than 5% of the OBD data was dropped for this reason.

When reviewing a vehicle's smoothed speed trace data, the coastdown rate of the vehicle is an important input for use in determining whether and when that vehicle's brakes were applied. Because the specific make and model of each participating vehicle in the Caltrans survey data was not available, ERG used a **Generalized Coastdown Curve** sourced from EPA emissions certification result report data. The road loads and inertia for different vehicles can be found in the EPA Certified Vehicle Test Results Reports published for each model year.[6] These reports include the road load curves used during emissions certification on the chassis dynamometer; these road loads are also relevant to the setup of a brake dynamometer. To determine a general coastdown curve for use in this work, ERG averaged the EPA-published target coastdown curves for the 6 vehicles chosen for testing on the test track. These 6 vehicles covered the range of light-duty vehicle types available and can therefore be used to represent an average or reasonably representative overall vehicle coastdown rate. The derivation of the generalized coastdown curve is described further in Appendix C, which also includes the target road load coefficients for the 6 test vehicles. Note also that specific vehicle coastdown coefficients are an input to brake dynamometer testing. The coastdown coefficients for the vehicle being simulated are entered into the dynamometer control at the start of a test, and these coefficients govern the system's application of brakes over the test cycle using the same type of calculation as was used to determine braking events in the Caltrans set.

ERG then assigned driving modes to the smoothed Caltrans survey data. There were only two important driving modes for this analysis, braking and non-braking. The braking driving mode was assigned any time the vehicle's deceleration rate exceeded that which would be experienced while following the generalized coastdown curve found previously. All remaining times in which the vehicle was not decelerating more rapidly than that coastdown curve were assigned as non-braking. Once the vehicle came to a stop, it was no longer considered to be braking (even through the brakes may have still been applied) because there was no further sliding at the brake friction interface and therefore no appreciable brake heating or PM emission taking place.

Further classifications of the survey data were applied for use in the overall cycle building process. The survey data was divided into **Microtrips**, defined as the period starting the moment a vehicle comes to a stop, through an idle period, acceleration, cruise, deceleration and ending at the next moment that vehicle comes to a stop. Each microtrip contains one or more **Braking Events**, defined as the moment the brakes are applied to the moment that either the brakes are released or the vehicle comes to a stop, whichever occurs first. The ERG new dynamometer cycle was constructed based on combining a selected series of braking events that actually occurred in the Caltrans survey data. Information about the microtrip from which each braking event was extracted was retained to associate the braking event with microtrip average speed and

[6] https://www.epa.gov/compliance-and-fuel-economy-data/annual-certification-data-vehicles-engines-and-equipment

distance traveled. This is done because, while some distance is traveled during braking, emission rate results from braking in EMFAC are given on a per-mile basis and these must also appropriately consider vehicle distance traveled between braking events for inventory purposes. An excerpt of a speed trace is presented in Figure 7, with graphical depictions of the start and end of a microtrip and its braking events.

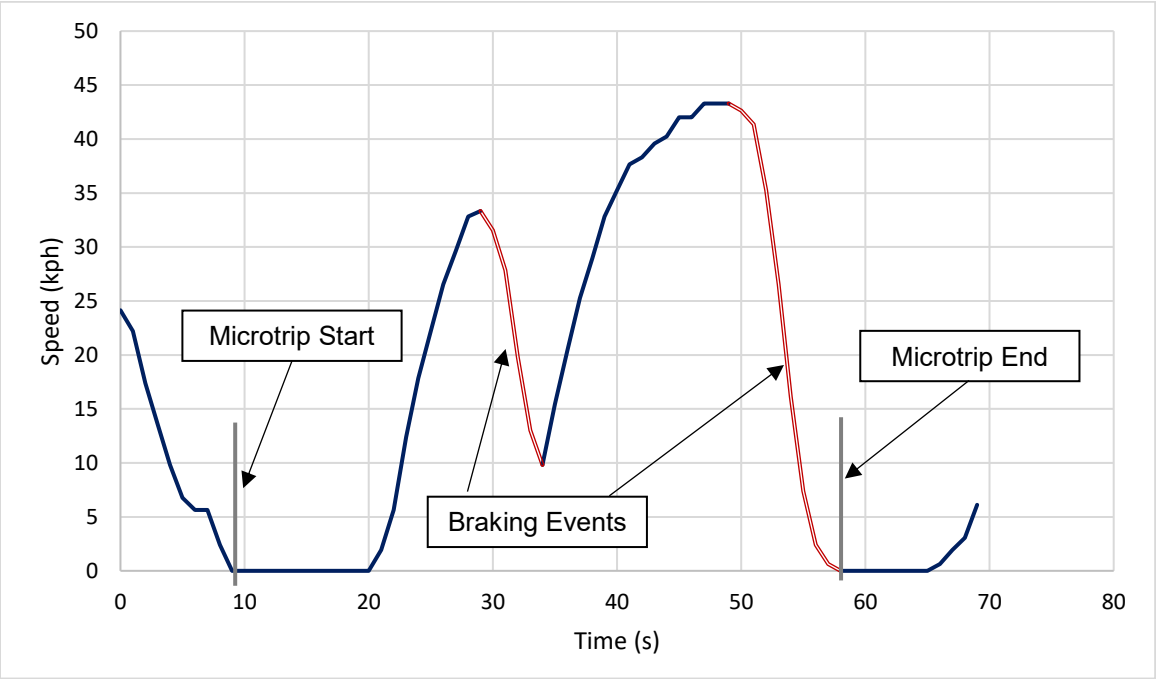

Figure 7. Illustration of microtrips and braking events within a speed trace

New Cycle Development and the Vector Collinearity Method

Over the last 25 years, ERG has developed and refined a method to measure agreement between a candidate test cycle and in-use data. The method is based on the determination of the angle between normalized vectors that represent the distributions of key time-series attributes in the candidate cycle and in the in-use data. An angle of zero degrees represents collinear vectors, that is, the key attributes of the candidate cycle and the in-use data times series would be the same (and normalized distributions of those attributes would be identical). Thus, the candidate cycle whose vector has the smallest angle with the vector of the in-use time series data is the best test cycle. Appendix D contains further information regarding the vector collinearity method including an excerpt from a previous ERG report in which the method was described in detail.

ERG used the vector collinearity approach to build the new brake dynamometer cycle from the Caltrans survey data. Put simply, the method involved sequentially selecting actual braking events from the Caltrans data so that the joint distribution of the key variables of the built-up cycle on the dynamometer best matched the same distribution of the braking events in the Caltrans data. Brake events continued to be selected in this

manner until the built-up cycle reached a target overall duration or distance. The key variables used in this work were:

- Vehicle speed (distribution)
- Modeled brake temperature (distribution)
- Deceleration (distribution)
- Braking event duration (single value for each event)

Three of the variables allow for a distribution of second-by-second values within any braking event, but the event duration is just a single value for each event. Each of the four parameters were weighted equally as there was no reason to justify prioritizing one of the parameters over the others. The resulting distributions of the parameters show that all matched the target reasonably well, so it wasn't necessary to weight the matching of one at the expense of any other (i.e. weighting them differently would not have significantly affected the outcome).

The vector collinearity method was applied to create a series of braking events whose distributions of speed, modeled temperature, deceleration, and event durations best matched those in the entire Caltrans set. It should be noted that this selection method results in selecting the group of braking events that best match the target, but the procedure does not result in any particular order for the events (meaning they need to be ordered later).

The evaluation of the distributions of the four different parameters of braking events on the millions of braking events present in the Caltrans survey data was extremely computationally intensive. To keep computation time reasonable, ERG randomly selected a pool of 1000 Caltrans survey braking events to choose from during the vector method. The target vector was created from the entire Caltrans dataset; however, the new cycle could be built up from only selections from the 1000 randomly-selected microtrips.

Matching the braking events' distribution for temperature created a new challenge for the cycle development process. During brake dynamometer testing, the test brake system cools according to how quickly it is rotating over time. However, applying the brakes is the only way to heat the brake system. Because of this, the method could select different braking events whose associated temperatures could result in temperature gaps between the different selected braking events, meaning one or more of the higher temperature events could not be reached by the temperature increases available from any of the other chosen events. As a result, ERG developed rules regarding temperature for selected events to allow for the testing to be as realistic in temperature as possible while also reaching all specified modeled temperatures.
To eliminate temperature gaps, in which one or more selected braking events had an initial temperature that couldn't be reached based on the heating of any of the others, ERG implemented rules regarding temperature selection. To be eligible for selection by the vector collinearity method, brake events had to have an initial temperature less than the maximum ending temperature of any of the events that had been previously selected. For the initial selection, any event with a starting temperature of less than 2°C

above ambient was eligible. While necessary to eliminate temperature gaps in which the highest temperatures could not be reached, this rule created a downward bias in temperature, as throughout the early stages of event selections only relatively low-temperature events were eligible for selection. To compensate for this, the selection pool of 1000 microtrips was adjusted to include 800 events selected at random, and 200 events selected at random from only those events with initial temperatures between 140°C and 190°C. As a result, ERG was able to develop a test cycle that could have completely reachable temperatures on the dynamometer as well as be representative of the distribution of modeled temperatures reached during on-road driving. The representativeness of the actual temperatures can be verified in histograms of operating temperature of the cycle and the target (included in the following sections).

After the microtrips were selected, they next needed to be ordered. Because of the rule that microtrips could only be selected if their initial temperature was less than the maximum temperature previously reached, they could, by definition, be ordered to increase without gaps (but there may be only one order that could reach the maximum without gaps). Braking events were ordered to achieve the maximum temperature relatively early in the cycle; those events that were needed to reach high temperatures were used to move rapidly up to the maximum. Otherwise, they could end up being "wasted" or lost by being followed by a cooler brake event leaving a temperature gap later in the cycle. So, the resulting trend of this process is a prompt rise to the maximum temperature followed by an oscillating and slowly decreasing temperature trend for the rest of the cycle. During cooling, brake events were ordered by always prioritizing the use of the highest starting temperature event that was accessible from the previous ending temperature. Sometimes, the time required by the dynamometer for speed changes after the point of highest temperature did result in a small number of temperature gaps. After the maximum-selected temperature had been reached, any further brake events with gaps were dropped from consideration. Dropping these events (after the maximum selected temperature had been reached) did not affect the resulting temperature distribution significantly. This is because there were generally few gaps at this point of ordering and they generally occurred across the entire temperature range such that their removal did not skew the resulting temperature distribution appreciably.

After each braking event was selected and ordered, the different events needed to be connected by a continuous speed trace that could be followed on the dynamometer. ERG added "engineered" segments between each braking event to allow the dynamometer speed and brake temperature to arrive at the initial speed and temperature of the next braking event. They included ramping to the next event's speed as well as allowing time to pass at constant speed if further cooling was necessary to match the starting temperature associated with the next selected event. Cooling was assumed to take place as a function of speed (simulated by dyno RPM) according to the temperature model. The dynamometer positive acceleration ramp rate was limited to a maximum of 8 kph/s to stay within typical brake dynamometer capability. Some brake events had initial speeds less than the ending speed of the previous brake event. The negative deceleration level was specified at -3 kph/s. If a large amount of cooling was needed to get to the next event's temperature, the speed was kept at the higher of either the previous event's end speed or the next event's initial speed to maximize the

cooling rate. For those segments in which the speed was held at the previous event end speed, deceleration took place at -3 kph/s near the end of the segment in order to arrive at the next event speed at the correct target temperature.

After the cycle was completely selected, ordered, and the engineered segments added, it was taken from that point as only a speed trace. The modeled temperatures are no longer a part of the trace, they were used in its creation only. The speed trace is the cycle and is independent of temperature now that it has been created. This means that testing of different brake assemblies will follow the same speed trace but will be allowed to run at completely different temperatures depending on the vehicle/brake assembly characteristics and modeled vehicle mass.

While some vehicle distance is traveled during the braking events selected in the cycle, each braking event actually represents a much greater distance traveled in the Caltrans set. Because the braking events were extracted from microtrips, the distance of the source microtrip must be accounted for to generate a representative on-road emission rate in g/mi. To do this, information on the microtrip source of each braking event was retained to associate braking events with a total distance traveled (which is greater than the distance traveled just during braking). For microtrips that contained multiple braking events, the braking energy for each event was used to proportionally assign the total microtrip distance traveled to that represented by each braking event. Dynamometer distance is also traveled during the engineered segments of the cycle; however, these segments only exist to set the dynamometer speed and the amount of brake cooling. The dynamometer operation during the engineered segments has no actual basis in vehicle distance traveled, which also contributes to why the dynamometer cycle distance traveled is not useful for g/mi calculations. The ERG cycle will specifically advise a **represented distance** to be used in all g/mi calculations and it will not be the same as the integrated distance traveled by the rotational assembly on the dynamometer. Figure 8 illustrates an example microtrip from which one braking event was selected and inserted into the test cycle. The speed trace of the braking event is identical, however the rest of the microtrip is excluded.

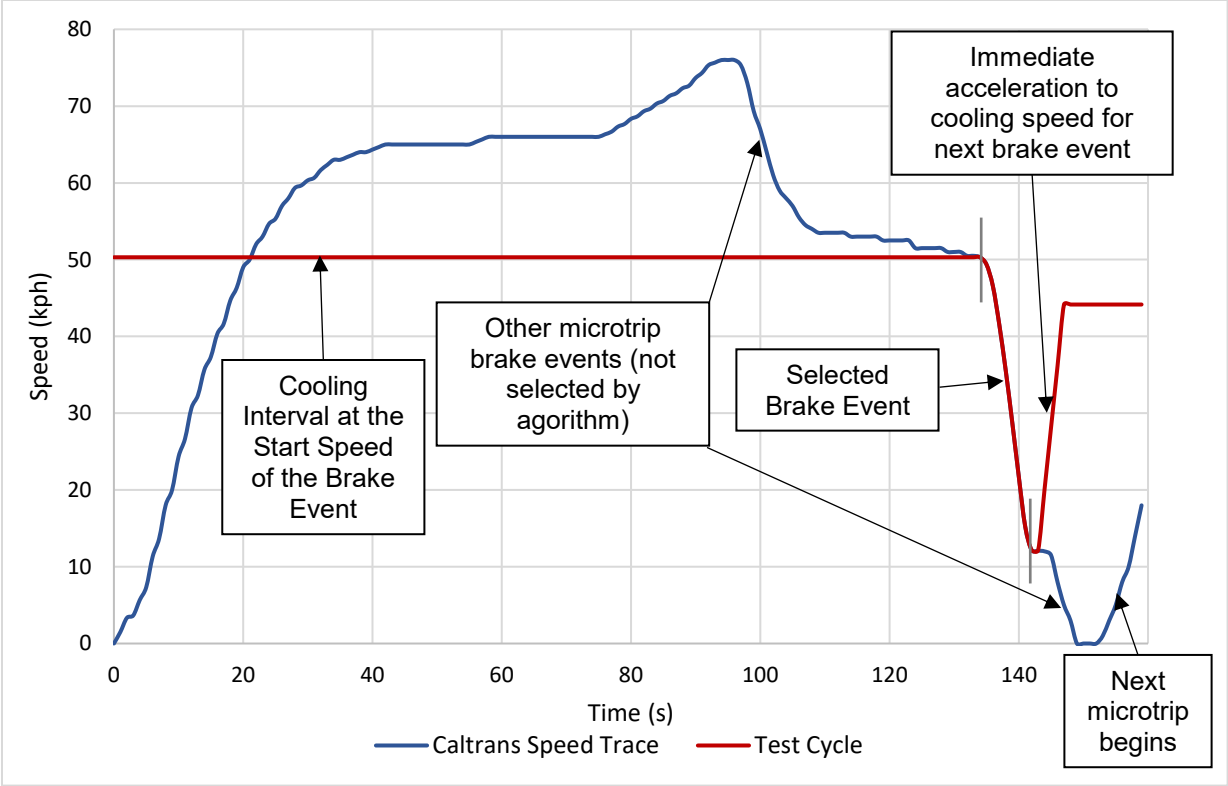

Figure 8. Illustration of a braking event, extracted from the original microtrip speed trace (blue), and inserted into the test cycle between engineered segments (red)

In addition to representativeness of California driving, the test cycle also needed to have the ability to resolve emission factors by speed. The ERG cycle is divided into three **speed segments** representing different average speed ranges. ERG selected three speed ranges based on trends in the average speed of all microtrips in the Caltrans data. Figure 9 depicts a histogram of the number of microtrips with each average speed. The histogram represents all microtrips in the Caltrans set, weighted by the duration of each microtrip (i.e. longer microtrips have higher weighting to reflect the greater duration and distance of driving that they represent). The average speed ranges for the segments of the new cycle were selected as 0-21 kph, 21-69 kph, and 69 kph and above. ERG used the cycle building approach to develop a brake dynamometer cycle for each average speed range. Each phase would contain braking events taken only from microtrips falling within its respective microtrip average speed range.

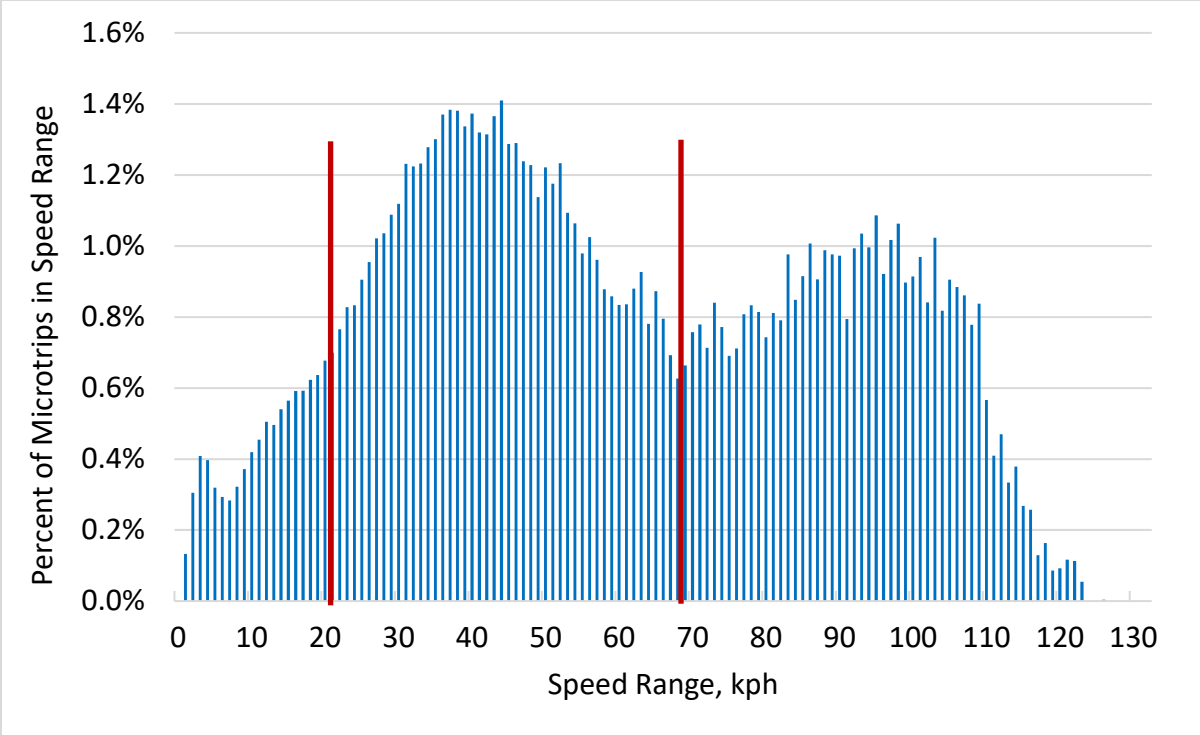

Figure 9. The percentage of the number of microtrips within each bin of average speed

ERG used the vector method described previously to construct each of the three speed segment. For a given speed segment, the selection pool of 1000 brake events were chosen from only those microtrips with an average speed within the segment's speed range. The target vector from Caltrans used for each speed segment was taken to be that made up of the braking events from all microtrips with an average speed in that range. The overall cycle is made up of the three speed segments run in succession. The representative distances of each was also taken to represent the relative distances traveled in the Caltrans survey by all microtrips falling within each speed range. This results in the overall per-distance emission rate being representative of overall brake emission rates in California. Because the speed segments are specified to run in succession, the speed-based emission factors could be based on either continuous or batch (i.e. filter-based) PM measurements.

ERG used a specific method to determine the overall duration/represented distance of the speed segments as well as how the distances were apportioned within each of the three speed segments. The following procedure was followed:

1. Use the vector collinearity method to build up 200 braking events for each of the three microtrip speed ranges
2. Determine the total distance represented by each range's 200 events
3. Determine the total distance traveled in the Caltrans dataset by microtrips in each of the 3 speed ranges and find the percentage for each
4. Correct the two speed segments that over-represent distance by removing trips at random, but do not remove trips that would cause a temperature gap in the cycle

After determining the relative distances of each cycle, ERG inserted engineered portions between each speed cycle to allow the brakes time to cool to a near-ambient starting temperature. The percentages of distance traveled in the overall Caltrans dataset of microtrips in each of the three speed ranges are presented in Table 11 along with the resulting represented distances and times for the new cycle.

Table 11. The percentage of Caltrans-survey and new test cycle total distance traveled by microtrips within each average speed range

Microtrip Avg. Speed Range	Percent of Total Caltrans Distance traveled	New Cycle Represented Distance (km)	New Cycle Represented Distance %	New Cycle Duration (s)
0 – 21 kph	3.96 %	6.163	4.7 %	2,741
21 – 69 kph	38.34 %	47.309	36.0 %	8,339
69+ kph	57.7 %	77.775	59.3 %	3,853
Total	100 %	131.247	100 %	14,933

Figure 10 presents a speed trace of the new ERG-developed braking cycle for this program.

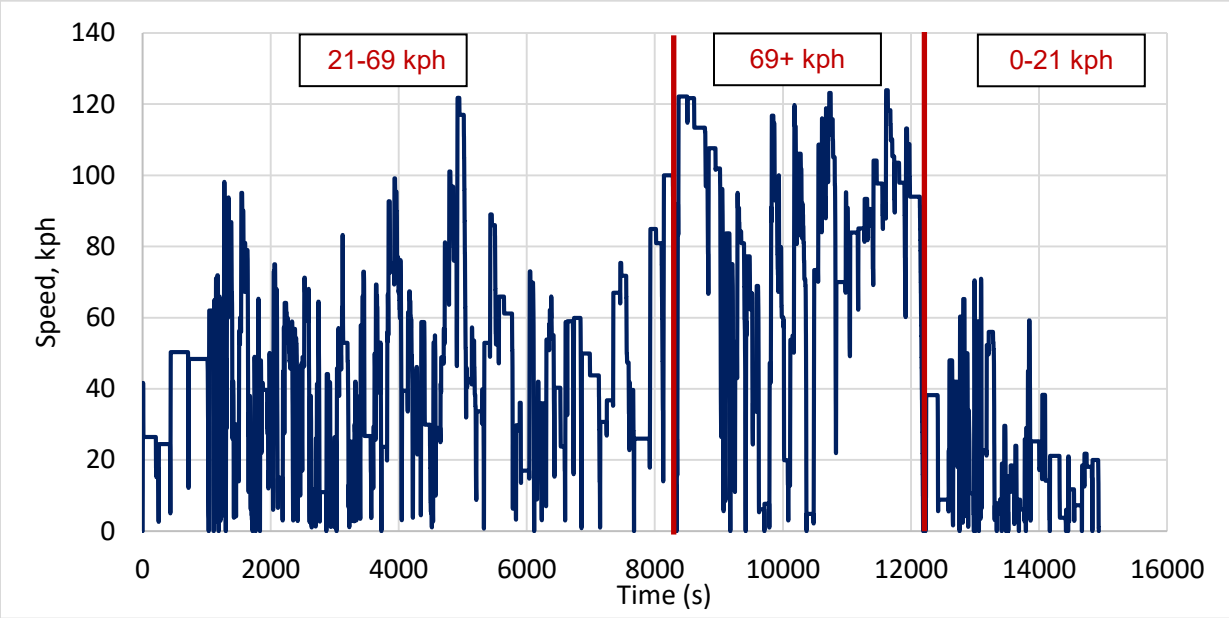

Figure 10. Speed trace of the braking cycle developed for this work

The new cycle developed from the vector collinearity method was evaluated against the two existing cycles, the EMFAC cycles and the WLTP-Brake. For each of these cycles, the same general coastdown curve was used to isolate braking events from the speed traces. The same temperature model was applied to these cycles to develop temperature distributions of each. To evaluate the EMFAC UC and SCCs, ERG created a single cycle from starting with the UC and appending all the SCCs to it. Modeled temperature was reset to ambient between each of the UC and SCCs. To develop distributions for the WLTP, the temperature was set to 10°C over ambient between each

of the 10 trips to reflect the cooling soaks to 30°C between trips as specified in the WLTP-Brake test procedure.

In this report, findings and comparisons for the EMFAC UC/SCCs are included, however these cycles may not be able to be repeatably run on the brake dynamometer. These cycles have a range of brake event durations that includes events down to 1s and 2s in duration. The LINK brake dynamometer cannot repeatably test braking events of this short of duration. This cycle could not be chosen for this project for this reason; however, the EMFAC cycles are left in the analyses in this section. Correspondingly, the ERG cycle development algorithm described previously was modified to only select braking events of 3s duration or longer to meet the dynamometer requirements for repeatable operation. Speed traces of the WLTP-Brake and the concatenated UC/SCCs are presented for reference in Figure 11.

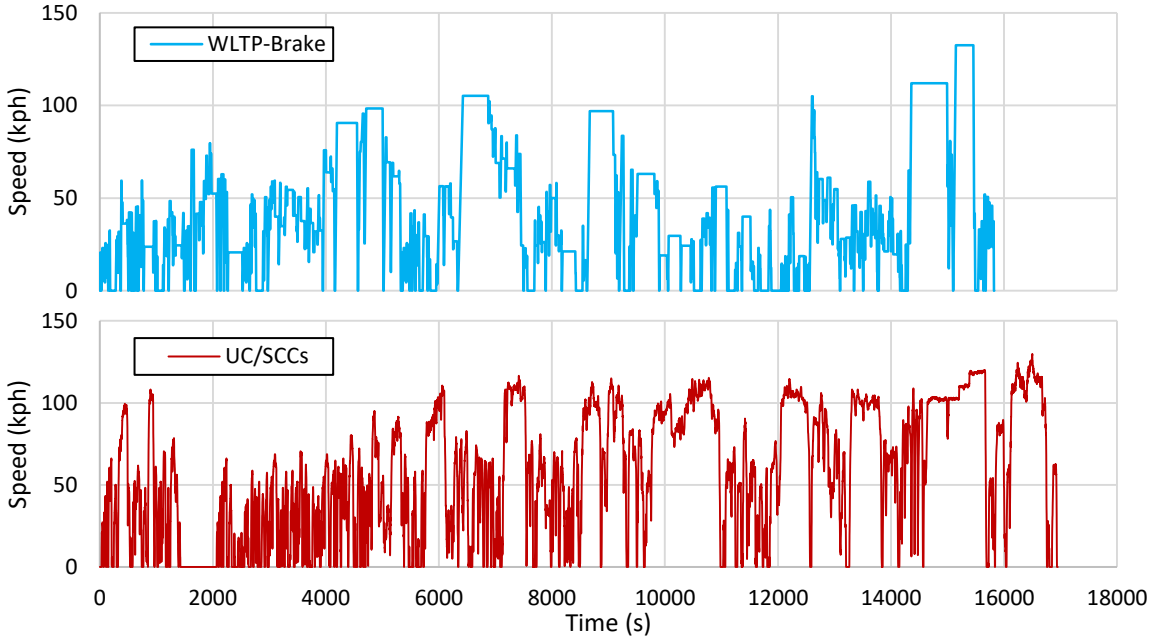

Figure 11. The Speed traces for the WTLP-Brake and the concatenated UC/SCC

Comparisons across the three cycles are presented in two ways. First, Table 12 describes some of the relevant properties of the three cycles. Later in this section, distributions of various parameters of interest are presented for the three cycles.

Table 12. Relevant parameters of the three candidate brake test cycles

	Duration (s)	Number of Braking Events	Distance (km)	Brake Events/ Distance (#/km)	Average Speed (kph)	Max. Speed (kph)
ERG Vector Method (Overall)	14,933	347	131	2.65	50.3[1]/30.3[2]	123.9
0-21 kph speed segment	2,741	65	6.16	10.55	21.7[1]/8.0[2]	70.9
21-69 kph speed segments	8,339	198	47.31	4.19	45.7[1]/19.4[2]	121.8
69+ kph speed segment	3,853	84	77.76	1.08	80.6[1]/69.8[2]	123.9
WLTP-Brake	15,826	303	192	1.58	43.7	132.5
EMFAC UC/SCCs	16,952	1,015	272	3.73	57.7	129.8

[1] – Calculated based on the actual number of dynamometer revolutions

[2] - Indicates the represented distance for inventory (accounting for brake cooling and elimination of unnecessary cruises – this is the value relevant for EMFAC)

It is important to note some specifics regarding the values in the table as follows:

- **Duration:** Duration is a count of the number of cycle-specified seconds only. The WLTP also includes cooling between most of the 10 Trips and so will take longer to complete. The time listed for the ERG method includes all required cooling.
- **Distance:** As described previously, the overall ERG cycle spins the dynamometer further than 131 km due to the engineered segments. The 131 km listed specifically describes the distance represented by those events for the purposes of g/mi calculations. The distance listed for the other two cycles describes the distance traveled by the dynamometer. The dynamometer spins a longer distance over the ERG cycle to allow the necessary amount of cooling.
- **Average Speed:** Because the ERG cycle spins the dynamometer farther than the on-road distance represented, the average speed is presented two different ways. For the ERG cycle and its constituent cycles, average speeds denoted with a "[1]" indicate the average speed of the **rotation on the dynamometer** including the cooling intervals. The average speeds denoted with a "[2]" indicate the average speed based on the distance represented by the cycle for the **purposes of inventory modeling**.

The following section includes distributions of various parameters of interest for the 3 cycles. The Caltrans survey data is shown as the target for representation of real California driving. In all plots, the distributions reflect the parameters from only the time

during brake events; the values during periods of time with accelerations and cruises are not included in the distributions. Braking events are defined by decelerations that exceed the generalized coastdown curve used in this work. Temperature distributions are estimated using the temperature model developed for the Camry test vehicle. Additional detail is presented in Appendix E, which contains similar distributions further broken down by each of the three speed segments that make up the new cycle.

The distributions of brake event durations are presented in Figure 12. Note that the ERG New Cycle does not have any brake events shorter than 3 seconds. This is intentional due to a limitation of the brake dynamometer used for testing and would otherwise be likely to result in the UC/SCCs not being repeatably testable as they have many 1s and 2s events. The number of events in the 3-second bin of the ERG cycle are higher as a result because the vector collinearity method was targeting the Caltrans distribution which contains a large number of 1s and 2s events.

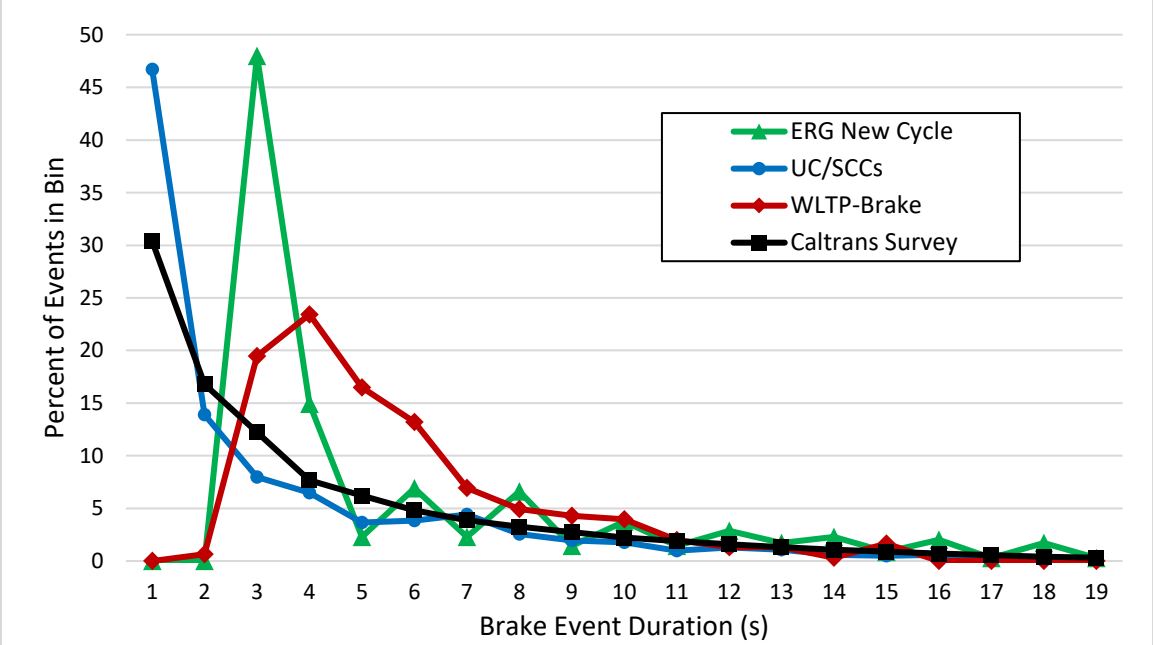

Figure 12. Distribution of brake event durations for the candidate cycles and the Caltrans data

The distributions of speeds encountered during braking events are presented in Figure 13. The distribution of (negative) acceleration rates during braking is presented in Figure 14.

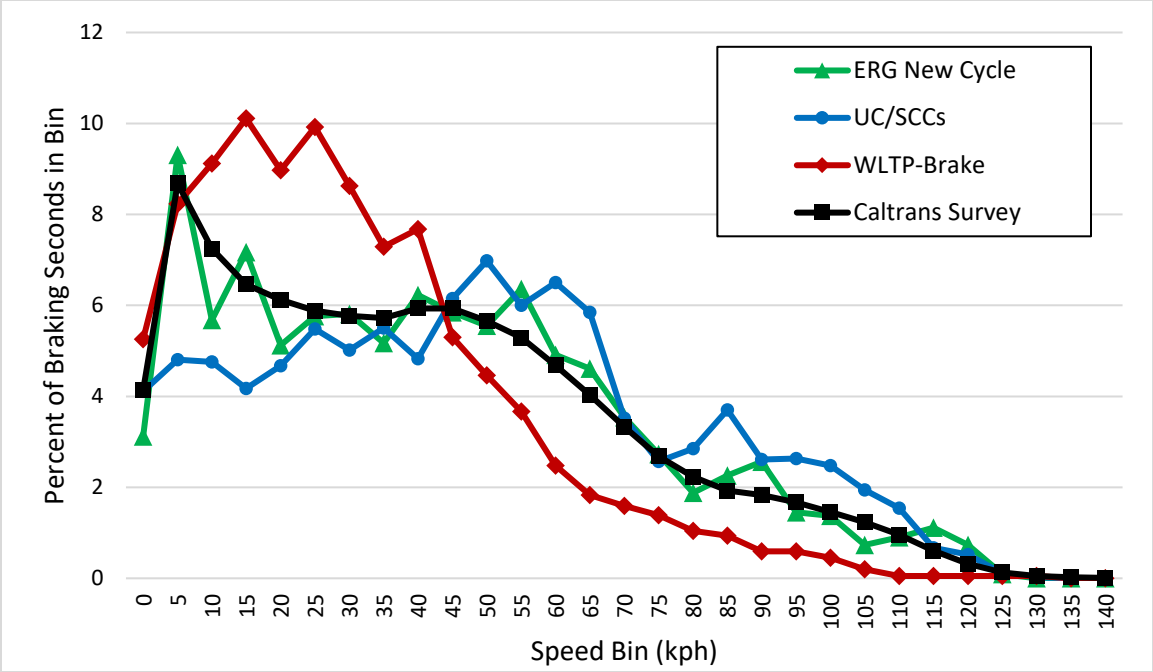

Figure 13. Distribution of vehicle speeds for the candidate cycles and the Caltrans data

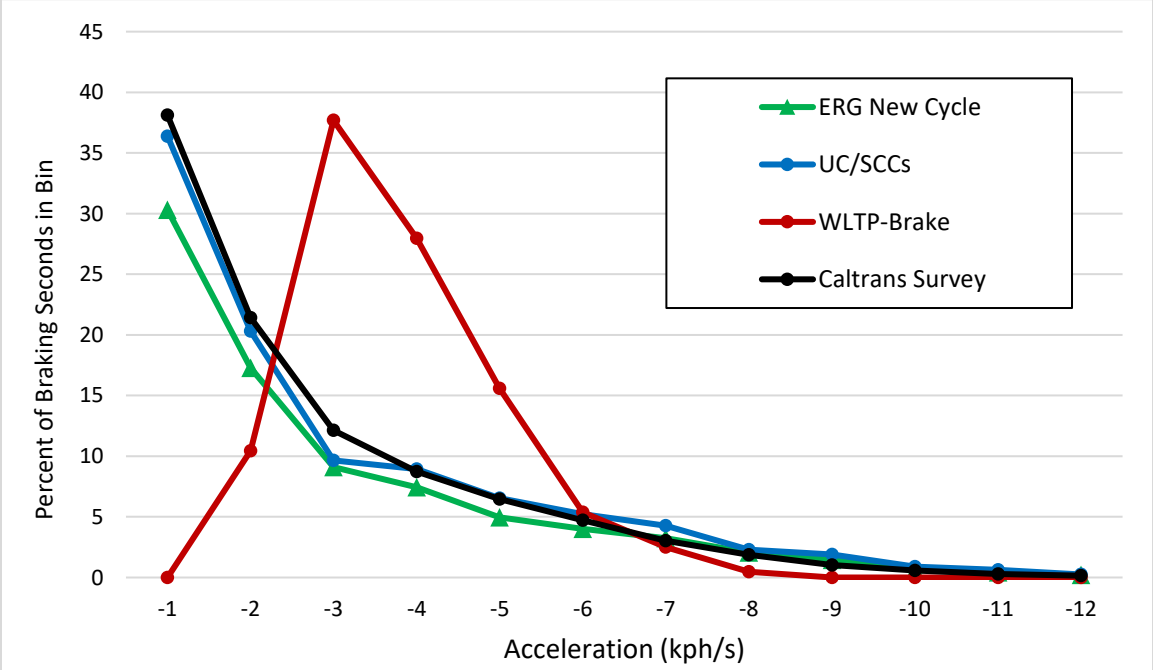

Figure 14. Distribution of braking event (negative) acceleration rates for the candidate cycles and the Caltrans data

The distributions of modeled brake temperatures for each cycle are presented in Figure 15. The same temperature model was used to estimate temperatures for the three candidate cycles as well as the Caltrans survey data.

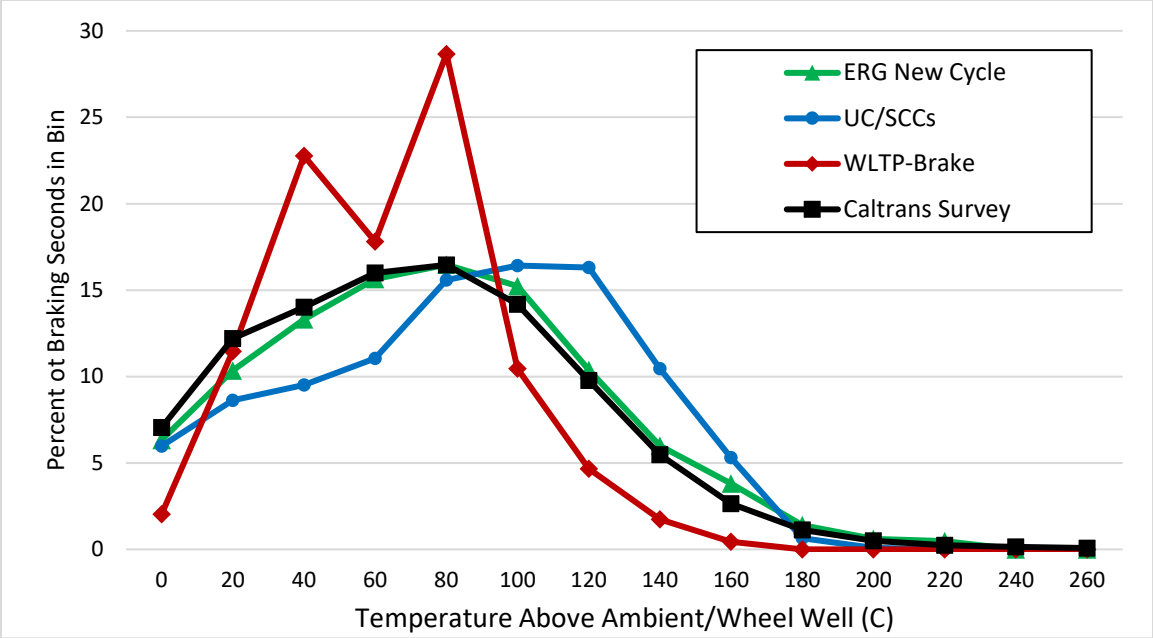

Figure 15. Distribution of modeled brake temperatures for the candidate cycles and the Caltrans data

The distribution of relative power per brake event is presented in Figure 16. In this plot, relative power is defined as the change in speed squared (accounting for the coastdown-rate of energy loss) divided by the duration for the entire brake event in seconds, with units of kph^2/s. Relative power was not one of the parameters used during cycle building, but is presented here for completeness.

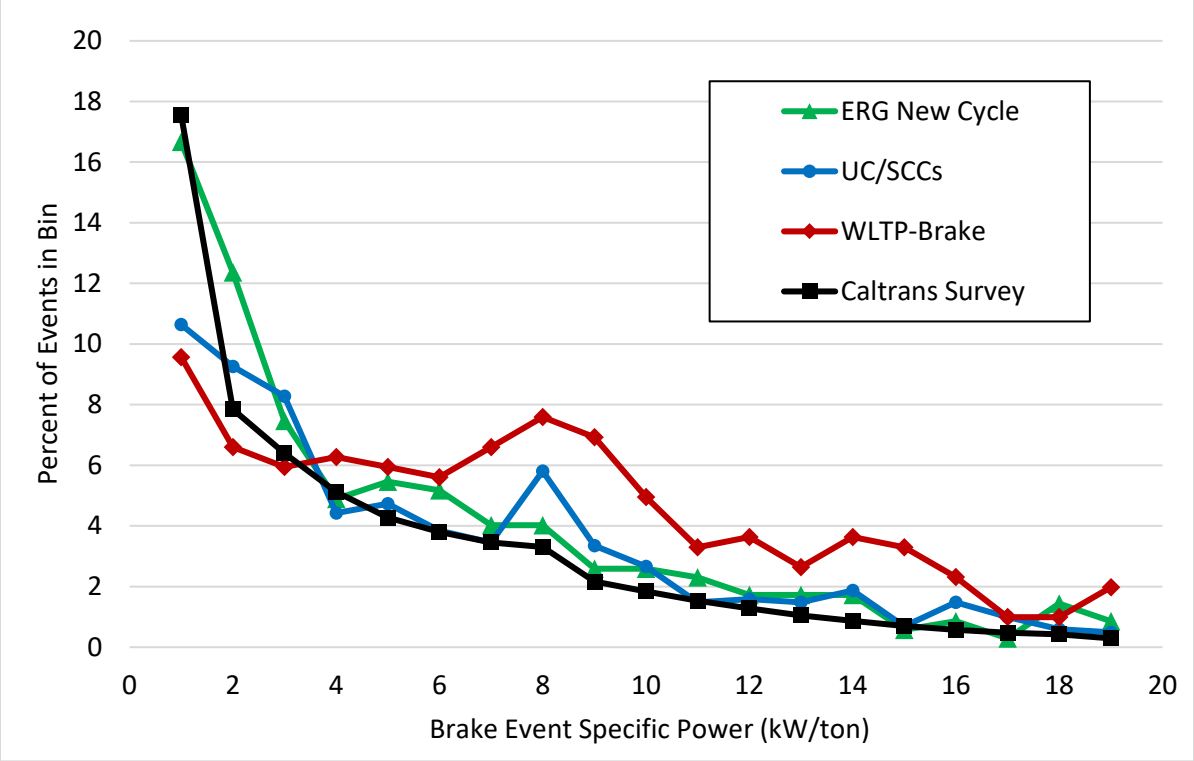

Figure 16. Distribution of brake event relative power for the candidate cycles and the Caltrans data

Each candidate cycle has advantages and disadvantages. The following summaries for each cycle describe the key considerations for the evaluation and final selection of the cycle used during dynamometer testing.

ERG Vector Method Cycle. The distributions on the parameters of interest for this cycle match very well with the Caltrans survey results because it was designed to result in a match on the four main parameters. It allows directly for determination of speed-based emission factors using its three constituent speed segments. However, it is an unproven cycle with no reputation across the research community. Some members of the community may not agree with the approach to have a represented distance for g/mi calculations (for the purposes of inventory modeling) that is separate from the actual dynamometer distance traveled. ERG planned to have a separately-specified represented distance from the start of this project as it ensures that g/mi calculations are appropriate for representing California driving.

WLTP-Brake. The WLTP-Brake is an engineered cycle designed for use on a brake dynamometer. As a result, it contains brake event durations appropriate for dynamometer testing. However, of the three candidate cycles, its distributions on the parameters of interest have the least similarity to the Caltrans survey results. Also, it was not designed to have the distance traveled over the cycle be on the same basis as PM emissions from California driving, resulting in potential error in g/mi calculations.

The WLTP-Brake cycle also does not necessarily lend itself to the measurement of speed-based emission factors. With this cycle, speed-based factors would only have been able to be generated from extracting different brake event segments from the continuous PM measurement traces. An advantage of the WLTP-Brake cycle is commonality and comparability with European brake testing which will heavily utilize the WLTP-Brake.

UC/SCCs. The analysis of braking events showed that the EMFAC cycles matched the Caltrans survey results reasonably well for the parameters of interest. The key limiting factor of these cycles will be that they contain a significant number of short duration (1-2s) brake events that cannot be repeatably simulated on the brake dynamometer. It is not possible to remove these short duration events without significantly reworking these cycles. For this reason, it would have been inadvisable to utilize these cycles for this program despite EMFAC being designed around them such that test results would be readily adapted into EMFAC emission factors including those that are speed based.

Cycle Selection. The three cycles were evaluated for how well they represented the driving logged during the Caltrans survey. The EMFAC UC and SCCs represented the Caltrans data fairly well and could be readily adapted to speed-based emission factors because the speed correction cycles already exist. However, the EMFAC cycle consisted of many 1s and 2s duration brake events, which cannot be repeatably simulated on the brake dynamometer. For this reason, the UC/SCCs could not be used in this work. The WLTP-Brake cycle is designed specifically for brake dynamometer testing but was not specifically designed to represent California (or US) driving as it was developed from data from multiple nations. The WLTP-Brake is also not designed to directly determine speed-based emission factors. The ERG vector-based method generated a cycle that both represented different speed ranges of operation and was very similar to the Caltrans travel survey data on the four important parameters of interest, so CARB and ERG staff agreed that ERG's newly-developed cycle would be used during the dynamometer testing in this work. From this point forward, it will be known as the **California Brake Dynamometer Cycle (CBDC)** for light duty vehicles.

Brake Burnish Cycle. Newly installed brake friction materials go through a process of "bedding in," in which the friction couple equilibrates and a layer of pad material becomes adhered to the disc or drum. Particulate emission rates may not be stable during this time. Also, brand new materials may have a protective coating to prevent oxidation prior to installation. After installation, this coating is worn off in the early stages of use but may result in particulate emissions that are not representative of emissions during the remaining life of the components. For this reason, a burnish procedure was performed after the installation of new components but prior to testing.

ERG developed a new brake burnish cycle with the goal of being as short as possible (to allow for a 24 hour test turnaround) while still resulting in a stable friction couple at completion. The PMP was developing a standardized burnish cycle concurrently with this project, and industry experts participating in the process indicated that a minimum of 5 repeats of the WLTP-Brake would be necessary for a stable burnish. ERG used this

as the source of the development of a new burnish cycle for this work. ERG developed a new burnishing cycle by using the following method:

- Calculate the total braking energy in 5 WLTP-Brake cycles
- Select a relatively high energy segment of the newly developed CBDC brake cycle that has a similar start and end temperature (starting at 707s, proceeding to 1740s)
- The burnish cycle starts from the beginning of the CBDC and runs through the end of the selected high-energy segment. Then, that segment is appended repeatedly until the total braking energy of 5-WLTP-Brake cycles is reached
- An engineered high-speed cruise is added to cool the brake assembly to near ambient temperature
- Finally, to cool down and equilibrate the friction couple so that it doesn't end during high intensity operation, a single, low speed segment is appended to the end of the burnish (the complete 0-21 kph speed segment).

The resulting burnish cycle has a duration of approximately 11 hrs 30 mins (as compared to approximately 30 hrs for 5 WLTP-Brake cycles when including the specified cooling between trips). A speed and temperature trace of the resulting burnish cycle (used for all tests in this program) is presented in Figure 17. The repetitive nature of the cycle facilitates the determination of whether PM emissions reach steady state.

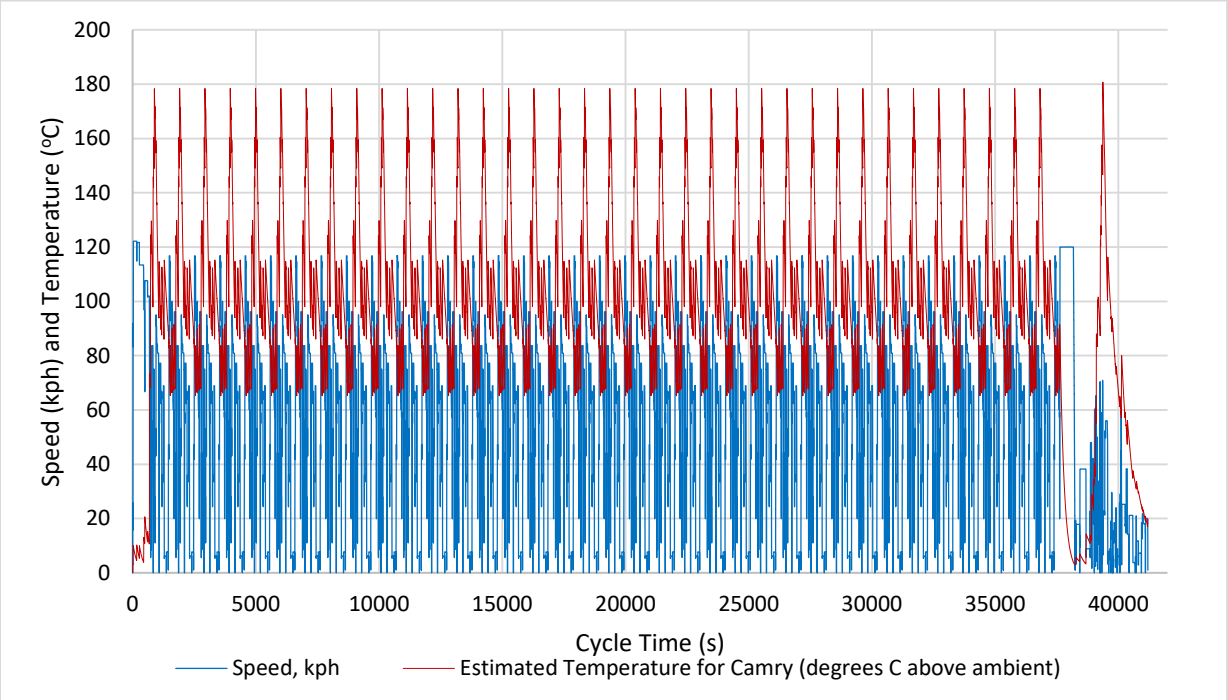

Figure 17. Dynamometer speed and estimated Camry front rotor temperature traces for the CBDC burnish cycle

Test Matrix

After the test cycle was developed, ERG and LINK then began the development of a test matrix that would describe the various tests that would be conducted during the dynamometer testing phase of the project. The first step in the development of a test matrix was to consider the parameters of interest to be tested. This section lists those parameters, the different options or values to test within each parameter, and their relative importance. The parameters that were considered are:

Vehicle make and model. The initial parameter that was considered was the vehicle make and model of each brake assembly. The selection of the test vehicles was described previously in the Representative Test Vehicle and Friction Material Selection section, in which the selection of the following 6 vehicles was documented:

- 2011 Toyota Camry LE
- 2013 Honda Civic LX
- 2013 Toyota Sienna LE
- 2015 Ford F-150 Supercrew
- 2016 Toyota Prius Two Eco
- 2016 Nissan Rogue S

These vehicles are all equipped with front and rear disc brake systems except for the Honda Civic, which utilizes front brake discs and rear brake drums. The Toyota Prius is a hybrid vehicle and is equipped with regenerative braking. The operation of the regenerative braking system was simulated by the brake dynamometer for this vehicle's assemblies only. These are the same vehicle make, model, and model year as those that were track tested during the development of the brake temperature model.

Vehicle front/rear brake assembly. The brake dynamometer tests the brake system components of a single vehicle wheel/hub assembly at a time. Because of weight distribution and weight transfer during braking, front and rear brake assemblies are designed differently. Front brakes typically receive a larger proportion of braking energy than do rear systems, and for this reason, their design is different from rear assemblies and the components typically have a greater mass and greater surface area for heat rejection. However, because they are generally lighter and less vented, rear brakes tend to operate within approximately the same temperature as front brakes. To estimate total PM emissions from braking, this project involved testing both front and rear assemblies to better understand the relative and total emission rates from these components.

Brake pad material. Modern brake pad materials fall into the categories of low metallic (LM) or NAO. A given vehicle may be fitted with different brake pad materials at different points in its life as aftermarket options may differ from original equipment components. Not all brake assemblies have the same brake lining materials available. Thus, brake lining materials were selected based on the individual vehicle assemblies tested. At a minimum, for each test vehicle the OES friction material was chosen for one of the pad material options (which was NAO for all models). Testing of each vehicle then included

one or two aftermarket options, either one or both of a common NAO aftermarket pad and/or a common metallic aftermarket pad depending on availability.

The test plan included matching the rotor selection (or drums in the case of the Civic) to the selected pad type where possible. OES pads were tested with OES rotors. For aftermarket pads, LINK used business intelligence and existing brake supplier relationships to determine the most likely/representative aftermarket rotor to be matched with each pad material during a real-world aftermarket purchase. This allowed for the friction couple between the pad and rotor to be more likely to be representative of real-world operation.

The selection of brake friction materials also included consideration of the copper content in each material formulation. California legislation in SB 346 specifies a phase-out of copper (as well as selected other metals[7]) in commercial brake pad formulations due to environmental harm associated with these compounds being carried into waterways by roadway runoff. Other states have also adopted the legislation and it is likely that, to simplify supply chains, eventually most or all brake manufacturers will produce only friction materials that meet SB 346 requirements nationwide. Under SB 346, copper must be reduced to 5% or less of total material content by weight by 2021, and to 0.5% or less by 2025. Friction material manufactured prior to the January 1, 2021 with <5.0% copper by weight may be sold until January 1, 2031. The Brake Manufacturer's Council has developed the LeafMark letter labeling design to indicate to consumers which of the above thresholds that a given pad meets. The LeafMark letter labels and their respective thresholds are defined as follows:

- A – formulation contains more than 5% copper by weight
- B – formulation contains between 0.5% and 5% copper by weight
- N – formulation contains less than 0.5% copper by weight.

In this work, LINK had limited control over which formulations were associated with the different brake assemblies that were tested. OES materials were tested in whichever formulation was used by the OES component. For aftermarket, in which a project goal is to test high-selling, representative components, one of two options existed:

- Only one LeafMark is associated with the best or second-best selling component. In this case, that LeafMark was selected.
- The LeafMark is not yet specified for a given aftermarket component. This situation exists for those components for which current inventory exists under multiple LeafMarks. In this case, the desired component was ordered and whichever LeafMark was delivered was tested (as there is no way to order these components based on the LeafMark).

Based on LINK business intelligence, there were no instances in which the top two selling components each had a different, specified LeafMark. So, there was no

[7] SB 346 also limits the presence of cadmium, chromium salts, lead, mercury and asbestiform fibers in brake friction materials sold in California during or after 2014. (https://leginfo.legislature.ca.gov/faces/billNavClient.xhtml?bill_id=200920100SB346)

assembly for which ERG and LINK had to select one LeafMark over another. The two vehicles for which metallic pads will be tested are most likely to carry the A label. The test matrix contains the LeafMark that was planned for testing if it was known for a given friction material.

Simulated vehicle weight/load. To decelerate at a given rate, more braking energy is required by a more heavily laden vehicle. To better understand the effect of this, additional tests of some vehicles will be performed at a higher weight than the normal test weight for each vehicle. The normal test weight simulated for each vehicle will be calculated as given for passenger cars in 40 CFR 86.129-00. The nominal equivalent test weight (ETW) for each vehicle will be the curb weight plus 300 lbs.

ERG selected the three vehicles with the largest cargo-carrying capacity for additional testing representing higher-laden weight operation. For these vehicles a heavily-laden weight (HLW) was defined as an additional two thirds of the capacity added between the curb weight and the gross vehicle weight (GVW). HLW was calculated as:

$$HLW = Curb\ Weight + \frac{2}{3} \cdot (GVW - Curb\ Weight)$$

Test cycle. For the majority of tests, ERG used the cycle that was developed and selected for use in this program. This cycle was developed based on actual in-use vehicle survey data from California. The new CBDC test cycle has a duration of approximately 4.3 hours and represents a total of about 81.55 miles of driving. It contains 347 braking events. The cycle consists of three different segments representing slow, medium, and high average speed driving. The three segments are proportioned in distance similarly to the actual in-use California distances driven in those average speed ranges based on the Caltrans survey data.

For comparison with outside brake PM research, a small number of tests with a subset of the test vehicles was conducted using the World Harmonized Brake Dynamometer Cycle (WLTP-Brake). The WLTP-Brake cycle has a duration of approximately 4.4 hours (plus cooling intervals) and represents approximately 119.3 miles of driving. It is divided into 10 trips containing a total of 303 braking events.

Test replicates and references. Conducting replicates helps determine the repeatability of the testing procedure. The selection of the quantity of replicates was optimized in terms of the number of replicates given that the total number of tests was limited. The number of replicates was decided prior to testing and was not adjusted during testing. Given that testing had not yet been conducted at the time of test matrix development, ERG had limited data from which to estimate the number of replicate tests required to determine statistical significance. Based on the total number of different brake materials and vehicles in the study, ERG decided to do two replicate tests for almost all test matrix combinations. Replicate tests were conducted using new components of the same specification (or part number) for each test. So, test repeatability could be influenced by both the test setup and the differences from using separate sets of friction materials manufactured to the same specification.

Additionally, one vehicle/assembly/material combination was selected to serve as a reference test. The single reference combination was repeated in the test matrix at regular intervals throughout the project. The reference test can help to better understand and track any measurement drift in the laboratory setup over time. ERG selected the F-150 front brake with OES pads (which are NAO) to serve as the reference. This was selected due to this vehicle being the most popular of the six test vehicles for brake component benchmarking based on LINK market research and business intelligence.

Additional considerations. In addition to the parameters that define the dimensions of the matrix, there were some additional considerations and line items in the matrix that were added to enhance the test plan. These include the types of filter blank measurements to be conducted, a planned testing pause, and additional notes regarding expected EPA and CARB chemical analyses to be conducted after the post-test weighing processes.

LINK conducted two types of filter blanks during the program, zero blanks and tunnel/background blanks. Zero blanks are intended to identify the level of contamination that may occur during the handling of the filter between weighings but outside of the actual test cycle. Zero blanks are not specifically listed in the matrix but were performed approximately once every two weeks during the testing program. Zero blanks were performed as follows:

1. Pre-weigh filter
2. Transport filter from weigh room to the test site and install normally
3. Pause and do not turn on sample pump or expose filter to any sample flow
4. Remove filter, transport back to weigh room and allow to stabilize
5. Post-weigh filter

Tunnel/background blanks required a more rigorous procedure and attempt to quantify not only the handling effects but also any contamination that exists within the complete sampling tunnel. Tunnel/background blanks are listed in the test matrix and were conducted as follows:

1. Pre-weigh filter
2. Transport filter from weigh room to the test site and install normally. Operate and/or log data with all measurement equipment.
3. Install the F-150 rotor, fixture, and caliper, but do not install brake pads. Run the tunnel dilution air pump as well as the relevant sample pump and cooling airflow for the test duration, however do not open the hydraulic brake line valve. Allow the installed rotor to rotate and follow the speed trace (as closely as possible given that no braking will take place). Run the cooling airflow at the flow rate used for the front assembly of the F-150 during tunnel blank measurements. The brake pads will not be present to eliminate any PM that could be generated from them lightly rubbing on the brake rotor.
4. Remove filter, transport back to weigh room and allow to stabilize
5. Post-weigh filter

As described in the original proposal, ERG and LINK planned a testing pause early in the program. This allowed time for an initial data review to determine if any problems exist with sampling plan or execution of testing. The pause allowed for specifically delineated time for any necessary changes to be made prior to conducting the bulk of the testing plan. The test matrix included the expected point for the testing pause.

In addition to the work conducted by LINK and ERG for this project, both CARB and EPA offered to contribute work in performing chemical speciation of some samples. For planning purposes, the labs that planned to perform different filter analyses are also presented in the matrix. Primarily this included the two different workflows to take place for the Teflon filters. One subset of them originated at CARB, were shipped to LINK for weighing and testing, and then were shipped back to CARB for XRF and/or ICP-MS analysis. A different subset originated at EPA's National Vehicle, Fuel, and Emissions Laboratory (NVFEL) and were used in a filter-weighing "round-robin" in which the pre-test and post-test weighings took place both at LINK and at EPA NVFEL in series. The test matrix includes the tests that were assigned for each of those two workflows.

The different parameters to be tested for each vehicle are presented in the following table. The total number of planned tests was 85.

Table 13. Brake Dynamometer Test Matrix Parameter Summary

Test Vehicle	Front/ Rear	Pad Material	Wheel load	# Replicates	Reference repeats	Test Cycle	Total Tests
Camry	Front Rear	OES After-Met. After-NAO	ETW	2 each	NA	CBDC, WLTP-Brake	14
Civic	Front Rear	OES After-NAO	ETW	2 each	NA	CBDC	8
F-150	Front Rear	OES After-Met. After-NAO	ETW HLW	2 each	5 of a single condition	CBDC WLTP-Brake	25
Sienna	Front Rear	OES After-NAO	ETW HLW	2 each	NA	CBDC	16
Prius	Front Rear	OES After-NAO	ETW	2 each	NA	CBDC	8
Rogue	Front Rear	OES After-NAO	ETW HLW	2 each	NA	CBDC	12
Tunnel Blanks				2 total			

The list of parameter options presented previously must then be ordered based on the relative quantities to be tested for each parameter. It was preferable to test as many different assemblies as possible prior to the pause, but it was also preferable to test at least one replicate prior to the pause to get an initial indication of the level of variability between two tests.

Where possible, the order was then randomized and mixed to reduce the likelihood of external factors biasing the measurements. So, most of the different assemblies were tested prior to the pause, but after the pause the testing order was assigned in groups in random order. Tests were conducted in blocks for each vehicle's front or rear brake assembly to reduce the turnaround time between testing where possible. The first replicates for each pad material were grouped together, but the order of these groups was then selected at random. For example, the "A" replicates of a given vehicle's front or rear assemblies for the OES, aftermarket NAO, and the aftermarket metallic friction materials make up a group to all be tested consecutively. These groups were then ordered, generally at random, to minimize the effects of any time-based biases that could be encountered during the test program. One exception to the complete randomization was that a few changes in order were made in order to reduce the turnaround time from switching between different assemblies. The LINK dynamometer system uses combinations of large and small inertia discs to simulate vehicle inertia. Where possible, assemblies using the same number of large inertia discs were grouped together to reduce the longer amount of time required to change these large discs. However, "A" and "B" replicates for a given vehicle were still kept separate in the matrix, and the vehicle order was not "sorted" by inertia (i.e. vehicles may be grouped together with a common number of required large discs, but the vehicles weren't ordered by ascending or descending number of discs).

The reference tests (of the F-150) were interspersed regularly throughout the testing program. One tunnel blank was conducted at the start of the program, and the other was conducted around two thirds of the way through the program. The complete test matrix, along with the dates of each test, is presented in Appendix F.

Procurement of Test Components

LINK began procuring brake parts once the test matrix was finalized. LINK procured OES components from local dealerships. Aftermarket components were prioritized based on sales levels and availability for non-asbestos organic (NAO) and low-metallic (LM) friction materials. The aftermarket components included several products acquired from Bosch, Wagner, Autozone, and RockAuto.

LINK Test Laboratory Setup

The LINK test laboratory that was used for this project is built around a constant volume (i.e. air velocity) sampling system that operates in a closed-airflow circuit. The cooling and airflow rates are fixed for a given test. The airflow through the test enclosure provides the sampling medium for emitted PM as well as the cooling flow for the brake assembly. The sampling airflow is filtered using HEPA filters after passing through the climate control unit and before entering the brake system enclosure. Figure 18 contains a schematic of the LINK laboratory layout that was used for this test program.

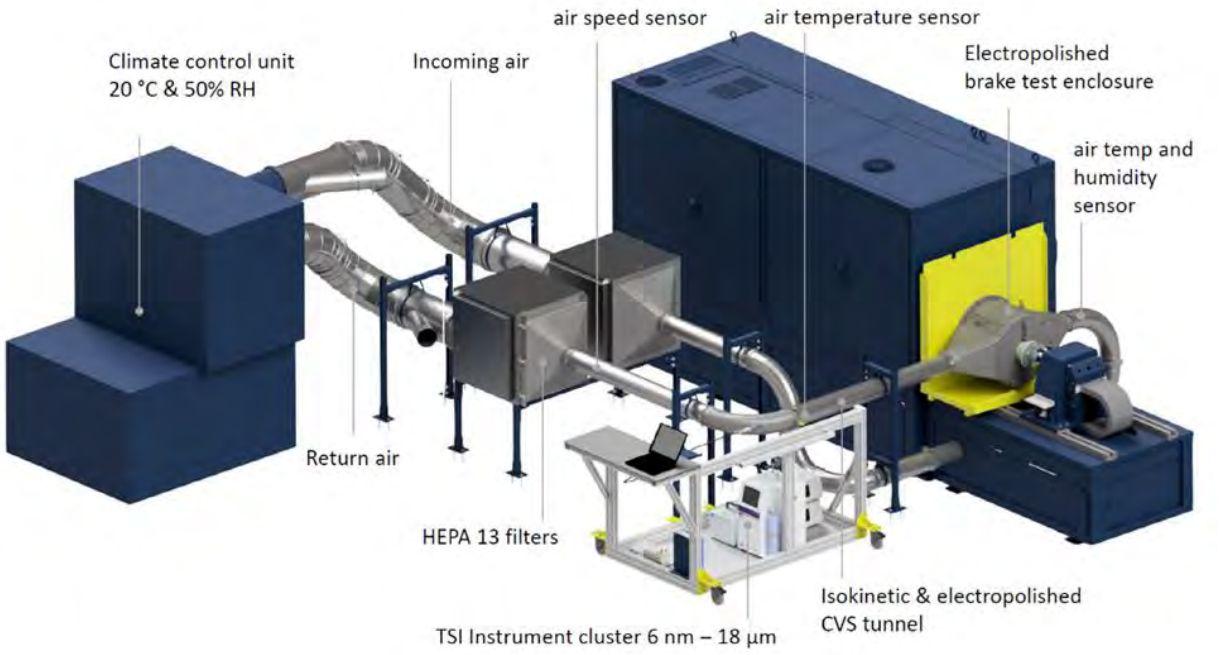

Figure 18. Schematic of LINK Laboratory Setup

The cooling air was controlled to stable temperature (within ± 5°C of the setpoint by vehicle) and held to a relative humidity of 50 ± 10%; this helps ensure a stable set of conditions when the particles enter the sampling train (between the aspiration position and the point of sampling). The LINK system allows for adjusting the airflow rate prior to each test to reflect the cooling rates established during the project for each brake assembly.

The airflow circulating layout involves the use of round ducting in stainless steel, with internal electropolished finish, with minimal constrictions and at least 8 diameters without disturbances between the brake assembly enclosure and the point of sampling. The sample duct is oriented horizontally, and samples are taken at the point of entry of flow into the 90° elbow downstream of the brake enclosure. Sampling is performed using four separate sampling lines, each originating from an isokinetic sample nozzle arranged in parallel at the upstream end of the sampling elbow. The sampling lines and instrumentation are described later in this document.

From the brake assembly enclosure to the sampling instrumentation, the layout is designed to minimize aerodynamic losses with minimal bends and constrictions. These design characteristics are intended to minimize turbophoretic losses, gravitational deposition, diffusion, and aspiration at the nozzle. Sampling is performed isokinetically (0.95 to 1.15 isokinetic according to ISO 9096) to avoid skewing the particle size distribution data. A transport time of less than 5 seconds from brake assembly to instrument is specified (with a target transport time of 2 seconds) to minimize potential changes in size distribution due to coagulation. In addition, the short transport time will allow the particle size distribution to be closer to the actual distribution as-generated by

the friction surface. A photograph of a brake rotor installed in the test enclosure is presented in Figure 19.

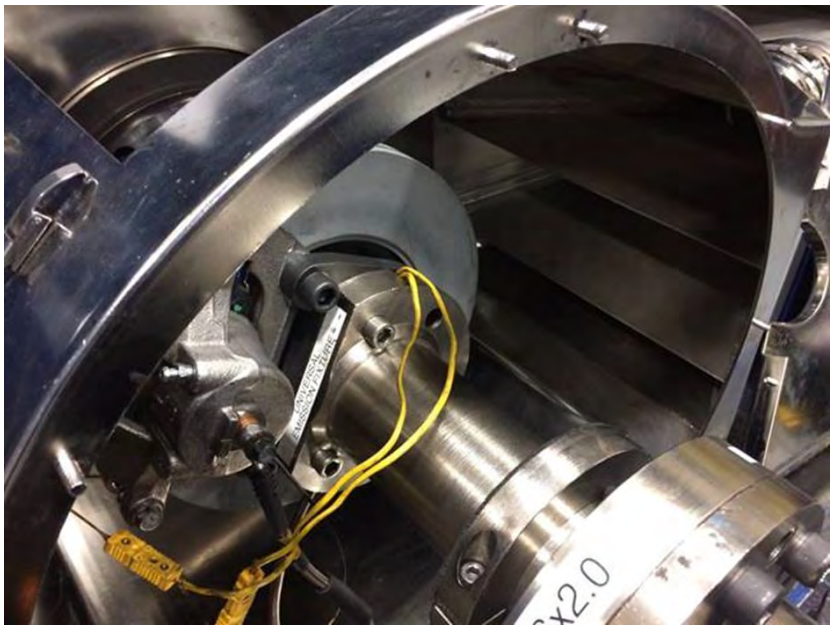

Figure 19. A brake rotor installed in the LINK test enclosure.

CVS Loop Cooling Airflow Setting

The air flow rate through the sampling chamber was set at different rates for the front and rear assemblies of each different test vehicle. The air flow rate was set in an attempt to best match the cooling that takes place in real-world operation, given that the flow rate must stay constant during a test to allow for constant volume PM sampling. During track testing, LINK logged temperature data for the front and rear assemblies of each of the six test vehicles when operating over the WLTP-Brake cycle driven on a test track. This data was used to determine the dyno cooling air flowrate for testing over the new CBDC.

Because all test vehicles were operated over the WLTP-Brake cycle on the test track with temperatures logged, this data was used as a source for flowrate setting. ERG and LINK selected a subset of the 10 WLTP-Brake trips that was most representative of the characteristics of the CBDC, and these were used to set the flowrate to best match the track temperature over the same subset when operating on the dynamometer. To select the WLTP trip or combination of trips to use for setting flow rate, ERG analyzed each WLTP trip in terms of distributions of the same parameters used during test cycle selection: deceleration rates, speed, brake event duration, temperature, and braking energy. From this, ERG determined that WLTP trips 1, 2, 5, and 10 were most similar in the above five parameters to the CBDC test cycle. As an example of the type of distribution that ERG reviewed, Figure 20 presents a cumulative distribution of modeled brake temperature for the Camry over the braking events of the CBDC and the 10 different trips of the WLTP-Brake.

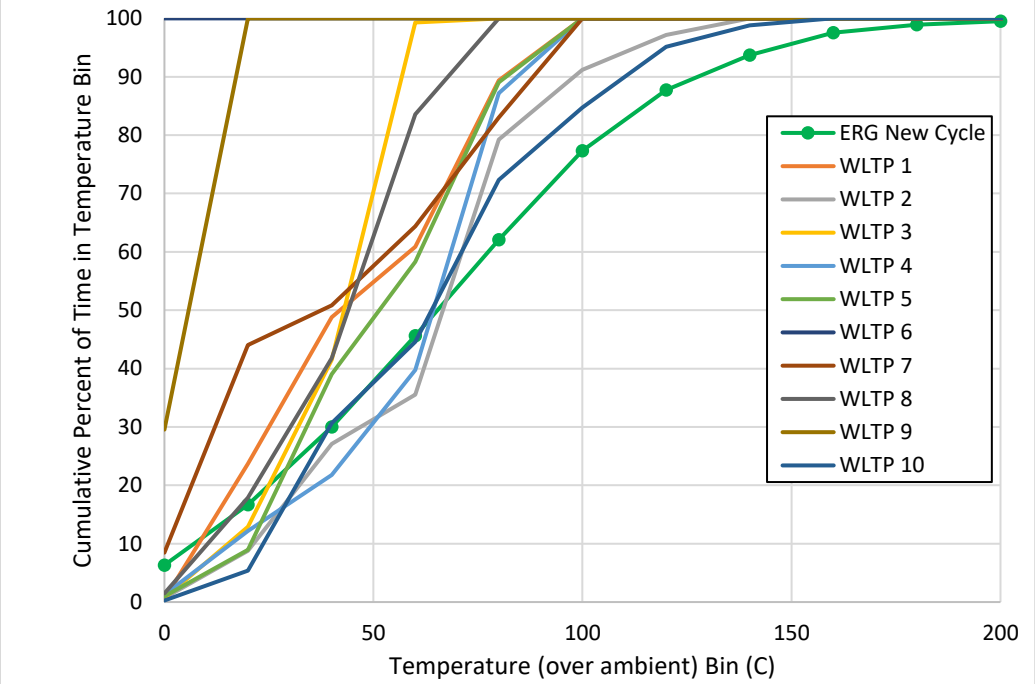

Figure 20. Cumulative distribution of brake temperature over ERG's New CBDC (Modeled) and the 10 trips of the WLTP-Brake (on track)

ERG then investigated the same distributions for various combinations of the four best-matching trips (1, 2, 5, and 10). This was done by comparing the sum of squares differences between the different trip combinations and the CBDC for the five parameters of interest. ERG determined that trip 10 was the best fit, and the addition of any other trip did not necessarily improve the representativeness. For this reason, LINK used only WLTP-Brake trip 10 for air flow rate setting for each different assembly.

LINK ran Trip 10 on the dynamometer for each brake assembly at three equally spaced flow rate settings. LINK then fit a curve to the average braking temperature at each flow rate and calculated the flow rate that best matched the track test temperatures for each brake assembly. Table 14 presents the flow rate used for all tests of each given assembly over the CBDC test cycle. These values represent the air flow speeds through the sampling duct that LINK found would allow the assembly temperatures to best match the temperatures measured on the test track. The cooling airstream speed was measured 8 diameters downstream of the sampling elbow, complying with the requirement defined in EPA Method 1A (the ducting has the same diameter over this entire length). Temperature plots comparing the measured dynamometer temperatures to the test track temperatures are presented for the front and rear assemblies of each vehicle in Appendix G.

Table 14. The CVS cooling/sample flow settings for each vehicle/axle combination

	Front Axle Flow Speed (kph)	Rear Axle Flow Speed (kph)
Camry	7.5	7.5
Civic	7.5	7.5
Sienna	7.5	7.5
F-150	51	7.5
Prius	28	28
Rogue	7.5	7.5

The different sample flow settings do affect the PM residence time between the brake enclosure and points of mass measurement (either the TSI 100S4 or 47mm filter). Overall nominal residence time varies from approximately 0.7s to 1.2s depending on the CVS flow rate.

Dynamometer Operation

The LINK brake dynamometer simulates the rotation and braking functions for a single brake assembly. The unit can simulate front or rear brakes depending on the brake-fixture assembly and the inertia. The system uses both an electric servo motor and the line pressure of the hydraulic brakes to follow a set speed trace over time. The dynamometer controller balances these two sets of torques based on the programmed vehicle road load and inertia. The inertia is the simulated wheel load at the tested brake corner, and the road load describes the force curve representing the drag on the vehicle across a range of speeds when traveling along a level road. During this work, the EPA-published coefficients from the annual certification reports for each model and model year were used to simulate road load for each test vehicle during brake dynamometer testing.

One significant difference in the operation of the brake dynamometer and a chassis dynamometer is the need to split the braking force between the front and rear brakes. Because vehicle weight is transferred forward during braking, the front brakes are designed to absorb and convert a larger amount of energy than rear brakes. The Society of Automotive Engineers (SAE) standard J2789, *Inertia Calculation for Single-Ended Inertia-Dynamometer Testing*, specifies how this energy split can be simulated.[8] Table 15 depicts the standard percentage torque splits for various vehicle categories for two levels of deceleration and two levels of vehicle loading, gross vehicle weight (i.e. fully laden) and lightly loaded vehicle weight (LLVW). Where possible, LINK followed J2789 for the proportioning of brake torque between front and rear assemblies in this work. All braking in the braking test cycles evaluated in this work consist of braking events falling within Low deceleration (< 0.65 g-force) as referenced in the table. One exception to the use of J2789 was made for vehicle types in which, during cooling flow

[8] https://www.sae.org/standards/content/j2789_201008/

setting, a temperature mismatch was observed between front and rear assemblies for a given vehicle compared to track test data. For example, if using J2789 resulted in the front assembly for a given vehicle running hotter than the track data and the rear assembly running cooler than track data, LINK adjusted the inertia split until the brake temperatures matched the track trends (this was the case for the F-150).

Table 15. Brake Torque Split Percentages Based on SAE Standard J2789

Percent of brake force done by each axle (X and Y values)								
Vehicle type	Fixed Proportioning							
	Low deceleration < 0.65 g				High deceleration > 0.65 g			
	GVWR		LLVW		GVWR		LLVW	
	Front X	Rear Y	Front X	Rear Y	Front X	Rear Y	Front X	Rear Y
Passenger car - FWD	78	28	78	28	80	25	80	25
Passenger car - RWD	78	28	78	28	75	30	75	30
Minivan and crossover	78	28	78	28	75	30	75	30
Pick-up trucks	68	38	63	45	80	25	80	25
SUV-RWD	73	33	73	33	75	30	75	30

Appendix C includes the road load coefficients for each model as well as the by-axle inertia settings programmed into the dynamometer for each vehicle, axle, and test weight combination.

Simulation of Regenerative Braking

The Toyota Prius test vehicle is equipped with regenerative braking, in which some amount of braking energy is converted to charge the vehicle's powertrain batteries instead of converting all energy to waste heat as is the case for the other test vehicles equipped with only the hydraulic brakes. LINK conducted the brake emissions testing for the Toyota Prius using their 'DutyCycleRegen' control program. This control program is a combination of two operating principles: Duty cycle simulation to simulate a given drive cycle (using the standard ProLINK 'DutyCycle' Program), and the addition of regenerative braking functions.

LINK first analyzed the operational accuracy of the 'DutyCycle' (non-regen) program on a ProLINK-controlled inertia dynamometer using the SAE J2951 procedure, *Drive Quality Evaluation for Chassis Dynamometer Testing*[9]. Table 16 presents the results of this analysis for the three segments of the CBDC for two vehicle assemblies.
The table presents the percent of time the parameter exceeded the control limits as well as the root mean squared speed error (RMSSE) for each segment of the test cycle and each assembly. RMSSE is the actual error as a percent of the maximum allowable error. At the initiation of this program, the PMP inter-laboratory round robin had begun the process of defining thresholds of acceptability for these two error metrics. At that time, PMP members indicated that approximately 10% violation time is acceptable for

[9] https://www.sae.org/standards/content/j2951_201111/

maximum violation time. The threshold for RMSSE was not yet completely defined, but was expected to be at or below 200%.

The overall error levels for both metrics were acceptable based on the threshold of the PMP inter-laboratory round robin (which assigned a threshold of 100% on RMSSE).

Table 16. Results of SAE J2951 Analysis of the Sienna Front Assembly Operating over the CBDC Test Cycle

		F150 Front			Sienna Front		
CBDC Segment	Duration (s)	Violation Time (s)	% Violation	RMSSE	Violation Time (s)	% Violation	RMSSE
1	8,767	308	4%	77%	578	7%	92%
2	4,011	109	3%	67%	207	5%	85%
3	2,784	77	3%	70%	290	10%	118%
Overall	15,562	494	3%	74%	1,075	7%	96%

Using the successful ‘Dutycycle’ program as a starting point, LINK created the ‘DutyCycleRegen’ program by adding the following primary features:

- A dedicated section for burnish, the actual test cycle, and any intermediary cooldown phases
- Import of vehicle speed profiles into the control program using ‘.csv’ file format
- User input window to enter the number of repeats of the test cycle (e.g. number of repeats of the ERG-CARB mini-trips for burnish or the WLTP-brake cycle)
- User input window to enter the vehicle coastdown coefficients to account for vehicle running resistance
- User-interface to enter the regenerative brake system specifications

The regenerative braking activity of the selected Toyota Prius vehicle was simulated using mainly four regenerative brake parameters of the electric motors:

- **Regensim_power**: This is the maximum power that the vehicle electric motors can convert to electrical energy
- **Regensim_Trq_Limit**: This is the maximum torque that the regenerative system can compensate for without any pressure applied tothe friction brakes.
- **Regensim_On_Above**: This is the minimum speed above which the regenerative system can operate at full capacity
- **Regensim_Off_Below**: This is the maximum speed below which the regenerative system cannot provide any braking support and all braking energy is handled by friction brakes.

The following scenario is an example of the function of the regenerative braking control feature. Consider a vehicle with regenerative system parameters shown in the screen capture presented in Figure 21. In addition to the four parameters specific for a vehicle, the program includes a generic parameter Regen_Brk_Trq_Min for additional control on brake actuation times. If set to 0, the friction brake torque may take some time to build as the brake is filled. This causes a delay and / or torque overshoot when the brake finally clamps down onto the rotor.

RegenSim | Safeties | Script | Service Brake | Servo Tuning

Vari	Desc (5 items)	Unit	Value
10080	Regensim_Power	kWatt	5
10081	Regensim_Trq_Limit	lb·ft	368.7816
10082	Regensim_On_Above	mph	6.21402
10083	Regensim_Off_Below	mph	1.2428
10084	Regensim_Brk_Trq_Min	lb·ft	0

Figure 21. ProLINK screen capture of regenerative braking parameters

If a brake application from 50 km/h to 0 km/h requires 200 N·m (368.78 lb·ft) of retarding torque, the graph in Figure 22 shows how the torque would be split between the regen system and the friction brakes at different stages of braking.

- **Stage A**: Power is speed· torque and thus for the first 5 seconds, the regenerative brake torque gradually ramps up as the speed comes down with a regenerative peak power of 5 kW.
- **Stage B**: Regenerative system provides all braking needed from 25 km/h (=5000 W/200 N·m) to 10 km/h (6.2 mph).
- **Stage C:** Once the vehicle speed is below the Regensim_On_Above value of 10 km/h (6.2 mph), the friction brake kicks in and ramps up. At the same time, the regenerative torque ramps down at the same rate. This is called “brake blending”.
- Below the Regensim_Off_Below speed, friction brakes absorb all torque.

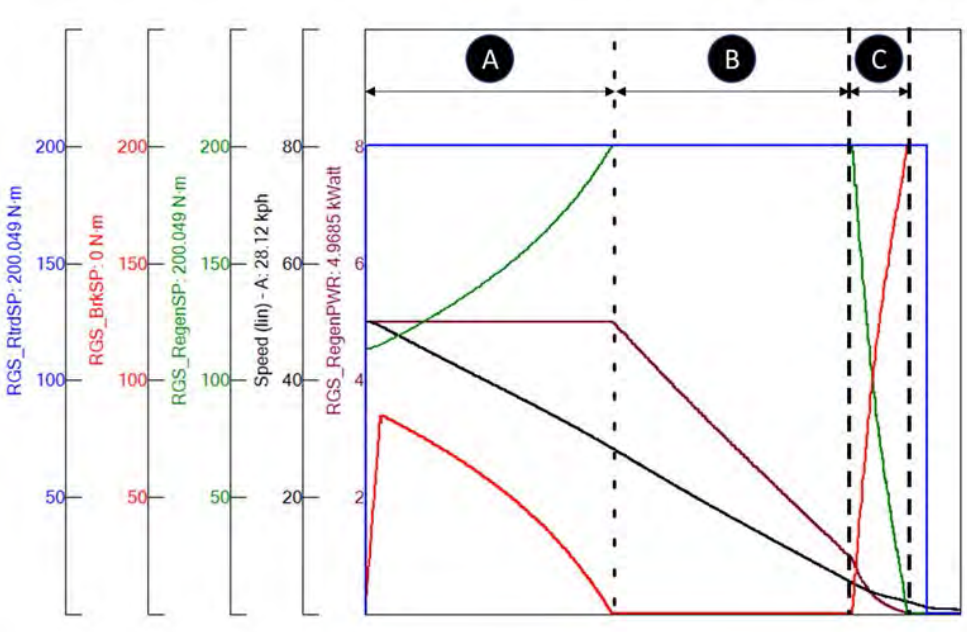

Figure 22. Plot of retarding torque (blue), friction brake torque (red), regenerative torque (green), wheel speed (black), and regenerative power (purple) during a regenerative-equipped braking event.

The original specifications for the Prius regenerative brake system were not available due to non-disclosure policies of the manufacturer so LINK developed preliminary estimates of the regenerative system parameters for the 2016 Toyota Prius Two-Eco vehicle based on previous experience of conducting dynamometer tests for a customer's Prius brake evaluation.

Figure 23 presents vehicle-to-dynamometer comparison plots of brake pressure and total retardation torque for two brake events. These brake events were run on the test track for a range of 0.1g-0.4g deceleration levels. Retardation torque is the combined torque of resistance provided by the friction brake as well as the regenerative motor. Torque was not measured during the track testing as torque wheels were not installed at the time. Instead, the vehicle torque 'Veh Trq' shown here correspond to the values calculated using the deceleration, tire rolling radius, and the wheel load front-to-rear split percent (according to SAE J2789).

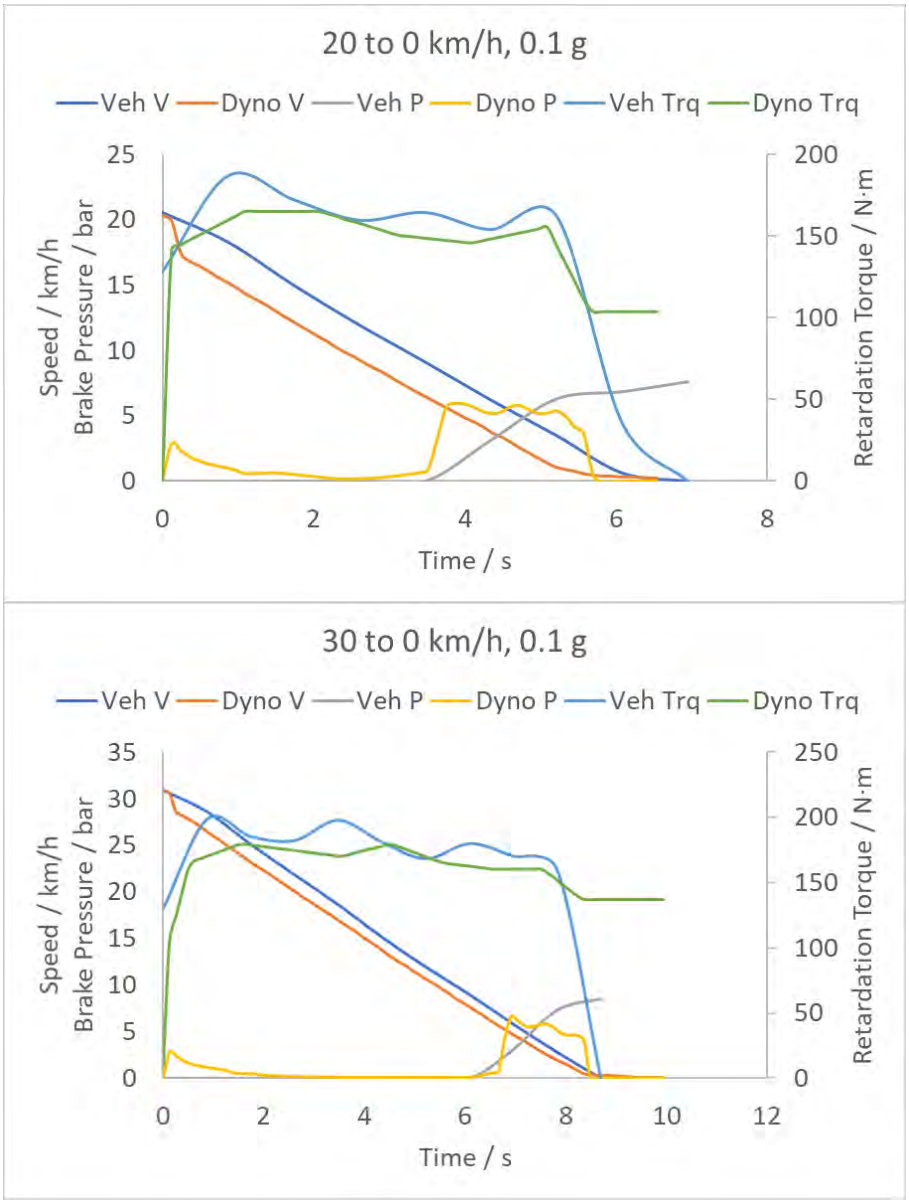

Figure 23. Dynamometer-to-track comparison of velocity, brake pressure, and wheel torque for example regenerative braking events

Torque measured on the dynamometer for a 0.1g deceleration level was within 10% of track-tested calculation. Actuation times of the friction brakes during the dynamometer test match well with the vehicle brake pressure. The Dyno brake pressure (P) was slightly lower than the Vehicle P. A brake event with the duty cycle program starts in a pressure-based control mode (more common in regular brake testing) and then switches to torque mode. This is the reason behind a small spike in brake pressure at the start of brake application on the dynamometer. This spike currently offsets the dyno speed profile with respect to the vehicle speed profile.

LINK refined their regeneration simulation parameters for the dynamometer simulation in the weeks leading up to testing based on continued review of the track test data. This

included creating a separate value for one parameter for tests of the front and rear axle assemblies of the Prius. Even though the Prius' regenerative system only acts on the front wheels of the vehicle, the system does affect the demand on the foundation brakes of both the front and rear axles. LINK used the parameters and values in Table 17 for the simulation of the Prius regeneration capacities and speed ranges during all tests of that model's components.

Table 17. Updated parameters used for the simulation of the Prius regenerative braking system on the dynamometer

Parameter	Front Axle Simulation	Rear Axle Simulation
Maximum Power	2.5 kW	2.5 kW
Maximum Torque	90 Nm	60 Nm
Speed above which 100% regeneration is available	8 kph	8 kph
Speed below which no regeneration is available	3 kph	3 kph

Measurement Instruments

LINK equipped its test laboratory with a variety of TSI instruments for the measurement of PM mass, count, and size distribution. This section describes the capabilities of the various instruments that were used during this program.

TSI 100S4. The TSI 100S4 is the central instrumentation for this project. It has 4 different particle size classifications for the measurement of PM mass. The 100-S4 has an 18 µm inlet stage (i.e. sampling is 18 µm and smaller), which is followed by cut-point stages of 10, 2.5, and 1 µm. The instrument has Micro-Orifice Uniform Deposition Impactors (MOUDI) for the collection of mass at each of these cutpoints. The impactors are followed by a final filter to collect particles smaller than 1 µm. In the 100S4, LINK used coated aluminum impactors, with a glass fiber final filter.

Figure 24. TSI 100S4 MOUDI

TSI QCM MOUDI 140. The Model 140 Quartz Crystal Microbalance (QCM) MOUDI is designed to perform continuous, real-time size-segregated mass concentration measurements of particles smaller than 2.5 µm. The system uses six cutpoint stages at 960, 510, 305, 156, 74 and 45 nm and operates at a 10 L/min inlet flow rate.

Figure 25. TSI QCM MOUDI

TSI CPC. The 3790A Condensation Particle Counter (CPC) is a full-flow design PM particle counter that has a particle size lower detection limit of 23 nm. The unit is designed to linearly respond to particle concentrations from 1 to 10,000 particles/cm^3 and can operate continuously taking 10Hz measurements. TSI indicates a counting accuracy of ± 10%. The PMP has specified the use of this unit as the baseline for brake particle counting without the use of a catalytic stripper or other volatile particle removal (VPR) device. No VPR device was used in this program.

Figure 26. TSI CPC

TSI APS. The 3321 Aerodynamic Particle Sizer (APS) measures the aerodynamic size of particles between 0.5 – 20 µm. The system operates using time-of-flight aerodynamic sizing to determine the particle's behavior while airborne and is unaffected by index of refraction or Mie scattering. The unit also measures light-scattering intensity in the equivalent optical size range of 0.37 to 20 µm. The system offers continuous sampling at 1 Hz.

Figure 27. TSI APS

TSI EEPS. The 3090 Engine Exhaust Particle Sizer (EEPS) is a spectrometer that measures the size distribution of particle emissions from 5.6 to 560 nm continuously at up to 10 Hz. The EEPS provides outputs of size distribution in the above range as well as particle number concentrations down to 200 particles/cm^3.

Figure 28. TSI EEPS

Additional sampling was performed on behalf of EPA through their participation in this project. EPA directed ERG and LINK to perform gravimetric sampling of brake PM during all tests planned in the test matrix in a manner consistent with 40 CFR 1065. Under this direction, LINK conducted parallel sampling of PM captured on 47 mm filters during the tests that were already planned for this work.

The other specific addition to the test plan funded by EPA was the collection of PM sample on Transmission Electron Microscope (TEM) grids using a Partector device during a large number of tests. NVFEL staff loaned this Partector system to LINK for the duration of the brake dynamometer testing. During use, this device only sampled for a part of each test cycle (automatically stopping when loaded completely) at a relatively low flow rate compared to the other instruments. These TEM grids were provided to EPA for analysis at the end of the program.

The sampling lines and instruments are arranged as shown in Figure 29. Flow splitters were used to separate the samples in Lines 2-4 into multiple instruments or components. Lines 1-3 provided sample to the TSI equipment described for use for CARB. Sample Line 4 provided sample to the filter equipment installed on behalf of

EPA. The four probes were arranged in an equally spaced fashion in a single plane of the sampling elbow.

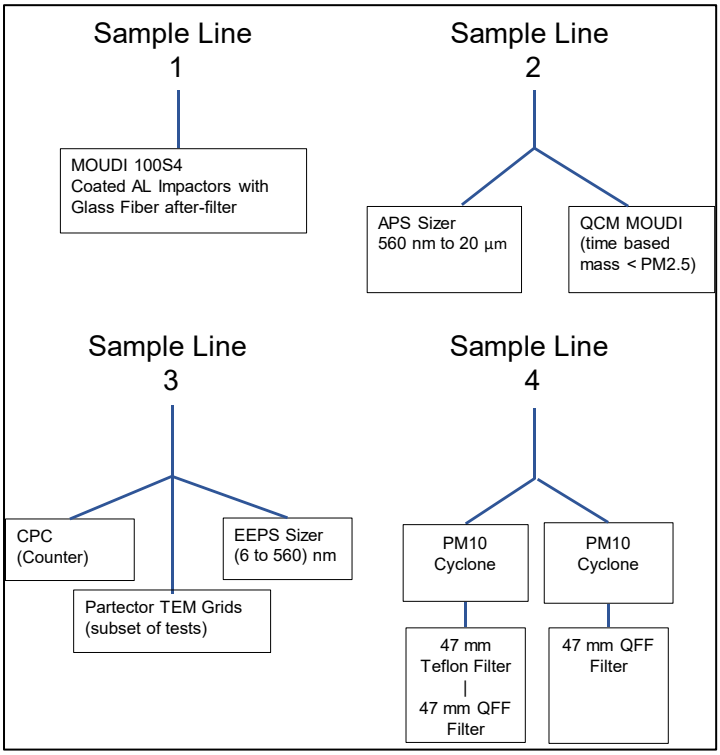

Figure 29. Sample line schematic for this program

Sample line 4 included the measurements added on behalf of EPA. This sample ran through a splitter into two PM10 cyclones. One leg of the splitter fed a 47 mm Teflon filter followed by a 47 mm Quartz fiber filter (QFF). The other leg of the splitter fed only a single 47 mm QFF. To equalize the pressures and flowrates, LINK installed a 47 mm Teflon filter after the lone QFF; however, this filter was not used for any analyses. A schematic of the layout of Sample Line 4 is presented in Figure 30.

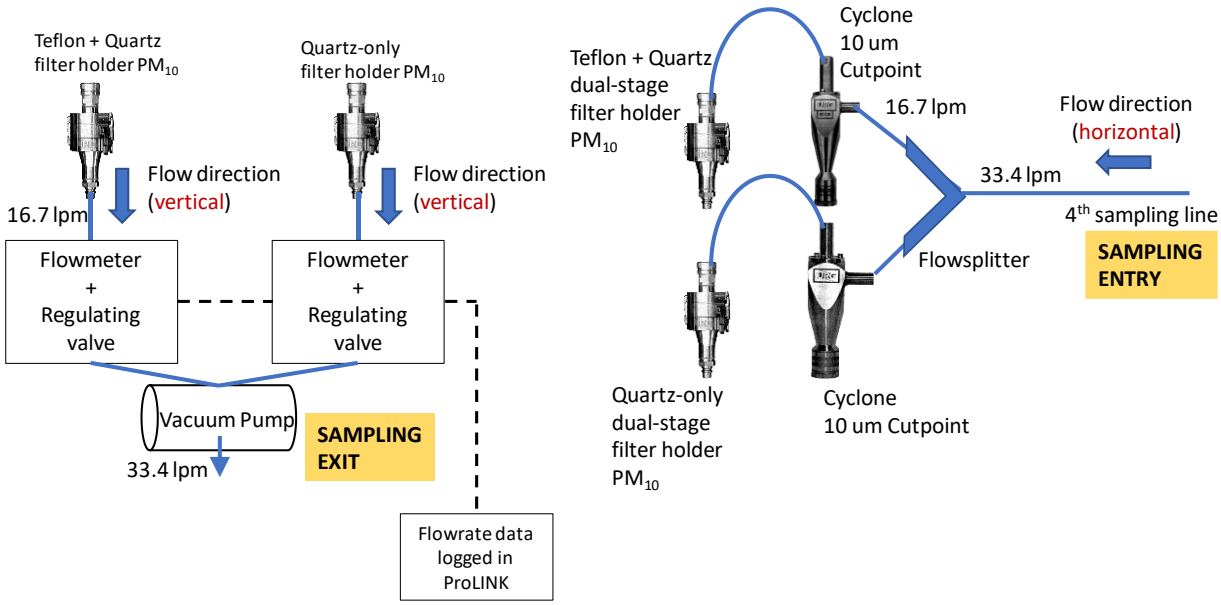

Figure 30. Detail schematic of Sample Line 4

The purpose of each of the three specified filters, along with potential analyses options that could be performed on the TSI equipment media or 47mm filters, is described in Table 18.

Table 18. The various filter media types and the respective analyses for each

Filter Material	Analysis Options
Teflon	• Gravimetric Mass • XRF elemental • ICP-MS
Quartz Fiber (QFF) – Following Teflon	• Volatile Organics that pass through Teflon (artifact collection)
Quartz Fiber (QFF) – Lone	• Particle Phase Organic Molecular Weight Distribution (on initial filters to inform further test types)
Coated AL Impactor	• Gravimetric mass
Glass Fiber	• Gravimetric Mass • Possibly ICP, TBD • No further chemical analysis recommended

In preparation for testing, LINK acquired the Teflon filters for use in gravimetric testing from two sources. Approximately half of the filters were provided by CARB, and half were sourced from EPA NVFEL in Ann Arbor, MI. EPA also provided all quartz fiber filters (QFFs) for use in capturing sample for later speciation analysis. Details of each filter type are presented in Table 19.

Table 19. The particulate filter types used during testing

Brand/Model	Diameter	Pore Size	Source	Material
Whatman 7592-104	47mm	2µm	CARB	Teflon
MTL PT47DMCAN	47mm	2µm	EPA	Teflon
PALL 2500QAO-UP	47mm	-	EPA	Quartz Fiber

For the TSI 100S4, LINK sourced impactor part number 0100-47-AF, and used silicone spray from MSP, Part #07041. LINK sourced two dual-stage stainless steel filter holders from URG, model URG 2000-30FVT, to collect PM samples on PTFE and QFF 47mm filters. A picture of this filter holder type is shown in Figure 31.
.

Figure 31. Dual-stage stainless steel filter holder for PM10 sampling

Arizona Dust Experiment

Prior to the commencement of testing, LINK evaluated the PM sampling system using Arizona dust as the particulate medium. Evaluations included the particle transport efficiency and system responses to different airflows, brake speed, brake rotation direction, and particle sampling setup. Arizona dust (per ISO 12103-1:2016) was used for these evaluations. The dust was injected at the brake enclosure, travelled through the sampling system, and collected on the 100S4 gravimetric filter. These experiments were conducted prior to the installation of the 47mm filter system, so only the 100S4 was used. Multiple experiments were conducted to determine the recovery efficiency, the repeatability, and the level of detection of the system.

Dust was emitted using a TSI 3410U dust aerosol generator. The generator's feed rate (i.e. dosing speed) was set to 5% and injector pressure was 1.2 bar. Different airflows

were evaluated to represent the possibility of covering various axles and vehicle combinations. A brake rotational speed of 45 km/h was chosen to match closely to average speed of WLTP cycle (and later for the CBDC), and a brake speed of 115 km/h was selected as the upper range value as it is equivalent to a typical highway speed. Brake rotation direction is designated viewing from the perspective opposite the dynamometer drive shaft, and both clockwise (CW, airflow opposed to particle exit direction from caliper) and counterclockwise (CCW, airflow parallel to particle exit from caliper)) rotation directions were evaluated. The dust injection duration was 3 minutes for each experiment. Table 20 presents the values that were tested during the Arizona dust evaluation.

Table 20. LINK Arizona Dust Test Parameters

Airflow (m^3/h)	500, 900
Brake speed (km/h)	45, 115
Brake rotation	CW, CCW
Sampling elbow	3-nozzle, 4-nozzle

Figure 32 shows the test setup for the dust injection experiments. Brake pads were not installed inside the caliper to avoid possible emission of particles from brake drag (rotor and pad surface interaction).

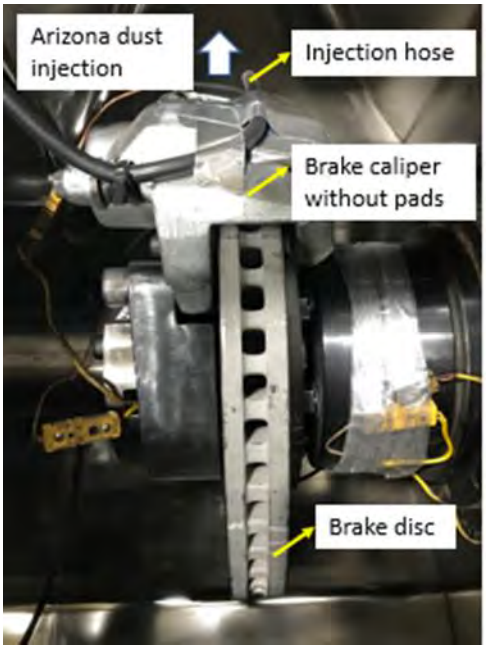

Figure 32. Brake assembly for PM system evaluation with Arizona dust

LINK utilized the 100S4 and APS to evaluate the test results. Figure 33 presents the mass collection results of two replicate tests (Test #67 and #68) for 500 m^3/h airflow, 45 kph brake speed, and CCW brake rotation. The PM system exhibits a collection efficiency (i.e. mass recovered / mass injected) of about 90% with Arizona dust.

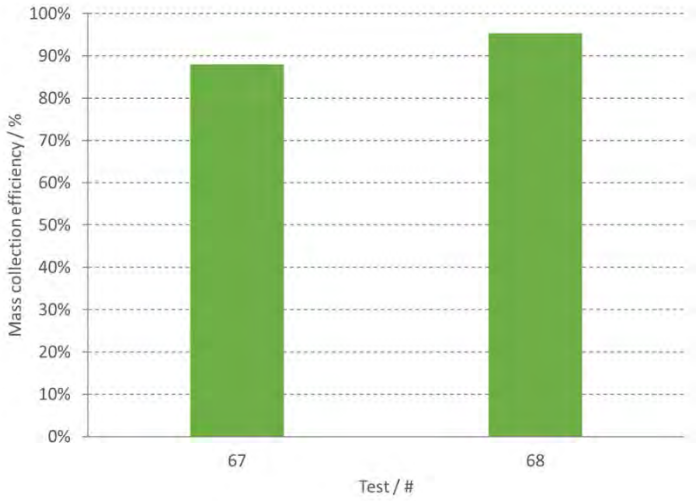

Figure 33. Mass collection efficiency results of two tests of the Arizona dust experiment as measured by the 100S4

In addition, LINK supervised a computational fluid dynamics (CFD) simulation of particle-laden airflow inside the brake enclosure and the sampling system. Arizona dust was used for the CFD study as well. Details of this study can be found in the technical paper SAE 2019-01-2139, *Design of Experiments for Effects and Interactions during Brake Emissions Testing Using High-Fidelity Computational Fluid Dynamics* [10]. Figure 34 presents the flow velocity contour inside the brake enclosure with brake assembly mounted, the stabilization duct, and into the sampling nozzles located at an 8 diameter distance from the enclosure exit.

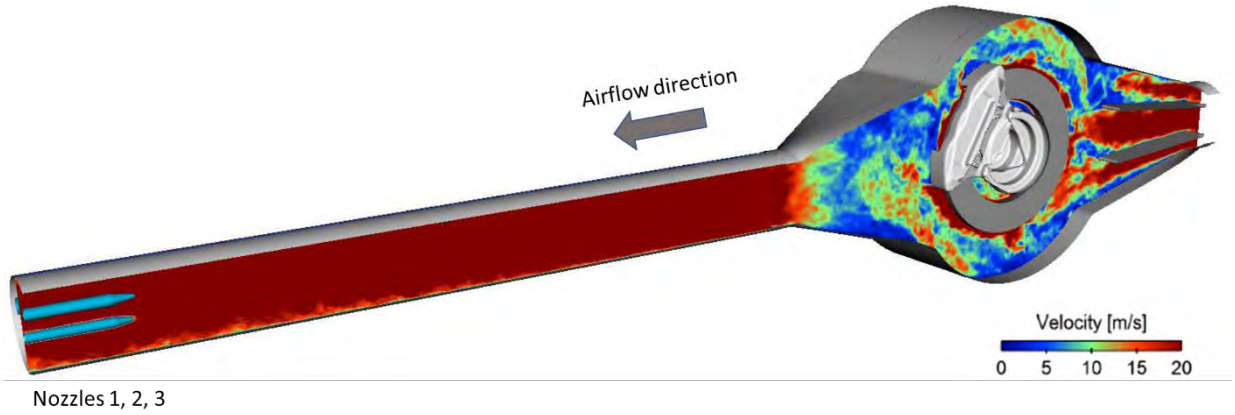

Figure 34. Velocity contour of cooling air resulting from CFD simulation

Figure 35 compares the particle count history of the Arizona dust test replicates, measured using APS, with the values calculated from the CFD simulations for various particle sizes. Probed locations for particle count in the CFD study are at the enclosure exit (inception), nozzle inlet, and inside the nozzles. Predicted particle counts (based on

[10] Agudelo et. al., "Design of Experiments for Effects and Interactions during Brake Emissions Testing Using High-Fidelity Computational Fluid Dynamics," SAE Technical Paper 2019-01-2139, 2019, https://doi.org/10.4271/2019-01-2139.

the Arizona dust size distribution) match well with the measured profiles. Also, particle count profile is seen to be very similar in nozzles 1, 2, and 3. This latter result indicates that the PN measurements are independent of sampling nozzle location radially along the duct cross section.

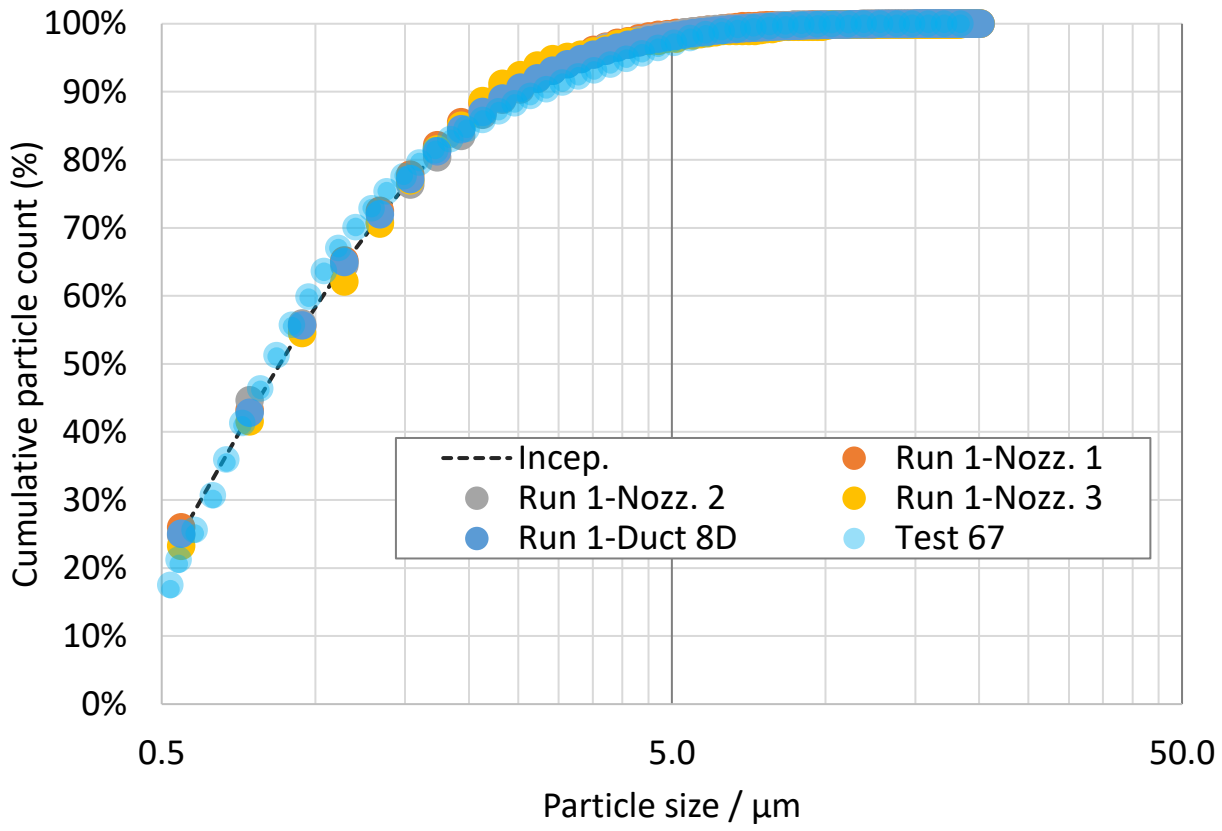

Figure 35. Simulated and measured cumulative particle count at different locations of PM sampling system

Figure 36 presents a graphical representation of a main effects analysis for measured PM mass emission rate after correcting for duct airflow (duct-to-sampling flow correction) in the Arizona dust experiment. Brake rotation direction showed significant variation in PM mass rate based on the steepness of its slope, with higher values (i.e. less mass loss) measured during tests with counterclockwise (CCW) direction of rotation. Sampling setup, airflow, and brake speed did not have noticeable effect on the measured PM mass rate. LINK conducted all brake emissions tests using the CCW direction for brake rotation as default because that direction resulted in higher measured PM mass (i.e. a higher collection efficiency) during the Arizona dust evaluation.

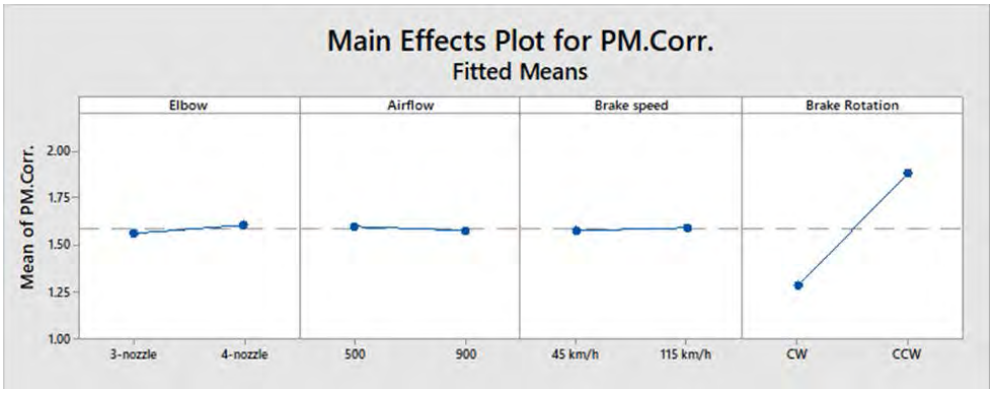

Figure 36. Graphical plot of the PM response to the parameters of the number of sampling nozzles, airflow rate, brake rotational speed, and brake rotational direction during the Arizona dust evaluation

Teflon Filter Weighing Interlaboratory Evaluation

At the completion of LINK's setup of the laboratory, EPA NVFEL staff participated in a filter "Round Robin" comparison with LINK. EPA NVFEL provided approximately half of the Teflon filters used during this work (CARB provided all others). After EPA provided all of the test filters, LINK staff selected 30 at random and weighted each of them three different times in their on-site weighing room. Then, the filters were returned to NVFEL, and allowed to stabilize. Then, EPA staff weighed the same 30 filters three times. This allowed for direct comparison to weights measured at NVFEL and at LINK. During transport between laboratories, the filters were kept cool and subject to minimal handling.

Results are presented as LINK measurements plotted against NVFEL measurements for each filter in Figure 37. Note that the plot includes all three measurements made by each lab on each filter (though they are superimposed over one another). The equation for a linear fit to the data is presented on the plot; the R^2 value of this fit is greater than 0.99999. The values in the plot are buoyancy corrected per 40 CFR 1065.690 by both laboratories. EPA data did include a further drift correction, however that data was not used in this discussion as, for the purposes of this evaluation, drift correction was not necessary.

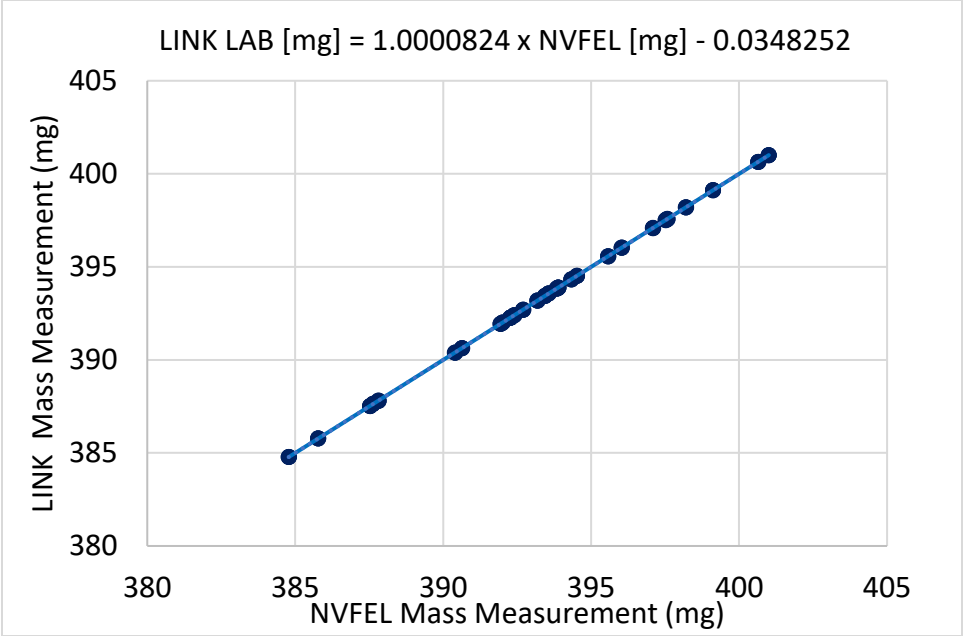

Figure 37. LINK Laboratory vs. NVFEL measurements for the 30 filters used in the interlaboratory evaluation.

The intercept of the linear fit was approximately 0.008 percent of the measured values, and the slopes agreed to within 0.008 percent. This represents an excellent level of agreement, and EPA, LINK, and ERG determined that any further interlaboratory investigations were not necessary.

Test Procedures and Quality Assurance Processes

Test Day Steps. One project goal was to be able to complete each test and turnaround in less than 24 hours. The following is a summary of the steps that were taken during each test day along with the estimated time required for those requiring a significant duration:

- Take the dimensions, weights, and pictures of the brake components before the test (15 min)
- After the removal of the previously-tested components, project staff clean the mounting hub as well as any debris that was deposited on the base or walls of the sampling enclosures. (15 min)
- The next test components are installed. On some days, the same caliper and adapter was used from the previous day. During all other days, the complete adapter and caliper was removed and replaced with the components used for the next test. After installation, the hydraulic system is bled of air. (30 min – 1.5 hrs)
- Install the correct isokinetic nozzles for the cooling airflow rate corresponding to the tested brake components

- Record pre-test background air data and then start the CBDC (California Light-Duty vehicle) burnish cycle to bed the friction materials together (approximately 11.5 hrs)
- Monitor the dynamometer and emission data recordings. PM mass was not measured during burnish. To protect from excessive amounts of brake dust noticed in some cases, CPC was turned off during burnish for one of the two replicates of the test matrix
- Record post-burnish background air data. Review burnish data after the cycle is complete.
- Clean the inlet cyclones of EEPS and CPC (whenever used during burnish)
- Take the QFF from freezer to the weighing room for 1 hr stabilization
- Weigh the pre-conditioned coated aluminum, glass fiber, and PTFE filters. PM Weighing is done only if the room temperature is within (22±1) ^{o}C and the dew point is within (9.5±1) ^{o}C.
- Turn on the QCM unit and install the sampling filters/media in the 100S4 stacks and 47mm particulate mass sampler (PMS) filter holders
- Connect 100S4 and PMS to the dynamometer system
- Run the CBDC brake emissions cycle (4.5 hrs)
- Upon test completion, perform data quality assurance test to check for any defects as defined in the Quality Assurance Project Plan (QAPP for EPA Work Assignment 1-04)
- Remove filters and media and return to weighing room for stabilization
- Remove brake assembly after the data passed the quality test (15 mins)
- Take the dimensions, weights, and pictures of the brake components after the test (15 mins)
- Weigh the post-tested coated aluminums, glass fiber, and PTFE filters.
- Store the QFFs and PTFEs at -20 ^{o}C in the freezer

The above schedule required approximately 18-19 hours if no issues were encountered. This allowed a reasonable margin of time to address any problems and with LINK staff working in shifts, the project was generally able to stay on a 1 test per day schedule.

Quality Assurance (QA) of Test Data

Both LINK and ERG staff performed a QA review of the results of each test. LINK completed their internal review first, then data was provided to ERG for further external review.

LINK developed a methodology to check the quality of data for various variables at the completion of each test. These variables include shaft speed (km/h), rotor temperature, cooling air settings, digital emission instruments, and the PM_{10} mass sampler. LINK staff:

- used the GTR15 drive quality regulation to assess the accuracy of the control program in simulating the CBDC test cycle on the dynamometer;

- checked the rotor temperature to ensure there were no loose-wires or defective thermocouples;
- checked that the cooling airflow settings i.e. temperature, relative humidity and air speed, were within the PMP (Particulate Measurement Programme) recommended limits;
- applied certain thresholds for specific channels of APS, CPC, and EEPS, to validate that the data recorded was well above background levels;
- evaluated the PMS flowmeter stability using certain criteria specified based on preliminary runs.

Figure 38 illustrates an example of the software tracking of LINK's quality assurance review for a selected test. It indicates the tolerance range for each parameter and provides a color-coded output indicating the status of the actual value.

Speed Conformity	**Condition**	**%Violation**		**RMSSE**		**PASS/FAIL**
Speed Profile	% Violation ≤ 10% and RMSSE ≤ 100%	0%		25%		Pass
Temperature Metrics	**Condition**	**Min Temp**		**Max Temp**		**PASS/FAIL**
Rotor Temperature	Must be > 15 °C and < 400°C	31 °C		273 °C		Pass
Cooling Air Check	**Condition**	**Trip Avg.**		**%Violation**		**PASS/FAIL**
Cooling Air Temperature	Trip Average within (20 ± 2) ℃ % Violation ≤ 15%	21.0		14%		Pass
Cooling Air Speed	% Violation ≤ 15%	7.5		0%		Pass
Cooling Air Humidity	Trip Average within (50 ± 5) %RH % Violation ≤ 15%	50.1		0%		Pass
Instrumentation Conditions	**Condition**	**Engineer Check**				**PASS/FAIL**
CPC	Blob 3 --- Col 3 from 40,000 to 50,000 sec average must be > 50	P				Pass
APS	Blob 2 from 40,000 to 50,000 sec averages --- Col 3 > 20 / Col 25 > 1	P				Pass
QCM	Blob 4 --- Col 7, 9, 11, 13, 15, 17 from 35,000 sec positive trend	P				Pass
PMS	**Condition**	**Min**	**Max**	**Avg**	**ineer Ch**	**PASS/FAIL**
PMS Flowmeter 1 (QFF)	Must be less than 15% fluctuation (14.195 ≤ X ≤ 19.205)	16.1	17.8	16.9	P	Pass
PMS Flowmeter 2 (PTFE)	Must be less than 5% fluctuation (15.865 ≤ X ≤ 17.535)	15.5	18.09	16.2	P	Pass

Figure 38. LINK software example quality review parameters and pass/fail indication

After test data passed the LINK review, datafiles were provided to ERG staff who then took the following steps:

- Cross reference of the test setup parameters as compared to those in the test matrix
- Review of select traces of second-by second data, both during the burnish and during testing
- Review for outliers in various parameters compared to the measurements of other tests. ERG developed a running tracking spreadsheet that would automatically color code outliers in any parameter that differed from other tests by more than two standard deviations- this tool facilitated the data review. In this review, ERG considered particulate mass measured by Teflon filter and by 100S4, particle count, average and peak temperatures, average brake pressure and measured torque, test distance traveled and duration, as well as selected other parameters as applicable.
- ERG reviewed the size distributions from both the aerodynamic particle sizer (APS) and the engine exhaust particle sizer (EEPS) and tracked the peak values for all tests to help track variation in the distributions
- ERG discussed any discrepancies with LINK to determine if any further investigation, explanation, or re-tests were needed

Results

This section presents the results of the brake dynamometer testing that took place during this program. Brake assemblies were tested using a brake dynamometer and CVS system for the measurement of PM. The air flow through the system provided cooling to the tested brake assembly during the test and also served as the medium to carry particulate to the point of sampling. PM mass was measured gravimetrically in batch and continuously. Particulate size and count were also measured continuously throughout each test. Assemblies from six light-duty vehicles equipped with various OES and aftermarket friction materials were tested between September 30, 2019, and January 29, 2020. Eighty-five valid tests (including 2 tunnel blanks) were conducted during this time, including a one-week pause to review the preliminary data after the first two weeks of testing. Appendix F includes the dates that each test in the matrix was conducted.

Where possible, testing was conducted according to the order in the test matrix. In some cases, certain external factors forced LINK to re-order the testing. For example, some of the aftermarket parts that were ordered did not arrive in time to be ready when their test was scheduled to take place. In these cases, the test order was re-arranged, and these tests were inserted into the test schedule once the parts arrived.

The following sections present various test results from this work in graphical and tabular form. Appendix H contains a table of numerical results of all direct measurements for all tests. The table includes the test parameters, gravimetric mass results, condensation particle counter (CPC) results, and some selected operational measurements such as temperatures and brake line pressures. Appendix I presents the test reports generated by LINK for each individual test. For brevity, in this section some plots or analyses refer broadly to the pads and rotor as the only components; in analyses that include the Civic rear axle these terms are intended to also include that vehicle’s brake shoes and drum, respectively.

Operational Parameter Results

This section presents a brief overview of relevant parameters measured over each test day. Test-level averages of three main parameters will be presented, average brake rotor temperature, maximum rotor temperature, and the average brake fixture torque. These values are averaged for each model, axle, and test weight in each of the following figures. Figure 39 presents the average rotor temperature during each test for each model, axle, and test weight combinations. Error bars present the 95% Confidence interval of the mean of all tests of each combination. Similarly, Figure 40 presents the peak rotor temperatures in each test, averaged by model, axle, and test weight.

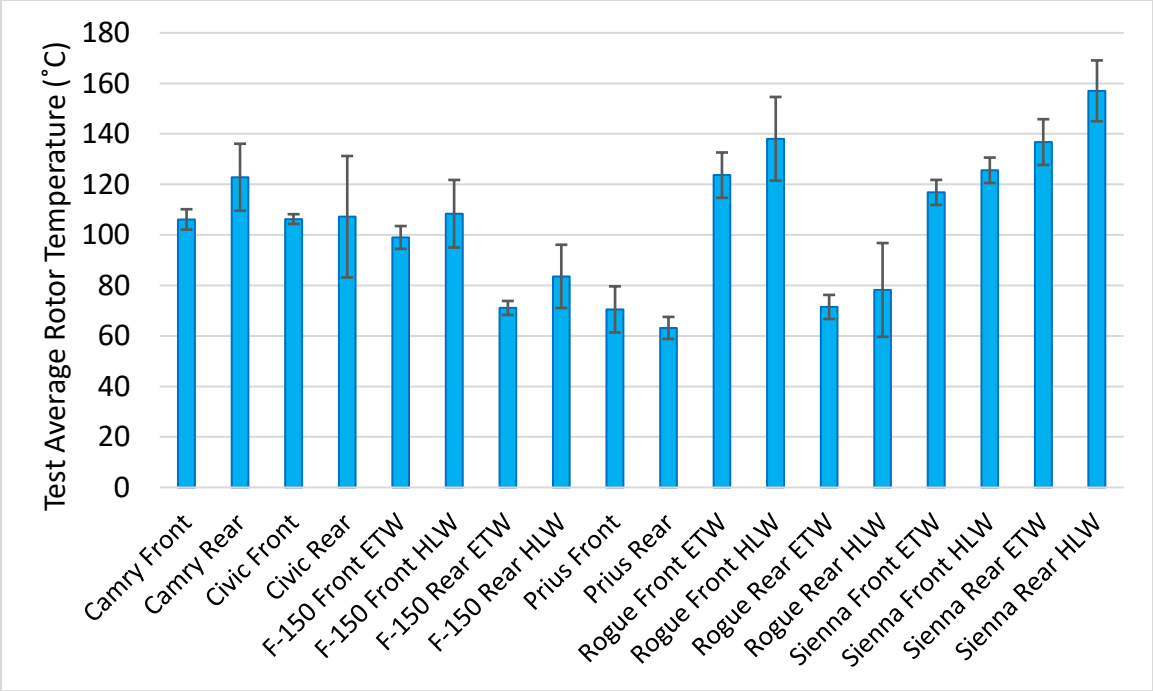

Figure 39. The average rotor temperature over the CBDC, averaged by model, axle and test weight. Error bars represent the 95% confidence interval of the mean of tests

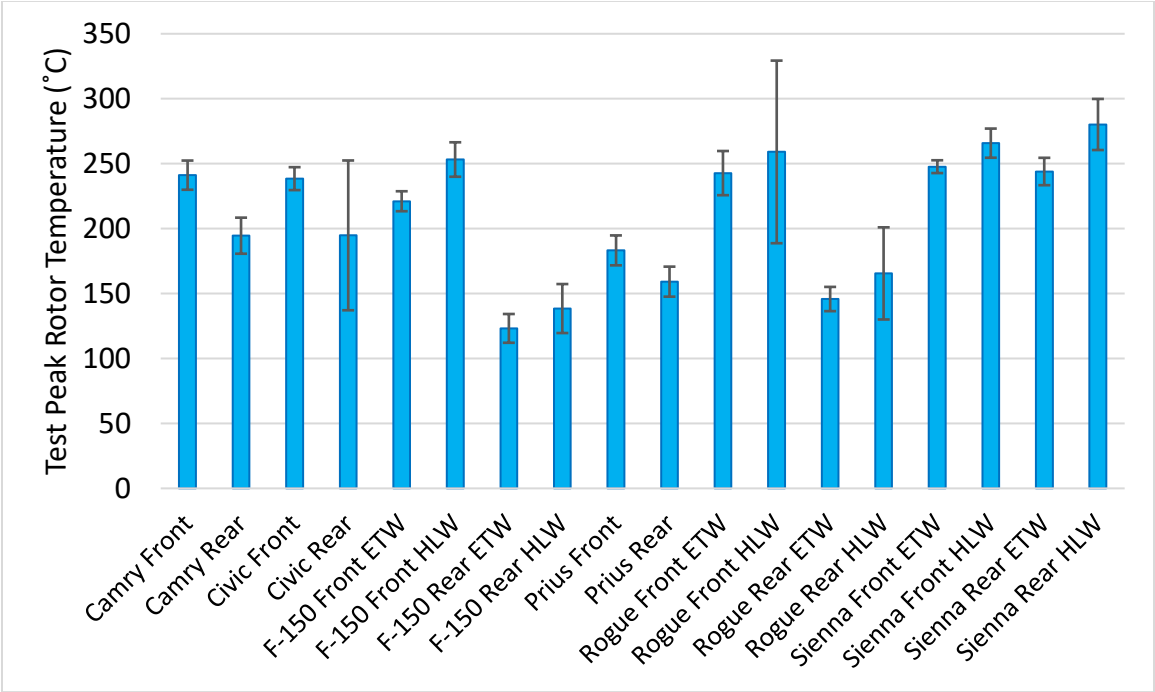

Figure 40. The peak rotor temperature during the CBDC, averaged across tests by model, axle and test weight. Error bars show the 95% confidence interval of the mean of tests

Figure 41 presents the average brake torque measured over each test, and then averaged across all combinations of model, axle, and test weight. The figures in this section are presented to provide some context to the subsequent PM analyses. For example, in terms of brake torque, the F-150 front axle tests exhibited the highest level of braking torque, and the Prius test resulted in the lowest braking torque due to the simulation of that vehicle's regeneration function.

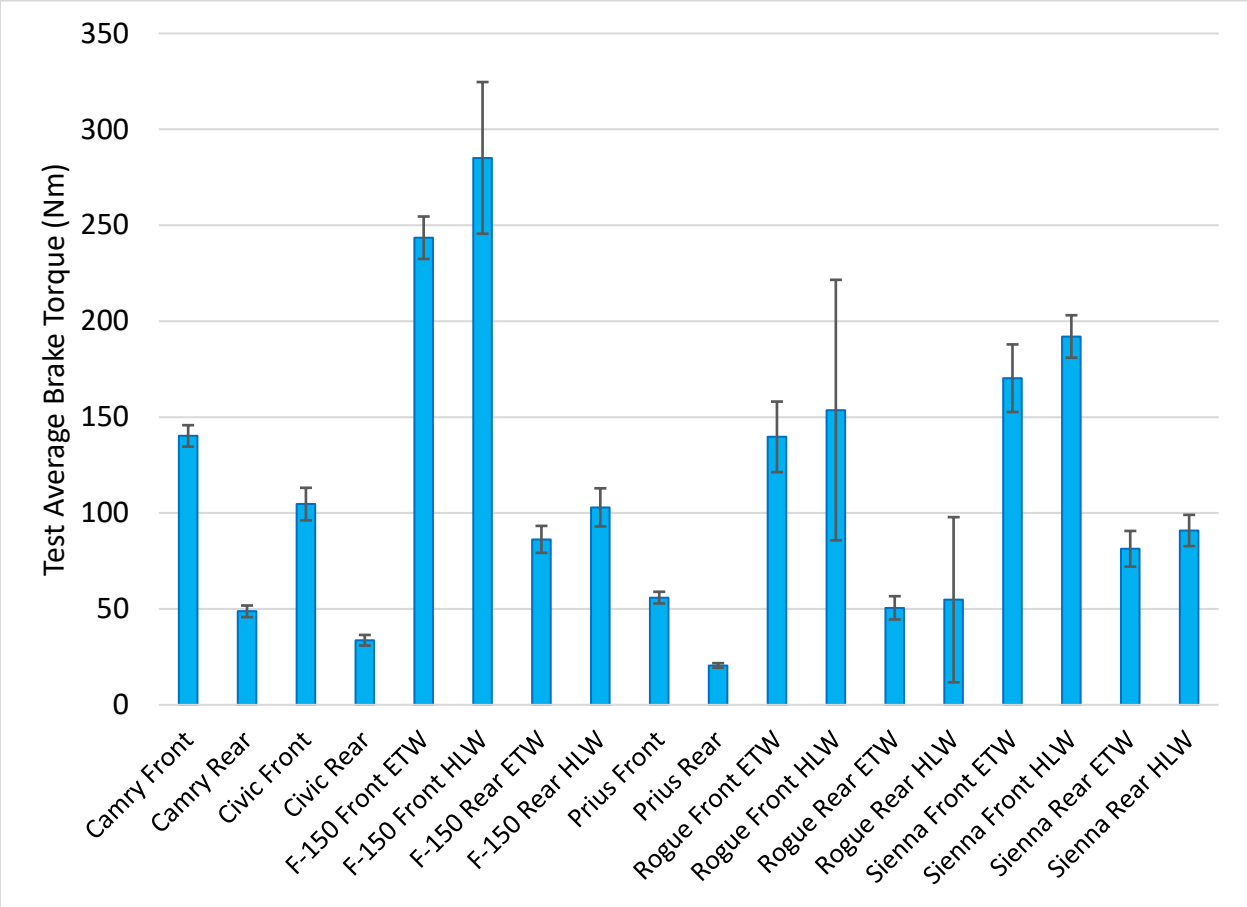

Figure 41. Average brake torque measured during the CBDC, averaged over all tests of each model, axle, and test weight combination.

Batch Gravimetric Results

The highest priority measurements during this project were the various gravimetric PM mass emissions, collected in batch for each test. This section presents those mass measurements, on a by-distance basis, for all tests. Results are shown in bar charts by test vehicle for single-wheel emission rates from front and rear axle assemblies as indicated. The 100S4 stages are shown in the blue bars (the left bar of each test pair) consisting of the three size cutpoints up to PM10. The Teflon filter system sampled PM10 mass and is shown in the green bars (the right bar of each pair). Tests are labeled with the vehicle model and the pad material. All tests can be assumed to be at

vehicle mass of ETW tests unless specifically labeled as an HLW test. Each figure depicts front axle results at left, and rear axle results at right.

Figure 42 presents the mass emission measurements for each test of the Camry. Three different pad materials were tested both front and rear. It can be seen that the low metallic pad materials resulted in the highest measured emissions. Figure 43 presents the mass emissions results for the Civic. Both the OES and aftermarket materials tested for the Civic are NAO formulations. Note that the Civic rear brake assembly is a drum; the drum brake geometry is likely the cause of the particularly low emission rate for that assembly, especially for the OES material.

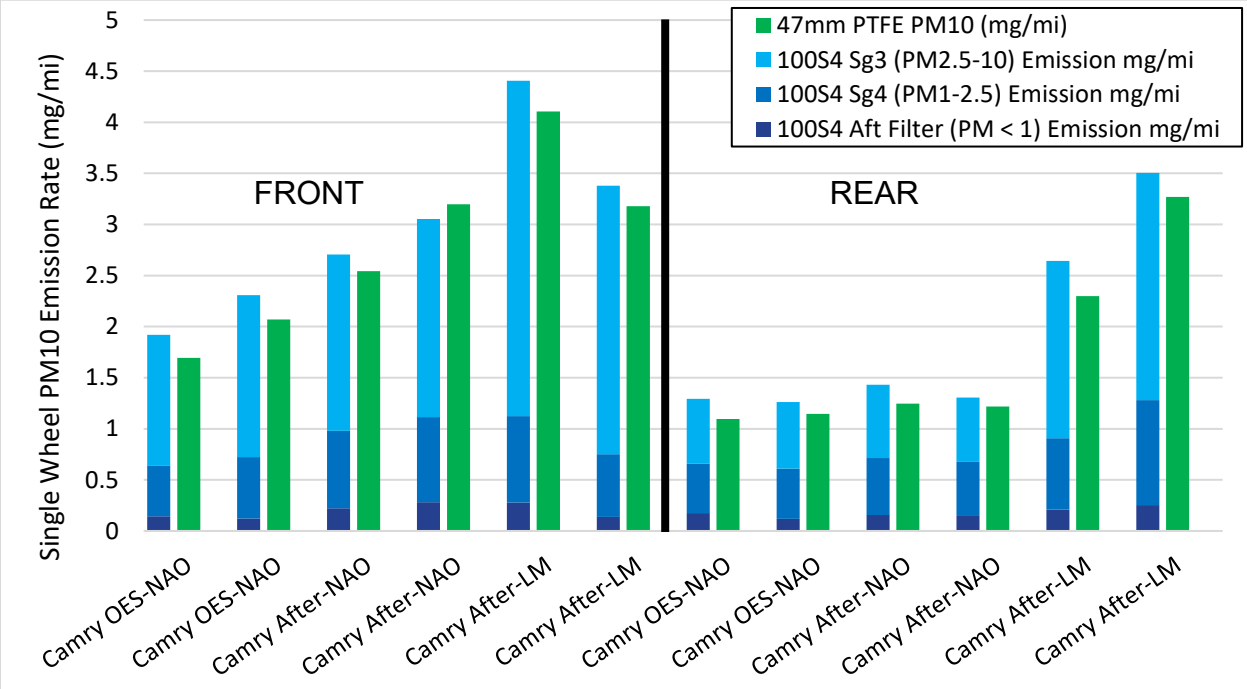

Figure 42. Single-wheel PM Mass Emission Rates for Camry as measured by 100S4 (Blue) and 47mm Teflon filter (Green)

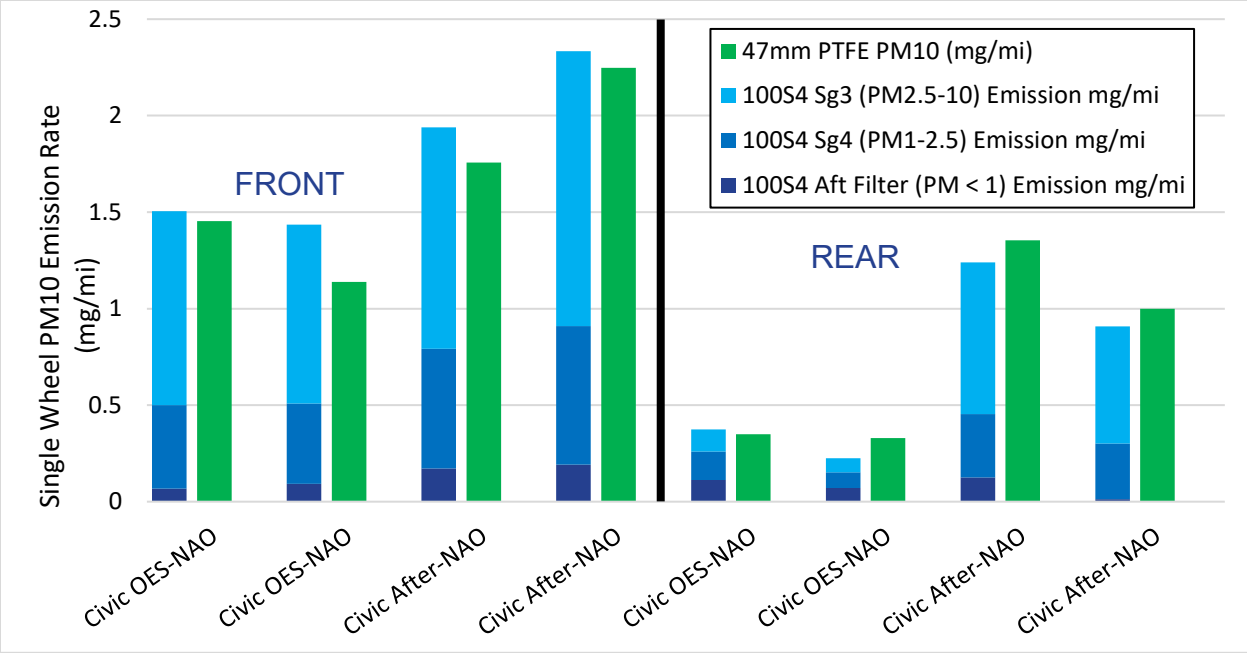

Figure 43. Single-wheel PM Mass Emission Rates for Civic as measured by 100S4 (Blue) and 47mm Teflon filter (Green). Note the Civic rear brake is a drum system

Figure 44 presents the mass emissions results for the F-150. This vehicle was represented in the greatest number of tests because it served as the reference vehicle, was tested with three different friction materials, and was tested at both test weight levels. The PM emissions of the low metallic material was measured at many factors higher than the NAO materials for the front axle assemblies. The various test matrix parameters tested for this vehicle model resulted in the widest range of resulting PM emissions of any model in this program.

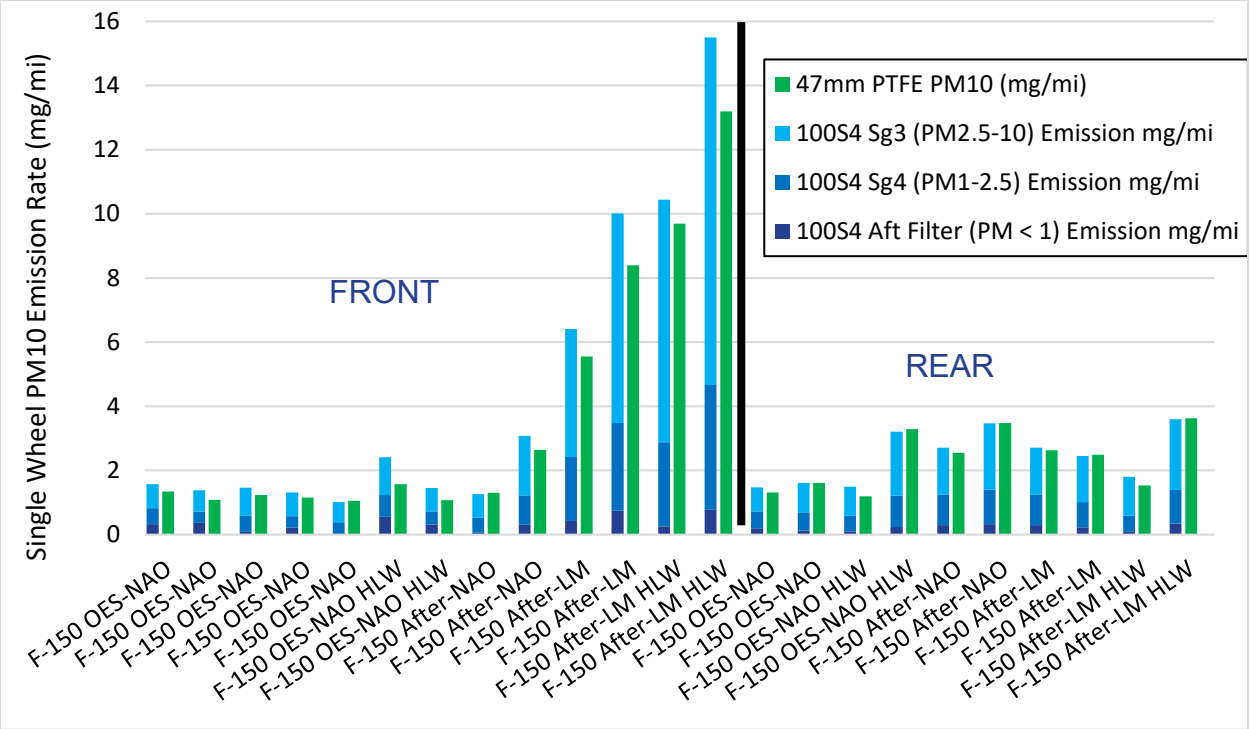

Figure 44. Single-wheel PM Mass Emission Rates for F-150 as measured by 100S4 (Blue) and 47mm Teflon filter (Green).

Figure 45 presents the mass emission rates for the Prius, which was tested with both OES and aftermarket NAO materials. While the Prius has a similar mass to the Camry, the mass emission rate tended to be approximately 50% lower for both the Prius front and rear axles. This is likely to be due to the reduction in demand on the hydraulic foundation brakes caused by the regenerative braking system function.

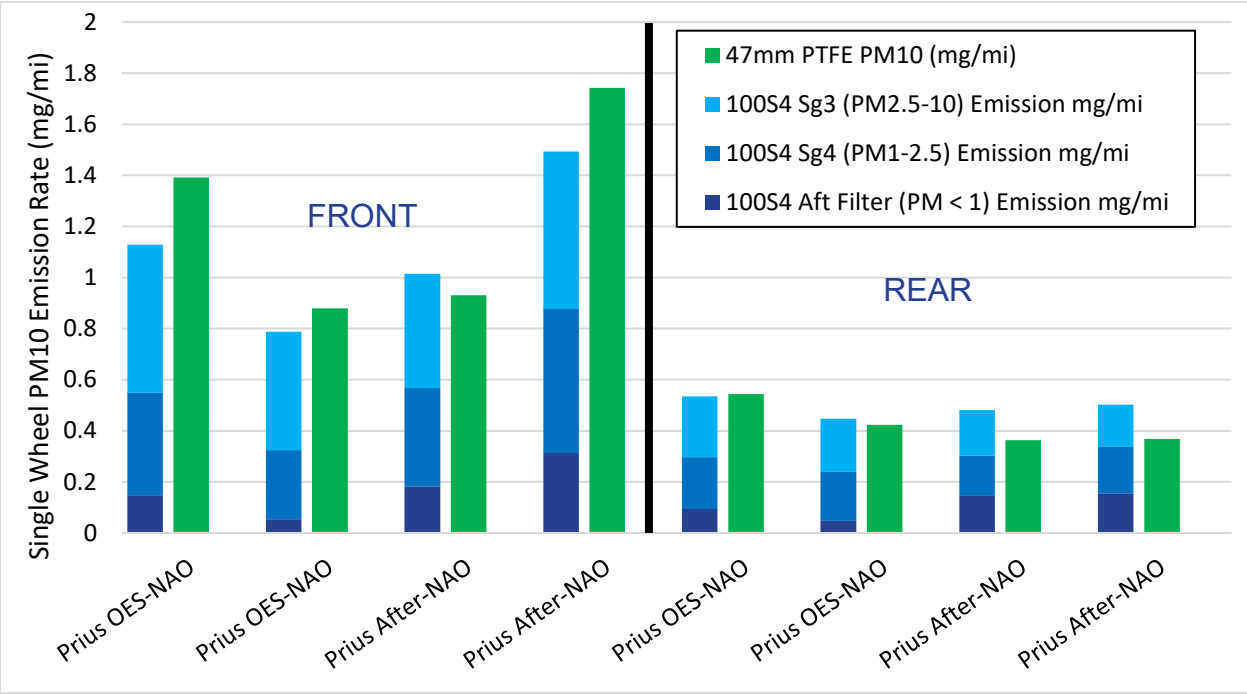

Figure 45. Single-wheel PM Mass Emission Rates for Prius as measured by 100S4 (Blue) and 47mm Teflon filter (Green).

Figure 46 displays the mass emission results for the Rogue, and Figure 47 presents the results for the Sienna. Both vehicles show elevated front-axle emission masses for the HLW tests. For the rear axle, the HLW tests did not result in appreciably higher emission masses, however the Sienna HLW test did result in a higher emission rate than the ETW tests.

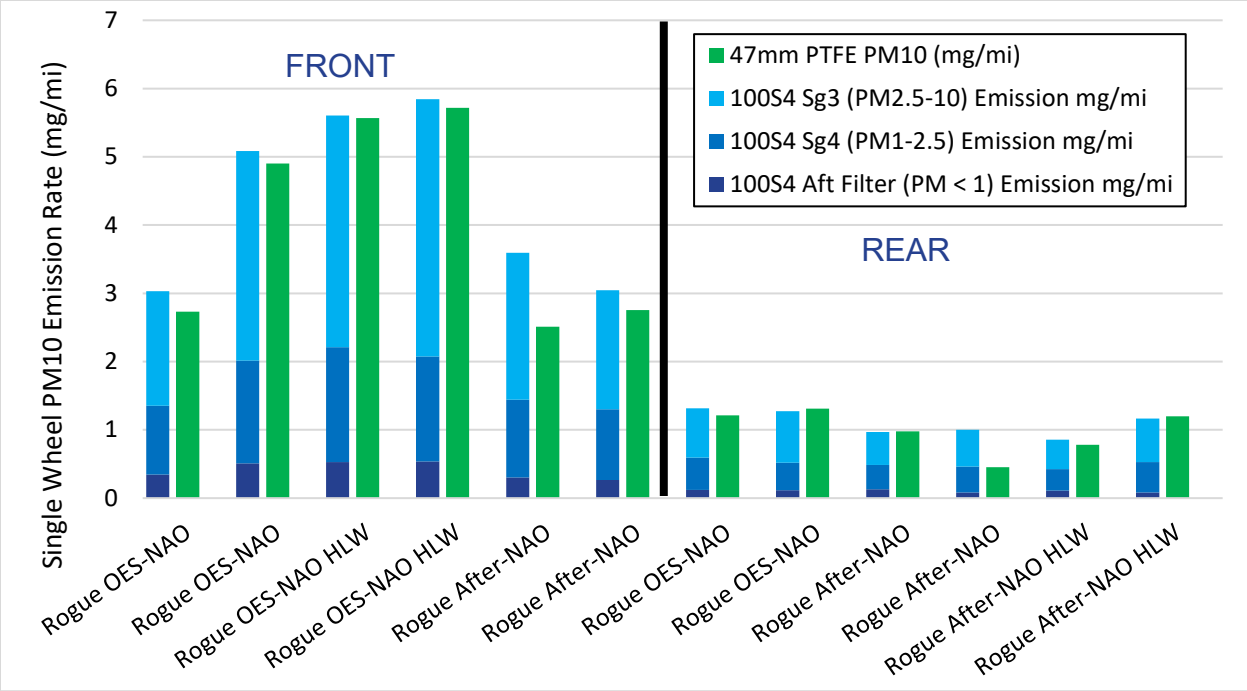

Figure 46. Single-wheel PM Mass Emission Rates for Rogue as measured by 100S4 (Blue) and 47mm Teflon filter (Green).

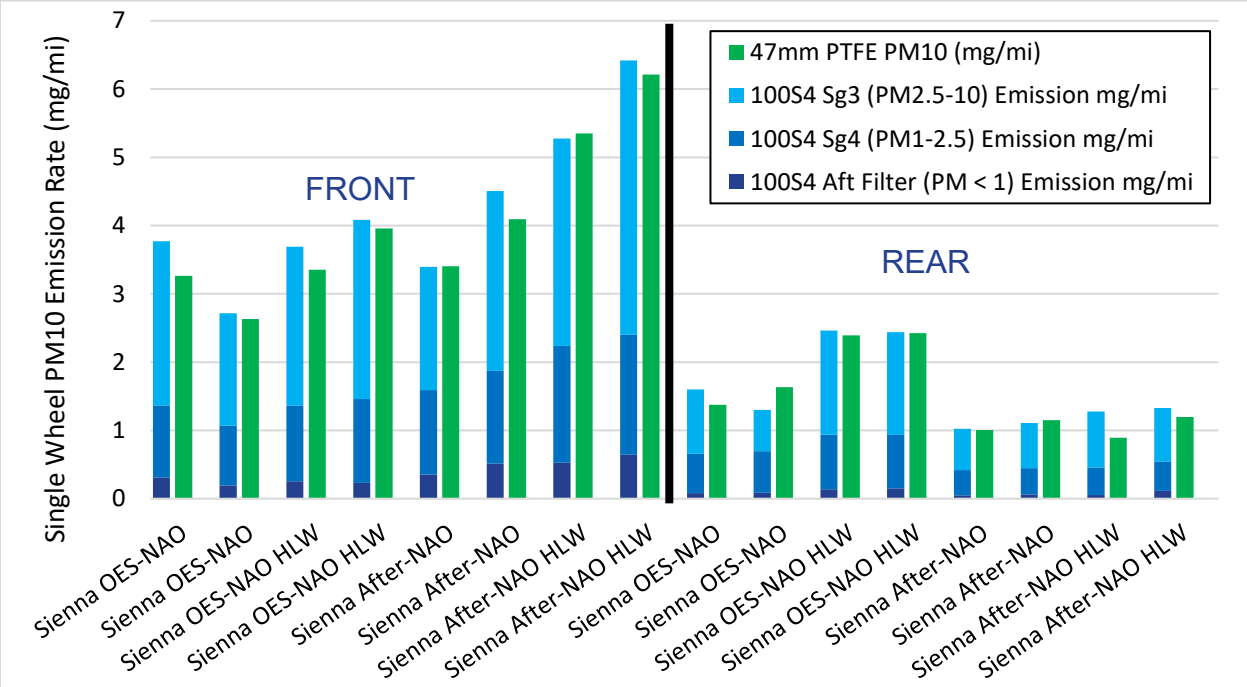

Figure 47. Single-wheel PM Mass Emission Rates for Sienna as measured by 100S4 (Blue) and 47mm Teflon filter (Green).

As presented in Table 19, two different Teflon filter types were used during testing (generally alternating across each test matrix replicate pair). Appendix J presents the initial and final weights of each filter along with the buoyancy-corrected weight gain. LINK performed buoyancy correction based on the laboratory ambient conditions as per the procedure outlined in 40 CFR 1065.690.

ERG also reviewed the test results against the as-delivered BMC Leafmarks for each pad material. The delivered LM pads all were assigned the letter “A” (the highest copper level). The overall material type appeared to have a larger effect on PM emission mass than the BMC Leafmark; after removing the LM pad tests with elevated emission levels, there was no apparent trend between emissions and BMC Leafmark across the OES and Aftermarket NAO tests.

Vehicle-Level Mass Results

Each test measured the PM emissions from a single wheel from either the front or rear axle. This section aggregates the test results to estimate vehicle-level emissions. For a given vehicle model, friction material, and test weight, the average front and rear emissions are added together and doubled to estimate 4-wheel emissions rates for each combination. Results presented in this section use only the PM mass measurements made by the 100S4 system.

Figure 48 presents the vehicle-level PM10 mass emission rates for each vehicle and test weight combination. Values are calculated as applicable for those friction materials that were tested on both front and rear assemblies within each model. Values range from approximately 3 mg/mi for the Prius OES material to nearly 30 mg/mi for the F-150 when heavily loaded with aftermarket low metallic pads.

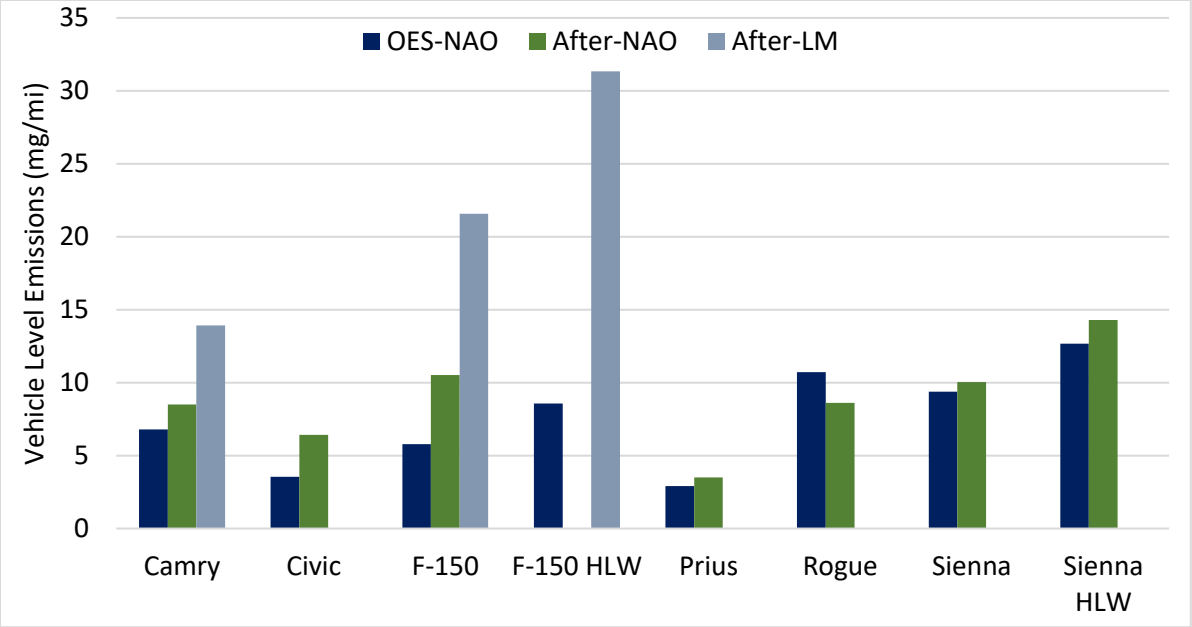

Figure 48. Vehicle-level PM10 mass emission rates for each vehicle, test weight, and friction material combination.

Next, these (along with the corresponding PM2.5) values are aggregated to estimate a single, average, on-road emission rate for each model at each PM size classification. These estimates will be based on the LINK breakdown of in-use pad materials on the road. A single emission value at each size classification for each model will be estimated for potential use as an emission factor in EMFAC. The estimate begins with the data provided by LINK regarding in-use balances of different materials based on their business intelligence. Those surveys involved estimates of pad material balances by vehicle model at 3 years old and 11 years old; those values were averaged to yield a simple estimate at 7 years of vehicle age. Those estimated are presented in Table 21. Note that aftermarket low metallic pads are only present in the estimate for those vehicles for which those materials were tested. The OES and aftermarket NAO materials are normalized to 100% for the other vehicles given that the test matrix did not involve testing these material/model combinations. One key assumption was necessary to develop the table; ERG assumed that when brake services are performed on vehicles in-use, that front and rear pads are typically replaced at the same time. This assumption was made based on looking at pad material wear rates as a percentage of total pad mass during each test. Front and rear pads generally lost approximately equivalent percentages of their total weight during the burnish and test cycle.

Table 21. Estimated balance of friction materials by model for vehicles models at 3 and 11 years old.

Age	Model	OES NAO%	AM NAO%	AM LM%
3 years old	Camry	29.8	57.8	12.5
	Civic	29.8	70.2	N/A
	F-150	78.8	8.8	12.4
	Prius	29.8	70.3	N/A
	Rogue	29.8	70.3	N/A
	Sienna	29.8	70.3	N/A
11 years old	Camry	22.4	43.6	34.0
	Civic	22.4	77.6	N/A
	F-150	59.4	6.6	34.0
	Prius	22.4	77.6	N/A
	Rogue	22.4	77.6	N/A
	Sienna	22.4	77.6	N/A

These values were then used to calculate overall by-model PM emission rates for these models in the in-use fleet. The values presented in Table 22 are multiplied by the in-use fleet balance to calculate an estimate of in-use emissions for each model and test weight combination at an average age of 7 years.

Table 22. Measured in-use brake emission rates by model, estimated for 7 year old vehicles.

Model	Estimated In-Use PM2.5 Emission Rate (mg/mi)	Estimated In-Use PM10 Emission Rate (mg/mi)
Camry	1.7	9.3
Civic	1.1	5.7
F-150	2.0	9.8
F-150 HLW	2.6	13.9
Prius	1.0	3.3
Rogue	2.0	9.2
Sienna	2.1	9.9
Sienna HLW	2.7	13.9

Results by Speed Segment

The CBDC test cycle was designed such that the relative distance traveled in each of the speed segment approximates the relative distances traveled by all microtrips within each speed range in the Caltrans dataset so that the overall cycle emissions represent real-world driving. However, the three speed segments were created to allow further refinement of the emissions factors based on trip average speeds as in EMFAC.

The EMFAC model uses speed correction curves (SCCs) to adjust pollutant emission factors for trips of varying average speeds. The test cycle in this work was comprised of three different cycles representing microtrips falling in average speed ranges of 0-21 kph, 21-69 kph and above 69 kph. ERG used these different speed ranges to develop trends for speed correction of the brake PM emission rates.

The QCM measures continuous mass (PM2.5) and is the measurement that can resolve differences across the 3 speed segments. (The 100S4 and 47mm Teflon systems were used for cumulative measurements over the cycle, not by speed segment). In this study, the QCM was considered a relative measurement; while it reports in units of mass, there was a large amount of noise (R^2 ~ 0.35) when comparing cumulative QCM mass for a test to the 100S4 PM2.5 results. To use it as a relative measurement only, ERG used the QCM results to apportion the 100S4 PM2.5 total mass to each speed segment based on the percentage of QCM mass recorded in each.

The QCM measures only PM2.5. However, the APS was measuring the size distributions throughout the tests as well. ERG used the APS size distribution to also estimate the PM10 mass in each speed segment from the QCM results. ERG took the following steps to perform this estimation:

- Gather APS data that indicates the particle size distribution (by counts) in the range from 0.5-20 µm.
- Assume that particles are spherical, then calculate ratio of PM10 particle volume to PM2.5 volume by summing the total particle volume measured at each APS cutpoint (counts of particles multiplied by the volume of a sphere at that cutpoint's diameter)
- Assume particles have a homogenous density such that mass is proportional to volume. Calculate the ratio of PM10 mass to PM2.5 mass based on the total volume.
- Multiply the apportioned PM2.5 by this ratio to estimate the percentage of the total PM10 emitted in each speed segment
- Use the calculated percentages of total PM10 for each cycle as weighting factors to apportion the cycle PM10 mass measured by 100S4 to each speed segment

This method required significant assumptions but did allow for the QCM to be used to estimate the PM2.5 and PM10 masses emitted within each speed segment. Figure 49 presents the overall mass emission trend by speed segment observed when averaging all tests. It can be seen that the 21-69 kph (13-42 mph) speed segment has the highest per-mile emissions, followed by the low speed segment with moderate per-mile emissions, and the high speed segment has the lowest per-mile emission rate. The error bars in the plot present the 95% confidence intervals based on the variability across all tests only (they do not necessarily indicate any error caused by the QCM or the assumptions used in this approach). Figure 50 presents, for the same data, the trend in the PM2.5 mass percentage of PM10 averaged across all tests. At higher speeds, the data indicate that PM2.5 makes up an increasing share of PM10 mass emissions.

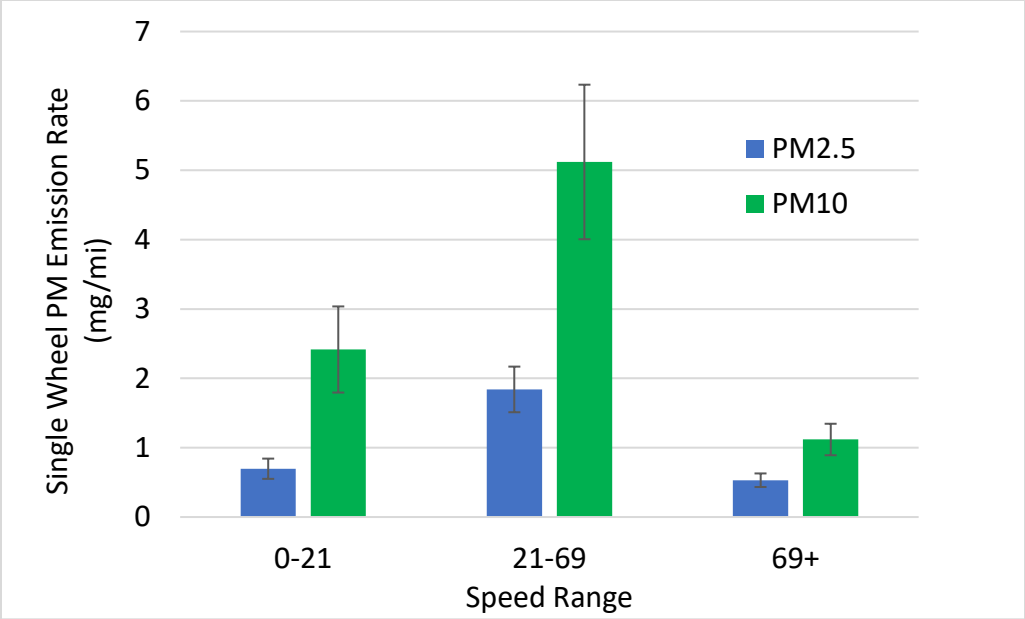

Figure 49. Overall trend in single-wheel mass emission rates over the three different speed segments making up the CBDC overall test cycle (averaged for all tests)

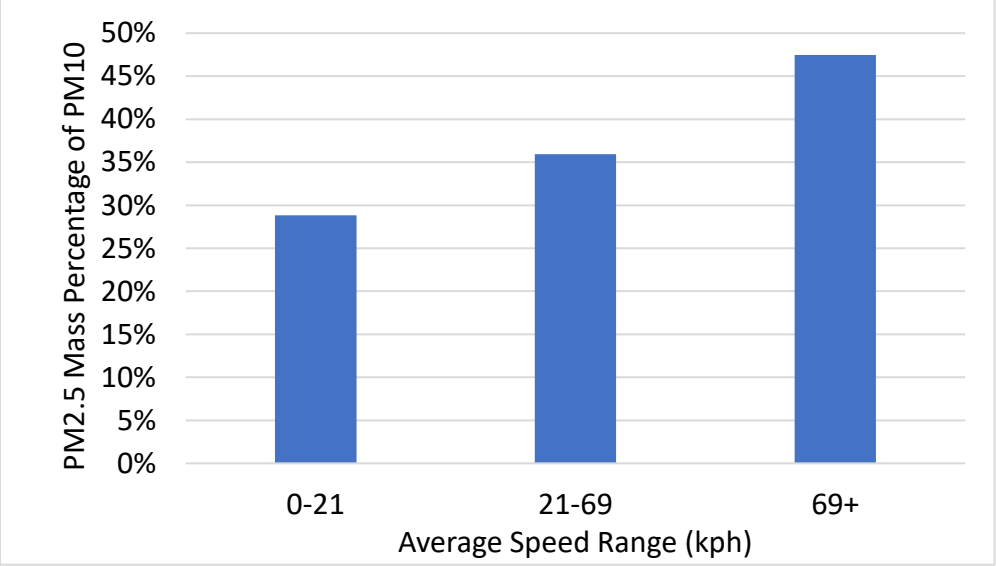

Figure 50. The PM2.5 mass fraction of PM10 for the different speed segments, averaged across all tests.

ERG used the relative emissions rates from Figure 49 to develop speed correction factors (SCFs) that can be applied to each overall CBDC result to calculate emission rates for trips of average speeds falling within the different ranges. Figure 52 presents the speed correction factor estimates for the three speed ranges. The factors are given separately for PM2.5 and PM10- these factors are to be multiplied by a given overall test cycle result for PM2.5 and PM10, respectively.

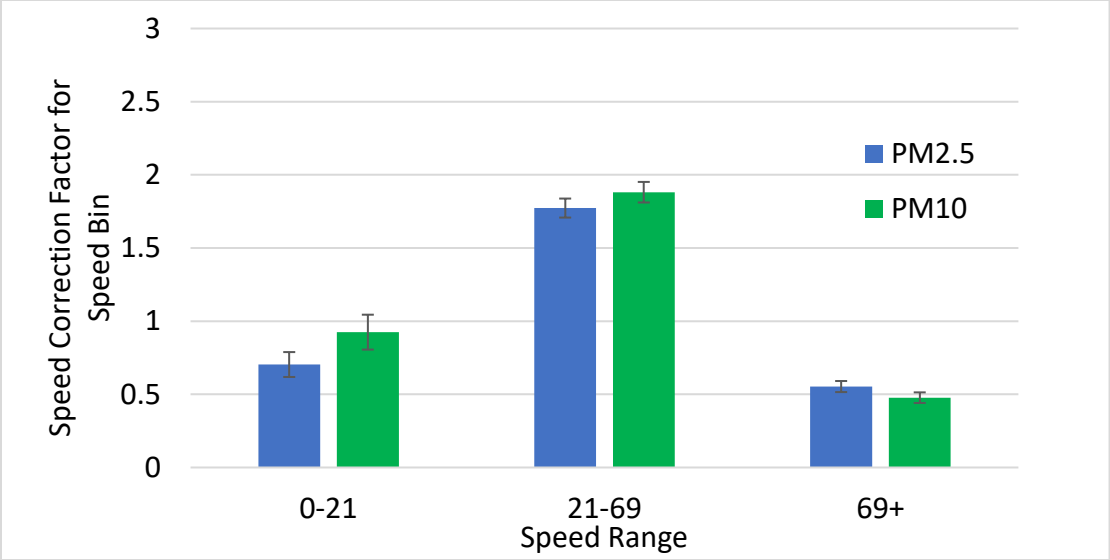

Figure 51. Speed correction factors for the three speed bins. These factors can be multiplied by the overall cycle emission rate to estimate the emissions of operation within each speed bin.

Because the speed-based emission results are not monotonic with respect to the speed cycle ranges, ERG further investigated the overall trend presented in the speed segment analysis. There are some potential factors that confound the agreement between speed segment and emissions, notably the distance represented by each cycle, the stops/distance, the braking energy/distance, and the actual duration of braking in each speed segment. Figure 52 presents a bar chart of total braking energy within each speed segment along with the total PM2.5 emission average of all 5 reference tests of the F-150 (axes are scaled differently to determine proportionality). In the high and medium speed segments, the energy and emissions are proportional. In the low speed segment, the relationship trends together (and neither are monotonic) but the energy is high relative to the emissions.

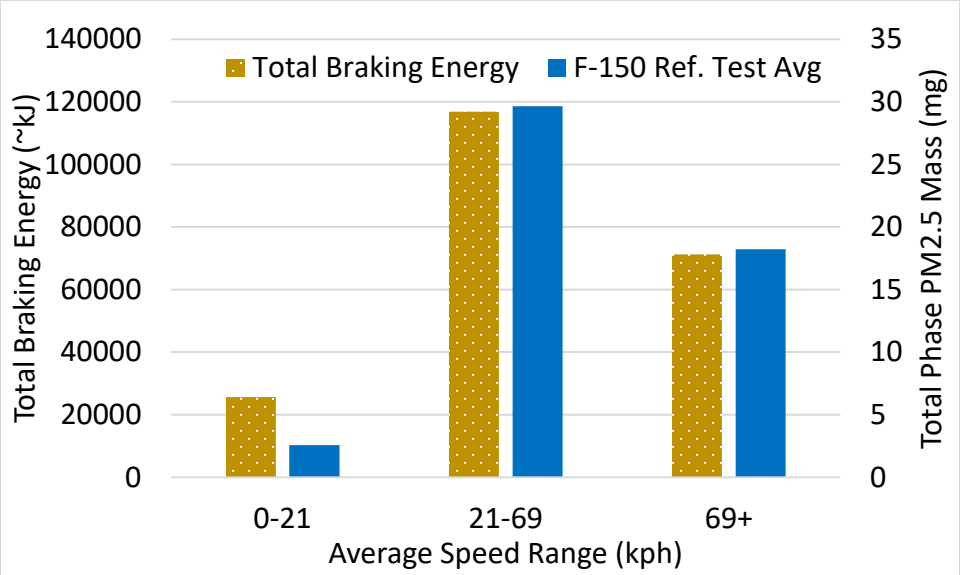

Figure 52. Total braking energy (proportional to kJ) within each speed segment and the F-150 Reference Test Average Total-Cycle PM2.5 emission mass for each speed segment

Figure 53 presents the total PM2.5 emission divided by the total seconds of braking time within each speed segment, averaged over the F-150 reference tests. Presented in this way, the emission measurements are monotonic. A key factor in the interpretation of the SCFs is the cycle-represented distance. Emissions per braking second trend with speed, however accounting for the distance traveled appears to confound that trend.

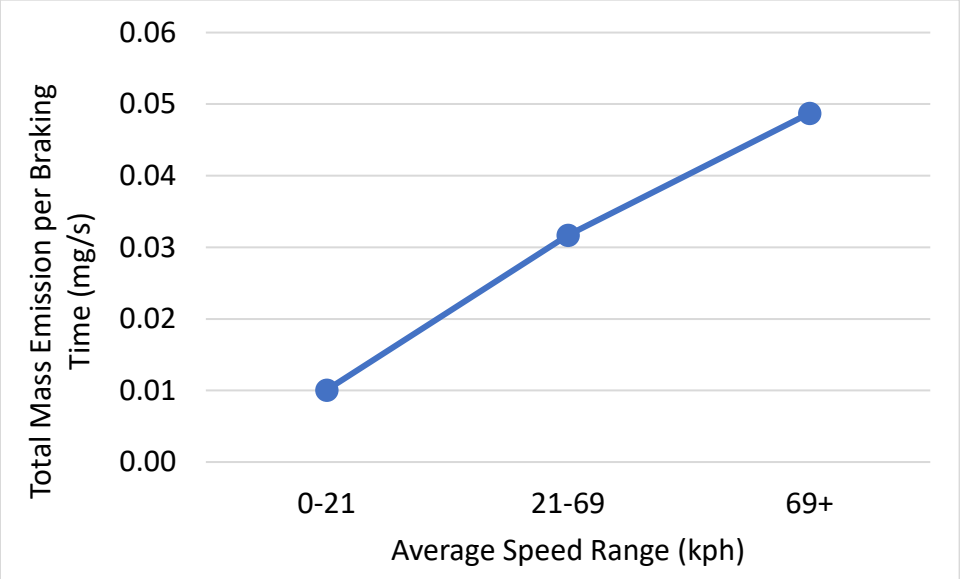

Figure 53. Total PM2.5 emission divided by total braking time in each speed segment, averaged for the F-150 reference tests

Emission Mass by Vehicle Weight

Figure 54 presents the vehicle-level test emission masses versus the simulated vehicle test weight, categorized by pad material. Labels of vehicle model are shown at the location of each model on the x-axis. The trends within each pad material do appear to be linear, so linear fits are shown by pad material. The fit to the aftermarket LM materials has the highest slope and the OES-NAO has the lowest slope. In this analysis, the fits are not forced through the origin (i.e. intercepts set to zero). The slopes and intercepts for these fits are presented in Table 23. While there may be engineering justification to set the intercepts to zero, there is little justification or utility in doing so as the Civic was the lightest vehicle tested (meaning no data is available near the origin) and is likely to be near the lower limit of weights of any light-duty vehicle to be modeled (meaning any modeling error at a zero vehicle weight will not affect results).

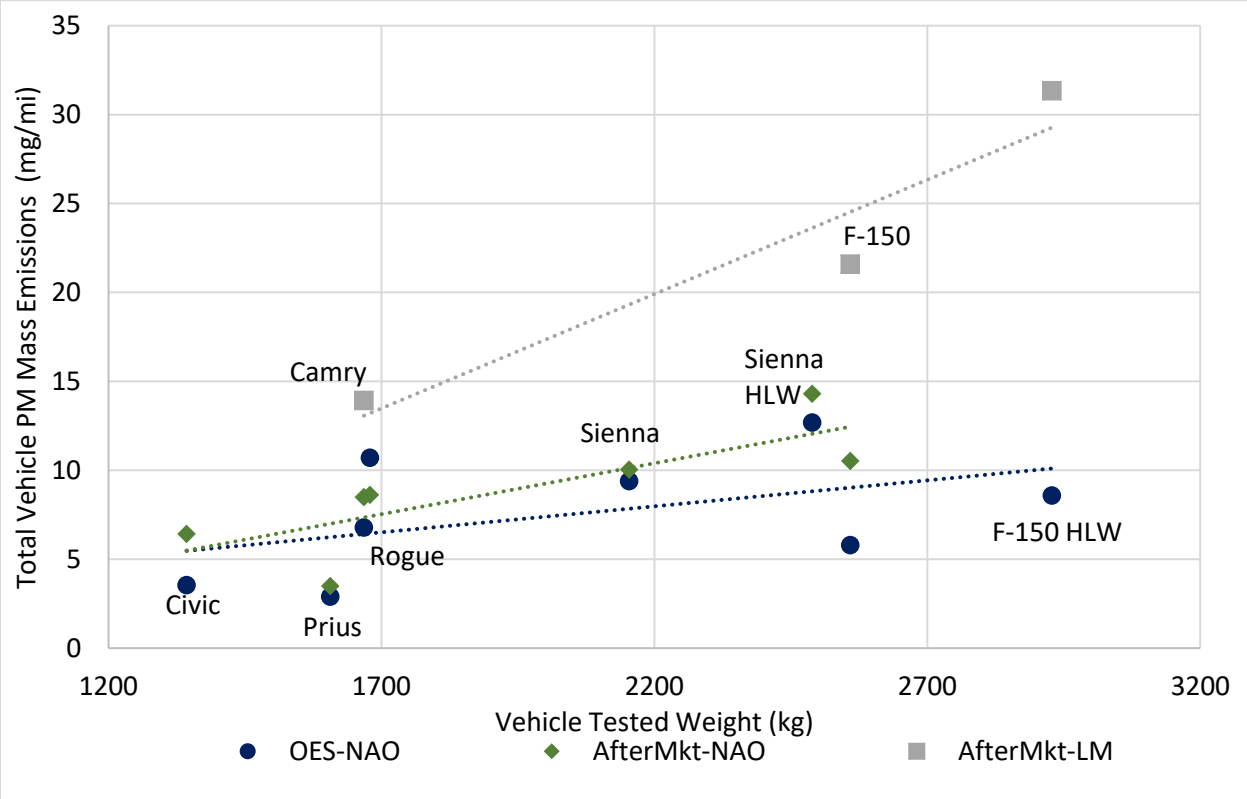

Figure 54. Total vehicle test cycle PM mass emissions vs simulated vehicle test weight, categorized by pad material.

Table 23. Slopes and intercepts for linear fits by material for PM mass emission rate (mg/mi) versus vehicle tested weight (kg)

Material	Slope (mg/kgmi)	Intercept (mg/mi)	Coefficient of Determination (R^2)	P Values, Slope, Intercept
OES NAO	0.003	1.55	0.91	0.23, 0.75
After NAO	0.006	-2.21	0.64	0.03, 0.58
After LM	0.013	-8.37	0.23	0.19, 0.55

Emission Mass and Component Mass Loss During Testing

LINK staff weighed the friction materials before and after each test. Rotors (or drums for the Civic) were weighed separately from pads. This allowed for the calculation of the total mass lost from the components over the course of the burnish and test cycles. Components could not be weighed after the burnish and before the test cycle because removal would have potentially upset the friction couple and nullified the burnishing process. ERG investigated the extent to which the total mass loss was proportional to measured PM mass emissions. This section references the components as pads and rotors generally, but for the Civic rear, the corresponding parts were shoes and drums and they are included.

Figure 55 presents the total PM mass emissions (y-axis) measured during the test cycle plotted against the total mass loss of pads and rotor for each burnish and test. The plot shows PM10 as measured by the 100S4 and has somewhat less noise than that of PM2.5 (though the trends are otherwise similar). Fits are not presented by material as the specific slope of the relationship between the test PM and the pad and mass loss is arbitrary due to the burnish cycle (for which emissions were not quantified by the 100S4). The relationship is presented to show the general level of proportionality.

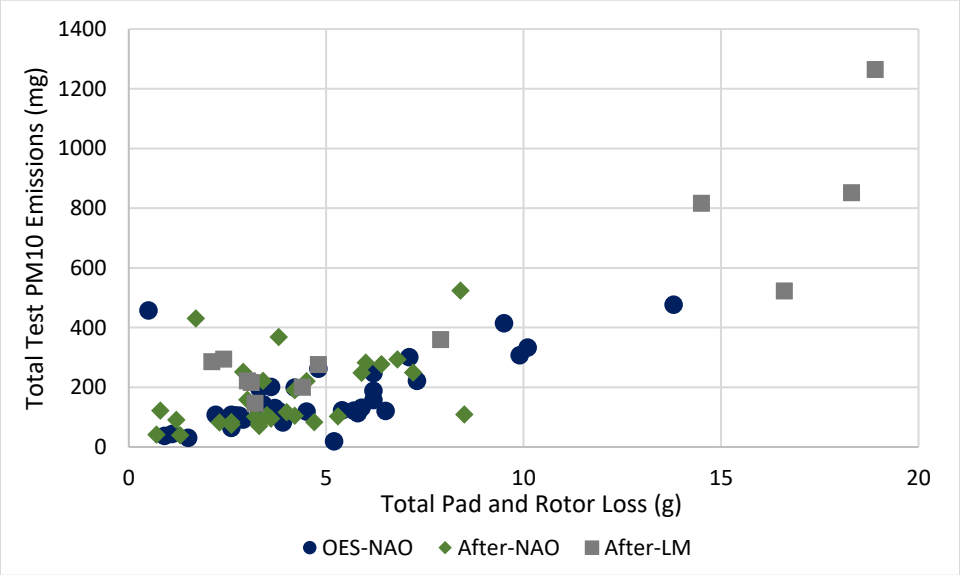

Figure 55. Total test-cycle PM10 emissions plotted against the total mass loss of the pad and rotor during the burnish and test cycle. Each point represents one test.

ERG also investigated whether the PM10 emission rates were more correlated to the mass of pad lost, the mass of rotor loss, or the sum of pad and rotor. Figure 56 presents the PM10 emissions totals for each test against the brake component mass loss for three categories: pad + rotor (same data as Figure 55), pads only, and rotor only. The plot includes R-squared values calculated for a linear fit made to each category. The best linear fit is for the sum of pad and rotor, and the noisiest fit is to the rotor only. This finding indicates that mass losses of both pads and rotors contribute to and are

correlated with emitted PM. However, it does appear as though the emitted PM mass is more responsive to the mass of pad lost. This could be because, in most tests, the pad mass loss exceeded that of the rotors. The pad mass loss averaged 3.2 times that of the rotor mass loss across all tests. However, this ratio varied widely across tests did not appear to be sensitive to the friction material type.

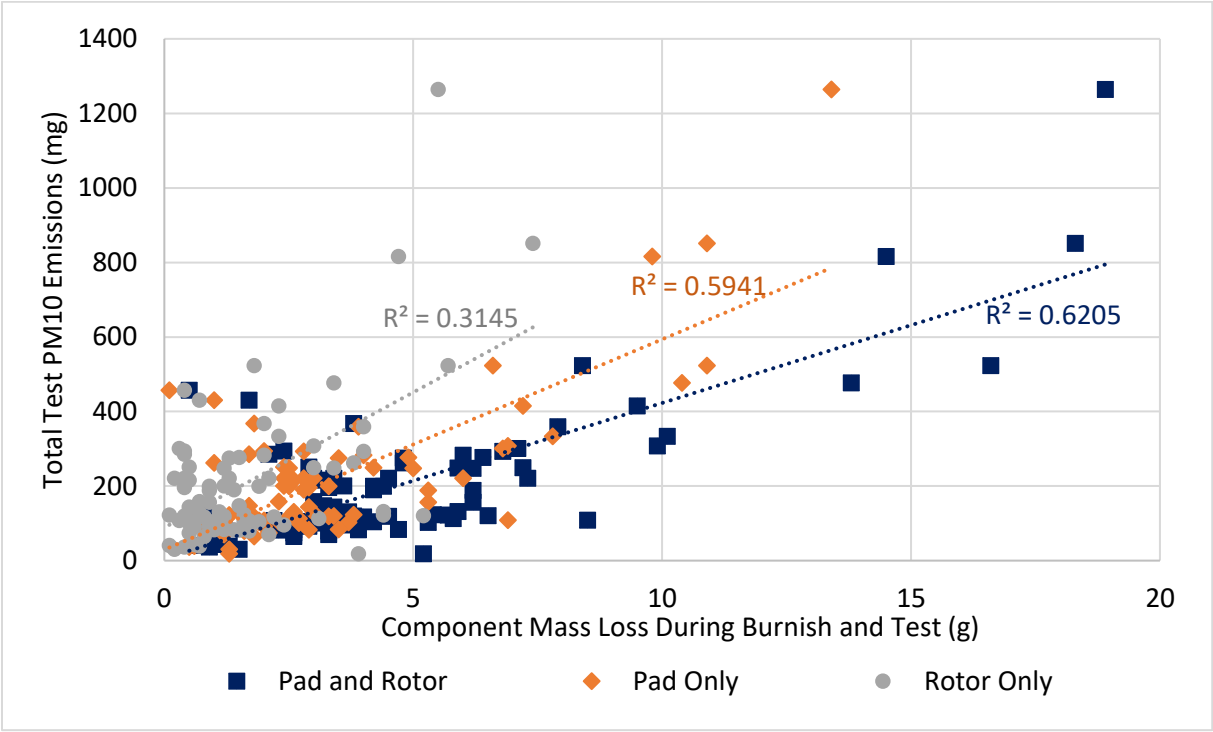

Figure 56. Total cycle PM10 emissions relative to mass lost for pads, rotors, or the sum of pads and rotors. R-squared values are presented for linear fits to each.

Particle Counts

The CPC was used to measure particle counts per unit of sample volume throughout the duration of each test. Particle number totals for each test are included in Appendix H. Table 24 presents the range, median, and average number of cumulative particles for all CBDC tests on a per-mile basis. In general, there was a weak trend in vehicle weight and particle count; larger vehicles tended to have larger particle counts.

Table 24. Selected statistics for single-wheel particle number counts for all tests (#/mi)

Test Statistic	Particle Number (#/mi)
Average	1.681×10^9
Median	1.258×10^9
Maximum	8.429×10^9
Minimum	3.913×10^8

ERG calculated vehicle-level particle number emission rates by doubling the single wheel emission averages for each model/material/test weight/axle combination. These axle-level values were summed within each model to calculate vehicle-level values. Figure 57 presents these estimates by vehicle model and categorized by pad material type. Compared to the mass results, the spanned range of values across models and pad materials appears lower for particle count results, meaning all vehicles appear to have more similar particle count emissions than they do mass. Generally, the trends otherwise follow those observed for PM mass with a notable exception of the Prius aftermarket NAO material. The elevated values for this combination were caused by high emissions measured in both tests of the front axle; the rear axle emission rates were in line with the other sedans.

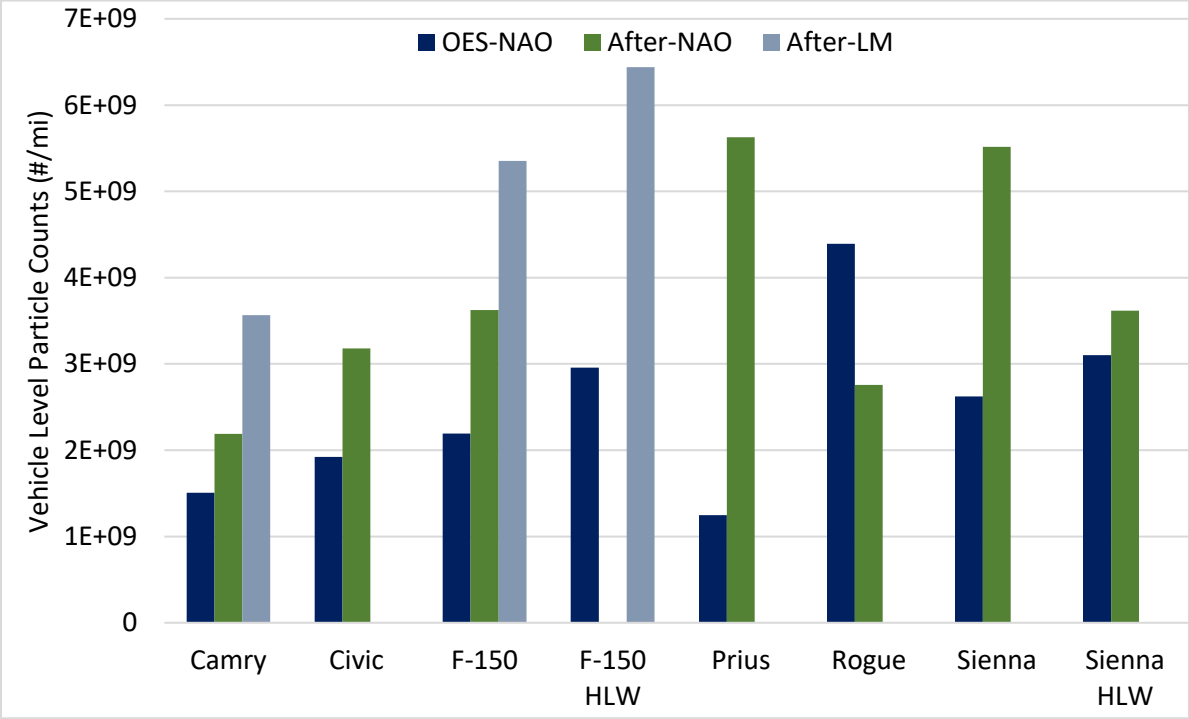

Figure 57. Vehicle-level particle number emission rates for each vehicle and friction material combination

Figure 58 presents the overall trends in single-wheel particle emission rates across the three speed segments. The figure presents the emission rates averaged across all tests. Error bars represent the 95% confidence interval for the mean of the results of all tests. Appendix K presents the corresponding vehicle-level results by individual model.

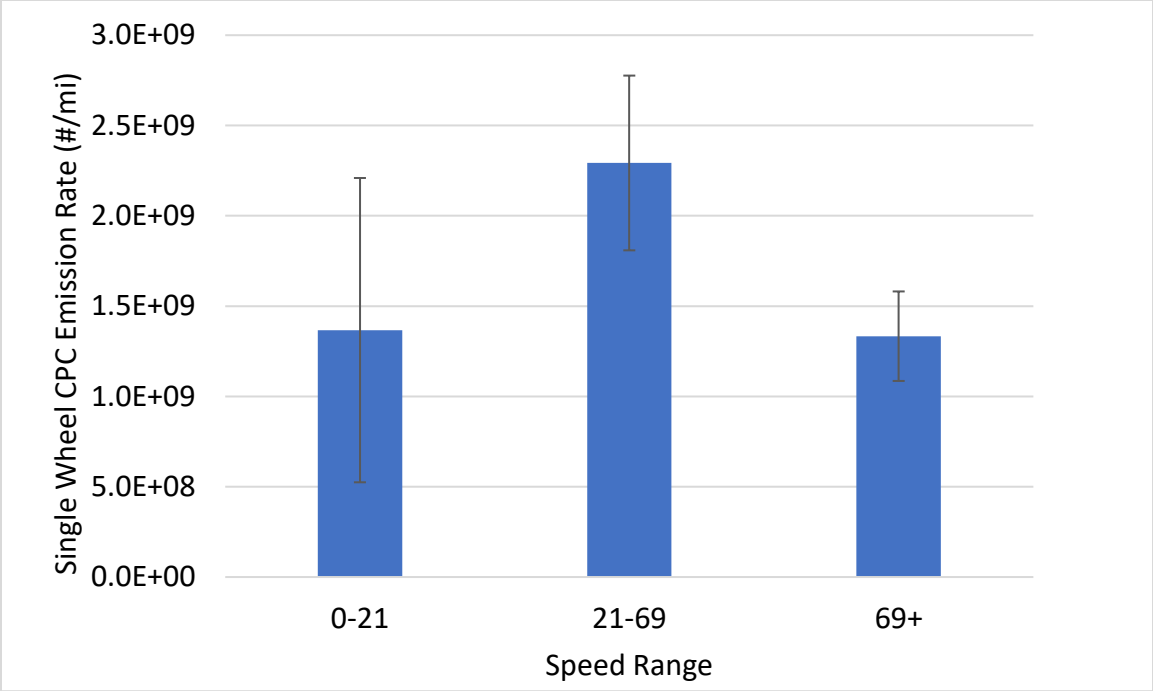

Figure 58. Overall average single-wheel particle number emission rate across the three speed ranges

Particle Size Distributions

Particle size was measured in two size ranges; the EEPS measured from 5.6 – 560 nm, and the APS measured from 0.5 – 20 µm. The APS results tended to show noticeable trends and responses to the test matrix parameters, and their results follow in this section. The EEPS results were more similar across all tests with a lower degree of apparent responsiveness to the test parameters, so EEPS results are presented only in Appendix L. Size distributions are presented in graphs by vehicle and axle, and each distribution is color coded by brake pad material. Note that all distributions in the size distribution figures are normalized to sum to 1. This is to enhance the comparability of particle size without any bias from particle number differences at the test level. Particle number is measured specifically by the CPC so reporting absolute count is not a necessary function of the particle sizers.

Figure 59 presents the size distribution of particles from the front brake tests of the Camry. It can be seen the test replicate pairs of the three different pad materials follow similar patterns. The low metallic material tends to emit larger particles, and the two NAO materials are relatively similar in particle size distribution.

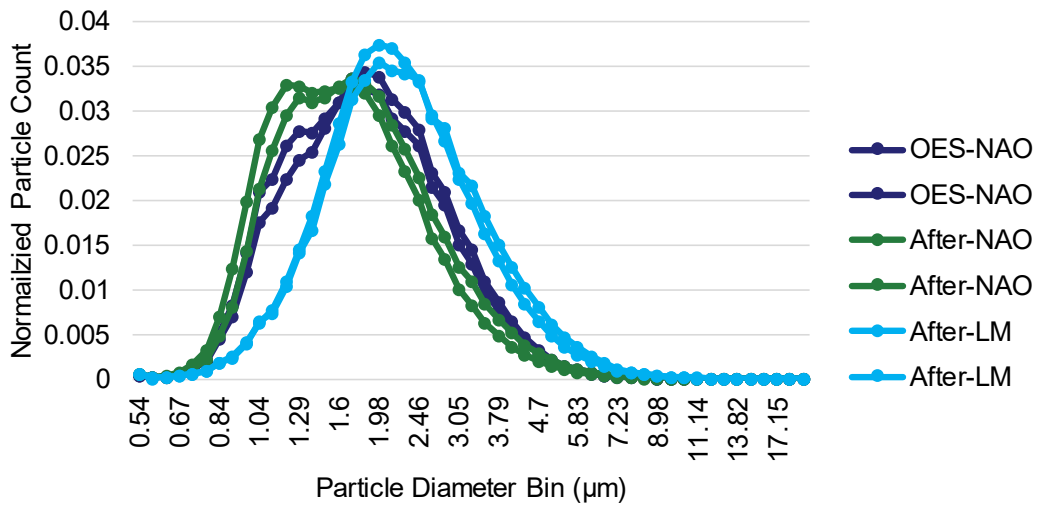

Figure 59. Size distribution of Camry front brake PM as measured by APS

The PM size distribution for the rear brake tests of the Camry is presented in Figure 60. The low metallic material has the largest particle sizes, and the aftermarket NAO tends to have the smallest.

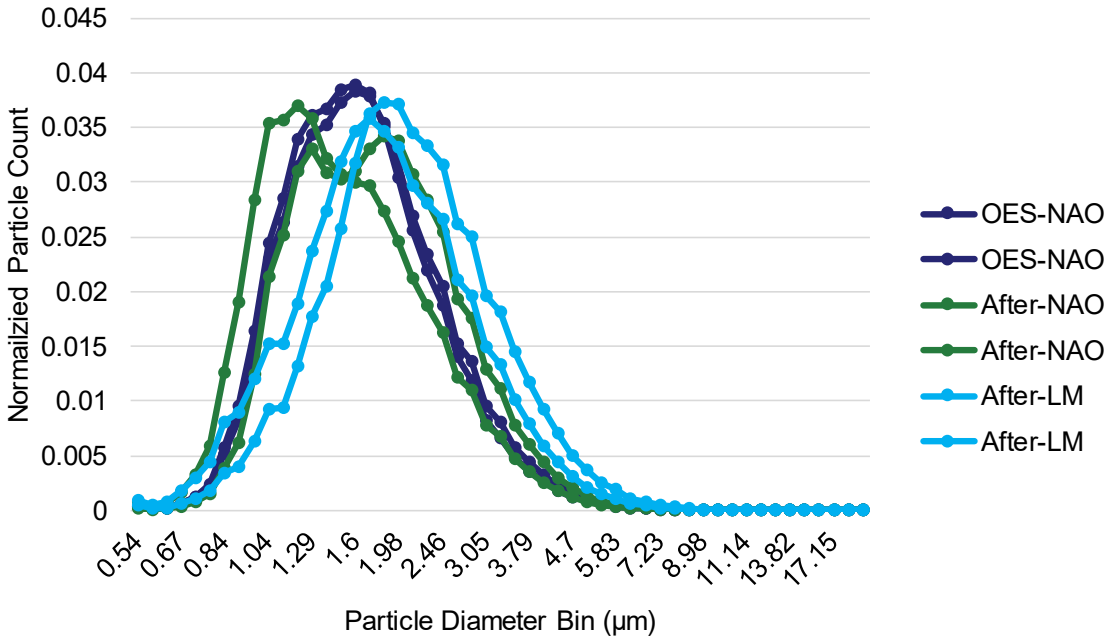

Figure 60. Size distribution of Camry rear brake PM as measured by APS

Figure 61 and Figure 62 present the size distributions for the Civic front and rear, respectively. The OES particles from the front tend to be larger than the aftermarket, but that trend appears to be reversed for the rear drum brake emitted particle size.

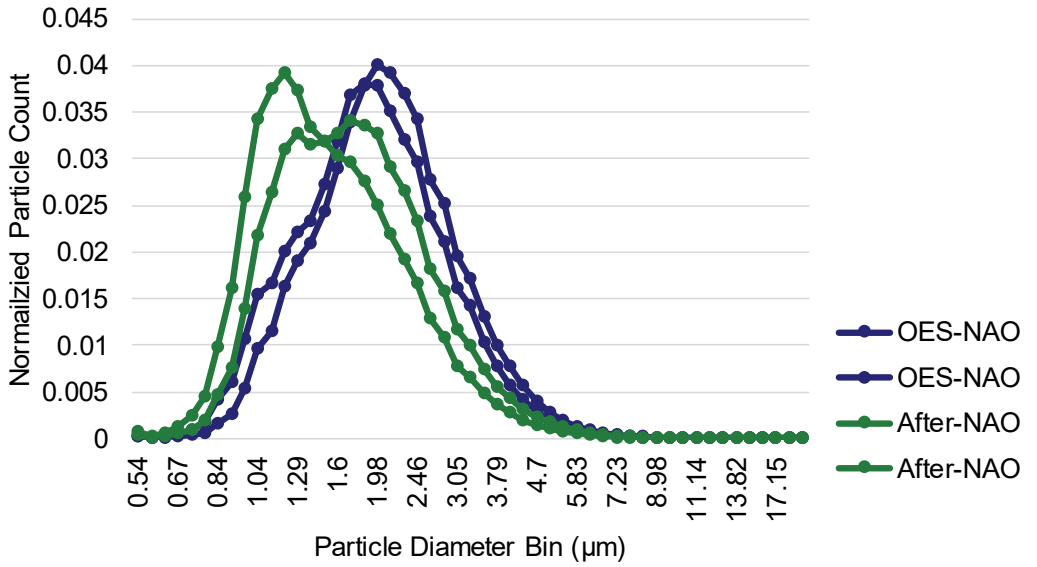

Figure 61. Size distribution of Civic front brake PM as measured by APS

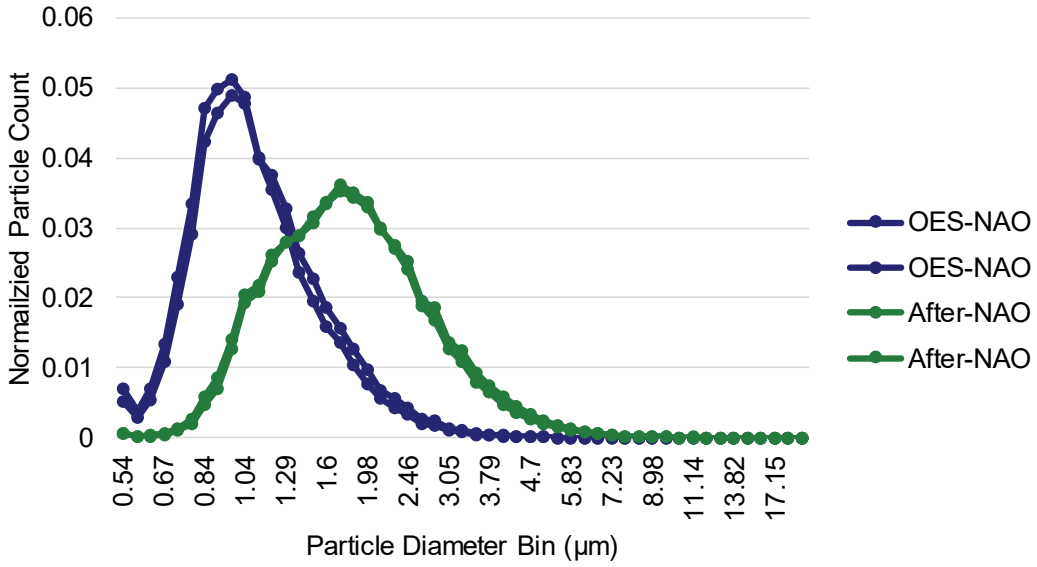

Figure 62. Size distribution of Civic rear brake PM as measured by APS

The size distributions for F-150 front and rear are presented in Figure 63 and Figure 64, respectively. For the front brakes, the low metallic pads have the largest particle size, but the trend is more inconclusive on particle size emitted from the various rear pads.

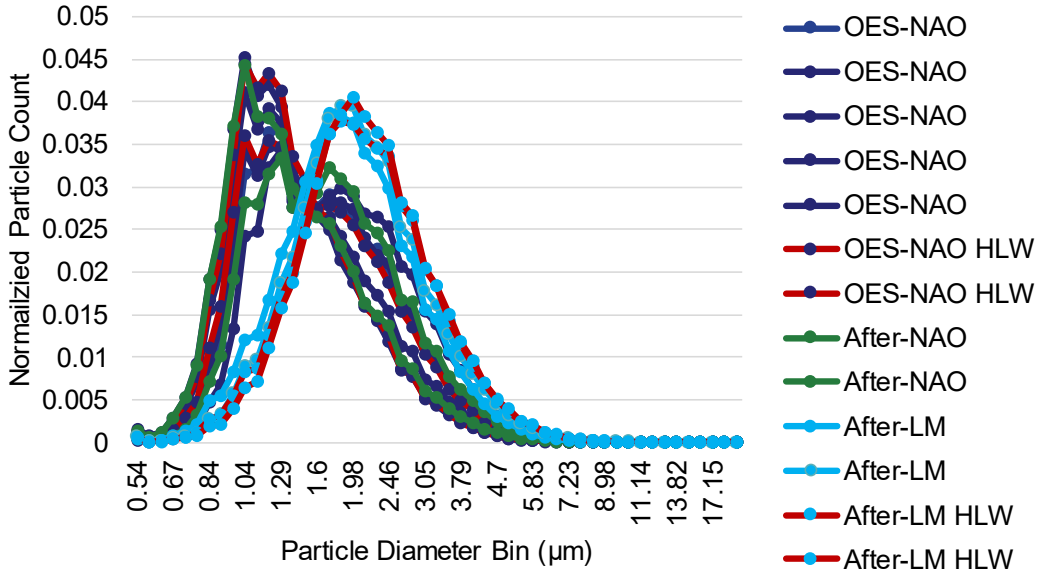

Figure 63. Size distribution of F-150 front brake PM as measured by APS

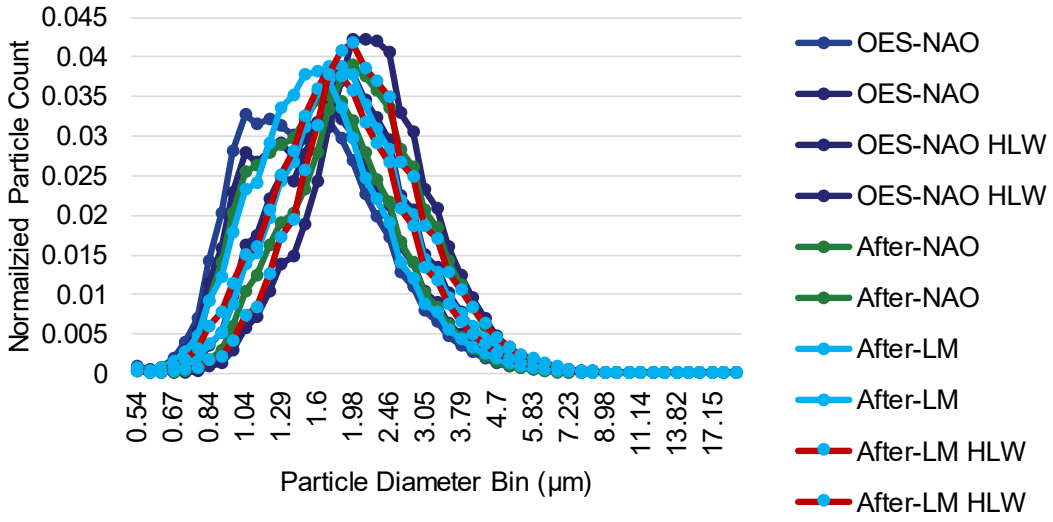

Figure 64. Size distribution of F-150 rear brake PM as measured by APS

Figure 65 and Figure 66 present size distributions for the Prius. The two NAO pad materials are largely overlapped in emissions from both the front and rear assemblies.

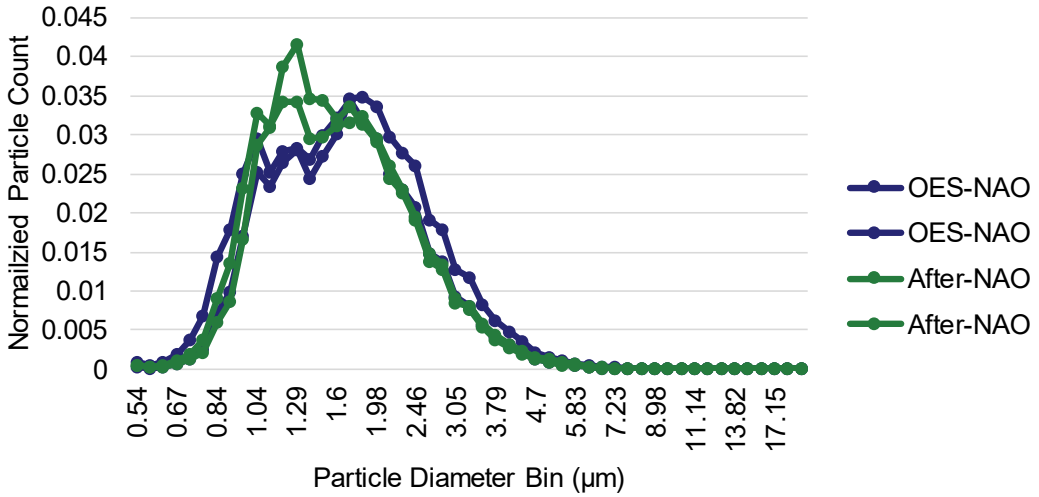

Figure 65. Size distribution of Prius front brake PM as measured by APS

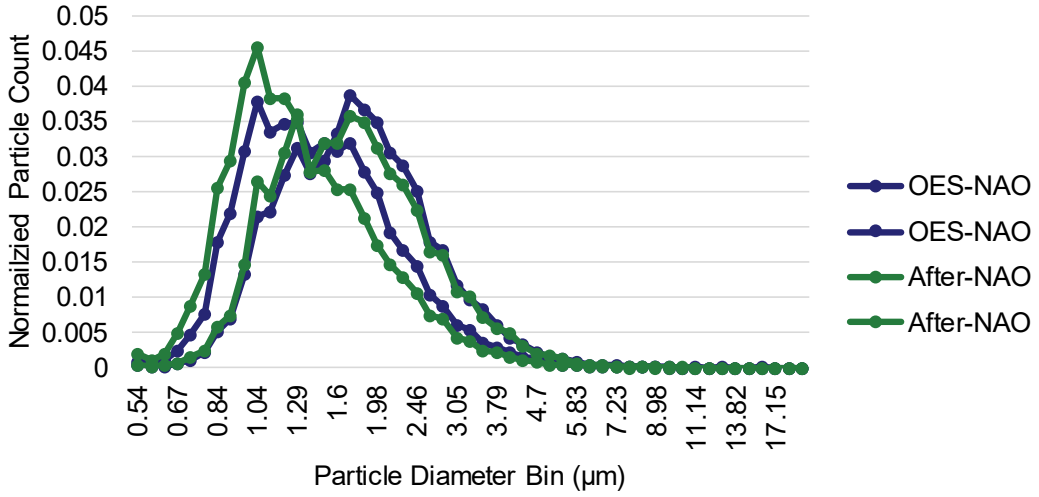

Figure 66. Size distribution of Prius rear brake PM as measured by APS

Figure 67 presents the size distribution of particles from the front brakes of the Rogue. The OES material tends to have a larger particle size than the aftermarket material. Figure 68 presents the findings for the Rogue rear, in which the distributions are largely overlapped.

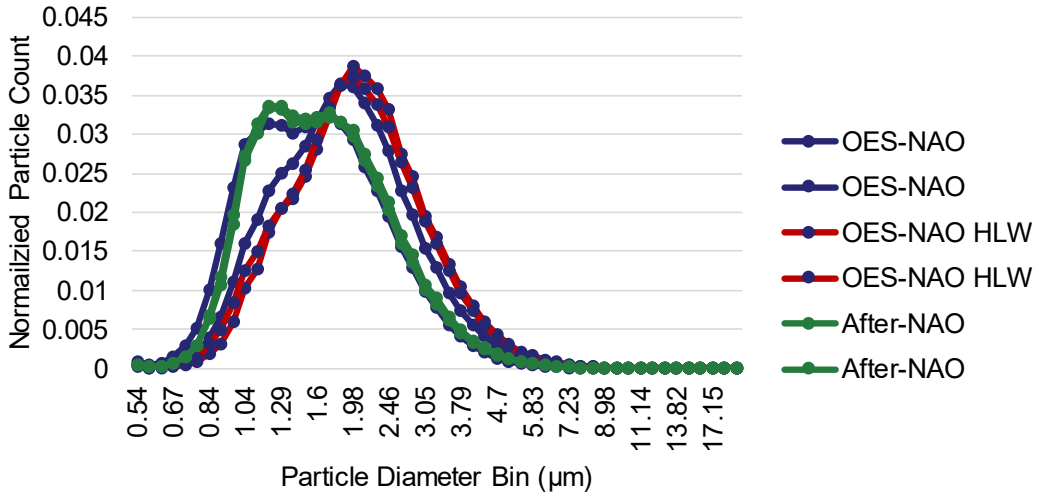

Figure 67. Size distribution of Rogue front brake PM as measured by APS

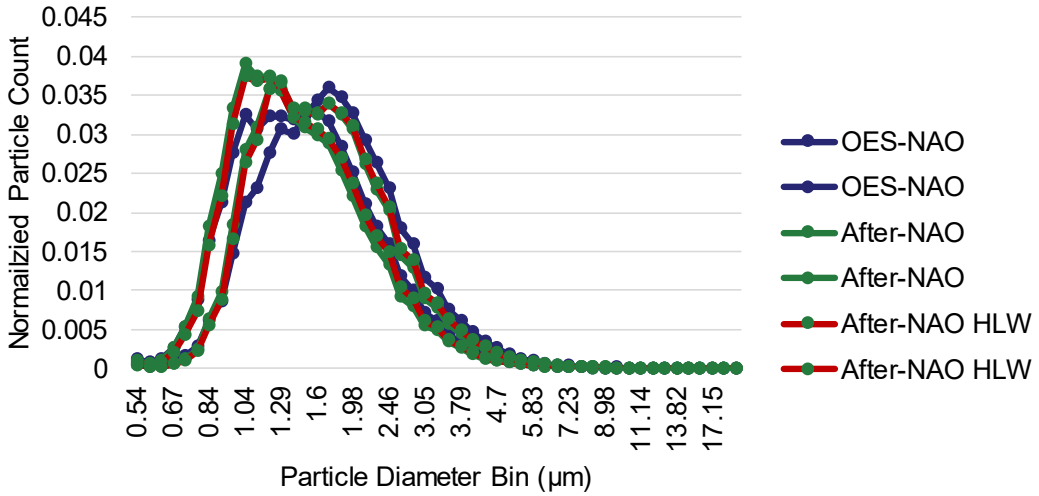

Figure 68. Size distribution of Rogue rear brake PM as measured by APS

Figure 69 and Figure 70 present the size distributions for the Sienna front and rear, respectively. Both display significant overlap in the size distributions of the different friction materials and test weight. Both the front and rear distributions tend to have a minor bimodal effect, with a major peak at 1.98 µm and a minor peak at 1.29 µm.

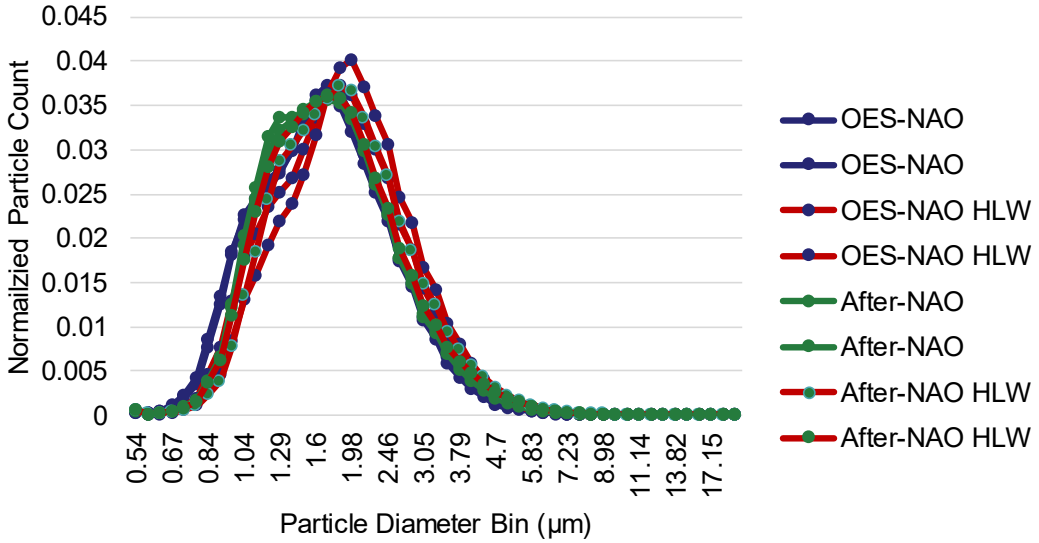

Figure 69. Size distribution of Sienna front brake PM as measured by APS

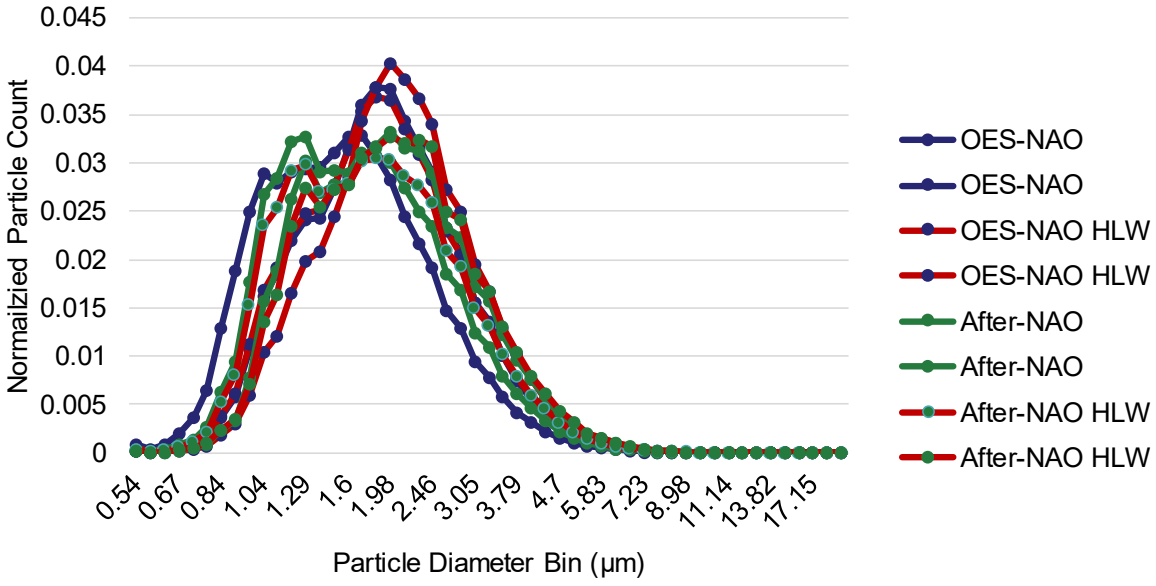

Figure 70. Size distribution of Sienna rear brake PM as measured by APS

Tunnel Blanks

LINK conducted two tunnel blank experiments, one early in the test program and the other late in the test program. Tunnel blanks involved running a complete CBDC test cycle without brake pads mounted or the brake hydraulic pressure active to help determine the level of background PM present during a test. Table 25 presents the results of the tunnel blank experiments as compared to all other brake assembly tests for particle counts and mass measurements. Mass measurements of PM10 were conducted with both the 100S4 as well as the two parallel 47 mm PTFE filter holder systems (note that in normal tests only 1 of the filters was directly measuring PM using a PTFE filter). The particle counts during blanks averaged approximately 0.2% of the test average. The 100S4 blank measurement was about 1% of the average test mass, and the PTFE filters averaged approximately 2.8% of the average value when including a single outlying high value during Tunnel Blank 2. No corrections were applied to the test results based on the tunnel blank findings. The main concern was that one of the mass measurements was an outlier in the 100S4 vs PTFE results by test. ERG and LINK were concerned that performing corrections based on an outlying point would have a detrimental effect on all results.

Table 25. PM counts and mass measurements for the two tunnel blank procedures as well as the averages for all brake emissions tests

	Test Day	CPC #	100S4 PM10 (mg)	47mm PM10 1 (mg)	47 PM10 mm 2 (mg)
Tunnel Blank 1	17	$9.5x10^7$	1.4	2.7	2.3
Tunnel Blank 2	66	$2.1x10^8$	2.7	3.7	12.5
Overall Test Average	All Others	$1.3x10^1$ [1]	208.3	192.3[1]	192.3[1]

[1]-Only 1 filter holder was used during non-blank dynamometer tests of brake components, so the average of those values is presented for both holders.

Figure 71 presents the particle size distributions measured by the APS during the two tunnel blank experiments. The measured size distributions are generally similar to the brake component tests with a peak around 1.6-2 µm. The similarity in shape between the tunnel blanks and actual tests may be due to the exchange of particles deposited within the tunnel and the sample airflow; the particles from previous tests that adhere to the surfaces during “seasoning” may be entrained into the sample flow during the blank, leaving a similar size distribution even though the total counts are far less. Appendix L includes the tunnel blank measurements from the EEPS. The EEPS measurements during tunnel blanks showed approximately 50% of the counts measured during CBDC tests, and the normalized size distributions were similar between tests and blanks. For this reason, ERG and LINK believe that the EEPS size distribution is strongly affected by the distribution of ambient dust that can pass through the CVS intake filter.

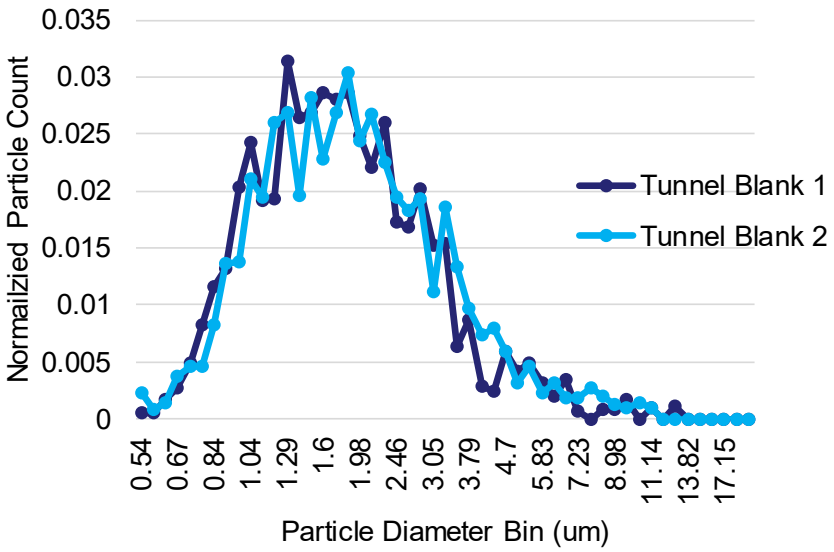

Figure 71. Size distribution of Tunnel Blanks as measured by APS

LINK also performed 6 zero blank experiments, in which filters were weighed, loaded into their respective sampling systems, then removed and re-weighted to determine any trends in weight gain or loss from handling. The weight gain of the PTFE filters during the 6 tunnel blanks averaged approximately 0.5% of the average weight gain measured in the PTFE filters during the CBDC tests. No corrections were applied based on the zero blank findings (as some filters gained weight and some lost weight during the zero blank process). The complete listing of zero blank results is presented in Appendix M.

Trends in Individual Brake Events

In addition to test level and phase level analysis, ERG also reviewed emissions for individual brake events. The QCM measured instantaneous mass and the CPC measured instantaneous particle count and findings of each are presented in this section.

For these analyses, event emissions for each measurement type are calculated as the sum of each deceleration event plus the emissions captured in the cruise or acceleration event following the braking. This segment is added to capture any emissions that might be released in the moments after the brake pressure is released and the friction materials move apart. The QCM data was processed similarly to the method presented in the Results by Speed Segment section; the QCM was used to estimate the emissions percentage of the 100S4-measured total PM2.5 across each brake event. These analyses present only findings for PM2.5 so no factor was used to estimate PM10. The CPC particle data was used directly as measured by the instrument.

ERG reviewed plots of the by-event emissions from both instruments as compared to parameters of the event, including the 4 parameters used in test cycle development. ERG reviewed emissions trends as a function of:

- Average vehicle speed during braking event
- Average event deceleration rate
- Brake rotor/drum temperature
- Brake event duration
- Total event braking energy
- Average event braking power

ERG reviewed plots of QCM and CPC data against each of the above parameters for every combination of model, axle, and pad material. No trends were apparent for deceleration rate, and a very weak trend was observed with temperature. Stronger trends were observed for speed, duration, energy, and power. This section presents the results overall for both measurement types across the five parameters in cases where trends were observed. In general, the QCM data appeared to have more noise than the CPC. The QCM appeared to have more noise in both measurement and time alignment. The time alignment noise is largely due to the QCM having a 1-minute time resolution during operation. This resulted in emissions responses that would appear to sometimes lead and sometimes lag the corresponding brake event, making complete time alignment impossible on a by-event basis (though brake events were typically on the order of 1 minute apart). In contrast, the CPC data responded favorably to time alignment. So, in the plots in this section, the CPC data has less overall observed noise. The following by-event plots include all braking events from all CBDC tests in this program. Note that all plots reflect single wheel emission rates.

Figure 72 presents the total brake event particle count against the braking event average speed. Power equation fits were performed by each friction material and are presented in the plot; the LM pads show the highest slope of the three materials. Figure 73 presents the corresponding plot for total event QCM-measured mass by brake event average speed.

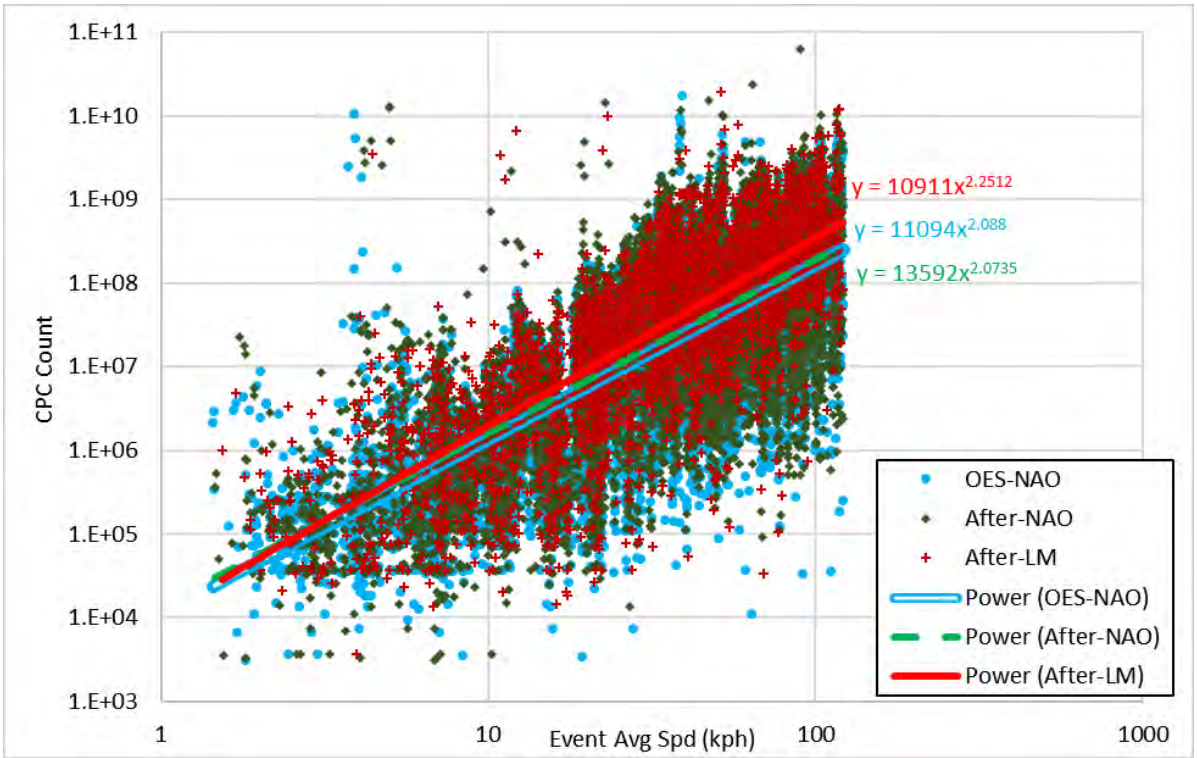

Figure 72. Trends in CPC count against braking event average speed, categorized by friction material

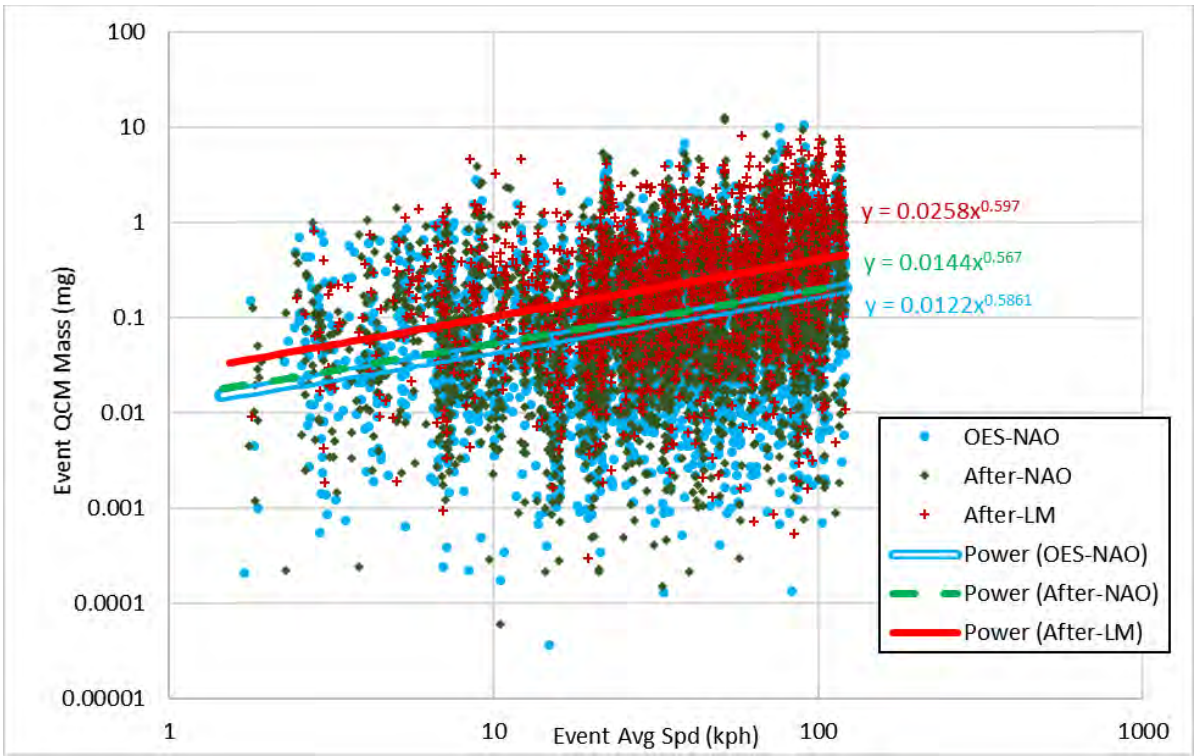

Figure 73. Trends in QCM brake event PM mass against braking event average speed, categorized by friction material

Figure 74 presents the total brake-event CPC count vs brake rotor temperature (note the linear scale of x-axis). Linear fits are applied to the data for reference and to indicate the gradual upward trend. The equations are not given, however, as the R^2 fits were all less than 0.05. Figure 75 presents the QCM-measured total brake event PM2.5 mass against average event rotor temperature. As with the CPC, linear trendlines are presented to show the very shallow increase in emission rate with temperature, but the fits have very low R^2 values. The temperature data in general did not show the level of responsiveness in emission rates as cited in literature. This is likely due to the relatively low temperatures used in this study (that is primarily intended to be representative of normal on-road use). The gradual uptrends in these plots may also be subjected to the confounding factor that the higher-temperature events are likely to be of higher intensity (since the rotor temperature is driven primarily by braking energy). So, it is difficult to draw meaningful conclusions of the effect of brake temperatures on on-road PM emission rates.

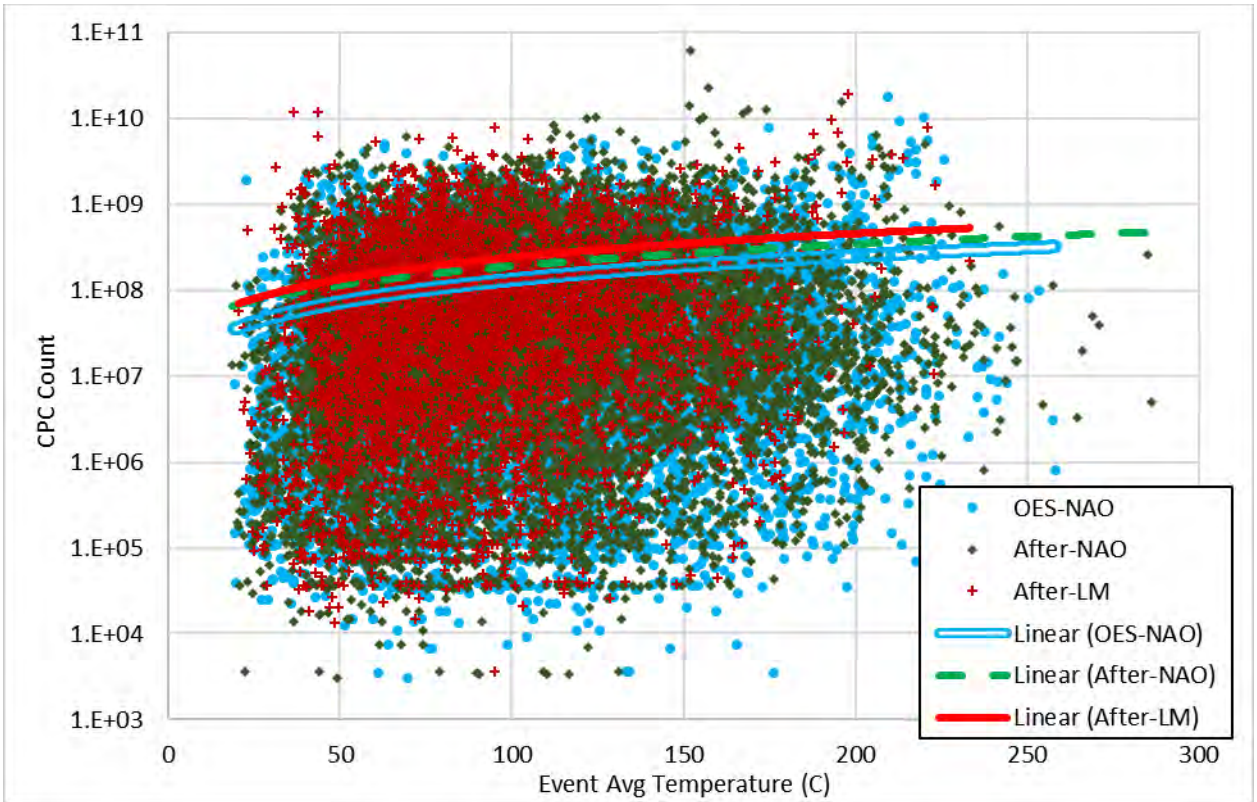

Figure 74. Trends in total braking event CPC count against average rotor temperature, categorized by friction material

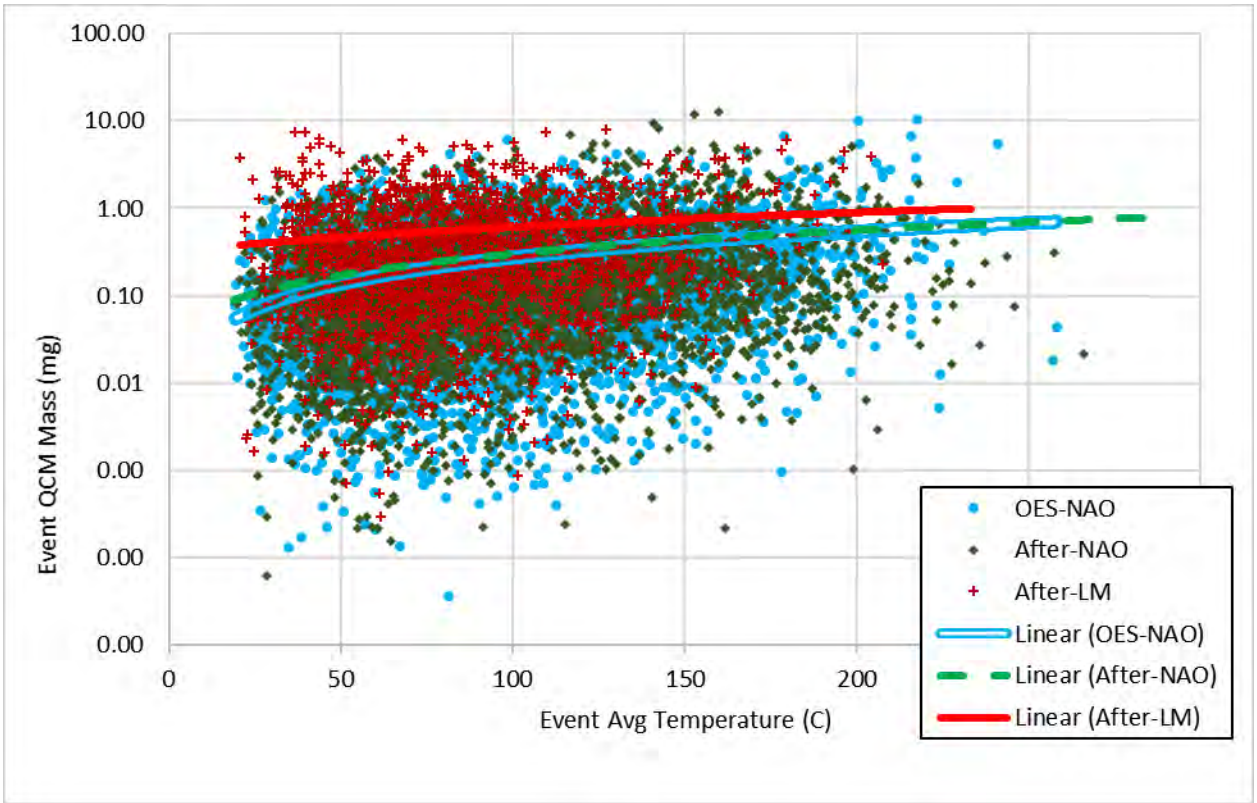

Figure 75. Trends in QCM brake event PM mass against braking event average rotor temperature, categorized by friction material

Figure 76 presents the by-event total particle count plotted against braking event duration. In this plot, it appears that there is less scatter in the data at the longer durations; however, it is likely that this is only because the events with durations over approximately 10 seconds are extremely rare in the tests performed over the CBDC. Analysis of the QCM -by-event PM mass data did not resolve an apparent upward or downward trend in emissions over duration, so that plot is not presented.

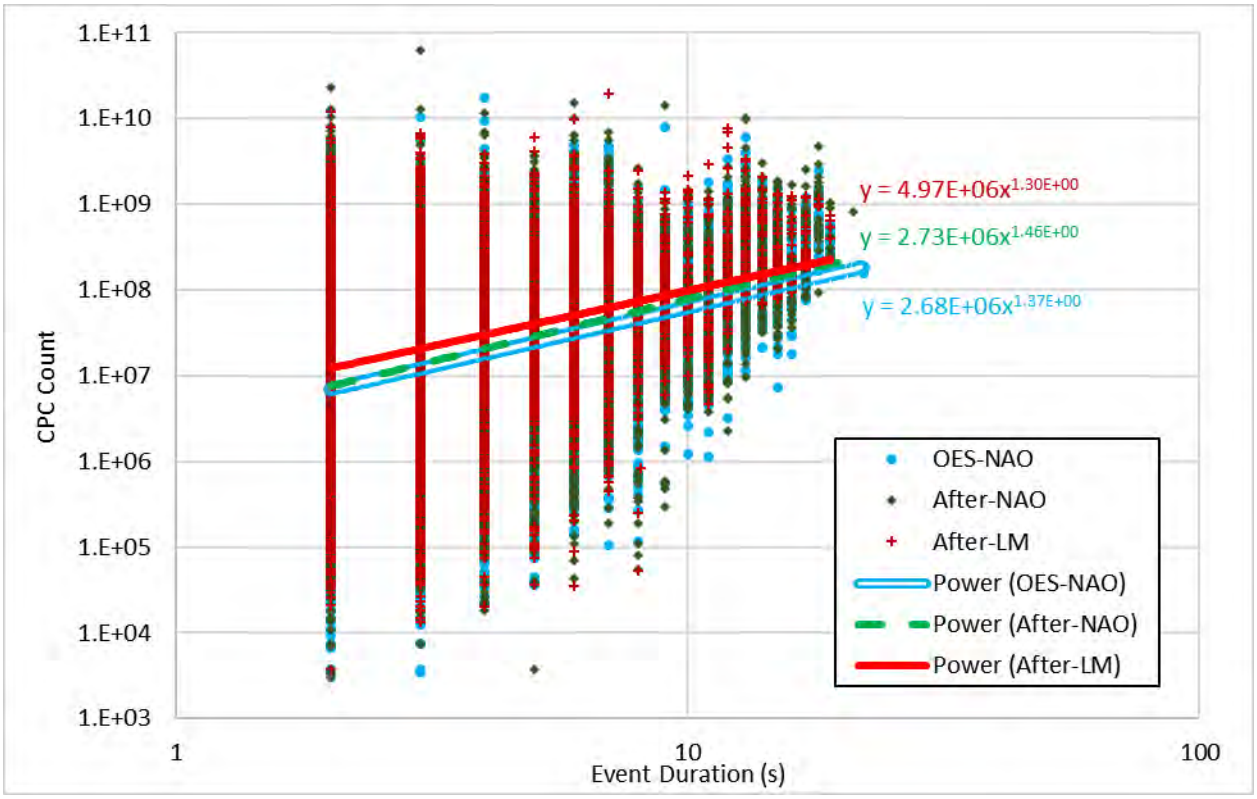

Figure 76. Trends in CPC count against braking event duration, categorized by friction material

Figure 77 presents the by-event total particle count against event total braking energy. The energy calculated in these plots does account for the differences in vehicle mass (it is not calculated purely on the speed change).

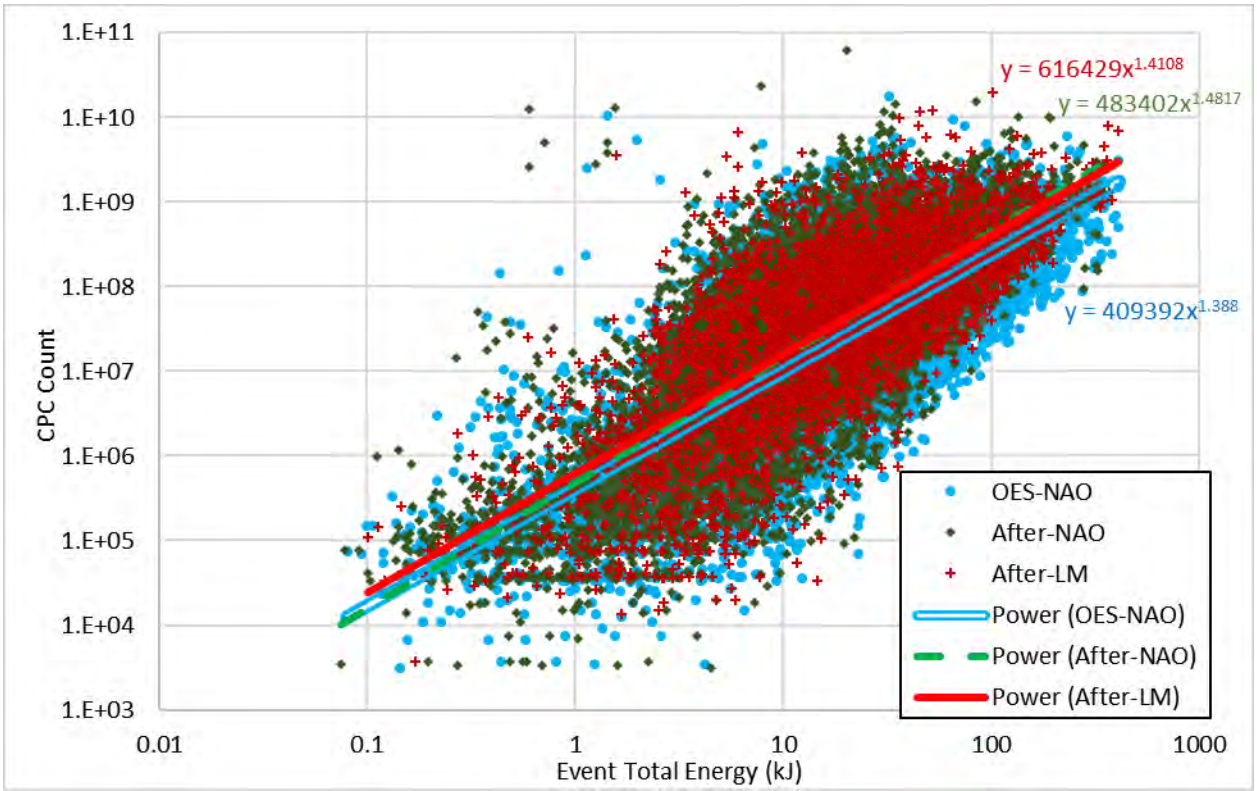

Figure 77. Trends in CPC count against braking event total braking energy, categorized by friction material

Figure 78 presents the by-event PM mass against the braking event total energy. As with the presentation of QCM mass against vehicle speed, it appears that the QCM was less responsive to total braking energy; this could be due to the noise in the instrument, especially in the time domain.

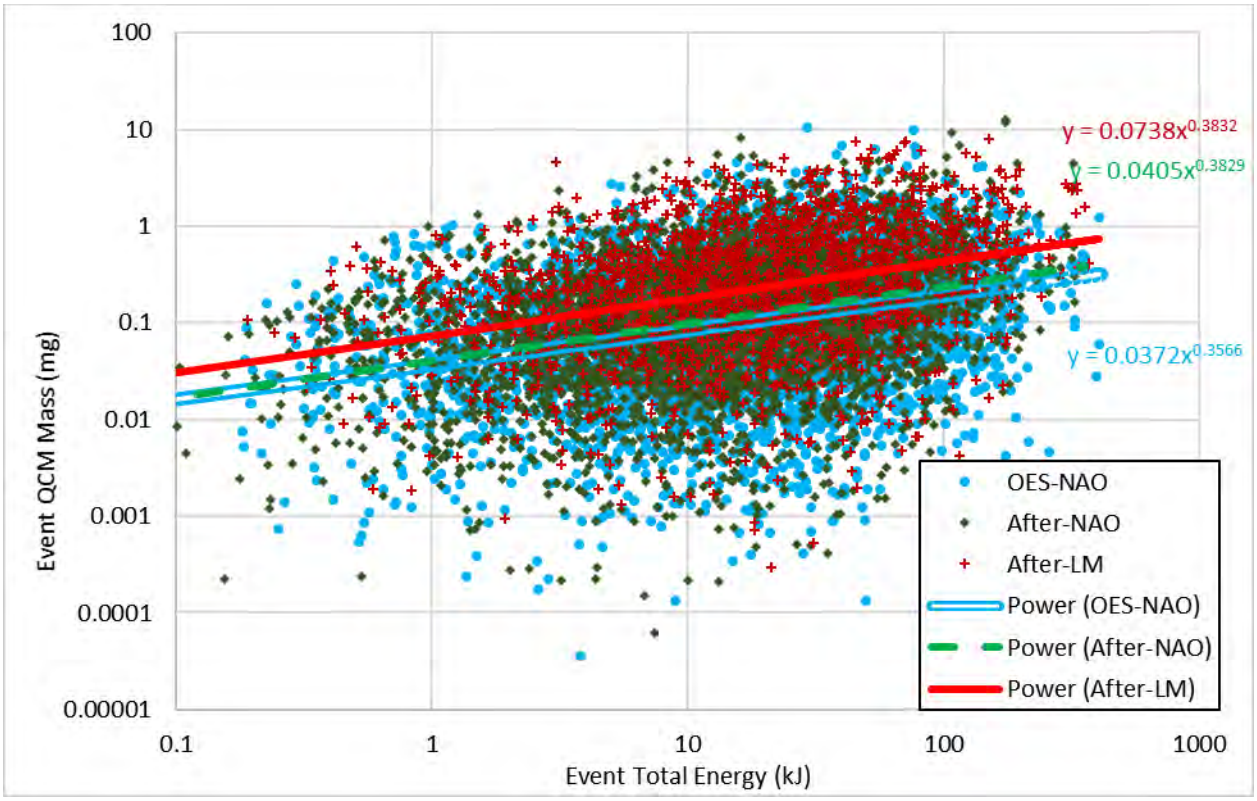

Figure 78. Trends in QCM braking event PM mass against braking event total energy, categorized by friction material

Figure 79 presents the by-event total particle number plotted against the average braking power for the event. It is interesting to see that the event duration, energy, and power all show identifiable responses in emissions. Given that the average power is the energy divided by the duration, it is not completely expected that power would also show such a clear trend.

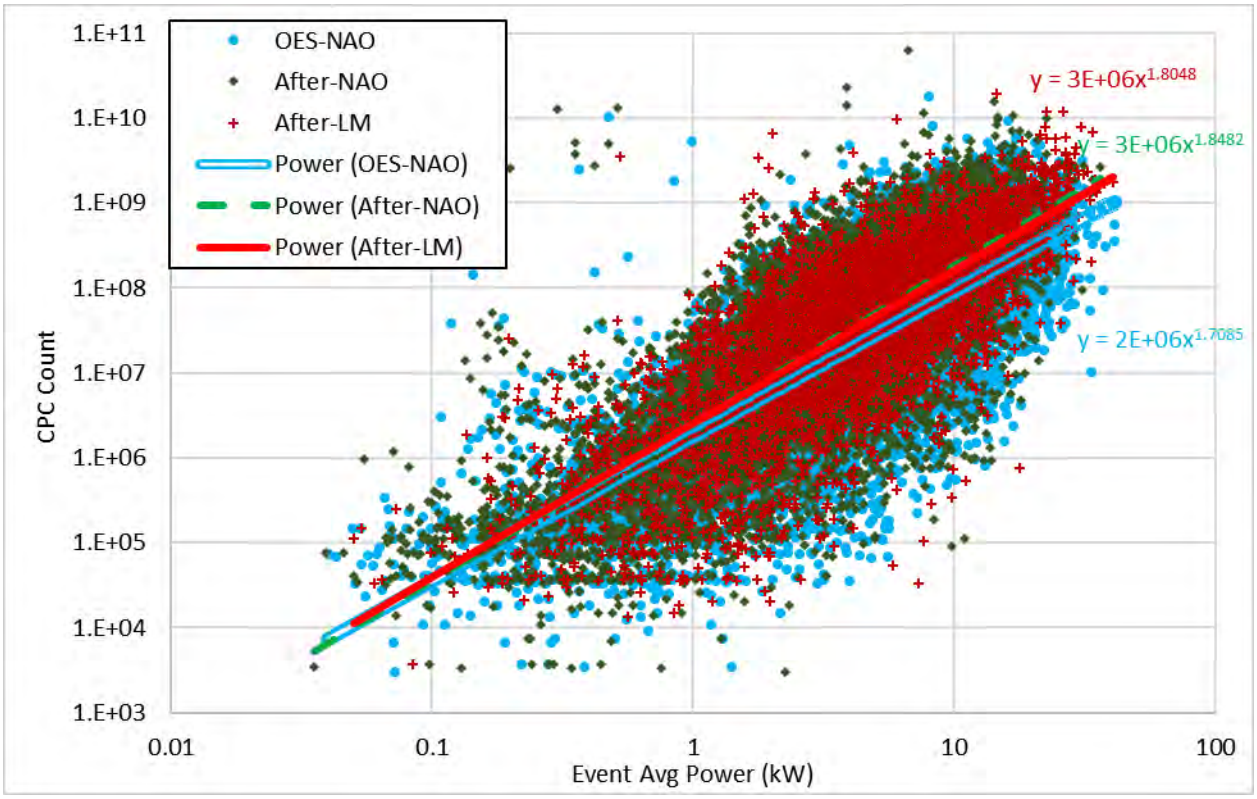

Figure 79. Trends in CPC count against braking event average braking power, categorized by friction material

Figure 80 presents the QCM-measured event PM mass against average braking event power. As with previous plots, the responsiveness appears reduced as compared to the CPC, but there are definite upward trends as shown in the power trendlines.

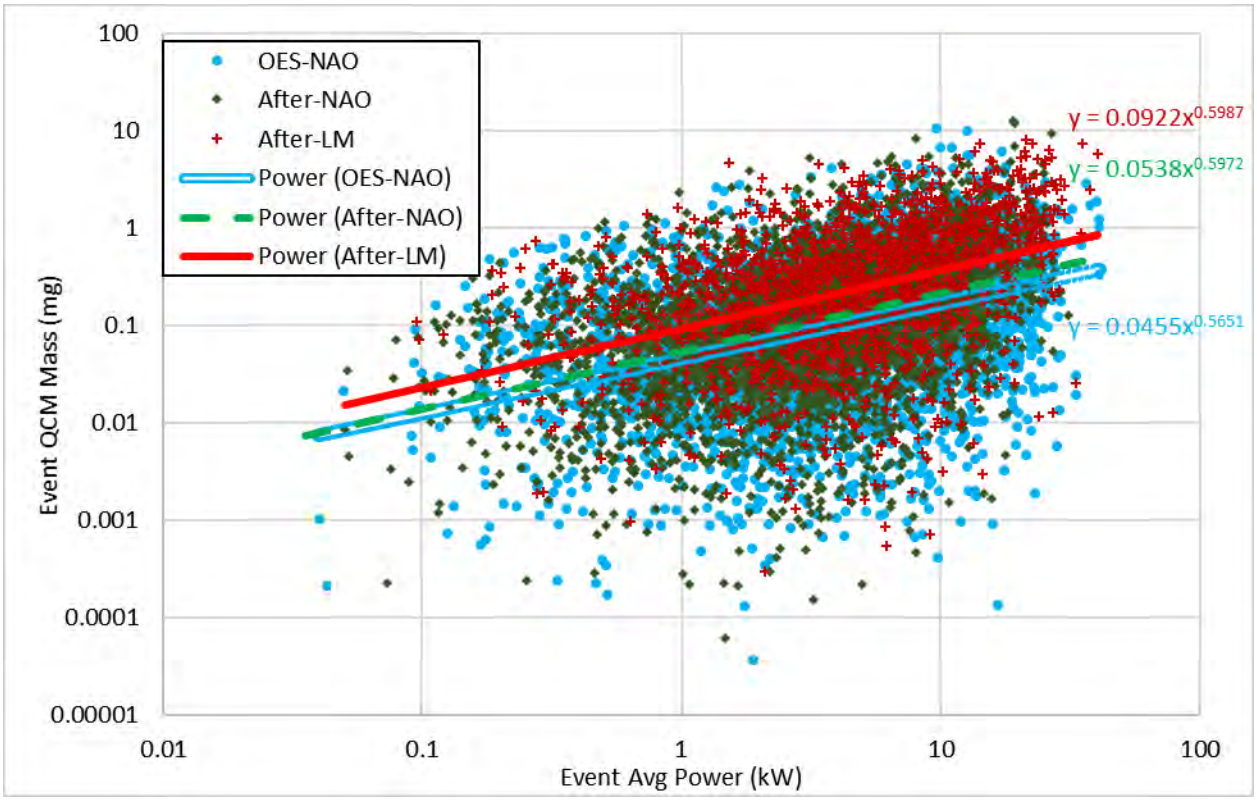

Figure 80. Trends in QCM brake event PM mass against braking event average power, categorized by friction material

It is not immediately clear what differences may have caused the relatively low correlation between emission rates and temperature in this work. Earlier studies, in which brake events were measured using matrix-style cycles instead of representative driving cycles, may have had a confounding factor that the type of braking events necessary to achieve high temperatures would necessarily be high energy events, and these two aspects were correlated in the previous works. There could also possibly be trends in temperature at brake temperatures greater than those encountered in this study, but the Caltrans data suggested that this would be encountered very rarely in on-road use. It is apparent that, of the parameters evaluated in this study, the energy and power are the most correlated to emission rates.

WTLP-Brake Tests

The test matrix included four tests over the WLTP-Brake cycle for the possibility of future benchmarking to other test programs that use that test cycle. Results are presented here primarily to allow for comparison between the WLTP-Brake and the CBDC results. Figure 81 presents a comparison of average emission mass results from

the CBDC to two replicate tests over the WLTP-Brake for each of the front OES-NAO friction materials for the Camry and F-150. The WLTP-Brake emissions for the Camry are approximately one third of that over the CBDC; while for the F-150, the results from the two cycles are much more similar.

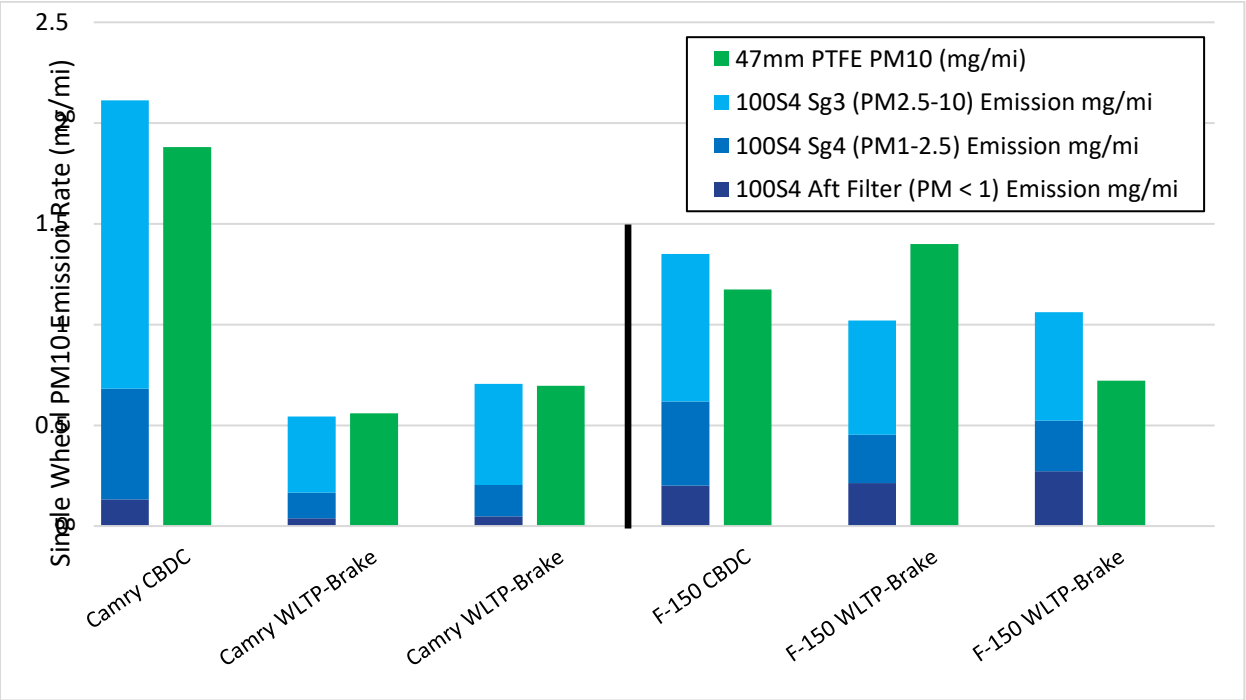

Figure 81. Comparison between the CBDC average results to replicate tests of the WLTP-Brake for the OES-NAO materials for the Camry and F-150 front axles

TEM Grid Loading

LINK attempted to collect sample on TEM grids using the Partector during almost all brake dynamometer tests. However, the system did not always successfully collect a fully loaded sample. Figure 82 presents results for each of the 75 TEM grid loading attempts; the x axis presents the time until loading was either manually or automatically stopped, and the y axis shows the indicated saturation level at the time sampling was stopped. Sixty six percent of the grids were loaded to more than 90 percent saturation, and half of the filters were loaded to 100 percent.

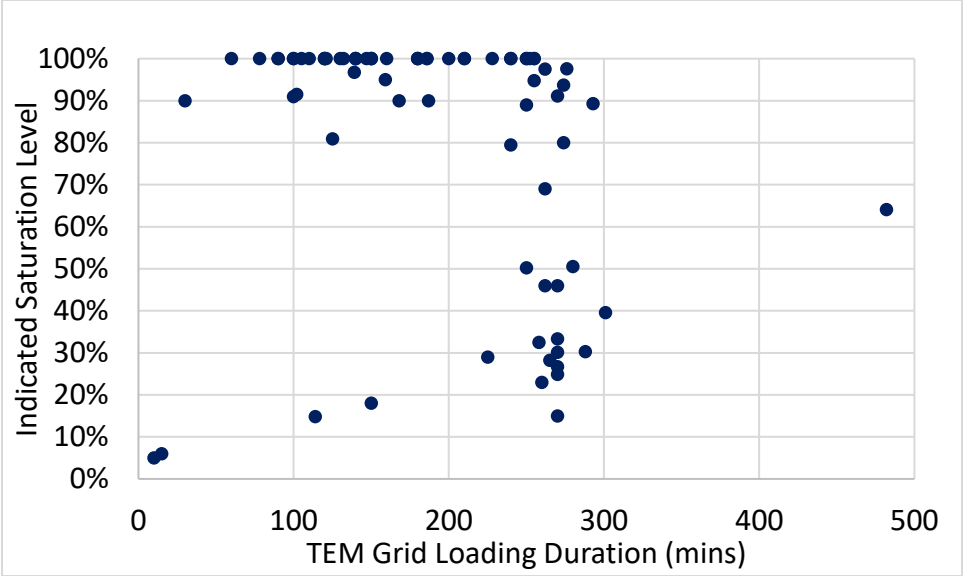

Figure 82. Partector-indicated saturation level plotted against the duration of loading time during the CBDC

Discussion

Brake dynamometer testing for drive-cycle based representative particulate emissions is a relatively new concept and few standard procedures existed at the time of the initiation of this project. During this project, ERG and LINK worked to modify existing exhaust emissions and brake durability testing procedures to create new appropriate and effective brake PM emissions test procedures. Some of these new procedures have already been adapted for use by the PMP within the EU's JRC as they develop brake PM related procedures in parallel with this work.

One early project goal was to be able to perform component installation, burnishing, emissions testing, and assembly removal within a 24 hour period. This goal was created to maximize the number of tests that could be completed within the limits of the project budget. This goal was achieved as LINK was able to conduct almost all tests within this amount of time, and LINK staff could keep a relatively consistent daily schedule throughout the work. In general, testing was reliable and no significant changes to the project plan were needed once testing began.

The results in the previous section show that the test setup was sensitive to the various parameters varied in the test matrix. The different vehicle platforms, brake pad materials, and test weights resulted in appreciable differences in PM mass emissions. This section aims to evaluate and discuss the experimental design, test methods employed, and test results.

Instrument Agreement in Mass Measurements

Generally, there was good agreement between the 100S4 and the 47mm Teflon filter mass measurement. Figure 83 presents a plot of the 100S4 vs the Teflon filter mass measurements, categorized by all emissions tests and the tunnel blanks. Note that two tunnel blanks were performed. In each, a single measurement of the 100S4 took place, and PTFE filters were placed in both legs of the filter system for parallel measurement. Both results for each blank are included as separate points with the same 100S4 value.

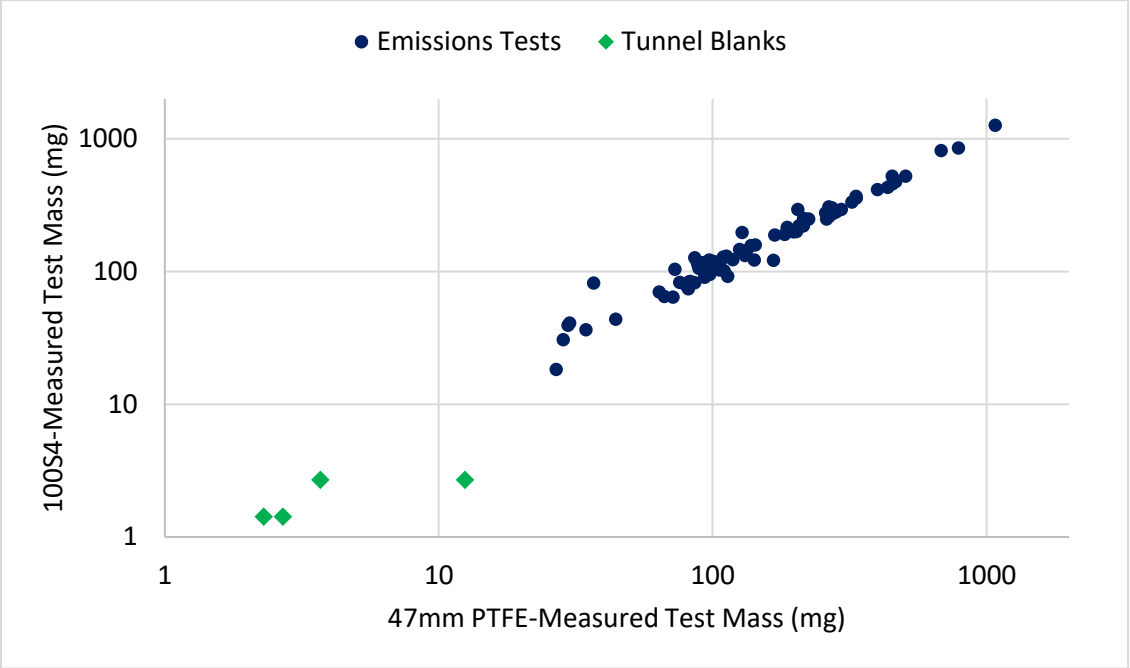

Figure 83. Agreement between 100S4 mass measurements (Y-axis) and 47mm PTFE mass measurements (X-axis) for all tests and tunnel blanks

Evaluation of the Burnish Procedure

The burnish procedure and dynamometer cycle were developed by ERG specifically for this work. The development of the cycle involved applying engineering judgement to early PMP burnish guidelines. This section is presented to evaluate the burnish procedure to determine the effectiveness of the cycle and inform any changes that may improve future testing. During burnish cycles, LINK operated the APS, EEPS, and logged brake temperature and hydraulic pressure data. LINK also ran the CPC during some burnish cycles but did not run that unit during all test days to reduce the amount of cleaning and maintenance required and prevent any delays to the test schedule. LINK did not run the QCM during the burnish cycle as that would have risked the unit becoming overloaded and losing data during the subsequent test cycle. So, plots of particle size, particle count, and the logged parameters of hydraulic pressure, speed, and brake temperature are available to evaluate the burnish cycle. For brevity, not all combinations of plots are shown; a representative plot is presented in this section for each vehicle model. The burnish cycle can be evaluated by determining where in the

cycle the measured values become stable (given that the cycle is made up of many repeats of the same speed trace)

Camry. Figure 84 presents the cumulative particle count measured during the burnish cycle on Test Day 59. This test day was the Camry rear assembly, equipped with aftermarket low metallic pads. The CPC trend stabilizes around 18,000 seconds into the test cycle (approximately 40% through the cycle).

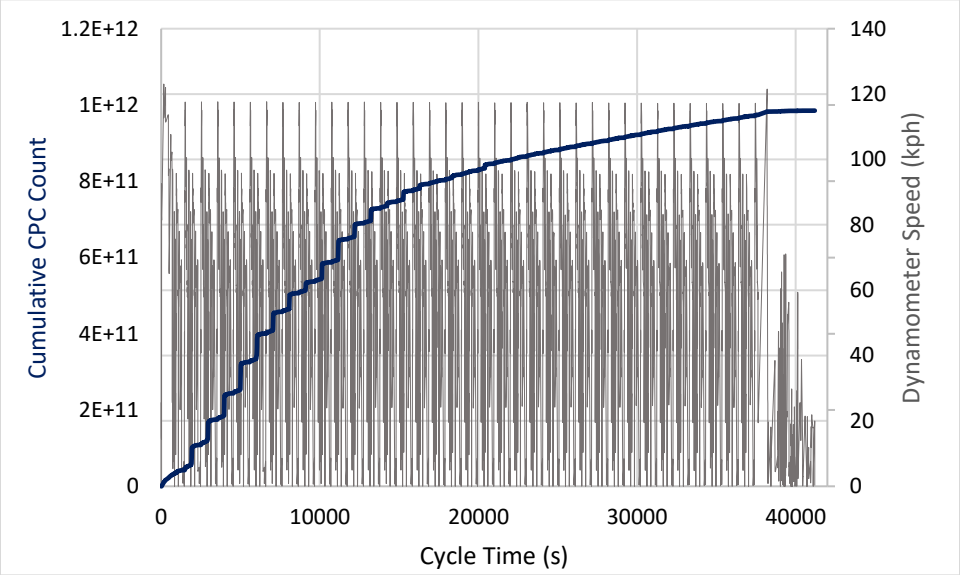

Figure 84. Cumulative CPC Particle Count Measured during a burnish of the Camry rear Aftermarket LM pads

Civic. Figure 85 presents the cumulative particle count measured during the burnish cycle on Test Day 84. This was a burnish of the Civic front assembly with OES-NAO friction materials installed. The particle count trend appears to stabilize at approximately 13,000 seconds (approximately 32% through the cycle).

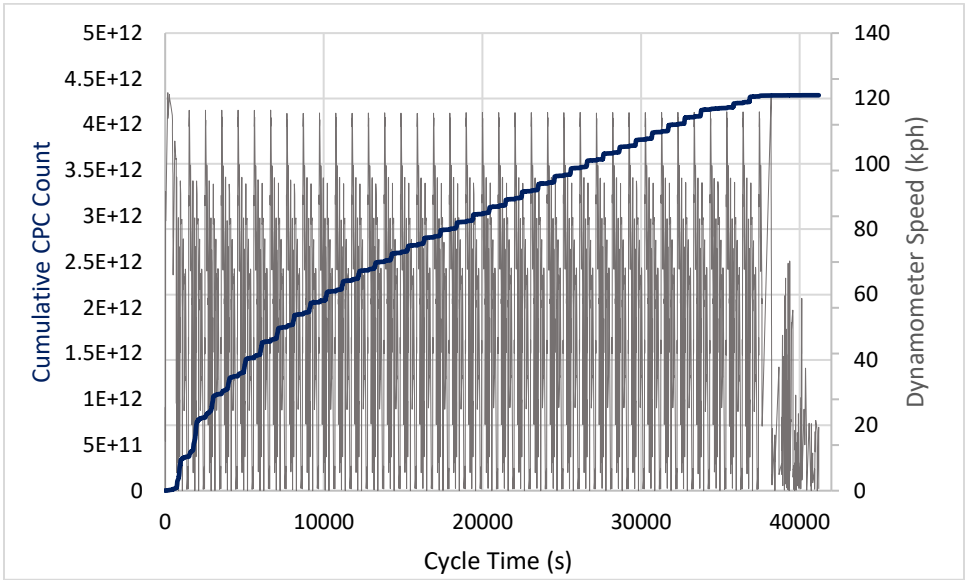

Figure 85. Cumulative CPC Particle Count Measured during a burnish of the Civic front OES-NAO pads

F-150. Figure 86 presents the calculated brake effectiveness over the burnish cycle of the F-150 front assembly during Test Day 63. Brake effectiveness is calculated by the deceleration torque divided by the brake hydraulic pressure and is proportional to the coefficient of friction between the pads and rotors. Each point on the plot represents the average effectiveness during a single braking event. This burnish took place with aftermarket metallic pads installed. The trend in effectiveness appears to stabilize at around 22,000 seconds (approximately 53% through the cycle). Note that the values are only an approximation of coefficient of friction and so they have a repetitive scattering across the different braking events. This is likely because there is some internal resistance in the hydraulic system that must be overcome such that the effectiveness is disproportionately lower in low intensity braking events (i.e. a larger proportion of the hydraulic pressure is used only to move the caliper pistons and pads prior to making significant contact with the rotors).

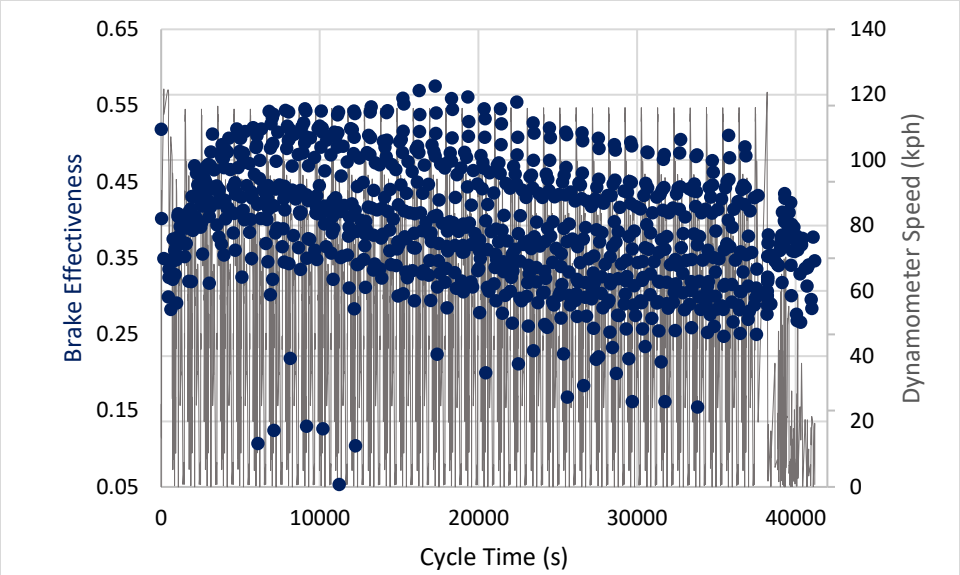

Figure 86. Calculated brake effectiveness (proportional to coefficient of friction) during a burnish of the F-150 front aftermarket metallic pads

Prius. Figure 87 presents the calculated brake effectiveness during the burnish of Test Day 49. This was a test of the front assembly with aftermarket-NAO friction materials installed. The effectiveness trend appears to stabilize at approximately 10,000 seconds into the cycle (24% through the cycle). The burnish of the Prius was a point of concern given that the burnish cycle was developed based on an assumed total amount of braking energy required. Given the simulation of the Prius' regenerative braking system, the friction materials for this vehicle did not receive the same amount of relative burnish energy as did the materials of the other vehicles. To further investigate this concern, Figure 88 presents another plot for the Prius, the cumulative particle count during the burnish for Test Day 27. This test day was a test of the rear assembly with OES-NAO materials. The figure indicates that the stabilization took place later in the cycle than that shown for the previous vehicles. It appears to stabilize at around 35,000 seconds (85% though the cycle. In future tests, to mitigate this potential concern, it may be beneficial to turn off the regenerative braking simulation during the some or all of the burnish cycle of regenerative braking-equipped vehicles.

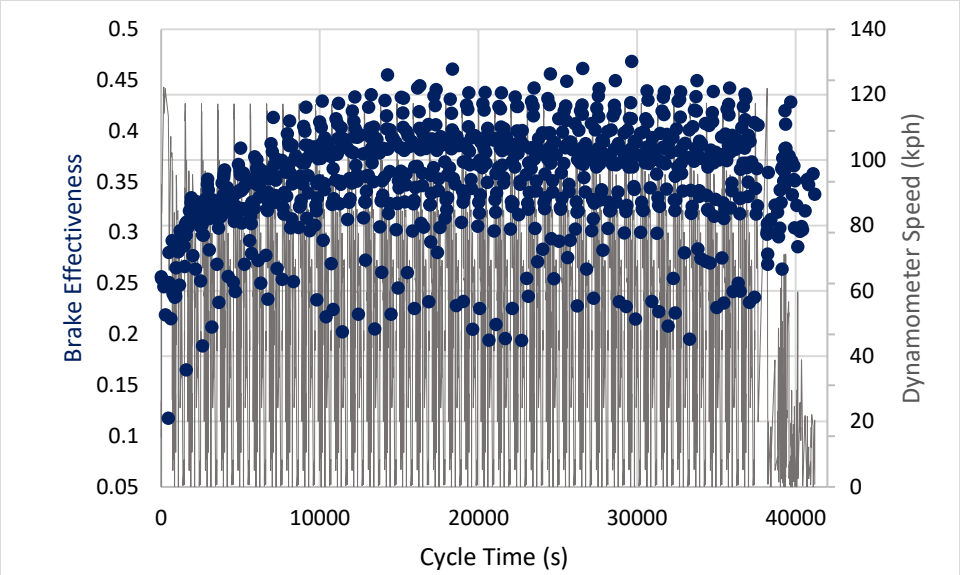

Figure 87. Calculated brake effectiveness (proportional to coefficient of friction) during a burnish of the Prius front aftermarket NAO pads

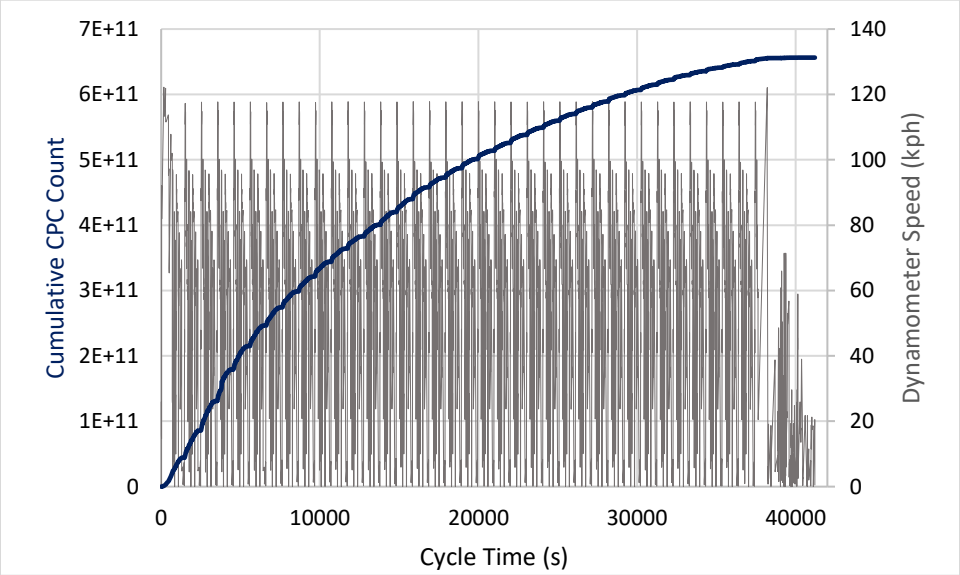

Figure 88. Cumulative CPC Particle Count Measured during a burnish of the Prius rear OES-NAO pads

Rogue. Figure 89 presents particle size data for the burnish cycle of Test Day 38. This test was a front-assembly test of the aftermarket-NAO pads for this vehicle. The APS size distribution (color coded by particle count) is the upper plot, and the EEPS side distribution (also color coded by count) is the lower plot. APS data appears to stabilize around 25,000 seconds (60% of the cycle), and the EEPS appears to stabilize around 30,000 seconds (73%).

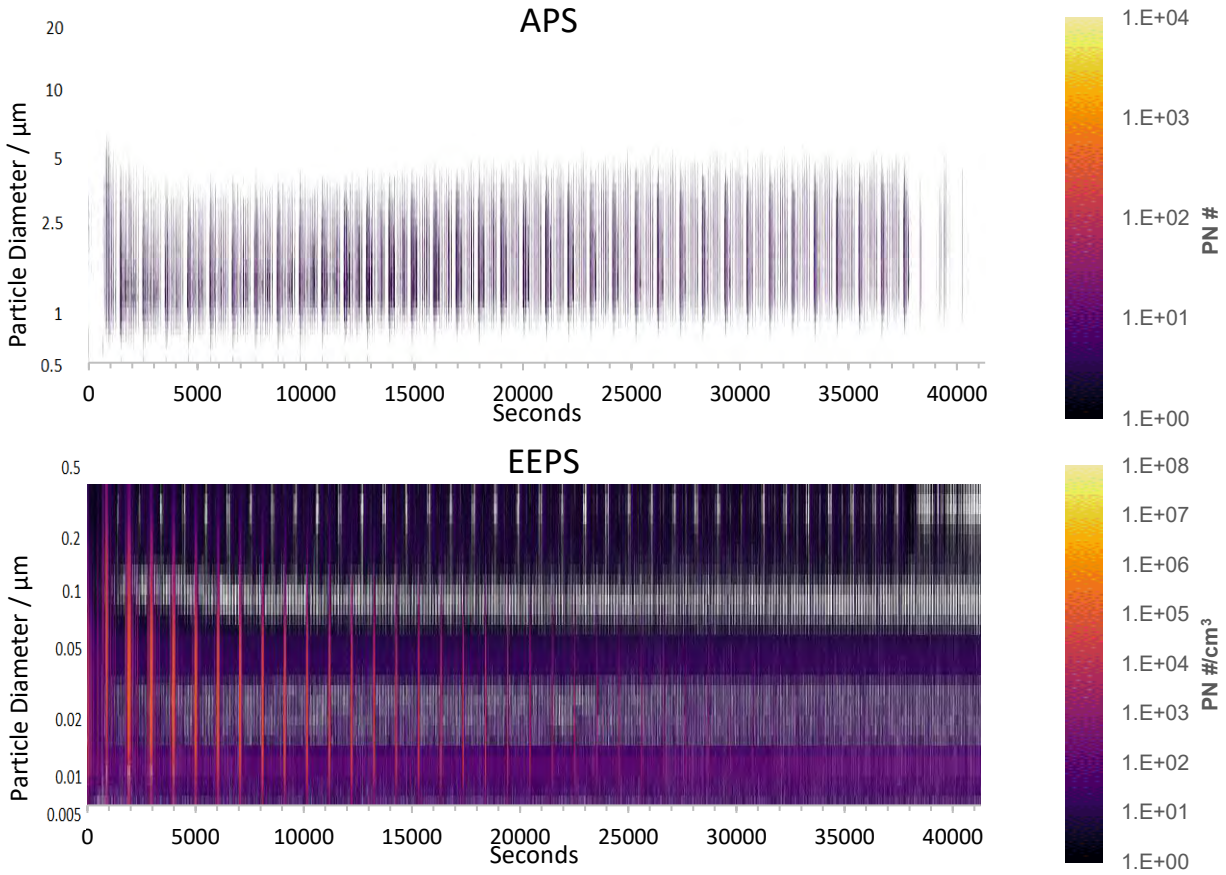

Figure 89. Particle size data during the burnish cycle of the Rogue front aftermarket-NAO pads. The upper plot presents the APS result and the lower presents the EEPS.

Sienna. Figure 90 presents particle size data for the burnish cycle of Test Day 13. This test was a rear-assembly test of the OES-NAO pads for this vehicle. The APS size distribution is the upper plot, and the EEPS side distribution is the lower plot. The APS data appears to stabilize around 20,000 seconds (49% of the cycle), and the EEPS appears to stabilize around 27,000 seconds (66%).

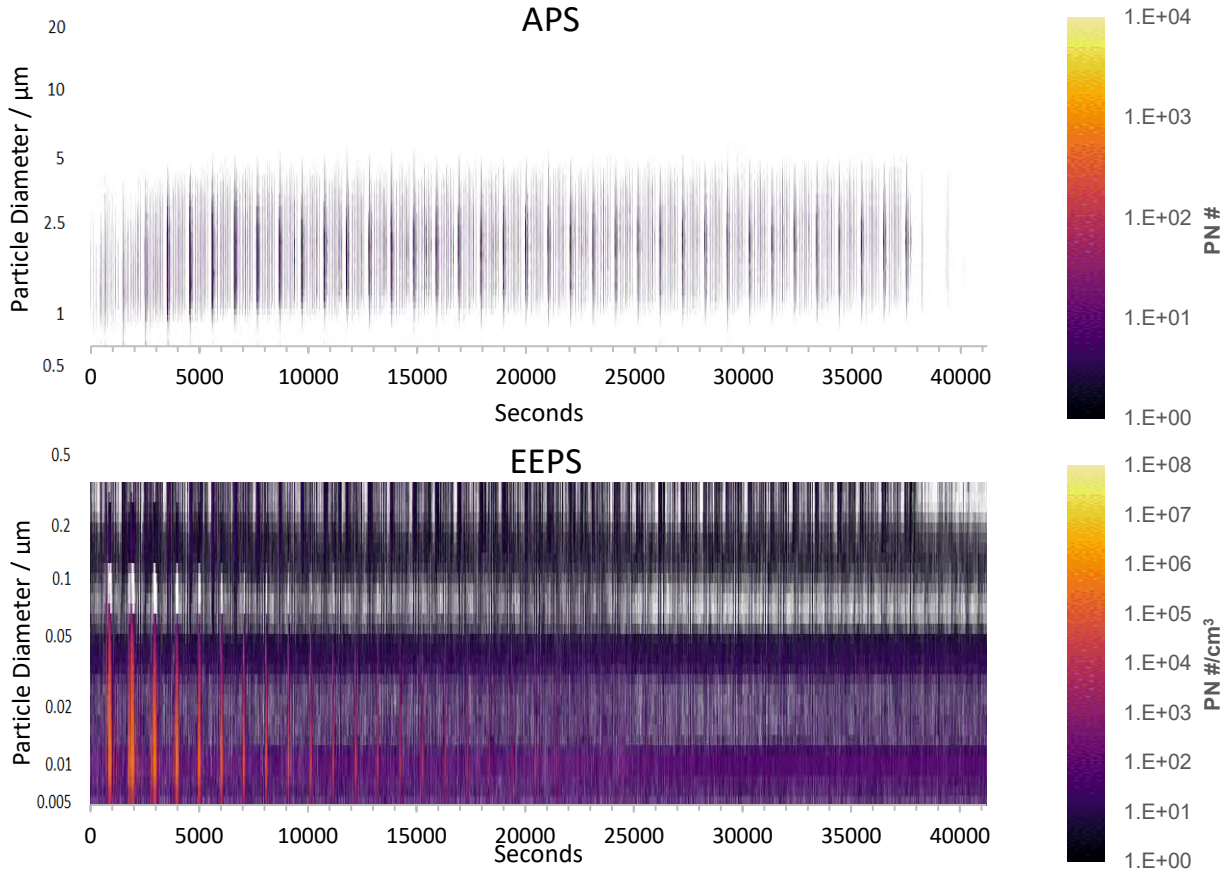

Figure 90. Particle size data during the burnish cycle of the Sienna rear OES-NAO pads. The upper plot presents the APS result and the lower presents the EEPS.

The burnish cycle appears to have included a large enough amount of braking energy for all friction materials to reach a stable condition from the various metrics presented in this section. The Prius rear assembly was a point of concern because it appeared to reach a stable level just as the burnish cycle was ending. This concern could be mitigated by disabling regenerative braking simulation during burnish of this type of vehicle in future testing. For all other vehicles, stabilization appeared to be reached at or before 30,000s into testing. So, the burnish cycle could potentially be reduced in length by up to approximately 3 hours and still achieve the desired level of stability for conventional-braking vehicles.

The CPC plots indicate that particle count emissions are elevated during the early stages of burnish after installation. Given that the duration of time that this elevated emission rate was observed (~5-6 hours typically), it is not likely that the burnishing process in-use has an appreciable effect on the overall emissions inventory given that

brake pads typically last for thousands of hours of operation, therefore this portion of brake service will not appreciably affect inventory values.

Evaluation of the Prius Regen Simulation

LINK used their internal 'DutyCycleRegen' program for the simulation of the Prius on the dynamometer. Given that brake dynamometer testing for emissions is a relatively new field, and the Prius (and most other regenerative braking equipped vehicles) operate using a proprietary algorithm, there is not a common or recognized procedure or approach for simulation of the regenerative system on a brake dynamometer. This section aims to evaluate the accuracy of the regenerative system used in this work. The Prius ETW was 1,606 kg in this work, and the Camry was the closest vehicle in weight at 1,668 kg ETW and so it is presented as the non-regenerative benchmark for comparison.

The first comparison is between the overall average brake torque measured during all dynamometer tests. Table 26 presents the overall average brake torque for Camry and Prius for front and rear assemblies. For direct comparison, only OES-NAO and Aftermarket-NAO pads are included (as the Prius was not tested with metallic pads). It can be seen that the Prius braking torque averages less than half of that of the Camry due to the simulation of the regenerative braking system.

Table 26. Comparison of Overall Average Measured Brake Torque for Camry and Prius

Test Vehicle	Avg. Front Brake Torque (nm)	Avg. Rear Brake Torque (nm)
Camry	138.4	48.3
Prius	55.9	20.5
Prius % of Camry Torque	40.4%	42.5%

Figure 91 presents an example instance of the source of the difference in torque trends between the Camry and Prius. The figure depicts a selected interval of the CBDC test cycle and presents traces of the speed and front brake hydraulic pressure for the two vehicles. The figure shows an example of how the hydraulic brake pressure differs during the same deceleration event, even approaching zero during moments that are most favorable to the regeneration system operation based on the regeneration parameters presented previously.

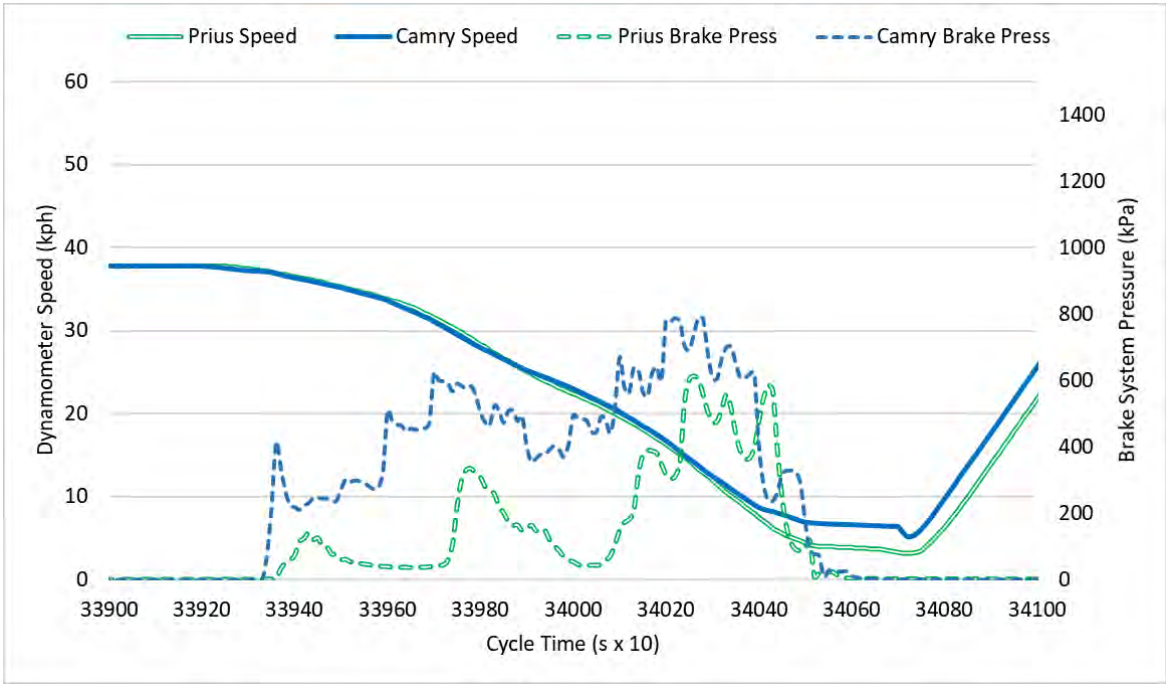

Figure 91. Speed and Brake Pressure traces for a selected point of the dynamometer test cycle for a test of the Camry and a test of the Prius

Another method to evaluate the accuracy and effectiveness of the regenerative system simulation is to make a comparison between the test track experiments and the dynamometer tests. On the test track, all models were driven over the WLTP-Brake cycle to inform the dynamometer cooling air flow setting process. During the cooling air flow setting, the WLTP-Brake Trip 10 was used as the test cycle. Comparing the brake heating trends between the dynamometer and the test track over Trip 10 can give an indication of the accuracy of the regenerative braking simulation. Figure 92 presents temperature traces for the front brake assemblies of the Camry and Prius operating over the WLTP-Brake Trip 10 on the test track and brake dynamometer. It can be seen that the rate of brake heating necessary to follow the same trace is much lower for the Prius than for the Camry. It can also be seen that the heating rates for the Prius are very similar between the test track and brake dynamometer, indicating that the regenerative simulation results in similar brake usage on the dynamometer as on the test track. Figure 93 presents similar data for the rear brake assemblies of both vehicles, and similar results are observed.

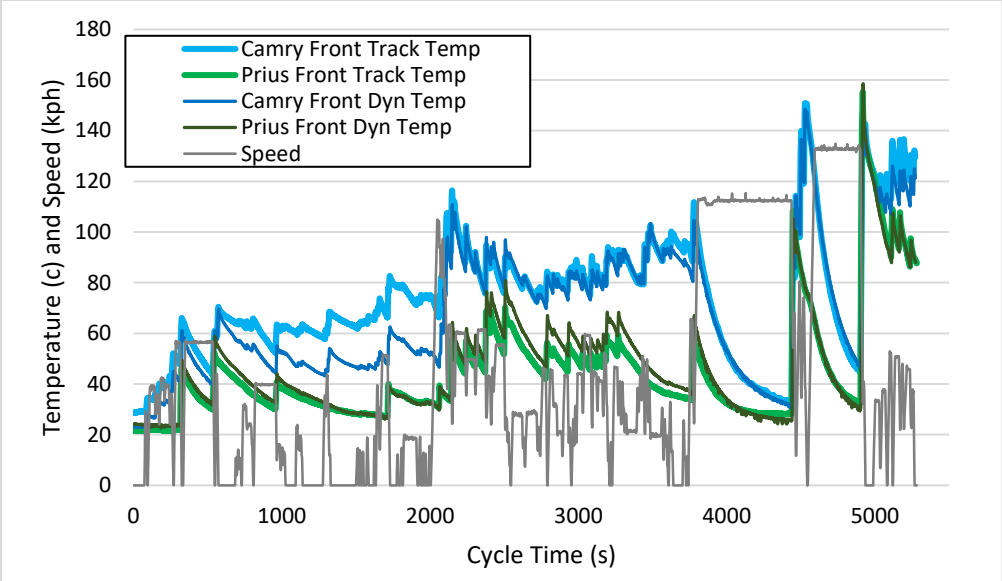

Figure 92. Temperature Traces of the Front Brakes of the Camry and Prius over WLTP-Brake Trip 10, operating on the test track and brake dynamometer

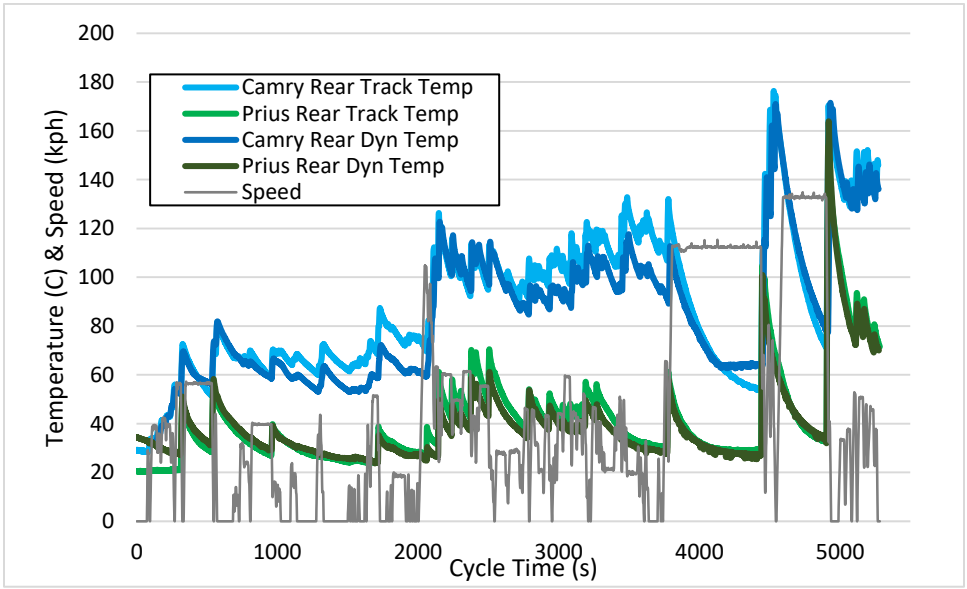

Figure 93. Temperature Traces of the rear Brakes of the Camry and Prius over WLTP-Brake Trip 10, operating on the test track and brake dynamometer

Reference Tests

The test matrix included additional replicate tests of one configuration to be run periodically throughout the program to potentially identify any sources of drift in the testing system. The reference test was chosen to be the front axle assembly of the F-150, equipped with OES-NAO friction materials and operating at ETW test weight. Figure 94 presents mass emission and particle count measurements by date. The original intent was to distribute the reference tests approximately equally throughout the

program, however the 4th test was swapped into the middle of the testing program due to a test that was scheduled as a WLTP-Brake being inadvertently run as a CBDC test and therefore matching the reference test parameters.

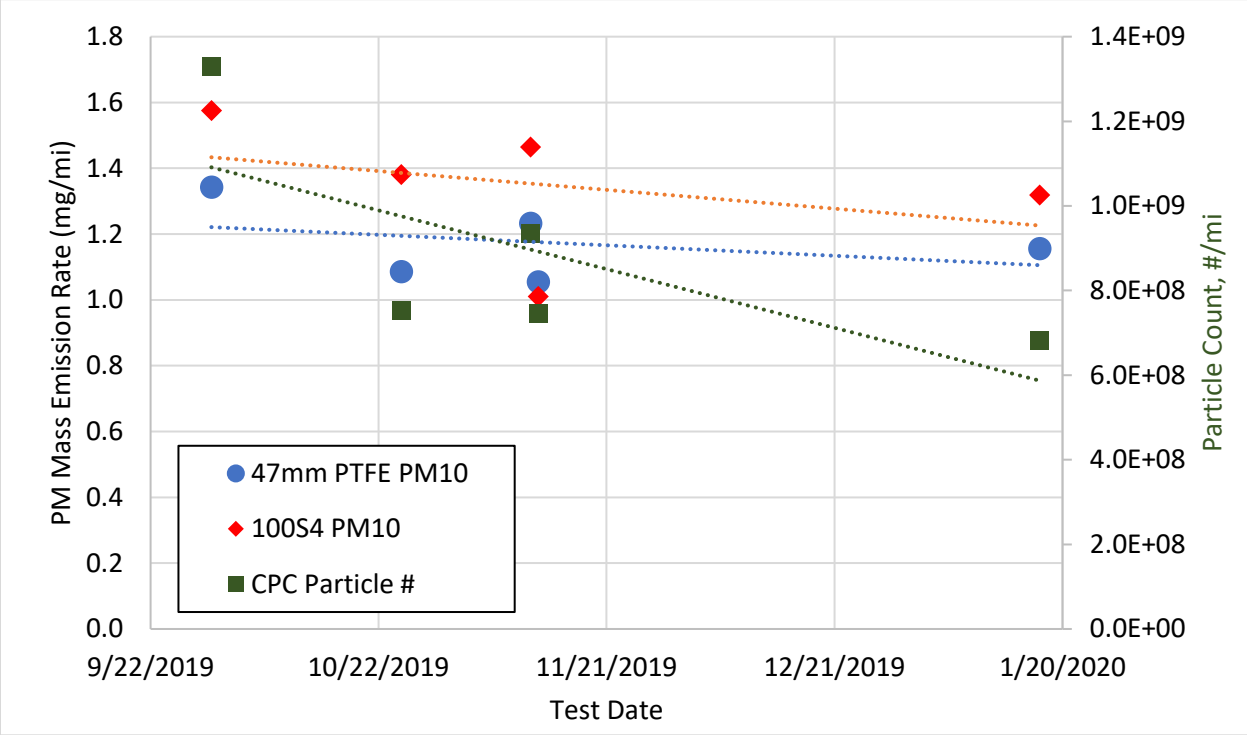

Figure 94. Reference trends by date for the 47mm PTFE and 100S4 PM10 mass measurements (left axis); and CPC particle count (right axis)

Trendlines fit to the test date are included for each of the three sets of values. Both mass measurement types have a minor downward trend over time. This appears to be driven primarily by the first test, which has the highest values for all three measurement types. From the time of the second test date, there is no discernable down trend in either mass measurement. The CPC trend has a steeper apparent down trend; the first value is the highest and the final value is the lowest. However, for both the mass and particle count plots, the noise in each variable appears to be equal or greater in magnitude than the strength of the trends. For this reason, ERG did not apply any corrections to the data based on test date.

Issues encountered

In early November, the humidity controller of CVS airflow loop failed, causing the humidity to eventually exceed the test limits (Limits are 50 +/- 10 %RH). LINK ordered a new control board to solve the problem. In the meantime, LINK continued running only the burnish cycle with the existing humidity controller for multiple upcoming tests without running the test cycle. This interim schedule lasted for approximately 1 week up until the humidity controller was repaired. After this, LINK re-mounted the previously burnished brakes, ran a partial burnish cycle (1 hour) to stabilize the contact surface of friction

couple, and measured emissions during the actual test cycle. *This issue resulted in slight downtimes to re-assemble tested parts and run the test cycle separate from the burnish cycle.*

LINK encountered another issue with the dynamometer control computer that aborted a test while conducting the burnish cycle. After troubleshooting this computer with limited staff during the holiday schedule, it was replaced with a new computer. *This issue caused approximately 5 days of delay in the test schedule*.

Comparison of Results to Literature

Studies in literature cite a variety of brake PM emissions test procedures and test cycles. As the concept of PM emissions testing for environmental protection is relatively new, there are few standard procedures and a wide variety of estimates of braking PM emissions factors. ERG reviewed a study that identified a range of published light-duty brake emissions rates.[11] This range of results, converted to mg/veh•mi for comparison to this study, is presented in Table 27. The results for this study tend to be lower in terms of PM2.5 and higher for PM10 than literature, though there is significant overlap in both sets of ranges.

Table 27. Ranges of vehicle-level PM emission rates (mg/mi), summarized in literature and for the vehicle models in this study

	Literature Range for Overall LD Emissions Factor (mg/mi)	Range of Emission Rates by Model in this Study (mg/mi)
PM2.5	1.3 - 3.4	1.0 - 2.7
PM10	1.9 - 5.0	3.3 - 13.9

Figure 95 presents a different review of past studies of brake wear emission rates of PM2.5 and PM10 for light- and heavy-duty vehicles.[12] The overlaid rectangles represent the range of emission rates by model in this study. In the figure, squares represent heavy-duty vehicles and circles represent light-duty vehicles. The figure shows a greater level of agreement with literature in terms of PM10 than the study in the previous table. However, the literature values are all higher than the range of results of this study for PM2.5. Notably, the findings from this study are lower in both PM2.5 and PM10 than values currently in EMFAC.

[11] Grigoratos, Theodoros & Martini, Giorgio. (2014). Brake wear particle emissions: a review. Environmental science and pollution research international. 22. 10.1007/s11356-014-3696-8.
[12] Sonntag et. al. *Modeling Brake and Tire Wear Emissions in Regulatory Models in the United States*, 2018 ISES-ISEE Joint Annual Meeting

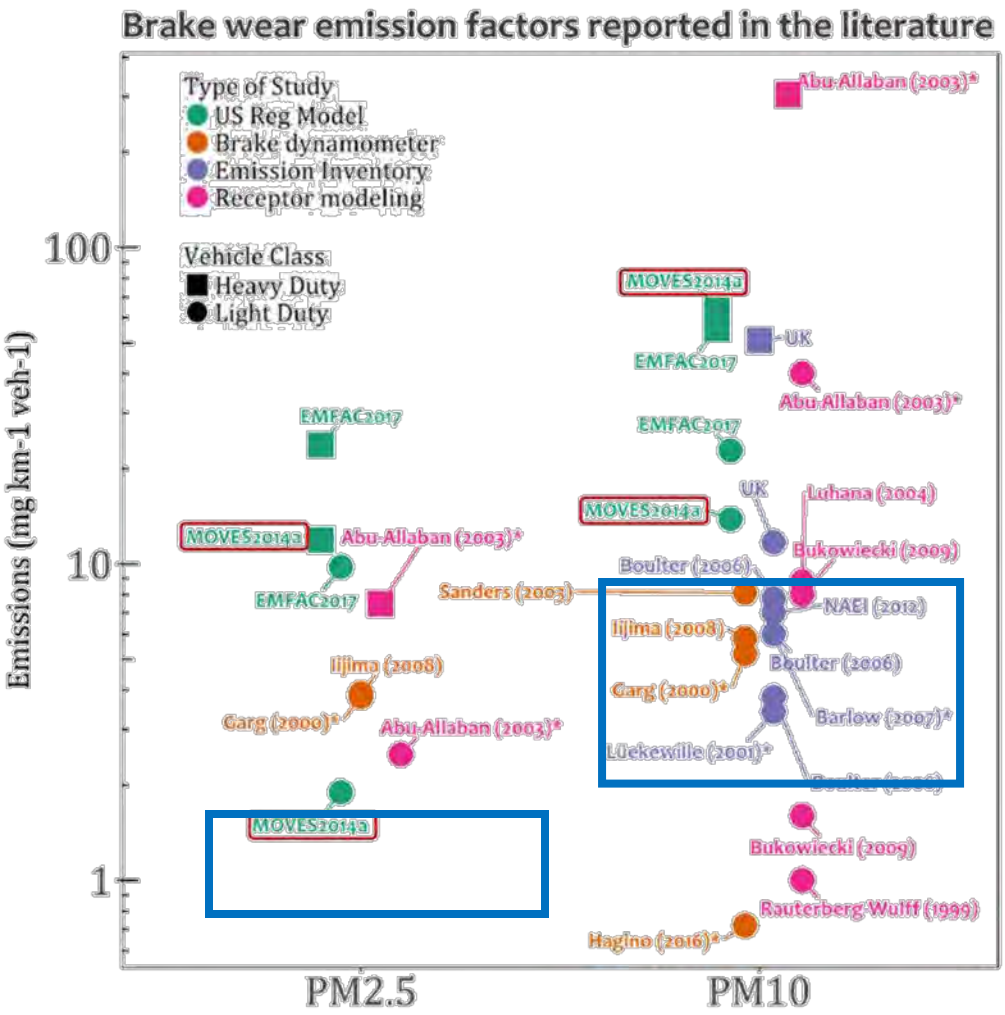

Figure 95. Various literature values for brake emissions, with the ranges from this study overlaid for comparison

PM emission rates cited in literature do appear to be trending down with time. Older emissions models may have been reliant on by-event type brake measurement with much higher temperatures (up to 400 °C), higher deceleration rates, and higher speeds. The prevalence of metallic friction materials is decreasing in the fleet with time and are therefore likely to be less prevalent in recent research. Also, friction material and rotor life has extended significantly in recent years, with current (OES and good quality aftermarket) formulations averaging 50-90k miles of life; based on the presented component mass loss vs PM emission plots, the longer life is indicative of lower PM emission rates.

Potential MOVES Emissions Factors

The Results section of this report presented emissions rates on the basis of grams per mile of represented distance traveled. For comparison to existing emissions factors in

MOVES, however, it is useful to present the emissions measured over the test cycle on a time basis. The Test Cycle Development section introduced the concept of the CBDC's represented distance, which is the distance of actual on-road travel that is represented by the braking events in the cycle when accounting for cooling and extended on-road cruises that were abridged to minimize the time required to run the cycle on the dynamometer. Just as the events that make up the CBDC have a represented distance, they also equivalently have a represented time, both for the overall cycle and for each speed segment. These times, along with the represented distances, are presented in Table 28 (in U.S. Customary units) for the Overall CBDC and the speed segments as well as the resulting calculated average speed. These values can be used to convert the previously given emissions per distance traveled to a time basis representing an overall trip.

Table 28. Represented time and represented distances for the overall CBDC and each speed segment

Cycle/Segment	Represented Distance (mi)	Represented Time (s)	Represented Average Speed (mi/hr)
CBDC Overall	81.56	11,564	25.39
0-21 kph	3.83	2,911	4.73
21-69 kph	47.31	5,438	19.46
69+ kph	48.33	3,215	54.12

For comparison with MOVES factors, however, it is of more interest to isolate the analysis from the overall test cycle (i.e. driving trip) down to time spent in actual braking. MOVES has various operational modes (Opmodes) for the purpose of binning emissions rates depending on the activity of a vehicle during a given second of operation. Some of the main opmodes are those for cruise/acceleration, which bin emissions factors based on the instantaneous level of engine power output on a vehicle-specific power (VSP) basis. MOVES also has a single opmode for braking, opmode 0, In general, the braking opmode is active when modeling deceleration rates either greater than 2 mph/s over 1 second or greater than 1 mph/s over 2 continuous seconds (the braking opmode also includes provision for braking over road grades equivalent to those levels of deceleration, however this project did not include any simulation of road grade). For comparison to MOVES, it should be noted that the CBDC was limited to not include any 1s or 2s braking events.

For comparison with the MOVES Braking opmode, braking emissions in this work must be presented as the total cycle emission rate divided by the total number of seconds of braking. For the CBDC, the conversion from mg/mi to mg/s (of braking) can be performed by multiplying by the factor of 0.052 [$mi/s_{braking}$], which is the cycle represented distance divided by the 1564 total seconds of braking in the CBDC. For this approach, it is not necessary to consider the cycle represented time, only the seconds of braking as the CBDC contains actual in-use braking events representative of real-world operation. However, the cycle does include some low-deceleration braking that would not fall into the requirements of opmode 0. The in-use data indicated that very light braking was performed frequently (even if accounting for vehicle coastdown deceleration rate). For this reason, approximately 60% of the braking events in the

CBDC falls in the category of opmode 0 and the remaining braking takes place at a deceleration rate less than 1 mph/s (Figure 14 presented the distribution of deceleration rates for the CBDC, note the units of that distribution are in kph).

Table 29 presents the vehicle-level emission rates on the basis of mass per second of braking. These values are based on the emission rates given previously in Table 22, corrected based on the factor of represented distance divided by seconds of braking. Values are presented based on measurements made by the 100S4 system so that factors can be generated for both PM2.5 and PM10. The values in the tables are based on batch gravimetric measurements made over the entire CBDC. Given that the test cycle is built specifically to reflect actual in-use light-duty braking, this is an appropriate approach for comparison to MOVES emissions factors. Appendix H, referenced earlier, includes overall tabulated test results including the average PM emissions rates per second of braking for each individual test.

Table 29. Estimated in-use brake emission rates per unit time of braking by model

Model	Estimated PM2.5 Emission Rate per Second of Braking (mg/s)	Estimated PM10 Emission Rate per Second of Braking (mg/s)
Camry	0.089	0.486
Civic	0.057	0.296
F-150	0.106	0.512
F-150 HLW	0.133	0.723
Prius	0.050	0.174
Rogue	0.102	0.478
Sienna	0.109	0.514
Sienna HLW	0.141	0.723

The average of the vehicle models in the table correspond to approximately 0.35 g/hr, which is somewhat lower than the MOVES2014 average PM2.5 braking emission rate of 0.558 g/hr.[13] However, a simple unweighted average of the vehicle models used in this program is not necessarily representative of the vehicles represented by MOVES; it is likely that lighter-weight and regenerative-braking equipped vehicles are overrepresented in this average as compared to the in-use fleet. Given that the test cycle represents in-use driving weighted appropriately across trip average speeds in-use, it is preferable to use these cycle-level emissions rates for comparison to existing MOVES factors as compared to the continuous measurements of the QCM system. This also has the co-benefit of minimizing the effect of the greater error level of the QCM system as compared to the 100S4.

[13] US EPA. Brake and Tire Wear Emissions from On-road Vehicles in MOVES2014. EPA-420-R-15-018, November 2015.

Informing Braking Emissions as a Function of Negative VSP

The Trends in Individual Brake Events section presented total event emission rate against various parameters such as deceleration, temperature, and power. To further inform brake modeling on a basis comparable to MOVES, it was also of interest to present the continuous emissions measurement data on the basis of emission rate per second plotted against VSP. Figure 96 presents the CPC-measured particle number emission rate (#/s) plotted against brake event averaged VSP (kW/ton) for all brake events in the test program. Points are colored by friction material and power fits are presented for each material.

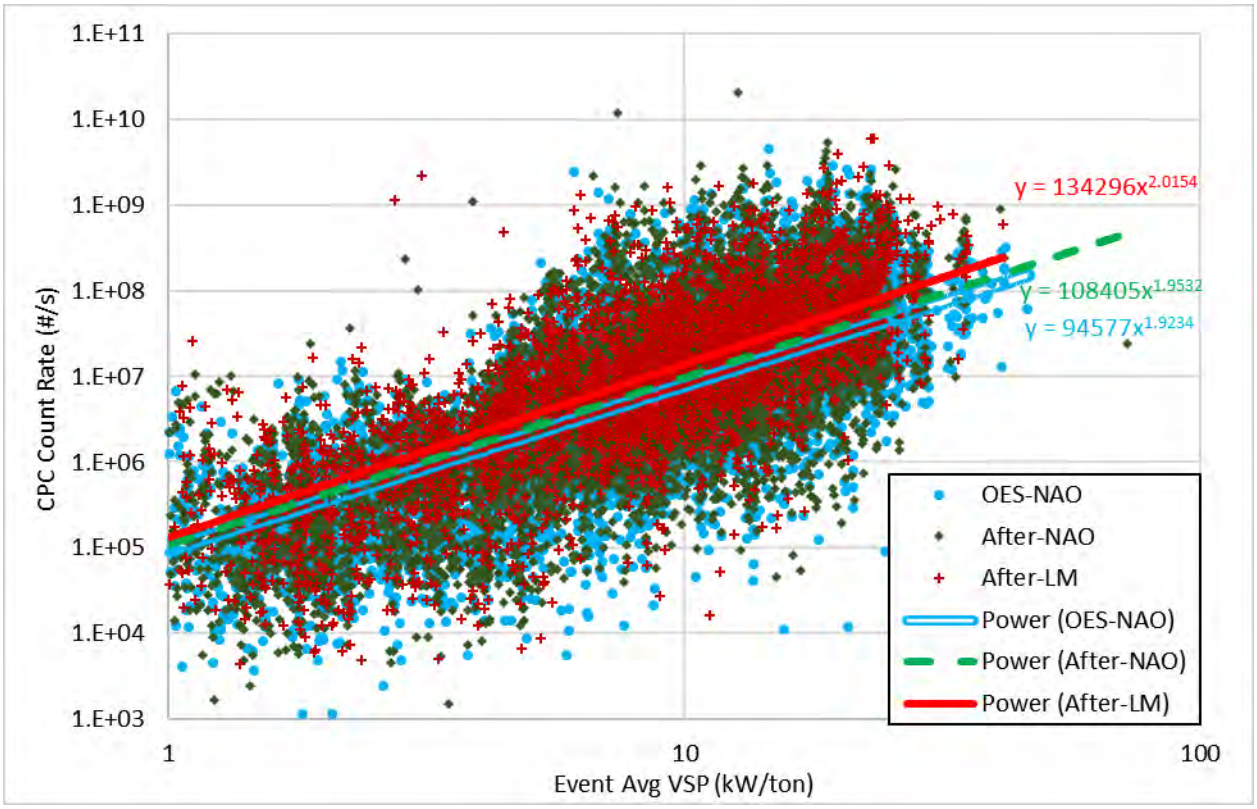

Figure 96. Particle number emission rates vs brake event average VSP for all braking events in the test program. Power fits are shown by friction material type

Similarly, Figure 97 presents the equivalent plot for the QCM measurements; PM2.5 mass emission rate (mg/s) is presented against event-average VSP. Power fits are presented for each material type. This type of analysis may be useful in informing the potential to expand the MOVES braking opmode into multiple negative VSP bins in a manner that is similar to the current cruise/acceleration VSP bins.

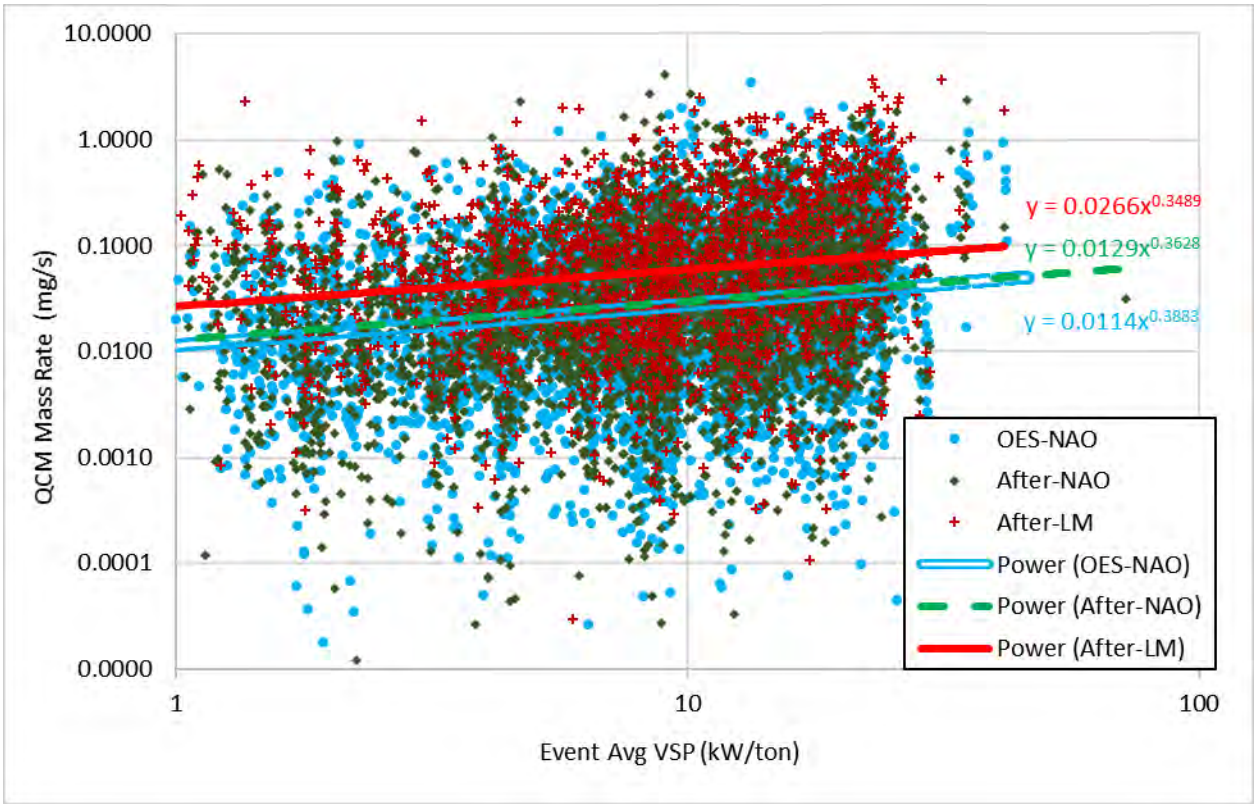

Figure 97. QCM-measured PM2.5 mass emission rate vs brake event average VSP for all braking events in the test program. Power fits are shown by friction material type

Modeling Emissions Deterioration

This study involved testing friction materials that were relatively new; they were purchased new, operated over an aggressive burnish cycle, and then were tested over the CBDC. As a result, the project did not generate emissions measurements indicating the deterioration of friction materials over time. Even if that effect had been quantified, vehicles periodically have their friction materials replaced with completely new components as the vehicle ages, potentially "resetting" the brake PM emission rates as compared to the age of the vehicle. However, the trend in change of installed friction materials was presented in the Representative Test Vehicle and Friction Material Selection section. Trends in the change in installed friction materials over time can potentially be used to estimate deterioration rates in braking PM emissions as vehicles age. LINK business intelligence was used to estimate the balance of materials at vehicle ages of 3 and 11 years, which were presented previously in Table 21. The business intelligence was based on vehicle age in years, and fitting a linear trend based on emission rates by material yields yearly deterioration rates as given in Table 30. These rates can be multiplied by the modeled vehicle age in years to adjust the previously presented emission rates (which were estimates for 7-year-old vehicles). Note these adjustment factors are based only on the estimated changes in installed friction materials as vehicles age. To estimate new-vehicle levels, these factors could be multiplied by 7 (years) and subtracted from the Table 29 emissions rates. Or, for older

vehicles, they could be multiplied by the number of years older than 7 and added to the estimates.

Table 30. Estimated Deterioration Rates Based on Friction Material Trend with Vehicle Age

Vehicle Type	PM2.5 Deterioration per year (mg/mi/yr)	PM10 Deterioration per year (mg/mi/yr)
Conventional Passenger Car	0.004	0.056
Light Truck	0.037	0.209
Regenerative-Equipped	0.003	0.005

Summary and Conclusions

This report presented the results from PM emissions testing of light-duty brake assemblies operating on a brake dynamometer. A new brake dynamometer test cycle was developed to represent the operation of real-world vehicles in California based on the Caltrans dataset. ERG adapted a previously developed algorithm to develop a test cycle that would be as similar as possible to the speeds, deceleration rates, temperatures, and braking durations encountered by real vehicles in the Caltrans survey. This new cycle was divided into three speed bins such that emission rates could be differentiated across different ranges of trip average speeds.

Six test vehicles (with common cross-platform brake components) were selected to represent the range of vehicle types in the light-duty fleet. Up to three different friction formulation types were tested for the front and rear assemblies of each model. Replicate tests were conducted for each test matrix combination.

The LINK lab site included a constant volume sampling (CVS) system with an integrated brake dynamometer. Measurements were made in batch and continuously by a variety of instruments including gravimetric sampling in parallel on coated aluminum impactors (TSI 100S4) as well as on 47mm Teflon filters. Instrumentation was also installed to measure particle size distributions, particle counts, and continuous particle mass.

Results were presented for emitted PM mass, particle count, and size distribution from the front and rear assemblies of six test vehicles. The test procedure developed for this work was able to resolve effects on particle mass emissions from the various parameters varied in the test matrix. Particulate mass emissions on a per-wheel-mile basis ranged from approximately 0.5 mg/wheel•mi for the Prius rear brakes operating at ETW with NAO pads up to 15 mg/wheel•mi for the front brake of an F-150 operating with a simulated cargo load and equipped with a low metallic friction material.

In most cases, low metallic friction materials resulted in higher mass emissions than NAO materials. Vehicles tested at higher simulated weights also tended to have higher mass emissions. For a given friction material type, PM emission masses trended linearly with vehicle test weight. Figure 98 presents the average by-vehicle emission mass vs test weight for each vehicle and test weight combination. The F-150 reference

vehicle tended to have relatively low PM emissions for its vehicle weight when equipped with OES friction materials (as compared to the other vehicles).

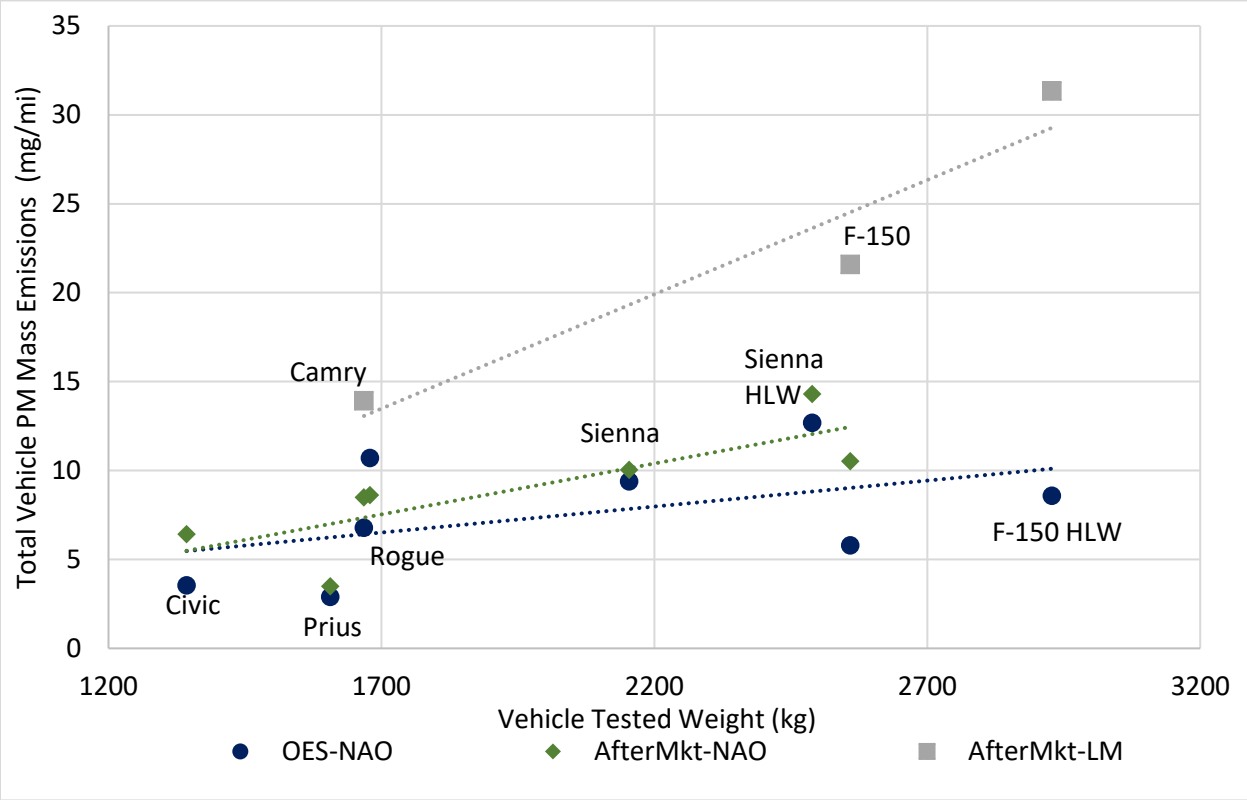

Figure 98. Total vehicle test cycle PM mass emissions vs simulated vehicle test weight, categorized by pad material

ERG used LINK business intelligence to estimate the in-use friction material fractions within each model. Using these fractions, ERG estimated the average in-use emission rates for each model. Table 31 presents these estimated emission rates of PM2.5 and PM10; they represent an inventory-level estimate for in-use emissions assuming an average vehicle age of 7 years.

Table 31. Estimated in-use brake PM emission rates by model (7 years old)

Model	Estimated In-Use PM2.5 Emission Rate (mg/mi)	Estimated In-Use PM10 Emission Rate (mg/mi)
Camry	1.7	9.3
Civic	1.1	5.7
F-150	2.0	9.8
F-150 HLW	2.6	13.9
Prius	1.0	3.3
Rogue	2.0	9.2
Sienna	2.1	9.9
Sienna HLW	2.7	13.9

For the purposes of comparison to the emission factors used in MOVES for opmode 0, the above values were also presented on the basis of mass emissions per second of braking. Table 32 presents these values by model on the basis of mg per second of braking.

Table 32. Estimated in-use brake emission rates per unit time of braking by model

Model	Estimated PM2.5 Emission Rate per Second of Braking (mg/s)	Estimated PM10 Emission Rate per Second of Braking (mg/s)
Camry	0.089	0.486
Civic	0.057	0.296
F-150	0.106	0.512
F-150 HLW	0.133	0.723
Prius	0.050	0.174
Rogue	0.102	0.478
Sienna	0.109	0.514
Sienna HLW	0.141	0.723

This report also presented emissions results for particle size distribution and particle counts. Particle count emissions generally trended with overall mass, however the observed range from the lowest to highest emitter was reduced as compared to measured mass. In general, low metallic pads resulted in somewhat larger particle sizes than did NAO pads.

Recommendations

The original project scope included a task in which ERG and LINK would use the experience in this work to develop recommendations for future work in the development of measurement techniques for non-exhaust PM emissions from vehicles.

Realistic Emissions Factors

The brake dynamometer system intentionally represents idealized braking particulate emission circumstances as compared to braking systems mounted on vehicles. They are idealized in that there is not a wheel/tire mounted, there is only the minimum hardware necessary for support of the components in the airflow, and there are not bodywork or vehicle frame elements in the airflow. This is intentional to maximize the repeatability of testing and to ensure that the maximum percentage of generated particles reach the point of sampling. The goal is to understand the particles generated at the friction couple, so it is important that the test setup maximize the sensitivity to particles originating at that point. In actual on-road use, however, some amount of brake-generated particulate settles on or adheres to vehicle components and surfaces. As a result, brake dynamometer testing may result in measurements that overestimate real in-use braking emissions.

ERG did not find any recent literature regarding the level of PM losses from settling. The Sanders (2003) study indicated estimates of the fraction of PM mass remaining airborne on a real vehicle being in the range of 50% - 70% of the emitted mass from the friction couple.[14] However, there was also some level of loss present in the dynamometer sampling system. The Arizona dust experiment indicated recovery percentages around 90%. **Accounting for this, a reasonable estimate for in-use emission rates would be 66% of the emission factors determined in this work.**

Further testing may help to inform a better understanding of the particle losses from settling, transient behavior like coagulation (and potential increased settling as a result), other dispersion considerations for brake particles, and temperature or meteorological effects on vehicle emissions in-use.

LINK and ERG recommend the following testing ideas for continued investigation into brake emissions:

Long-term effects. In this work, the tested friction materials were relatively new as they were tested after approximately 11 hours of burnishing. While the friction materials used in a given pad or shoe are likely to be homogenous throughout in terms of chemistry, it may be beneficial to determine whether there is a PM emissions trend as the pad or shoe proceeds through its life toward end-of-life. Also, the friction materials in this program were free of corrosion or any other wear outside of that caused by the burnish cycle. One potentially valuable subject to research in future work would be to determine any effect of corrosion (especially for metallic materials), other environmental effects, or mal-maintenance and mechanical problems on PM emissions. This could include stuck or constantly wearing brakes that could be emitting at disproportionate levels as compared to other vehicles. This could potentially be done by working with vehicle fleets to make an agreement to acquire and/or evaluate their used brake components for testing. A more costly option would be to conduct a full aging program in which the aging, corrosion, wear, and/or mechanical defects would be conducted as a part of the experimental design.

Meteorological effects. Weather can affect both driving habits as well as the morphology of particles as they are released into the atmosphere. The Caltrans travel survey that formed the basis for the development of the CBDC test cycle was a wide-ranging project that would have captured various weather events across the state, however the weather was not logged or noted so no analysis is possible on that basis. Additionally, rain may have a large effect on mitigating PM emissions (though this would be likely to shift air quality effects of PM to watershed effects). Understanding these effects, taken with climate data for the state, may allow for a correction to be applied to the brake PM emissions factors based on weather.

[14] Sanders, Paul G. et. al. “Airborne Brake Wear Debris: Size Distributions, Composition, and a Comparison of Dynamometer and Vehicle Tests.” Environmental Science & Technology 37 (2003): 4060–4069

(Urban) Geographic location. There may also be reason to prioritize the analysis of urban environments (and their associated driving styles) in which vehicle and pedestrians would be grouped together in large numbers and close proximity. The test cycle in this work represented vehicle use across the state, but PM emissions may be a higher priority in urban areas due to population density. The low-speed portion of the CBDC reflects the driving in low-speed trips from across the state, not necessarily those from urban environments.

By event analysis. To further inform the understanding of the mechanisms and physical causes of varying levels of braking events, it may be of interest to conduct testing over a prescribed or gridded set of stops instead of the representative driving cycle used in this program. It could resemble the Heating and Cooling Matrix used in this work to develop the brake temperature model. A series of the same engineered stops could be performed repeatedly and characterized as a group. This could reduce the noise observed in the Individual Brake Event analysis in this work.

Alternative brake dynamometer setup. For dynamometer testing in which the intent is not necessarily to attempt to capture all of the PM from the brake friction interface, minor changes from the design used in this work may be beneficial. For example, with a slightly larger brake enclosure, it may be feasible to mount a “dummy wheel” to the tested brake rotor to determine whether it would collect a measureable amount of PM (i.e. measurably less PM would reach the point of sampling). The dummy wheel could be a typical vehicle wheel with just the spokes and inner drum, with some of the outer drum machined off so that it would fit in the enclosure. Depending on the design, it may also need to have a hole drilled out at the center to accommodate the dynamometer’s brake hub support. Likewise, it may be possible to add an inner fender shape to the enclosure to disturb the airflow to determine if there is a measurable amount of particle loss. These are speculative ideas but potentially worth investigating.

Empirical/numerical models for transport losses. LINK developed a model of the transport losses of the CVS and sampling train setup used in this project. This was a relatively simple model assuming little turbulence and gradual curves in sample ducting. It may be of benefit to pursue modeling of transport losses in greater detail to create estimates of particulate settling on in-use vehicles, though this would require a much more complicated model than that used by LINK in analyzing the smooth surfaces of the setup used in this work.

Heavy Duty Vehicles

This work focused on light duty vehicles ranging in size from a Honda Civic up to a Ford F-150. For on-road inventory modeling, however, heavy-duty vehicles may be the source of a significant amount of PM emissions from the on-road vehicle fleet. The increased weight of these vehicles means that braking energy to stop from a given speed is much higher than that for a light-duty vehicle. As a result, even though the population of these vehicles is lower than that of light-duty, the total emissions may be equivalent or even higher. One confounding factor is that heavy duty vehicles are more

often equipped with drum brakes than their light-duty counterparts. In this study, the Civic rear axle was drum brake equipped and emitted at lower rates than the other vehicles, likely due to particles being trapped within the drum assembly. So, it is possible that heavy duty brake PM emissions do not completely scale up with weight at the same slope as the light-duty vehicles in this study.

Since the time of the project initiation, Caltrans has initiated a parallel project to measure the PM emissions associated with heavy duty vehicle braking. One of the key challenges to this work involves the wide variety of vehicle types and vocations in the heavy-duty fleet. Additionally, heavy duty vehicles tend to have multiple axles (including trailer axles) that all may have different braking characteristics and associated emission rates. The Caltrans project will include 36 dynamometer tests from different axles of Class 8 tractor trailers, refuse trucks, beverage haul trucks, and urban buses. The results of this project will better inform the need for and direction for potential further testing.

Tire Wear

The other potentially significant source of non-exhaust PM from vehicles is that of tire wear. The tire slip between the tire and roadway during operation results in abrasion of both sides of the friction couple. Rolling tires can also lift roadway debris and cause it to become airborne, and it is not always possible to determine whether the source of particulate is the tire, roadway material, or settled debris without chemical analysis. For the sake of measurement of all PM emission caused at the tire/road interface, the source is not important as all three directly contribute. However, if reductions are to be made possible, awareness of the source (either the roadway material or tire material) is critical to informing possibilities for reduction. Tire formulations generally consist primarily of styrene butadiene rubber, natural rubber, and polybutadiene. To enhance the engineering properties of the tire, zinc oxide is often present at levels of approximately one to two percent, and this zinc can comprise some percentage of the emitted particulate. Roadway surfaces vary more in material formulation, including stone/mineral matter, bituminous binder, sand, and various binders.[15]

The most common research publications discussing tire and roadway PM emissions are roadside or tunnel studies of the ambient air around vehicles traveling the roadway. These types of experiments reflect real in-use values but do not have the same level of control over vehicle types, tire materials, and driving styles as a dynamometer study in which a complete test matrix can be prescribed. Because many literature references describe roadside studies, many of the available emissions factors relate to ambient air

[15] Ntziachristos and Boulter. (2013). EMEP/EEA air pollutant emission inventory guidebook - 2013: 1.A.3.b.vi Road vehicle tyre and brake wear.

on a by-volume basis, not to a per-mile or per-second basis as needed for informing emissions models.[16,17]

Some studies have used a test vehicle with an onboard portable emissions measurement (PEMS) system mounted in such a way that it draws in tire and road or brake PM. These types of measurements generally involve a funnel-shaped capturing device with a sample pump that draws the air and PM into the system for measurement. Depending on the size and shape of the funnel, it can sample either tire/road interface PM or brake PM (with some risk of cross-contamination). These types of measurements allow for control of the test vehicle operational conditions and the tire and roadway materials. This type of testing is also subject to environmental conditions and contaminations, unlike the controllable conditions in a lab.

There have been studies involving various laboratory dyno systems that simulate the tire/road interface within controlled laboratory conditions. Like the brake dynamometer, these systems were generally developed for testing other tire parameters (such as tread life or noise) and were then adapted to PM testing. It is challenging to develop a representative laboratory simulation of the tire/road interface, however. Two existing designs are the system used by the German Federal Highway Research Institute (BASt), in which a large cylinder is fabricated, and the inside surface is made of roadway material. A wheel and tire combination is driven around the inside of this loop in a manner similar to a planetary gear in a gearset. Turning loads, tire scrubbing, acceleration, and deceleration can all be simulated with this design, and the volume within the confines of the cylindrical enclosure can be sampled for emitted PM.

Another method is a flat circular roadway surface with a centrally mounted arm that supports a wheel and tire traveling around the roadway surface. Acceleration, deceleration, and scrubbing can also be simulated with this design; however, the constant turning may emit a greater number of particles due to shear than would be emitted while traveling along a straight path. This type of laboratory setup has been used by the Swedish National Road and Transport Research Institute (VTI).

There is also the design that operates more like a light-duty chassis dynamometer in which a wheel and tire rides on the outside of a large textured drum, such as a 48” dynamometer roll. This interface can be mounted within an enclosure and the generated particles drawn and sampled from that enclosure. Because the tire is riding against a round surface, the tire stresses, deformation, and likely PM emissions would be higher than that from driving along a flat surface.[18] Some adjustment factor to account for this

---

[16] Panko, Julie & Hitchcock, Kristen & Fuller, Gary & Green, David. (2019). Evaluation of Tire Wear Contribution to PM2.5 in Urban Environments. Atmosphere. 10. 99. 10.3390/atmos10020099.

[17] Sommer et. Al. (2018). Tire Abrasion as a Major Source of Microplastics in the Environment. Aerosol and Air Quality Research. 18. 10.4209/aaqr.2018.03.0099.

[18] Dalmau, Eugenia & Augsburg, Klaus & Wenzel, Felix & Ivanov, Valentin. (2017). Tire particle emissions: Demand on reliable characterization.

would be necessary. Of the various laboratory designs, this design appears to be the most cost-effective to fabricate, especially in a lab already containing a chassis dynamometer and PM sampling equipment.

The literature reveals a wide range of particle emissions estimates and wear factors. One aspect that adds complexity is that tires can sometimes separate larger particles up into the ~1mm range. These particles settle immediately so do not become airborne particulate, but they are a part of the mass represented by reported "wear factors."[19] So, literature review must take care to specify the type of emission of interest. This difference contributes to the wide range of observed values for tire wear in literature. ERG has attempted to compile some estimates of tire and road wear and they are presented in Table 33. The table presents two emission sources, tires only or the tire and road interface. For comparison, value ranges are given for PM2.5, PM10, and all wear. Some values are given in literature on a per-tire basis and some are given at the vehicle distance traveled level, indicated by vkm.

Table 33. Selected light-duty tire and roadway PM emission factors from literature

Emission Source	PM2.5	PM10	All Mass
Tire Only			0.02-0.11 g/vkm[20];
Tire + Roadway	0.31-0.5 ug/tire•km	0.54-0.95 ug/tire•km; 3.5-9.0 mg/vkm[21]	3.5-6.4 mg/km (>PM10)[22]

Based on literature, there appears to be a wide variety of research into measuring particulate emissions from tires, however there does not appear to be a consensus or any standardization of test processes. One potential avenue of work would be to conduct a survey or poll from various researchers to start developing a consensus on what can be agreed upon and standardized to start moving toward a test method that can be widely accepted.

[19] Sommer et. Al. (2018). Tire Abrasion as a Major Source of Microplastics in the Environment. Aerosol and Air Quality Research. 18. 10.4209/aaqr.2018.03.0099.
[20] Ntziachristos and Boulter. (2013). EMEP/EEA air pollutant emission inventory guidebook - 2013: 1.A.3.b.vi Road vehicle tyre and brake wear.
[21] PMP – Particle Measurement Program UNECE Informal Group, Non-exhaust traffic related particle emissions. Non-exhaust traffic related particle emissions (brake and tyre/road wear). Informal document GRPE-73-14 73rd GRPE, 6-10 June 2016. https://www.unece.org/fileadmin/DAM/trans/doc/2016/wp29grpe/GRPE-73-14.pdf
[22] Aatmeeyata, D.S. Kaul, Mukesh Sharma,*Traffic generated non-exhaust particulate emissions from concrete pavement: A mass and particle size study for two-wheelers and small cars*, Atmospheric Environment, Volume 43, Issue 35, 2009, Pages 5691-5697

References

Mathissen, M. et. al., A novel real-world braking cycle for studying brake wear particle emissions, Wear, Volumes 414–415, 2018

Garg, Bhagwan D. et. al. “Brake Wear Particulate Matter Emissions.” Environmental Science & Technology 34.21 (2000): 4463–4469

Sanders, Paul G. et. al. “Airborne Brake Wear Debris: Size Distributions, Composition, and a Comparison of Dynamometer and Vehicle Tests.” Environmental Science & Technology 37 (2003): 4060–4069

Marcel Mathissen, Jaroslaw Grochowicz, Christian Schmidt, Rainer Vogt, Ferdinand H. Farwick zum Hagen, Tomasz Grabiec, Heinz Steven and Theodoros Grigoratos, A novel real-world braking cycle for studying brake wear particle emissions, Wear, https://doi.org/10.1016/j.wear.2018.07.020e

EPA Annual Certification Data for Vehicles, Engines, and Equipment https://www.epa.gov/compliance-and-fuel-economy-data/annual-certification-data-vehicles-engines-and-equipment

Society of Automotive Engineers (SAE) Standard J2789, Inertia Calculation for Single-Ended Inertia-Dynamometer Testing https://www.sae.org/standards/content/j2789_201008/

Grigoratos, Theodoros & Martini, Giorgio. (2014). Brake wear particle emissions: a review. Environmental science and pollution research international. 22. 10.1007/s11356-014-3696-8.

US EPA. Brake and Tire Wear Emissions from On-road Vehicles in MOVES2014. EPA-420-R-15-018, November 2015

Ntziachristos and Boulter. (2013). EMEP/EEA air pollutant emission inventory guidebook - 2013: 1.A.3.b.vi Road vehicle tyre and brake wear.

Panko, Julie & Hitchcock, Kristen & Fuller, Gary & Green, David. (2019). Evaluation of Tire Wear Contribution to PM2.5 in Urban Environments. Atmosphere. 10. 99. 10.3390/atmos10020099.

Sommer et. Al. (2018). Tire Abrasion as a Major Source of Microplastics in the Environment. Aerosol and Air Quality Research. 18. 10.4209/aaqr.2018.03.0099.

Dalmau, Eugenia & Augsburg, Klaus & Wenzel, Felix & Ivanov, Valentin. (2017). Tire particle emissions: Demand on reliable characterization.

PMP – Particle Measurement Program UNECE Informal Group, Non-exhaust traffic related particle emissions. Non-exhaust traffic related particle emissions (brake and

tyre/road wear). Informal document GRPE-73-14 73rd GRPE, 6-10 June 2016. https://www.unece.org/fileadmin/DAM/trans/doc/2016/wp29grpe/GRPE-73-14.pdf

Aatmeeyata, D.S. Kaul, Mukesh Sharma,Traffic generated non-exhaust particulate emissions from concrete pavement: A mass and particle size study for two-wheelers and small cars, Atmospheric Environment, Volume 43, Issue 35, 2009, Pages 5691-5697

Glossary of Terms, Abbreviations, and Symbols

100S4 – The TSI instrument used in this work to measure gravimetric PM mass at various size classifications using coated aluminum impactors

APS – Aerodynamic Particle Sizer, the TSI instrument used to measure particle size distributions in the range from 0.5 – 20 μm

Brake Event – In a driving trace, the period of time from the initial application of the brakes until the brakes are either released or the vehicle comes to a stop

BWI – Brake Wear Index (or Indices), a measure of the amount of brake emissions potential from a given vehicle or brake component, weighted by friction material mass and the counts in-use in the fleet

California Brake Dynamometer Cycle (CBDC) – The new brake dynamometer test cycle developed and used during this test program

EEPS – Engine Exhaust Particle Sizer, the TSI instrument used to measure particle size distributions in the range from 5.6 to 560 nm

ETW – Equivalent test weight, the simulated test weight used for most tests in this program; corresponds to curb weight + 300 lbs.

Generalized Coastdown Curve – The estimated coastdown curve, derived from the average of the road load coastdowns of the 6 test vehicles in this program, used to identify braking events in the Caltrans dataset (any decelerations greater than this curve were flagged as braking events)

Heating and Cooling Matrix – The test matrix of standardized braking events and cruise intervals followed by each vehicle on the test track while recording brake temperatures in order to provide inputs to the temperature model.

HLW – Heavily laden weight, the test weight used in some tests of the cargo-carrying vehicles amounting to two thirds of the difference between the curb weight and gross vehicle weight

LM – Low metallic friction materials used in some tests of the Camry and F-150 assemblies. Indicates the materials have a larger amount of metal than NAO

Microtrip – An identified portion of the Caltrans driving trace consisting of the time that a vehicle starts moving, through the cruise and lasting until the next stop.

NAO – Non asbestos organic friction materials, the most common friction material and that comprising all OES pads

OES – Original Equipment Service, the friction material specified in dealer-sourced replacement parts

PM – Particulate Matter, often classified by PM2.5, indicating particulate up to 2.5μm in diameter, and PM10, particulate up to 10μm in diameter

QCM – Quartz Crystal Microbalance, the TSI instrument used to measure continuous PM2.5 mass

Represented distance – the distance represented by the CBDC for inventory purposes; the cycle consists of braking events extracted from real trips as well as engineered cruises added for cooling, neither of which has distance basis in real use; represented distiance also includes the actual distance traveled between each braking event

SCC – Speed Correction Cycles, the EMFAC speed cycles used to factor UC emission rates into the different EMFAC speed bins

SCF – Speed Correction Factors, the values provided in this work that may be used to to factor the overall vehicle-level emission rates found in this work into groups of EMFAC speed bins

UC – The EMFAC Unified Cycle, the standard basis for exhaust emissions factors in EMFAC

WLTP-Brake – The World-Harmonized Brake cycle, developed recently in Europe in cooperation with the JRC; a new cycle designed specifically for measuring brake PM emissions.

Appendix A

Vehicle and Friction Material Selection Supporting Data

This Appendix includes supporting data for the Representative Test Vehicle and Friction Material Selection section of the report. This table presents the details of the top-25 vehicle analysis including the calculated values for the two brake wear indices (BWI). In the table, VIO indicates vehicles in operation. BWI1 is VIO x total wearable mass, and BWI2 is VIO x total wearable mass x replacement rate.

MAKE	MODEL	MY	Common for bench-marking	Curb wt (kg)	Brake system	VIO	**VIO Rnk**	Total wear mass per vehicle / g	BWI1 = (VIO x total wearable mass) / ton	**BWI1 Rnk**	Repl. Rate (%)	OE/OES mkt share (%)	BWI2 (tons)	**BWI2 Rnk**
TOYOTA	CAMRY (BASE, L, LE)	2009-2016	yes-FA	1460	Disc/ Disc	342992	1	2133	732	1	16%	34.0%	117	1
HONDA	CIVIC LX	2012-2015		1221	Disc/ Drum	140733	5	2322	327	4	14%	34.0%	46	3
NISSAN	ROGUE S	2014-2016		1550	Disc/ Disc	41213	10	1845	76	14	11%	34.0%	8	16
TOYOTA	SIENNA LE	2011-2015		1940	Disc/ Disc	44921	8	2717	122	8	14%	34.0%	17	6
FORD	F150 SPRCREW	2015-2016	yes-FA & RA	2206	Disc/ Disc	32921	17	2895	95	11	11%	90.0%	10	10
TOYOTA	PRIUS REGULAR	2010-2016		1382	Disc/ Disc	241055	2	1749	422	3	2%	34.0%	8	15
TOYOTA	COROLLA L	2014-2016		1265	Disc/ Drum	159154	3	3028	482	2	11%	53.5%	53	2
NISSAN	ALTIMA (BASE, 2.5)	2012-2016	yes-FA	1429	Disc/ Disc	149096	4	1510	225	5	14%	40.7%	32	4
NISSAN	SENTRA S	2013-2016		1277	Disc/ Disc	110629	6	1436	159	7	11%	53.5%	17	5
FORD	F150 SPRCREW	2013-2014	yes-FA	2549	Disc/ Disc	33721	16	2878	97	10	16%	17.0%	16	7
LEXUS	RX 350	2014-2015		1900	Disc/ Disc	43306	9	2707	117	9	11%	34.0%	13	8
CHEVROLET	TAHOE C1500	2007	yes-FA	2462	Disc/ Disc	19517	23	2521	49	18	23%	14.0%	11	9

MAKE	MODEL	MY	Common for bench-marking	Curb wt (kg)	Brake system	VIO	**VIO Rnk**	Total wear mass per vehicle / g	BWI1 = (VIO x total wearable mass) / ton	**BWI1 Rnk**	Repl. Rate (%)	OE/OES mkt share (%)	BWI2 (tons)	**BWI2 Rnk**
TOYOTA	RAV4 XLE	2014-2016		1560	Disc/ Disc	36803	14	2462	91	12	11%	34.0%	10	11
TOYOTA	TACOMA DOUBLE CAB	2015-2016		1975	Disc/ Drum	36052	15	5256	189	6	5%	90.0%	9	12
HONDA	ACCORD LX	2014-2016	yes-FA	1465	Disc/ Disc	52193	7	1598	83	13	11%	53.5%	9	13
DODGE	RAM 1500 ST	2004		2260	Disc/ Disc	19739	22	2180	43	19	21%	5.0%	9	14
HYUNDAI	ELANTRA GLS	2013		1207	Disc/ Disc	30566	18	1649	50	17	16%	17.0%	8	17
HYUNDAI	SONATA (GLS, SE, SPORT)	2013-2015		1486	Disc/ Disc	40117	11	1678	67	15	11%	90.0%	7	18
CHEVROLET	SILVERADO 1500	2014-2015	yes-FA	2240	Disc/ Disc	27578	19	2431	67	16	11%	53.5%	7	19
HONDA	ACCORD EX	2014-2016		1492	Disc/ Disc	39344	12	993	39	21	11%	53.5%	4	20
HONDA	ACCORD SPORT	2014-2015		1468	Disc/ Disc	37332	13	803	30	23	11%	34.0%	3	21
HONDA	CIVIC LX	2016		1276	Disc/ Disc	25782	20	1666	43	20	5%	90.0%	2	22
LEXUS	RX 350	2016		1970	Disc/ Disc	12540	24	2668	33	22	5%	90.0%	2	23
HYUNDAI	SONATA SE	2016		1486	Disc/ Disc	11363	25	1803	20	24	5%	90.0%	1	24
HONDA	ACCORD SPORT	2016		1507	Disc/ Disc	22978	21	803	18	25	5%	90.0%	1	25

Appendix B

Heating and Cooling Matrix for Track Testing

The following table depicts the braking events that made up the ERG heating and cooling matrix conducted by LINK at the test track. Each vehicle was subject to a series of braking snubs to achieve the desired initial temperature. The initial and final speeds, along with the deceleration rate is given for each braking event. The cooling speed, where applicable, refers to the steady-state speed that should be held after the braking event to allow the brakes to cool down below 50°C.

Event #	Initial Front Axle disc temperature, °C	Initial speed, km/h	Final speed, km/h	Cooling speed, km/h	Deceleration, g
1	60	55	0	0	0.10
2	60	55	< 5	55	0.25
3	160	55	< 5	55	0.25
4	160	55	< 5	NA	0.35
Warm-up	open	120	60	55	0.40
5	300-350	55	55	55	-
6	60	55	< 5	NA	0.25
Warm-up	open	120	60	55	0.40
7	300-350	55	55	55	-
8	60	55	< 5	55	0.35
9	60	95	0	0	0.10
10	60	95	< 5	55	0.10
11	60	95	< 5	95	0.25
12	160	95	< 5	95	0.25
13	160	95	< 5	NA	0.35
Warm-up	open	120	60	95	0.40
14	300-350	95	95	95	-
15	60	95	< 5	NA	0.35
Warm-up	open	120	60	95	0.40
16	300-350	95	95	95	-
17	60	95	< 5	95	0.35
18	60	130	0	0	0.10
19	60	130	< 5	55	0.10
20	60	130	< 5	130	0.25
21	160	130	< 5	130	0.10
22	160	130	< 5	NA	0.25
Warm-up	open	120	60	130	0.40
23	300-350	130	130	130	-
24	60	130	< 5	NA	0.35
Warm-up	open	120	60	130	0.40
25	300-350	130	130	130	-
26	60	130	< 5	95	0.35
Warm-up	open	120	60	NA	0.40
post Warm-up	300-350	60	0	0	0.25
27	300-350	0	0	0	-
Warm-up	open	120	60	NA	0.40
Warm-up	300-350	60	0	0	0.25
28	300-350	0	0	0	-

Appendix C

Derivation of the Generalized Coastdown Curve and Road Load Coefficients

The generalized coastdown curve was determined using the EPA-published road load coefficients for the six test vehicles used in this project. EPA publishes these values, including test weight, yearly as a part of new-vehicle exhaust emissions certification.1 The coefficients are used to allow determination of the simulated dynamometer drag force on the vehicle as a function of speed. The published coefficients for the test vehicles used in this work are shown in the following table.

	Target Coef. A (lbf)	Target Coef. B (lbf/mph)	Target Coef. C (lbf/mph**2)	Weight, lbs
Toyota Camry	35.941	-0.01201	0.020084	3670
Honda Civic	21.290	0.11890	0.018670	2970
Toyota Sienna	37.384	0.03816	0.029553	4810
Ford F-150	46.83	0.7658	0.03132	5770
Toyota Prius	31.145	0.35285	0.013956	3510
Nissan Rogue	35.59	-0.1577	0.028	3640

The EPA target coefficients are the target that the vehicle will experience as a function of speed. For this project, the force was not the parameter of interest as the main focus was on the vehicle deceleration rate. Using the weight and the road load force curve, ERG determined the expected deceleration rate as a function of speed for the six vehicles. ERG performed a polynomial curve fit to the average (by speed) of the deceleration rates for the six vehicles. The calculated coastdown deceleration rates as a function of speed are presented for the six test vehicles in the following figure. The larger black curve represents a fit to the average of the six vehicles and forms the basis of the generalized coastdown curve. The generalized coastdown curve used in this work was:

$$\Delta V = -7.931x10^{-5} \bullet V^2 - 8.558x10^{-4} \bullet V - 0.3023$$

where ΔV has units of kph/s and V has units of kph.

[1] https://www.epa.gov/compliance-and-fuel-economy-data/annual-certification-data-vehicles-engines-and-equipment

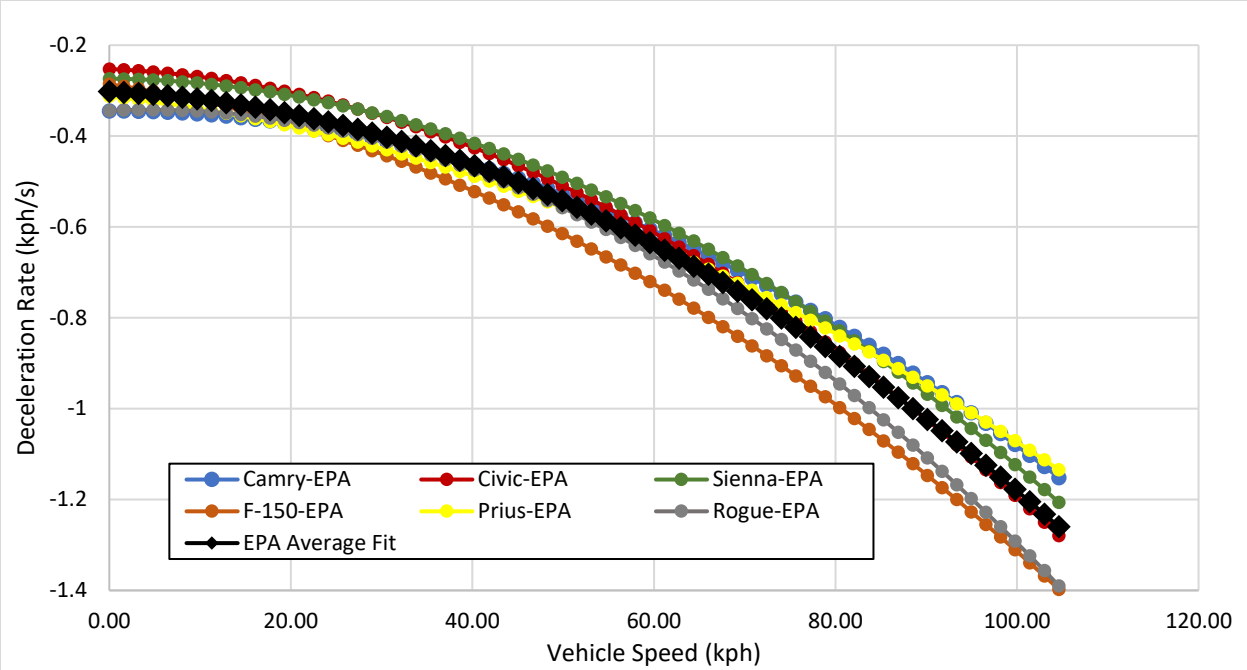

The following table presents the actual inertia values used by LINK when programming tests of each vehicle/axle combination into the dynamometer control software:

Vehicle	**Front Inertia (kg•m^2)**	**Rear Inertia (kg•m^2)**
Camry ETW	79.8	28.6
Civic ETW	55.1	19.8
F-150 ETW	161.0	58.6
F-150 HLW	184.3	67.0
Prius ETW	53.0	26.5
Rogue ETW	85.9	30.8
Rogue HLW	95.9	34.4
Sienna ETW	98.0	47.5
Sienna HLW	113.2	54.9

Appendix D

The ERG Vector Collinearity Cycle Building Approach

This section references two past reports in which ERG described the use of the vector collinearity method to build up a cycle from a larger in-use dataset. The process required further refinement for use in 17RD016 because of the temperature requirements and that temperature could not be directly controlled on the brake dynamometer (as the temperature is a function of only speed, braking intensity, and time).

The first reference was included as a footnote in ERG's proposal for this project. This reference is *Roadway-Specific Driving Schedules for Heavy-Duty Vehicles*, an ERG report to EPA, August 15, 2003. Section 5 of that document includes the description of the implementation of the vector method. This report is available at: http://nepis.epa.gov/Exe/ZyPURL.cgi?Dockey=P100LWCT.TXT

The next reference is presented as an excerpt, and is from *Development of NONROAD Load Factors, Emission Factors, Duty Cycles, and Activity Estimates*, an ERG report to EPA, February 12, 2013. In this reference, the term microtrip is the equivalent to the brake event in Project 17RD016 (meaning it is the building block taken from the larger dataset and used to build up the new cycle). The section describing the technique reads as follows:

In 1995 we developed a technique for creating duty cycles based on the microtrip concept. Since then, we have built engine dynamometer cycles (load and RPM vs. time) for wheeled loaders[2] and telescoping boom excavators,[4] and chassis dynamometer cycles (speed vs. time) for drayage trucks, heavy-duty trucks[3], dump trucks, and Bangkok cars and motorcycles. In most cases we also collected the data used to build those duty cycles. In addition, many of the cycles built were actually used to make dynamometer measurements of the emissions of engines and POEs.

The idea of a duty cycle is that it contains the essence of actual operating behavior. To make a representative cycle practical, it should be no longer than needed. A key challenge for the cycle builder is to compress the dataset collected on each type of construction equipment to produce a reasonably short cycle while maintaining the essence of the engine operating behavior. Such a short cycle can then be used to characterize engine operation to estimate engine emissions for a type of construction equipment during typical operation for that type of equipment.

---

[2] T.H. DeFries, G.F. Baker, B. Limsakul, M.A. Sabisch, P. Henson, S. Kishan, "ERG Contributions to the Texas Department of Transportation Evaluation of PuriNOx Diesel Fuel," prepared for R.D. Matthews, University of Texas at Austin, prepared by Eastern Research Group, TxDOT-030218, February 18, 2003.

[3] T.H. DeFries, S. Kishan, B. Limsakul, M.J. Hebets, "Roadway-Specific Driving Schedules for Heavy-Duty Vehicles," prepared for U.S. Environmental Protection Agency, prepared by Eastern Research Group, EPA-030815, August 15, 2003.

Representative cycles can be built using different methodologies. The methodology we have chosen for this study is to use pieces of real engine operation, called microtrips, from the data collected on construction equipment, which when connected together can be expected to have similar emissions behavior to the same type of equipment in normal operation. The cycle is built around parameters of equipment operation and usage that are known to be important to exhaust emissions. By building up a duty cycle from snippets (microtrips) of actual engine operation such that the characteristics of the cycle in some way matches the characteristics of a database of typical engine operation, it can be inferred that the emissions behavior of the engine over the cycle will be similar to the emissions behavior of the engine in a particular type of construction equipment.

The cycle is created by selecting and combining microtrips taken from the dataset of actual engine operation for each type of construction equipment. Two or more variables are used to define and select microtrips for the cycle. This cycle-building introduction uses relative mass fuel rate and relative RPM as the two variables used to define engine operation. To identify specific segments of equipment operation for inclusion in the cycle, the entire activity dataset is converted to a set of microtrips. Typically, a microtrip is defined as a contiguous time trace of engine operation that is an all-non-idle period or that is an all-idle period.

To use the microtrip cycle development approach, all of the microtrips in the dataset need to have all of their second-by-second observations binned in terms of relative mass fuel rate and relative RPM. While the size of the bins is arbitrary, bins in general need to be narrow enough to resolve important emissions effects. On the other hand, from a practical perspective, the number of bins needs to be small so that the program that selects microtrips can run in a reasonable amount of time.

Selecting microtrips for the cycle is based on a strategy of minimizing the difference between a cycle vector **C** representing operation in the candidate cycle and a target vector **T** representing operation in the activity database. As microtrips are added to the kernel of the candidate cycle, the difference between the two vectors **C** and **T** tends to become smaller and smaller. The build-up process ends when the cycle developer decides that the two vectors are substantially the same and the duration of the cycle that has been built up is acceptably short. The multi-dimensional space that these vectors are in will be described shortly, but first let us consider how the build-up process works for developing a cycle.

The goal of building the cycle is to select microtrips such that when their vectors $\mathbf{M_i}$ are added together, the vector **C** of the resulting cycle is as similar as possible to the target vector **T** of the activity database. Figure A3-1 shows the hypothetical situation of the vectors after two microtrips have been used to create a cycle. In this hypothetical example, the first microtrip was selected from the activity database for the case as the one whose vector $\mathbf{M_1}$ was closest to the target vector **T** for the database. Then, a second microtrip is searched for such that when its vector $\mathbf{M_2}$ is added to $\mathbf{M_1}$ to create the resultant vector **C** shown in Figure A3-1, the distance between the tips of **C** and **T** is minimized. This distance is the length of the vector **T-C** as denoted in the figure by the dashed vector. As microtrips are added to create the built-up cycle represented by **C**, the length of **T-C** is calculated after each additional microtrip is added to the cycle to follow the progress of the build-up process. It should be noted that the order of the microtrips in the final cycle is unimportant from the point of view of the selection of the microtrips. The reason for this is that the resultant **C** is independent of the order in which the microtrip vectors $\mathbf{M_i}$ are added together.

Figure A3-1. Vector Description of Comparing Target and Cycle Activity

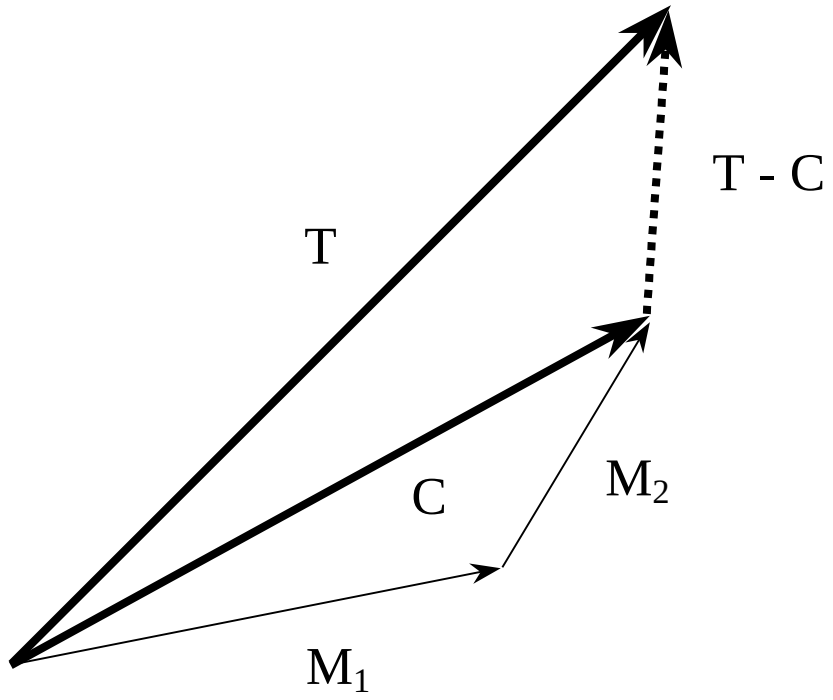

It should also be noted that we are forcing microtrips to be added to the candidate cycle. This is done even if the addition of the best incremental microtrip causes the length of **T-C** to increase in some instances. Generally, as the cycle is built up there will be a decrease in the length of **T-C**. After several microtrips have been added, the length of **T-C** may increase slightly. Later, with the addition of more

microtrips, a "discovery" will be made that will produce a relatively abrupt decrease in the length of **T-C** so that the accumulated cycle will be substantially better than the cycle was much earlier in the build-up process.

All of the vectors used above to describe the build-up process are based on representations of the cumulative frequency distributions of observations in relative mass fuel rate / relative RPM space. This statement requires some explanation. A segment of operation, whether it is a microtrip, a piece of a duty cycle, or the entire activity database can be described as a frequency distribution. The distribution consists of combinations of the two variables: relative mass fuel rate and relative RPM. The continuous values for these variables were converted into frequency distributions through the use of bins. Each one-second observation in the database was placed in a particular relative mass fuel rate / relative RPM bin. The cumulative frequency distribution is made up of the number of observations that fall “below” the current bin for each of the two-binned variables. The binning criteria for the variables will be described in Section 5.2. To help the reader understand the process, we will present a numerical example in one dimension and another example in two dimensions to demonstrate how the comparison of the vectors **T** and **C** works.

Suppose we wanted to compare a candidate cycle with the database using a single POE operation variable that was monitored second-by-second in the collection of data for the activity database. The single variable might be engine load. In this hypothetical example, we have 35,900 one-second observations of engine load in the target activity database and 68 one-second observations in the cycle. The first step in comparing **T** and **C** is to bin the observations of load in the target data and in the cycle data. TableTable A3-1 shows the binning of the hypothetical data in Columns 2 and 3. Note that the number of observations in the target data in Column 2 is much higher than the number of observations in the cycle data in Column 3. This is a consequence of the activity database containing all of the observations for all microtrips and the cycle having just one microtrip. The frequency counts in Columns 2 and 3 are then converted to cumulative frequency counts in Columns 4 and 5. This is done to provide proximity information for the microtrip searching algorithm. In other words, we wanted the algorithm to be able to select a microtrip even if the observations for a given microtrip were not in exactly the same bins as the target but did have observations at least in a nearby bin. The use of the cumulative distributions helps ensure that proximity information is available.

Table A3-1. Comparison of Cycle and Target Vectors for a Hypothetical One-Dimensional Example

	Counts		Cumulative Counts		Vector (Normalized Cumulative Counts)		Square of Difference
Bin	Target	Cycle	Target	Cycle	T	C	T-C
1	1000	0	1000	0	0.028	0.000	0.001
2	11000	30	12000	30	0.334	0.441	0.011
3	7000	10	19000	40	0.529	0.588	0.003
4	6000	7	25000	47	0.696	0.691	0.000
5	4500	5	29500	52	0.822	0.765	0.003
6	2800	1	32300	53	0.900	0.779	0.014
7	1500	4	33800	57	0.942	0.838	0.011
8	800	6	34600	63	0.964	0.926	0.001
9	600	1	35200	64	0.981	0.941	0.002
10	700	4	35900	68	1.000	1.000	0.000
				Sum of Squares	6.139	5.657	0.047
				Vector Length	2.478	2.379	0.217

A comparison of the cumulative counts for the target and cycle information in Columns 4 and 5 shows that if we used these counts to create the **T** and **C** vectors, the lengths of the vectors would be greatly different simply because the target vector, which is made up of the 10 elements in Column 4, would be a much longer vector then the cycle vector, which is made up of the 10 elements in Column 5. Accordingly, we normalize the target and cycle cumulative counts in 4 and 5 to produce the target vector elements and the cycle vector elements as the fractional values between 0 and 1 shown in Columns 6 and 7.

The values in Columns 6 and 7 become the elements of the **T** and **C** vectors, which are in 10-dimensional space. A visualization of the elements of these vectors is provided in Figure A3-2. This figure shows the normalized cumulative counts of the target and cycle from Columns 6 and 7 as a function of the bin number. What we want to do in developing the cycle is select microtrips so that the curve for the cycle is as close as possible to the curve for the target in this figure. The way we do this is to minimize the sums of the squares of the differences between the value for the corresponding elements of the target and cycle vectors. This corresponds to the square of the length of **T**-**C**. TableA3-1 shows the calculated length of **T**, **C**, and **T**-**C**. These lengths can be determined from the values of the elements for **T** and **C** in Columns 6

and 7 using the standard relationship for determining the length of a vector when its elements are known.

Figure A3-2. Visual Comparison of Vector Elements

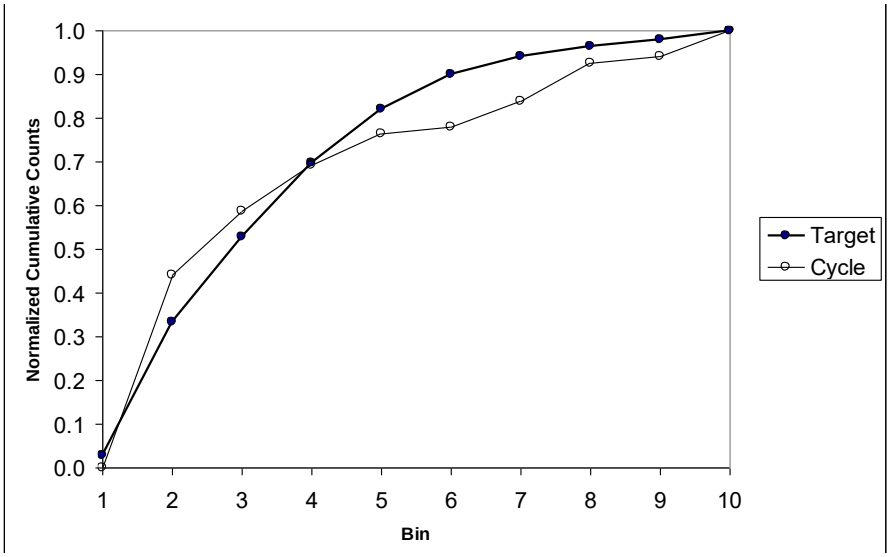

Extension of the one-dimensional example shown in TableA3-1 and Figure A3-1 to multiple dimensions is demonstrated by the spreadsheet calculations shown in Table A3-2. In this example, 100 matrix elements are used. The table shows 10 rows which might be relative mass fuel rate and 10 columns which might be relative RPM. The left side of Table A3-2 shows the calculations for the target matrix and the right side shows the calculations for the cycle matrix. In Tables a) and b), the second-by-second observations of the target and cycle data are binned. The numbers in each bin represent the frequency of observations that meet the criteria for those bins. In Tables c) and d), the counts in the Tables a) and b) are accumulated across each row. Then, in Tables e) and f), the accumulated frequencies in Tables c) and d) are accumulated down each column. This produces a field of frequencies on a cumulative basis that run from a low value in the upper left corner of each matrix to a high number in the lower right corner of each matrix. The value in the lower right hand corner of Tables e) and f) is equal to the total number of observations in the target or cycle matrix. These total observation numbers in the lower right hand corner of e) and f) are used to normalize all of the frequencies in Tables e) and f) to arrive at the normalized cumulative matrices in g) and h). The values in g) and h) are then used to calculate the square of the differences in each corresponding matrix element to produce the values in Table i). The value in Table j) is just the summation of all of the elements of Table i) and represents the square of the length of the **T-C** vector. This is the value that we attempt to minimize when selecting microtrips for the cycle. Note that the counts in a) and b) did not need to

be in corresponding bins for this comparison process to work. The use of cumulative distributions permitted the two matrices to be compared successfully.

Extension of the technique to more than two dimensions can be made by analogy.

Table A3-2. Comparison of Cycle and Target Matrices for a Hypothetical Two-Dimensional Example

Target Activity Matrix

a) Count the second-by-second observations in each bin.

	A	B	C	D	E	F	G	H	I	J
1	2									
2		1								
3		2		5						
4			5		3		2	1		
5		5		9	1			2	9	3
6			2			4	1			
7										
8			6			1				
9		1								
10										

c) Accumulate the above frequencies across each row

1	2	2	2	2	2	2	2	2	2	2
2	0	1	1	1	1	1	1	1	1	1
3	0	2	2	7	7	7	7	7	7	7
4	0	0	5	5	8	8	10	11	11	11
5	0	5	5	14	15	15	15	17	26	29
6	0	0	2	2	2	6	7	7	7	7
7	0	0	0	0	0	0	0	0	0	0
8	0	0	6	6	6	7	7	7	7	7
9	0	1	1	1	1	1	1	1	1	1
10	0	0	0	0	0	0	0	0	0	0

e) Accumulate the above frequencies down each column.

1	2	2	2	2	2	2	2	2	2	2
2	2	3	3	3	3	3	3	3	3	3
3	2	5	5	10	10	10	10	10	10	10
4	2	5	10	15	18	18	20	21	21	21
5	2	10	15	29	33	33	35	38	47	50
6	2	10	17	31	35	39	42	45	54	57
7	2	10	17	31	35	39	42	45	54	57
8	2	10	23	37	41	46	49	52	61	64
9	2	11	24	38	42	47	50	53	62	65
10	2	11	24	38	42	47	50	53	62	65

g) Normalize the elements in the above matrix.

1	0.031	0.031	0.031	0.031	0.031	0.031	0.031	0.031	0.031	0.031
2	0.031	0.046	0.046	0.046	0.046	0.046	0.046	0.046	0.046	0.046
3	0.031	0.077	0.077	0.154	0.154	0.154	0.154	0.154	0.154	0.154
4	0.031	0.077	0.154	0.231	0.277	0.277	0.308	0.323	0.323	0.323
5	0.031	0.154	0.231	0.446	0.508	0.508	0.538	0.585	0.723	0.769
6	0.031	0.154	0.262	0.477	0.538	0.600	0.646	0.692	0.831	0.877
7	0.031	0.154	0.262	0.477	0.538	0.600	0.646	0.692	0.831	0.877
8	0.031	0.154	0.354	0.569	0.631	0.708	0.754	0.800	0.938	0.985
9	0.031	0.169	0.369	0.585	0.646	0.723	0.769	0.815	0.954	1.000
10	0.031	0.169	0.369	0.585	0.646	0.723	0.769	0.815	0.954	1.000

Cycle Activity Matrix

b) Count the second-by-second observations in each bin.

	A	B	C	D	E	F	G	H	I	J
		1								
				4						
		4				3		1		
								4	1	
				8						2
					3					
							1			
	1	5								

d) Accumulate the above frequencies across each row

	0	0	0	0	0	0	0	0	0	0
	0	1	1	1	1	1	1	1	1	1
	0	0	0	4	4	4	4	4	4	4
	0	4	4	4	4	7	7	8	8	8
	0	0	0	0	0	0	0	4	5	5
	0	0	0	8	8	8	8	8	8	10
	0	0	0	0	3	3	3	3	3	3
	0	0	0	0	0	0	1	1	1	1
	1	6	6	6	6	6	6	6	6	6
	0	0	0	0	0	0	0	0	0	0

f) Accumulate the above frequencies down each column.

	0	0	0	0	0	0	0	0	0	0
	0	1	1	1	1	1	1	1	1	1
	0	1	1	5	5	5	5	5	5	5
	0	5	5	9	9	12	12	13	13	13
	0	5	5	9	9	12	12	17	18	18
	0	5	5	17	17	20	20	25	26	28
	0	5	5	17	20	23	23	28	29	31
	0	5	5	17	20	23	24	29	30	32
	1	11	11	23	26	29	30	35	36	38
	1	11	11	23	26	29	30	35	36	38

h) Normalize the elements in the above matrix.

	0.000	0.000	0.000	0.000	0.000	0.000	0.000	0.000	0.000	0.000
	0.000	0.026	0.026	0.026	0.026	0.026	0.026	0.026	0.026	0.026
	0.000	0.026	0.026	0.132	0.132	0.132	0.132	0.132	0.132	0.132
	0.000	0.132	0.132	0.237	0.237	0.316	0.316	0.342	0.342	0.342
	0.000	0.132	0.132	0.237	0.237	0.316	0.316	0.447	0.474	0.474
	0.000	0.132	0.132	0.447	0.447	0.526	0.526	0.658	0.684	0.737
	0.000	0.132	0.132	0.447	0.526	0.605	0.605	0.737	0.763	0.816
	0.000	0.132	0.132	0.447	0.526	0.605	0.632	0.763	0.789	0.842
	0.026	0.289	0.289	0.605	0.684	0.763	0.789	0.921	0.947	1.000
	0.026	0.289	0.289	0.605	0.684	0.763	0.789	0.921	0.947	1.000

i) Calculate the squares of the differences in corresponding elements of the above two matrices.

	A	B	C	D	E	F	G	H	I	J
1	0.001	0.001	0.001	0.001	0.001	0.001	0.001	0.001	0.001	0.001
2	0.001	0.000	0.000	0.000	0.000	0.000	0.000	0.000	0.000	0.000
3	0.001	0.003	0.003	0.000	0.000	0.000	0.000	0.000	0.000	0.000
4	0.001	0.003	0.000	0.000	0.002	0.002	0.000	0.000	0.000	0.000
5	0.001	0.000	0.010	0.044	0.073	0.037	0.050	0.019	0.062	0.087
6	0.001	0.000	0.017	0.001	0.008	0.005	0.014	0.001	0.021	0.020
7	0.001	0.000	0.017	0.001	0.000	0.000	0.002	0.002	0.005	0.004
8	0.001	0.000	0.049	0.015	0.011	0.010	0.015	0.001	0.022	0.020
9	0.000	0.014	0.006	0.000	0.001	0.002	0.000	0.011	0.000	0.000
10	0.000	0.014	0.006	0.000	0.001	0.002	0.000	0.011	0.000	0.000

j) Sum the squares of the differences.

0.754

An example of the discovery process as microtrips are built up is shown in Figure A3-2. The figure shows a plot of the length of the **T-C** vector as microtrips were added to a cycle for wheeled backhoe loaders. The figure shows that as microtrips were added, the length of the vector first dropped to a local minimum after 12 microtrips were added. The next minimum vector length was encountered after 14 microtrips were added. Subsequent lower minima were achieved when 20, 23, 28, 30, … microtrips were added. Major decreases in the length of the **T-C** vector occurred after 14, 28, and 59 microtrips were added. This alternate drop/plateau/increase/drop behavior is commonly seen when using this method of cycle building. At this point in cycle development, the duration of the cycle becomes important. Depending on the acceptability of the duration of the cycle being built up, a cycle with any of the specific 14, 28, or 59 microtrips could be used. These three candidate cycles would have durations of 73, 124, and 437 seconds, respectively.

Figure A3-2. Square of the Length of T-C as MicroTrips are Added: Example for Wheeled Backhoe Loaders

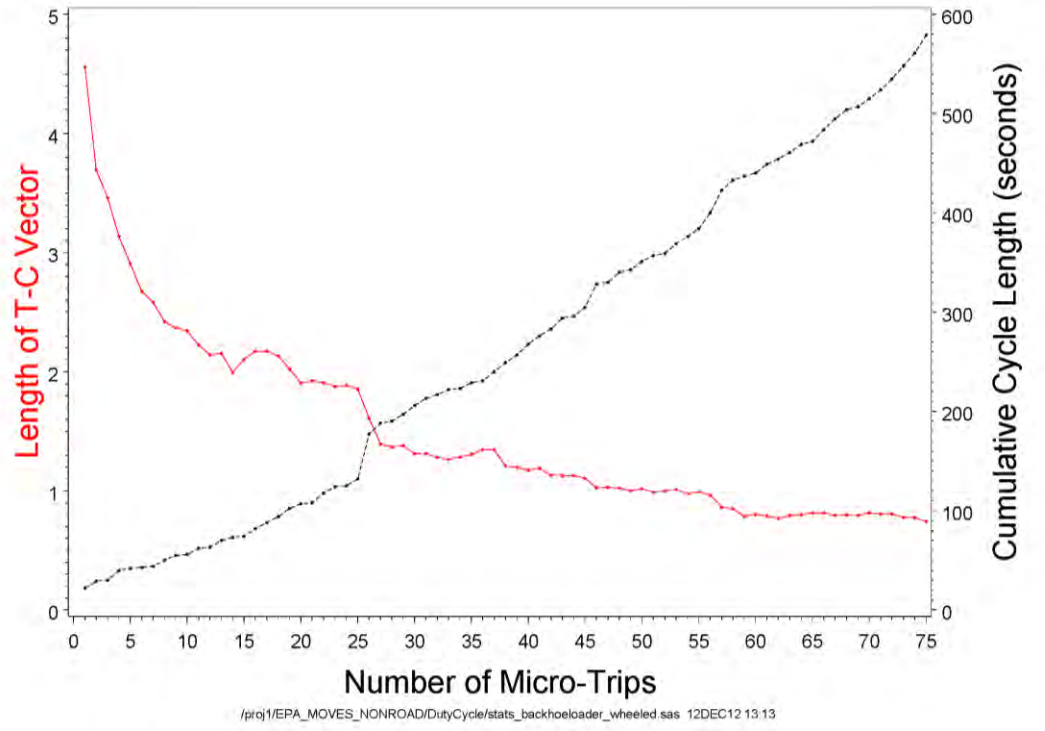

Appendix E

Distributions of Parameters of Interest for the Vector Method's (New CBDC) 3 Speed Segments

Further distributions of the four parameters of interest, broken down by the three speed segments created by the vector method, are presented in this Appendix. The distribution for the overall vector cycle (previously shown in the distributions in the *Results* section) is presented for comparison. Note again that the distributions are for the periods during brake events only; acceleration and cooling/cruise periods are not included.

The distributions of brake event durations are presented in the following figure. As described previously, the ERG cycle intentionally does not have any brake events shorter than 3 seconds.

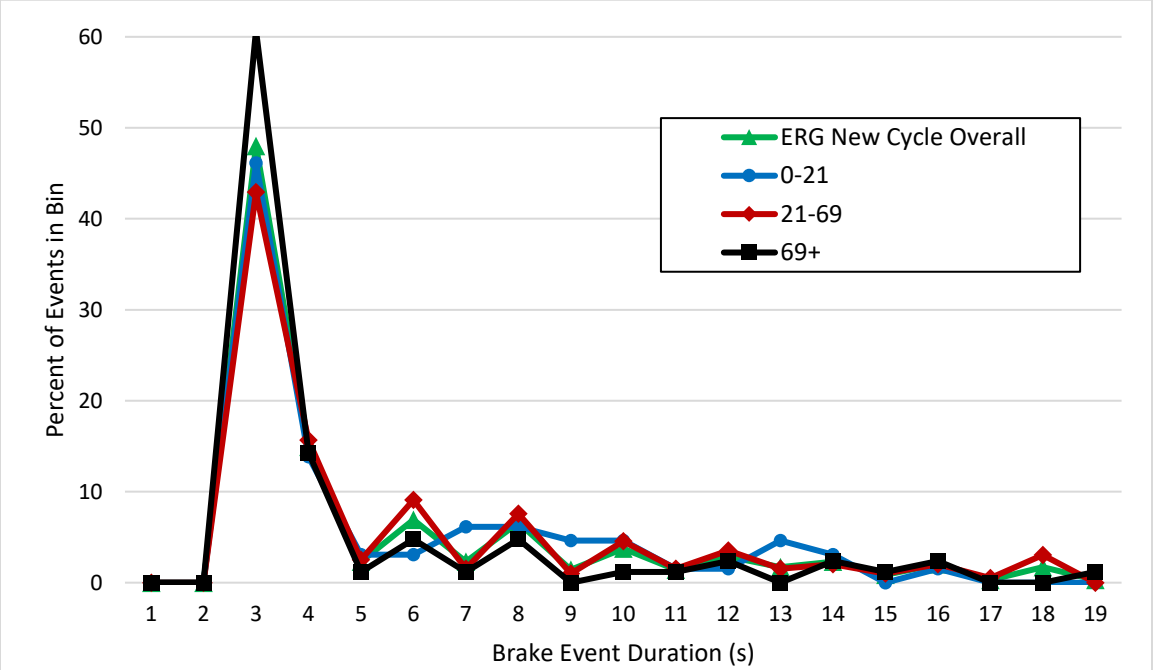

The distributions of speeds encountered during braking events are presented in the following figure. It can clearly be seen that the slow speed segment has more time in the slow speed bins, and the high speed segment has more time in the high speed bins. The distribution of (negative) acceleration rates during braking is presented in the subsequent figure.

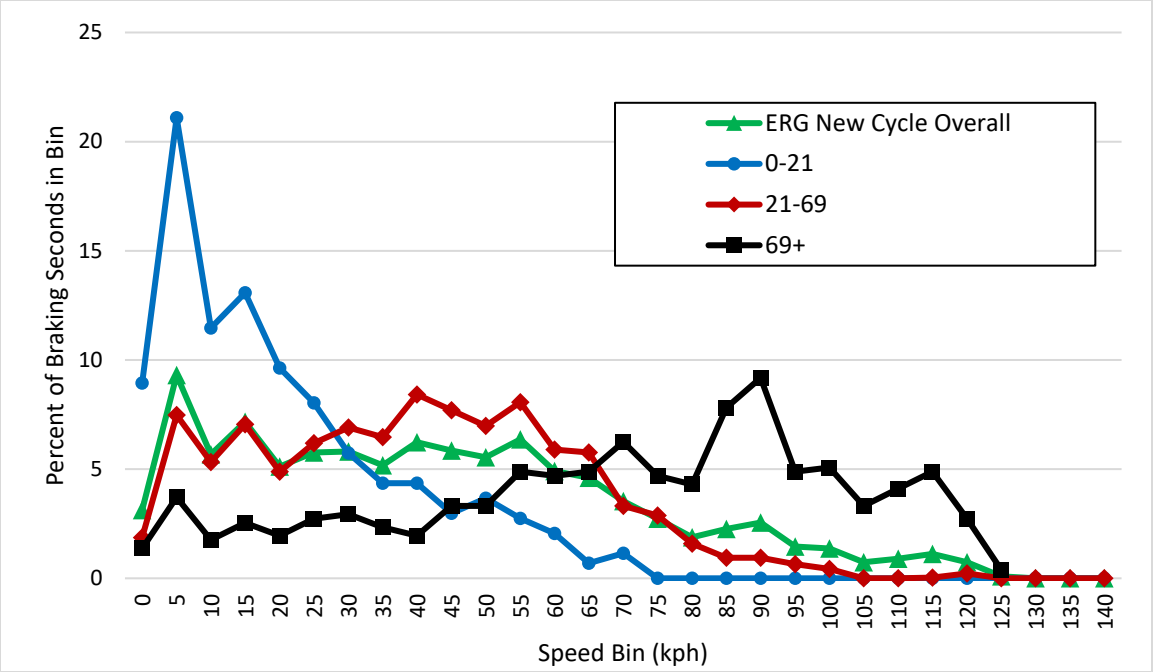

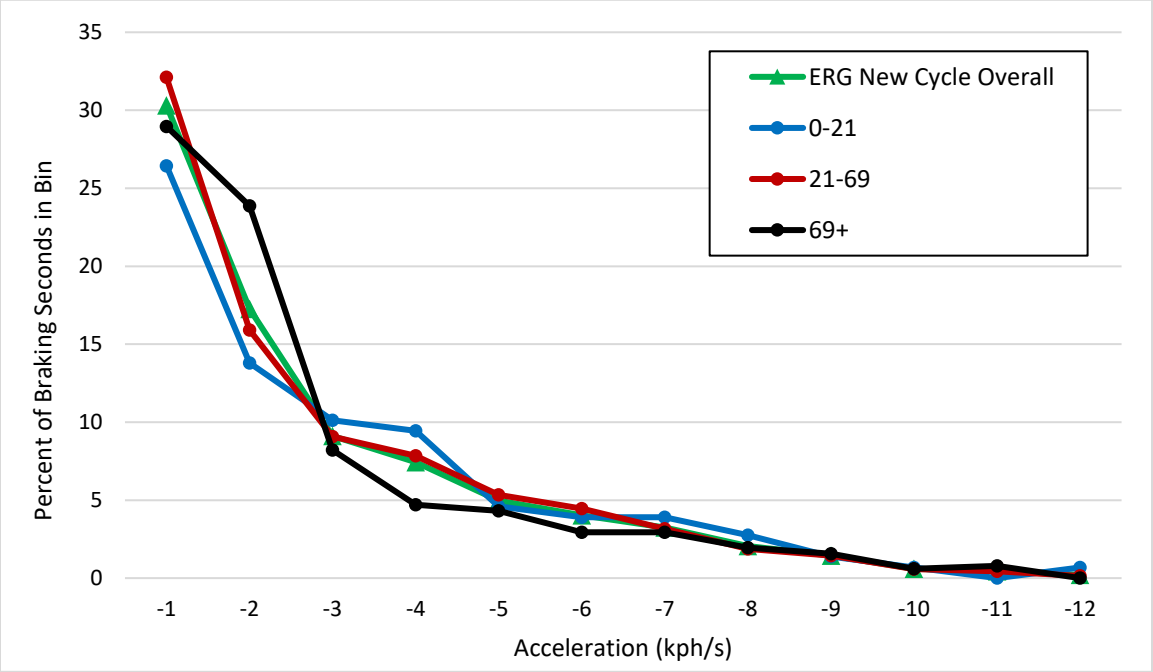

The distributions of modeled brake temperatures for each speed segment are presented in the following figure. It can be generally seen that the temperatures for the high speed segment tend to be somewhat lower (where there would be more cooling taking place) than the temperatures for the other two speed segments.

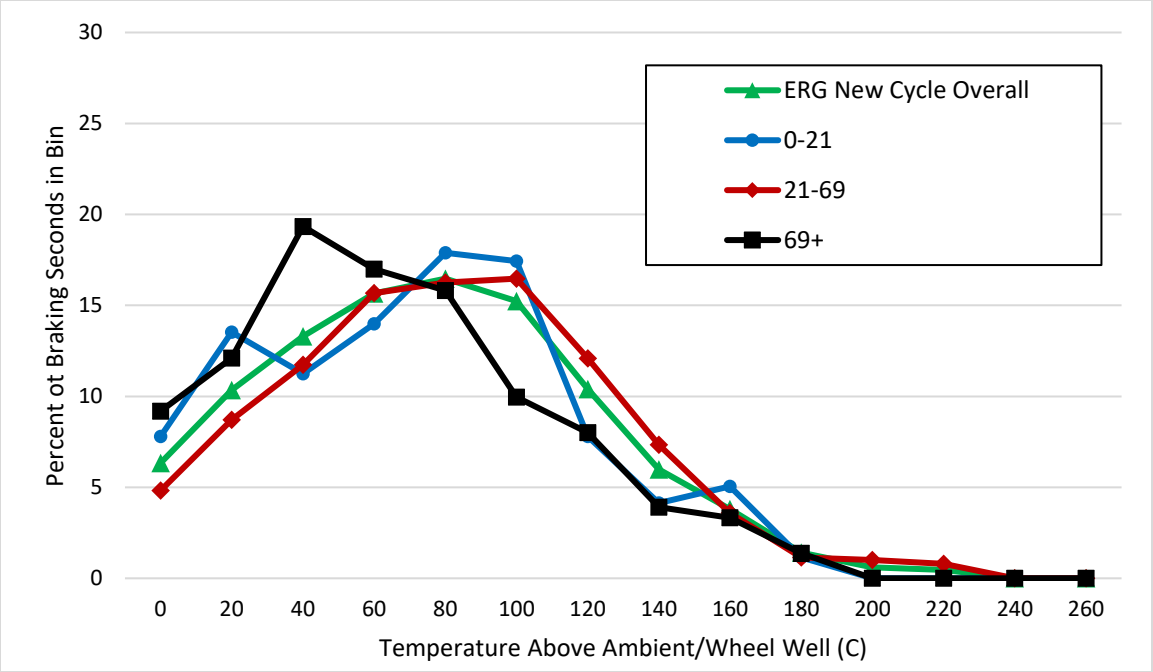
30
25
20
15
10
5
0
Percent ot Braking Seconds in Bin
0
20
40
60
80
100
120
140
160
180
200
220
240
260
Temperature Above Ambient/Wheel Well (C)
ERG New Cycle Overall
0-21
21-69
69+

Appendix F

Test Matrix and Test Dates

The complete test matrix is presented in this Appendix. Note under Teflon Filter analysis, all planned tests in which CARB was planned for analysis of the Teflon filters are indicated. Tests in which this column is left blank may be either analyzed by EPA or not subject to any further speciation analyses depending on EPA preferences. There are four tests in the matrix that were conducted over the WLTP-Brake cycle. These are labeled in the Replicates column as WLTP-Brake A or B; there were 2 replicates of each planned WLTP-Brake test. The BMC LeafMark is listed if known and listed as Indeterminate (Ind.) if it was not known until ordered components are delivered. The 17RD016 proposal included provision for 90 days of available dynamometer time. LINK estimated that the cooling air flow setting experimentation for all assemblies would require a minimum of 5 days of dynamometer time. So, in the matrix the first 5 test days were reserved for cooling air flow rate setting, 85 tests were prescribed (including the 2 tunnel blanks), adding to a total of 90. This matrix presents the planned tests and order at the onset of the program. During the program, minor changes to the order were made for the following reasons:

- Aftermarket components were not received in time for their planned tests after ordering
- Tests were voided due to equipment malfunctions or other issues that invalidated a test that had been initiated. In this case, this test was postponed if new components needed to be ordered and the matrix was continued
- One test that was scheduled to run over the WLTP-Brake cycle was inadvertently run over the CBDC; this test was kept and the planned WLTP-Brake test was swapped into the place of an equivalent upcoming CBDC test.

As mentioned in the report, there were various reasons why the originally planned testing order was not maintained throughout the program. Delays in sourcing brake components, voided and repeat tests and other minor reasons resulted in the actual test order being changed; however LINK kept to the original plan where possible The table in this appendix also includes the actual date of all valid tests.

Test Matrix Including Planned Test Order and Actual Test Dates

Test Day #	Test Vehicle	Front/Rear	Pad Material	BMC Leaf Mark	Wheel load	# Replicates	Ref. repeat #	Teflon Filter Analysis	Test Date
1-5	Air/Sample flow setting days for each assembly								
6	F-150	Front	OES-NAO	N	ETW	N/A	1	ARB	9/30/2019
7	F-150	Front	OES-NAO	N	HLW	A		EPA	10/13/2019
8	Camry	Front	OES-NAO	A	ETW	A		ARB	10/2/2019
9	Civic	Rear (Drum)	OES-NAO	N	ETW	A		EPA	10/3/2019
10	Camry	Rear	OES-NAO	A	ETW	A		ARB	10/5/2019
11	Sienna	Front	OES-NAO	A	ETW	A		EPA	10/6/2019
12	Prius	Front	OES-NAO	A	ETW	A		EPA	10/7/2019
13	Sienna	Rear	OES-NAO	B	ETW	A		EPA	10/7/2019
14	Rogue	Front	OES-NAO	A	ETW	A			10/12/2019
15	Camry	Front	OES-NAO	A	ETW	B		EPA	10/9/2019
16	F-150	Rear	OES-NAO	A	ETW	A		EPA	10/10/2019
Testing PAUSE									10/14-20/2019
17	Tunnel Blank 1					A			10/29/2019
18	Rogue	Rear	After-NAO	Ind.	HLW	A			10/28/2019
19	Rogue	Rear	OES-NAO	A	ETW	A		ARB	10/21/2019
20	Rogue	Rear	After-NAO	Ind.	ETW	A		ARB	10/29/2019
21	Camry	Rear	OES-NAO	A	ETW	B			10/22/2019
22	Camry	Rear	After-NAO	Ind.	ETW	B			10/24/2019
23	Camry	Rear	After-LM	A?	ETW	B			10/23/2019
24	F-150	Front	OES-NAO	N	ETW	N/A	2		10/25/2019
25	Civic	Rear (Drum)	OES-NAO	N	ETW	B		ARB	10/30/2019
26	Civic	Rear (Drum)	After-NAO	Ind.	ETW	B			12/13/2019
27	Prius	Rear	OES-NAO	A	ETW	A		EPA	10/27/2019
28	Prius	Rear	After-NAO	Ind.	ETW	A		ARB	10/27/2019
29	F-150	Rear	After-NAO	N	ETW	A		ARB	11/1/2019

Test Day #	Test Vehicle	Front/Rear	Pad Material	BMC Leaf Mark	Wheel load	# Replicates	Ref. repeat #	Teflon Filter Analysis	Test Date
30	F-150	Rear	After-LM	A	ETW	A		ARB	11/2/2019
31	F-150	Rear	OES-NAO	A	HLW	A		ARB	11/2/2019
32	F-150	Rear	After-LM	A	HLW	A		ARB	11/3/2019
33	Sienna	Front	OES-NAO	A	ETW	B		ARB	11/4/2019
34	Sienna	Front	OES-NAO	A	HLW	B			11/19/2019
35	Sienna	Front	After-NAO	N	ETW	B			12/26/2019
36	Sienna	Front	After-NAO	N	HLW	B			1/26/2020
37	Rogue	Front	OES-NAO	A	HLW	A		ARB	1/26/2020
38	Rogue	Front	After-NAO	Ind.	ETW	A		ARB	11/20/2019
39	F-150	Front	OES-NAO	N	HLW	B			11/9/2019
40	F-150	Front	After-LM	A	ETW	B			11/10/2019
41	F-150	Front	After-LM	A	HLW	B			11/21/2019
42	F-150	Front	After-NAO	N	ETW	B			11/10/2019
43	F-150	Front	OES-NAO	N	ETW	N/A	3	ARB	11/11/2019
44	F-150	Front	OES	N	ETW	WLTP A			11/12/2019
45	Camry	Front	After-NAO	Ind.	ETW	A		ARB	11/22/2019
46	Camry	Front	After-LM	A?	ETW	A		ARB	11/23/2019
47	Camry	Front	OES	A	ETW	WLTP A			1/18/2020
48	Prius	Front	OES-NAO	A	ETW	B		ARB	11/26/2019
49	Prius	Front	After-NAO	Ind.	ETW	A		ARB	11/26/2019
50	Prius	Front	After-NAO	Ind.	ETW	B			1/27/2020
51	Civic	Front	OES-NAO	A	ETW	A		ARB	12/6/2019
52	Civic	Front	After-NAO	Ind.	ETW	A		ARB	12/7/2019
53	Sienna	Rear	OES-NAO	B	ETW	B		ARB	12/8/2019
54	Sienna	Rear	OES-NAO	B	HLW	B			12/9/2019
55	Sienna	Rear	After-NAO	N	ETW	B			12/10/2019
56	Sienna	Rear	After-NAO	N	HLW	B			12/11/2019
57	Civic	Rear (Drum)	After-NAO	Ind.	ETW	A		ARB	12/12/2019

Test Day #	Test Vehicle	Front/Rear	Pad Material	BMC Leaf Mark	Wheel load	# Replicates	Ref. repeat #	Teflon Filter Analysis	Test Date
58	Camry	Rear	After-NAO	Ind.	ETW	A		ARB	12/19/2019
59	Camry	Rear	After-LM	A?	ETW	A		ARB	12/20/2019
60	Rogue	Front	OES-NAO	A	ETW	B		ARB	12/16/2019
61	Rogue	Front	OES-NAO	A	HLW	B			12/17/2019
62	Rogue	Front	After-NAO	Ind.	ETW	B			12/18/2019
63	F-150	Front	After-LM	A	ETW	A		ARB	12/20/2019
64	F-150	Front	After-LM	A	HLW	A		ARB	12/21/2019
65	F-150	Front	After-NAO	N	ETW	A		ARB	12/22/2019
66	Tunnel Blank 2					B			1/5/2020
67	F-150	Front	OES-NAO	N	ETW	N/A	4		1/16/2020
68	Sienna	Front	OES-NAO	A	HLW	A		ARB	12/23/2019
69	Sienna	Front	After-NAO	N	ETW	A		ARB	12/24/2019
70	Sienna	Front	After-NAO	N	HLW	A		ARB	12/25/2019
71	Camry	Front	After-NAO	Ind.	ETW	B			12/27/2019
72	Camry	Front	After-LM	A?	ETW	B			12/28/2019
73	Camry	Front	OES	A	ETW	WLTP B			1/21/2020
74	F-150	Rear	OES-NAO	A	ETW	B		ARB	12/29/2019
75	F-150	Rear	After-NAO	N	ETW	B			12/30/2019
76	F-150	Rear	After-LM	A	ETW	B			12/31/2019
77	F-150	Rear	OES-NAO	A	HLW	B			1/19/2020
78	F-150	Rear	After-LM	A	HLW	B			1/25/2020
79	Prius	Rear	OES-NAO	A	ETW	B		ARB	1/12/2020
80	Prius	Rear	After-NAO	Ind.	ETW	B			1/28/2020
81	Rogue	Rear	OES-NAO	A	ETW	B			1/4/2020
82	Rogue	Rear	After-NAO	Ind.	ETW	B			1/4/2020
83	Rogue	Rear	After-NAO	Ind.	HLW	B			1/5/2020
84	Civic	Front	OES-NAO	A	ETW	B			1/10/2020
85	Civic	Front	After-NAO	Ind.	ETW	B			1/11/2020

Test Day #	Test Vehicle	Front/Rear	Pad Material	BMC Leaf Mark	Wheel load	# Replicates	Ref. repeat #	Teflon Filter Analysis	Test Date
86	Sienna	Rear	OES-NAO	B	HLW	A		ARB	1/13/2020
87	Sienna	Rear	After-NAO	N	ETW	A		ARB	1/29/2020
88	Sienna	Rear	After-NAO	N	HLW	A		ARB	1/14/2020
89	F-150	Front	OES	N	ETW	WLTP B			1/17/2020
90	F-150	Front	OES-NAO	N	ETW	N/A	5	ARB	1/17/2020

Appendix G

CVS Flow Setting Results

This appendix presents the temperatures measured to validate the CVS air flowrate setting. Brake rotor temperatures as measured on the proving ground track over the WLTP-Brake Trip 10 are presented as the target for matching. The measured brake rotor temperatures from the same speed trace run on the dynamometer are presented for comparison. Results are shown for the final selected flowrate for each brake assembly (that shown in **Error! Reference source not found.** of the main report). Note that the selection method biased the temperature match to be best around the peak temperature for each assembly; ERG's literature search indicated that high temperatures represent the driving mode in which brake emissions could be expected to be highest[4], and matching at elevated temperatures also allowed a similar temperature range to be covered during each test as the track given that tests begin at room temperature. Temperature traces are presented for the front and rear assemblies of each vehicle.

Temperature and speed traces for each assembly are presented; traces labeled as "PG" represent the proving ground track testing, and those labeled "D" represent the dynamometer test. At the right of each trace are corresponding box plots indicating various statistics on the proving ground and dynamometer temperature traces. The central line of each box is the median temperature, and the top and bottom of each box are the 75th and 25th percentile values, respectively. The ends of each bar display the maximum and minimum values for each trace.

[4] B.D. Garg, S.H. Cadle, P.A. Mulawa, P.J. Groblicki, C. Laroo, G.A. Parr, "Brake Wear Particulate Matter Emissions," Environmental Science and Technology, 2000, Volume 34, Number 21, pages 4463-4469, DOI: 10.1021/es001108h.

Camry Temperature Traces for CVS Flow Rate Setting

Front

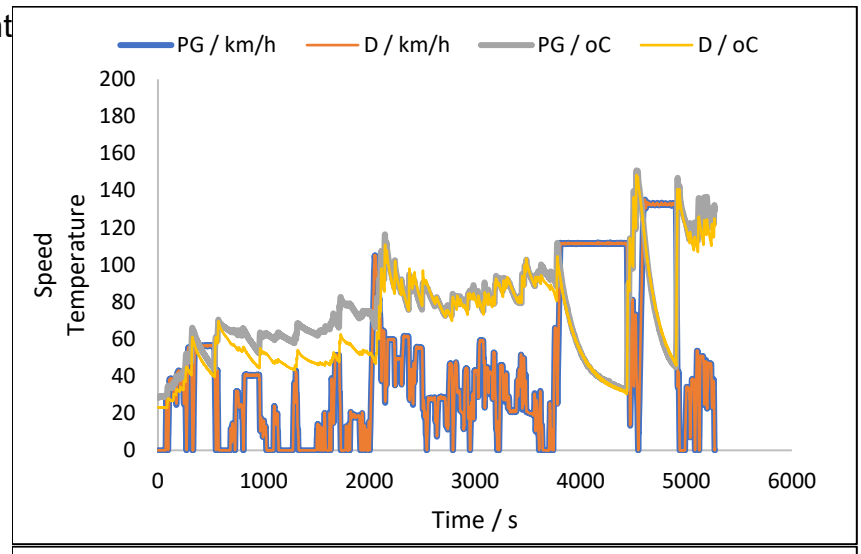

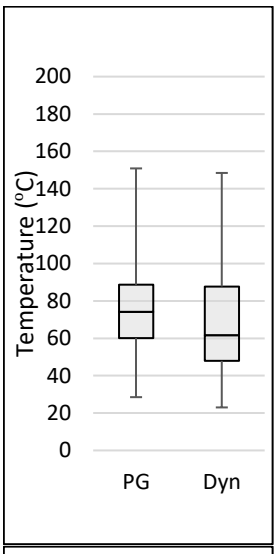

Rear

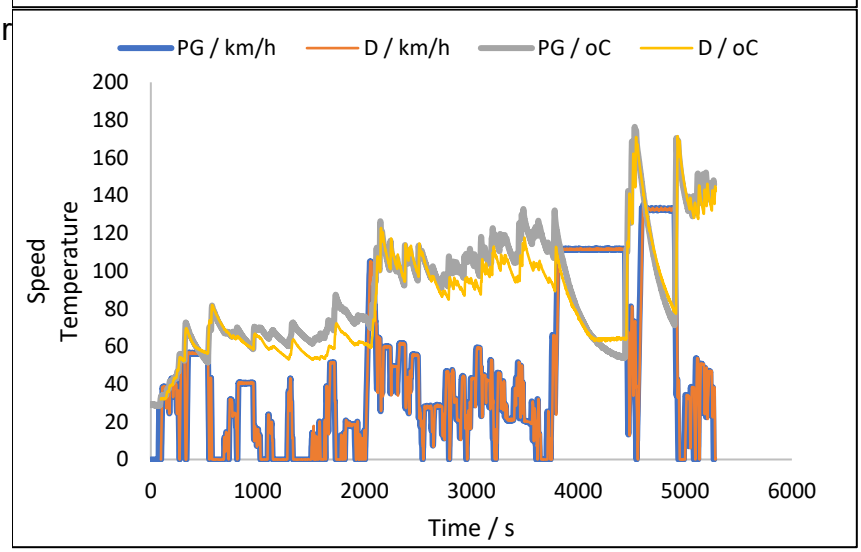

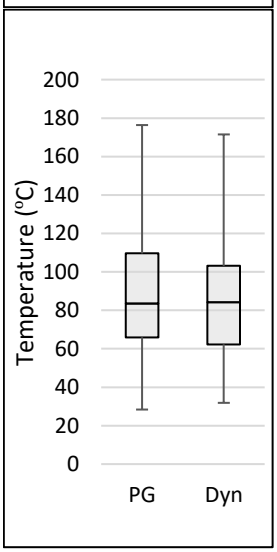

Civic Temperature Traces for CVS Flow Rate Setting

Front

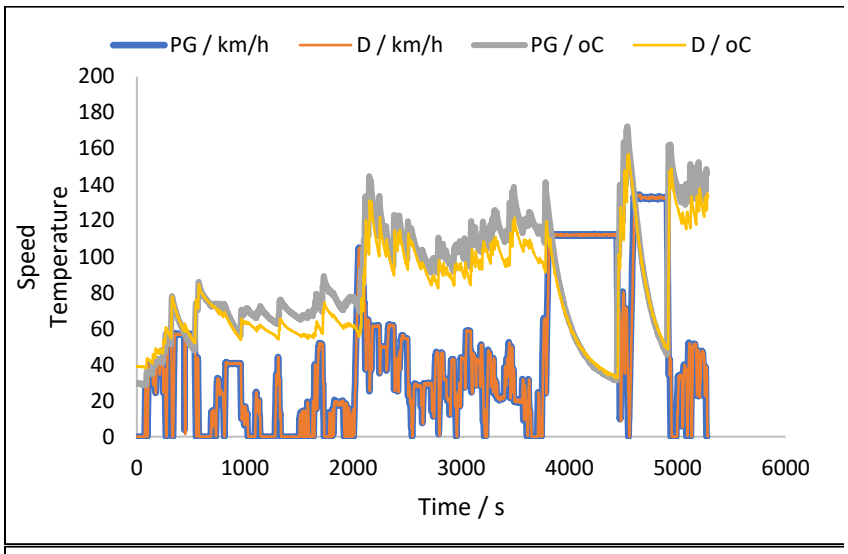

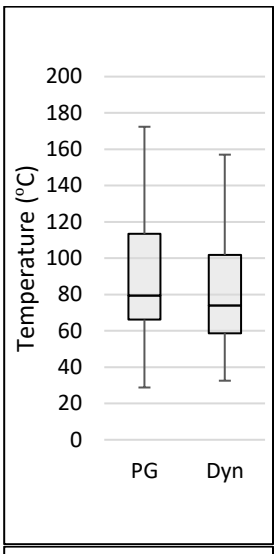

Rear

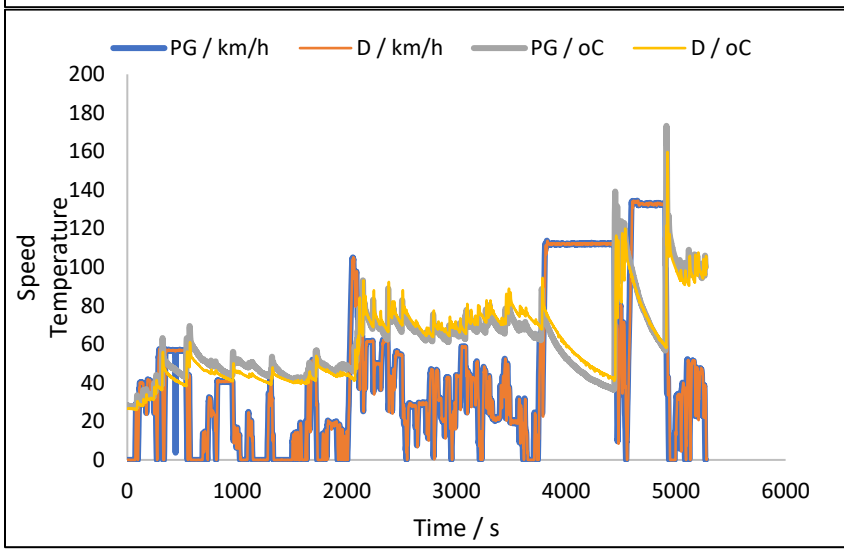

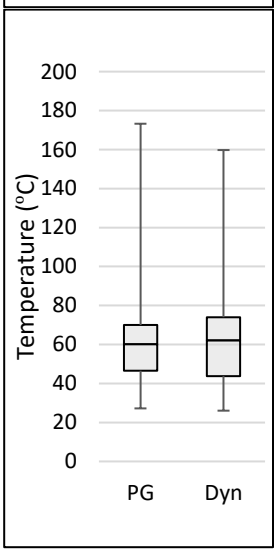

F-150 Temperature Traces for CVS Flow Rate Setting

Front

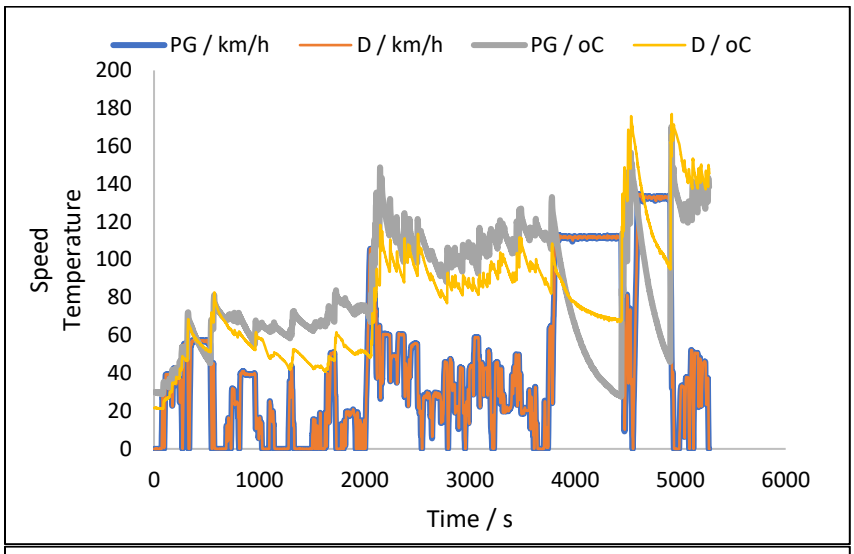

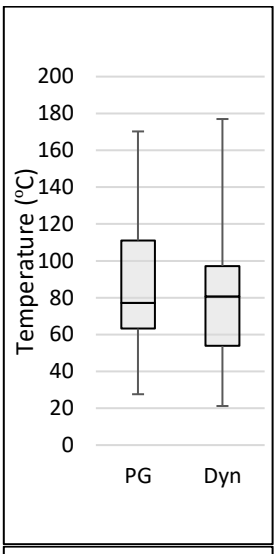

Rear

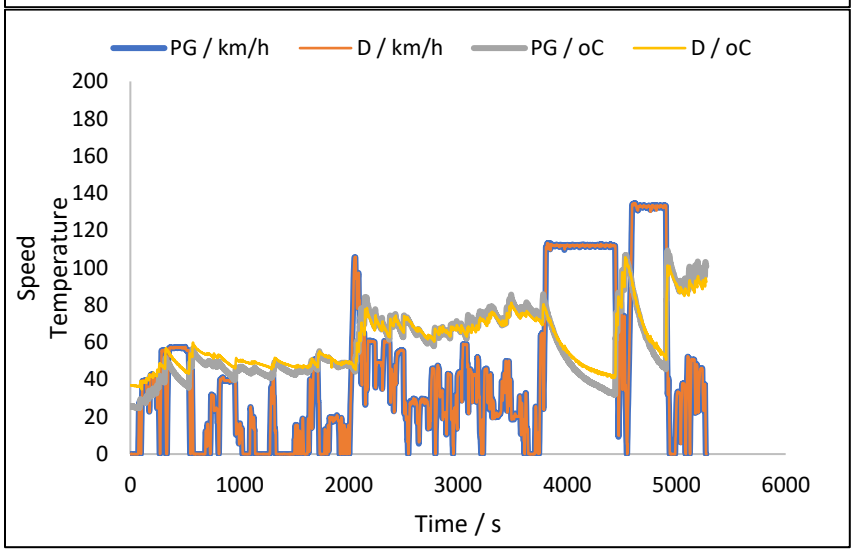

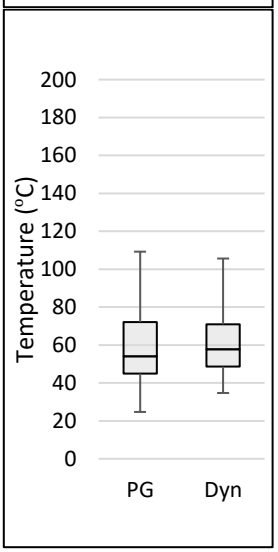

Prius Temperature Traces for CVS Flow Rate Setting

Front

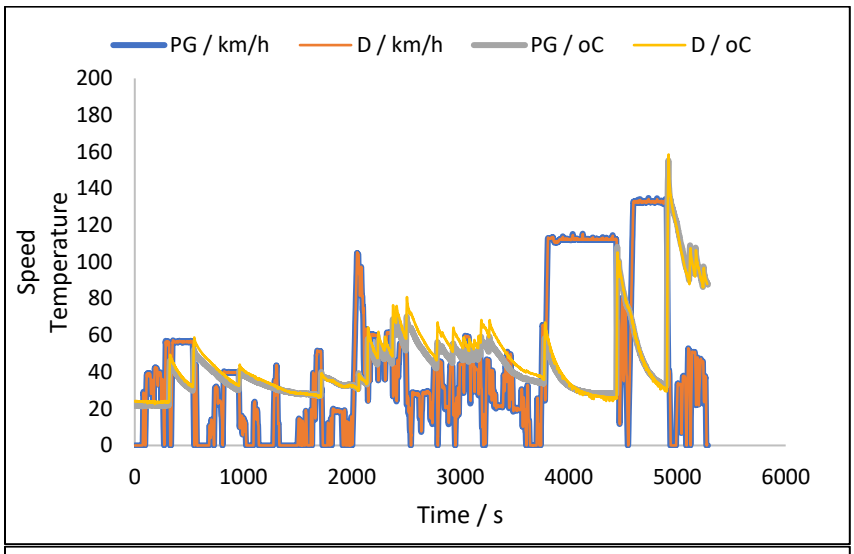

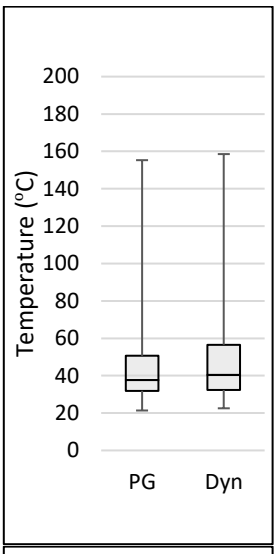

Rear

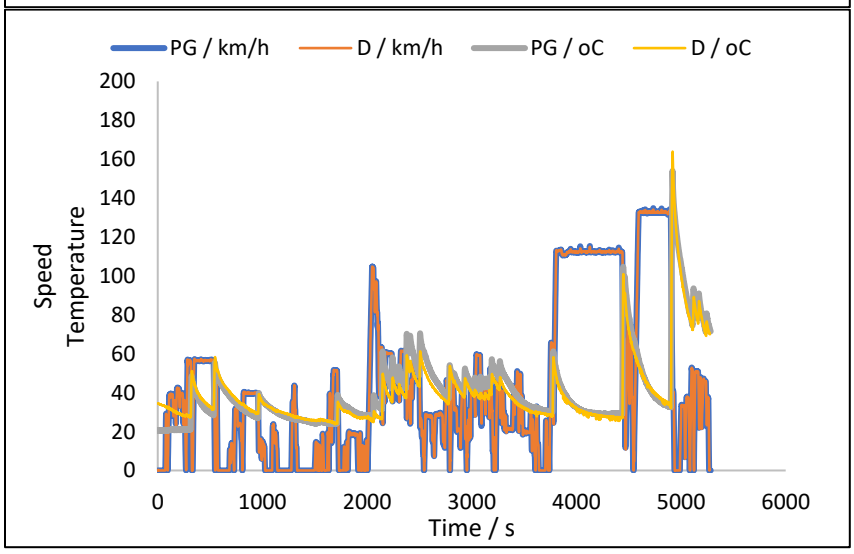

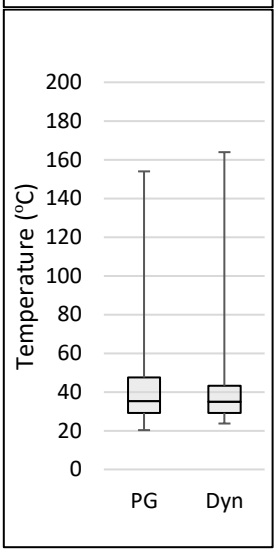

Rogue Temperature Traces for CVS Flow Rate Setting

Front

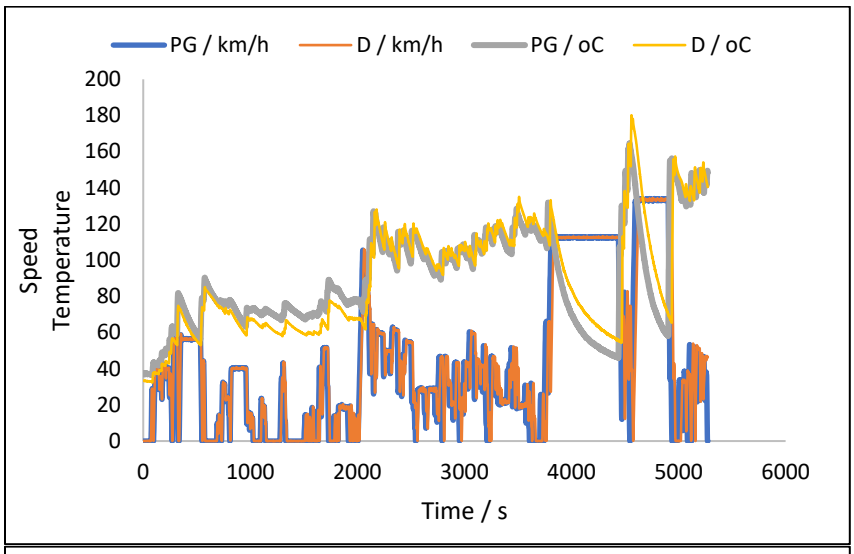

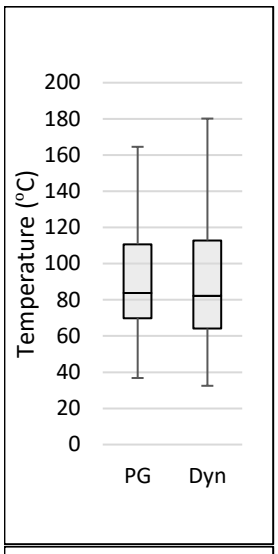

Rear

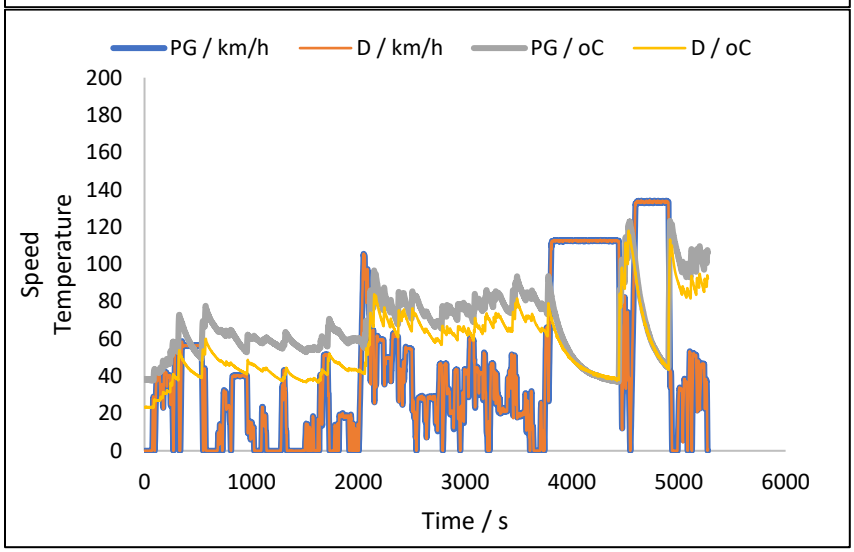

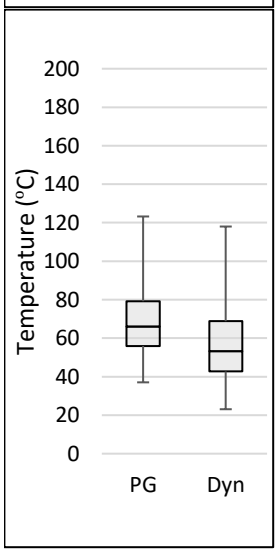

Sienna Temperature Traces for CVS Flow Rate Setting

Front

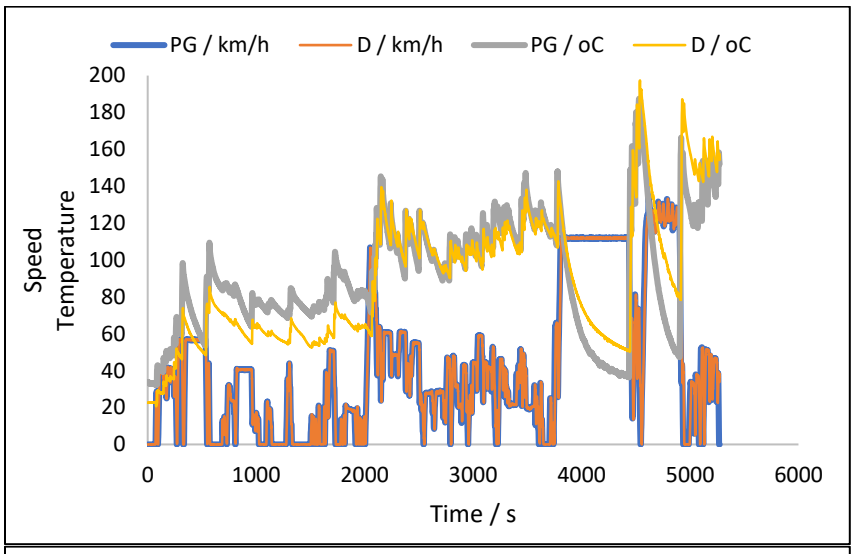

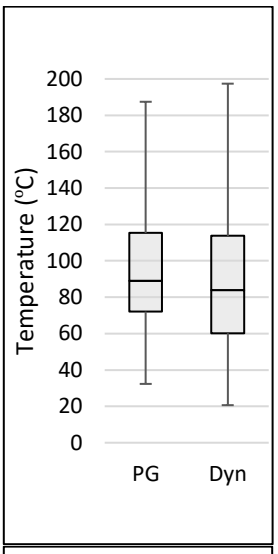

Rear

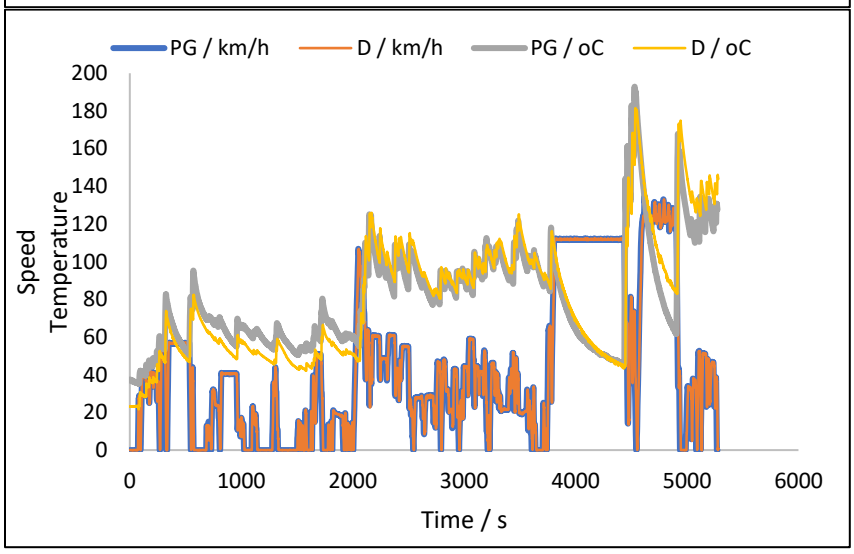

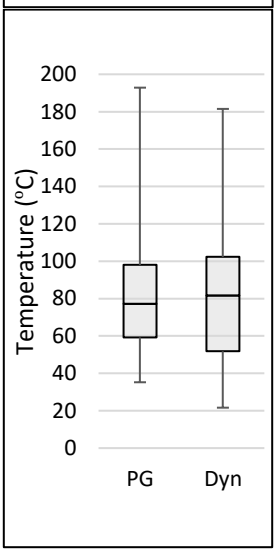

Appendix H

Tabulated Test Result Summary

Test results and measured operational parameters are presented in this appendix. “Test day” refers to the test day number given in the Task 2 test matrix, not necessarily the actual order in which tests were conducted. “F/R” indicates the front or rear axle assembly being tested. “Pad” indicates the friction material used during the test; OES indicates the OES material, all of which were NAO, NAO indicates Aftermarket NAO, and LM indicates the aftermarket low metallic. “Avg. Torq” refers to the average torque applied to the dynamometer drive shaft by the hydraulic brakes during the test, and “Avg. Press” refers to the average brake-circuit hydraulic pressure during the test. “PN” refers to particle number count as measured by the condensation particle counter (CPC), which measures between the range of 23 nm to 2.1 µm. The three size cutpoints are given for the gravimetric mass measurement of the 100S4, and the PM10, as measured by the 47mm Teflon PMS, is given in next column. The rightmost columns indicate the 100S4 PM2.5 and PM10 values presented on the basis of mass per second of braking to be on the same basis as MOVES opmode 0.

Test Day #	Test Veh.	F / R	Pad	Tst Wt	Avg. Torq N·m	Avg. Press kPa	Avg. Rotor Temp °C	Peak Rotor Temp °C	PN 23 nm-2.1 µm CPC #/cc	Avg. CPC PN 23 nm - 2.1 µm #	Total Pad and Rotor Wear (g)[a]	100S4 Sg3 (PM2.5-10) Emission mg/mi	100S4 Sg4 (PM1-2.5) Emission mg/mi	100S4 Aft Filter (PM < 1) Emission mg/mi	Brake PM_{10} per PMS (mg/mi)	100S4 PM2.5 per s braking time (mg/s)	100S4 PM10 per s braking time (mg/s)
6	F-150	F	OES	ETW	259	594	103.2	234.9	29.0	1.072E+11	3.7	0.7512	0.4933	0.3315	1.3432	0.0430	0.0822
7	F-150	F	OES	HLW	316	674	119.2	251.2	33.9	1.252E+11	3.3	1.1711	0.6792	0.5587	1.5741	0.0645	0.1256
8	Camry	F	OES	ETW	146	570	110.4	246.3	83.6	4.532E+10	6.2	1.2773	0.4987	0.1436	1.6942	0.0335	0.1001
9	Civic	R	OES	ETW	34	832	125.2	231.7	91.9	4.977E+10	1.5	0.1156	0.1472	0.1120	0.3493	0.0135	0.0195
10	Camry	R	OES	ETW	51	497	114.3	181.9	118.7	6.430E+10	2.7	0.6329	0.4848	0.1752	1.0943	0.0344	0.0674
11	Sienna	F	OES	ETW	183	493	117.6	243.4	255.3	1.341E+11	9.9	2.4060	1.0530	0.3115	3.2632	0.0711	0.1966
12	Prius	F	OES	ETW	58	302	73.1	186.0	41.1	8.311E+10	2.9	0.5794	0.4008	0.1483	1.3922	0.0286	0.0588
13	Sienna	R	OES	ETW	88	792	134.1	237.5	149.6	8.110E+10	3.7	0.9403	0.5772	0.0831	1.3773	0.0344	0.0835
14	Rogue	F	OES	ETW	152	646	118.1	236.5	577.1	3.130E+11	6.2	1.6787	1.0086	0.3467	2.7309	0.0707	0.1582
15	Camry	F	OES	ETW	133	526	110.4	245.3	138.0	7.522E+10	6.2	1.5849	0.5995	0.1228	2.0689	0.0377	0.1203
16	F-150	R	OES	ETW	95	430	73.5	119.1	184.4	1.000E+11	6.5	0.7476	0.5345	0.1941	1.3135	0.0380	0.0770
17	**Tunnel Blank 1**								0.2						0.0291		
18	Rogue	R	NAO	HLW	58	599	76.8	162.7	80.4	4.405E+10	3.3	0.4307	0.3169	0.1102	0.7834	0.0223	0.0447
19	Rogue	R	OES	ETW	56	661	70.2	142.3	151.8	8.223E+10	2.6	0.7191	0.4743	0.1219	1.2108	0.0311	0.0686
20	Rogue	R	NAO	ETW	50	564	75.3	154.2	132.0	7.227E+10	3.3	0.4856	0.3565	0.1291	0.9789	0.0253	0.0506
21	Camry	R	OES	ETW	51	552	116.2	186.2	107.4	5.819E+10	2.8	0.6533	0.4907	0.1183	1.1458	0.0318	0.0658

Test Day #	Test Veh.	F / R	Pad	Tst Wt	Avg. Torq N·m	Avg. Press kPa	Avg. Rotor Temp °C	Peak Rotor Temp °C	PN 23 nm-2.1 µm CPC #/cc	Avg. CPC PN 23 nm - 2.1 µm #	Total Pad and Rotor Wear (g)[a]	100S4 Sg3 (PM2.5-10) Emission mg/mi	100S4 Sg4 (PM1-2.5) Emission mg/mi	100S4 Aft Filter (PM < 1) Emission mg/mi	Brake PM_{10} per PMS (mg/mi)	100S4 PM2.5 per s braking time (mg/s)	100S4 PM10 per s braking time (mg/s)
22	Camry	R	NAO	ETW	45	413	127.7	206.6	128.1	7.014E+10	4	0.7179	0.5572	0.1571	1.2446	0.0372	0.0747
23	Camry	R	LM	ETW	51	552	111.1	185.6	186.6	1.022E+11	3.1	1.7370	0.6974	0.2095	2.2983	0.0473	0.1379
24	F-150	F	OES	ETW	249	549	103.5	237.1	16.4	6.123E+10	5.8	0.6689	0.3496	0.3622	1.0859	0.0371	0.0720
25	Civic	R	OES	ETW	32	788	96.9	153.9	58.1	3.179E+10	5.2	0.0731	0.0804	0.0713	0.3296	0.0079	0.0117
26	Civic	R	NAO	ETW	33	739	92.8	175.6	104.2	5.707E+10	3.2	0.7868	0.3270	0.1264	1.3536	0.0236	0.0647
27	Prius	R	OES	ETW	20	246	62.3	156.1	17.7	3.630E+10	1.1	0.2391	0.2019	0.0944	0.5442	0.0154	0.0279
28	Prius	R	NAO	ETW	21	274	63.7	160.9	25.6	5.229E+10	1.3	0.1784	0.1582	0.1449	0.3637	0.0158	0.0251
29	F-150	R	NAO	ETW	84	329	70.9	117.8	269.0	1.475E+11	3.4	1.4611	0.9500	0.2989	2.5550	0.0651	0.1413
30	F-150	R	LM	ETW	88	579	67.4	117.6	144.5	7.918E+10	3	1.4611	0.9500	0.2989	2.6306	0.0651	0.1413
31	F-150	R	OES	HLW	105	453	86.5	146.2	164.0	9.176E+10	5.7	0.8994	0.4939	0.1011	1.1918	0.0310	0.0779
32	F-150	R	LM	HLW	111	631	72.8	125.4	139.0	7.619E+10	3.2	1.2050	0.5050	0.0903	1.5381	0.0310	0.0939
33	Sienna	F	OES	ETW	172	504	113.8	248.3	240.0	1.316E+11	7.3	1.6431	0.8754	0.1959	2.6295	0.0559	0.1415
34	Sienna	F	OES	HLW	197	523	121.8	268.3	266.6	1.462E+11	7.1	2.3284	1.1091	0.2546	3.3531	0.0711	0.1925
35	Sienna	F	NAO	ETW	170	520	120.9	250.8	663.3	3.641E+11	6.4	1.8041	1.2351	0.3557	3.4047	0.0829	0.1770
36	Sienna	F	NAO	HLW	189	530	129.3	260.6	424.5	2.331E+11	1.7	3.0364	1.7150	0.5246	5.3524	0.1168	0.2751
37	Rogue	F	OES	HLW	159	622	139.4	264.6	438.4	2.403E+11	0.5	3.3931	1.6843	0.5282	5.5660	0.1154	0.2923
38	Rogue	F	NAO	ETW	146	530	122.4	255.4	312.3	1.712E+11	6.8	2.1538	1.1387	0.3025	2.5123	0.0751	0.1874
39	F-150	F	OES	HLW	257	559	104.1	253.6	36.8	1.372E+11	4.5	0.7348	0.4031	0.3193	1.0776	0.0377	0.0760
40	F-150	F	LM	ETW	226	557	91.6	213.1	62.2	2.322E+11	16.6	3.9896	1.9996	0.4236	5.5549	0.1264	0.3344
41	F-150	F	LM	HLW	276	635	99.9	244.0	88.4	3.301E+11	18.3	7.5629	2.6190	0.2579	9.6947	0.1500	0.5443
42	F-150	F	NAO	ETW	226	651	98.5	214.4	31.8	1.188E+11	5.3	0.7222	0.4763	0.0614	1.3003	0.0280	0.0657
43	F-150	F	OES	ETW	241	456	106.4	218.9	20.4	7.612E+10	3.8	0.8705	0.5081	0.0860	1.2329	0.0310	0.0764
44	F-150	F	OES	ETW	228	487	96.9	211.4	16.3	6.070E+10	3.9	0.6250	0.3792	0.0061	1.0556	0.0201	0.0527
45	Camry	F	NAO	ETW	135	505	103.1	234.5	188.9	1.035E+11	4.5	1.7274	0.7565	0.2221	2.5411	0.0510	0.1411
46	Camry	F	LM	ETW	144	523	107.0	243.2	383.0	2.084E+11	7.9	3.2827	0.8459	0.2772	4.1068	0.0586	0.2297
47	Camry	F	OES	ETW	149	613	76.9	165.6	17.0	1.664E+10	6.4	0.3780	0.1267	0.0383	0.5591	0.0126	0.0414

Test Day #	Test Veh.	F / R	Pad	Tst Wt	Avg. Torq N·m	Avg. Press kPa	Avg. Rotor Temp °C	Peak Rotor Temp °C	PN 23 nm-2.1 µm CPC #/cc	Avg. CPC PN 23 nm - 2.1 µm #	Total Pad and Rotor Wear (g)[a]	100S4 Sg3 (PM2.5-10) Emission mg/mi	100S4 Sg4 (PM1-2.5) Emission mg/mi	100S4 Aft Filter (PM < 1) Emission mg/mi	Brake PM_{10} per PMS (mg/mi)	100S4 PM2.5 per s braking time (mg/s)	100S4 PM10 per s braking time (mg/s)
48	Prius	F	OES	ETW	56	300	64.0	173.2	20.1	4.113E+10	2.6	0.4632	0.2710	0.0539	0.8795	0.0169	0.0411
49	Prius	F	NAO	ETW	56	304	67.8	190.3	66.8	1.368E+11	2.6	0.4466	0.3859	0.1820	0.9305	0.0296	0.0529
50	Prius	F	NAO	ETW	54	257	77.0	183.5	334.9	6.860E+11	0.8	0.6171	0.5630	0.3135	1.7420	0.0457	0.0779
51	Civic	F	OES	ETW	106	542	104.7	235.4	263.3	1.446E+11	5.4	1.0051	0.4334	0.0668	1.4537	0.0261	0.0785
52	Civic	F	NAO	ETW	99	531	107.1	239.9	364.0	1.999E+11	3	1.1477	0.6194	0.1725	1.7565	0.0413	0.1011
53	Sienna	R	OES	ETW	74	657	130.5	239.1	144.3	7.919E+10	3.4	0.6065	0.6103	0.0849	1.6315	0.0362	0.0918
54	Sienna	R	OES	HLW	84	765	149.1	274.5	184.3	1.012E+11	3.6	1.5234	0.8009	0.1372	2.3943	0.0489	0.1284
55	Sienna	R	NAO	ETW	79	715	138.9	250.7	79.2	4.349E+10	4.7	0.6038	0.3699	0.0488	1.0051	0.0218	0.0533
56	Sienna	R	NAO	HLW	92	822	156.2	274.0	71.6	3.930E+10	4.2	0.8197	0.4015	0.0542	0.8939	0.0238	0.0665
57	Civic	R	NAO	ETW	36	755	113.9	218.0	65.9	3.609E+10	2.6	0.6065	0.2886	0.0135	0.9999	0.0158	0.0474
58	Camry	R	NAO	ETW	46	387	145.6	214.9	143.5	7.865E+10	3.5	0.6286	0.5292	0.1481	1.2192	0.0353	0.0681
59	Camry	R	LM	ETW	48	511	122.1	192.1	342.0	1.874E+11	2.1	2.2237	1.0269	0.2528	3.2695	0.0667	0.1827
60	Rogue	F	OES	ETW	127	548	122.6	231.7	412.5	2.269E+11	9.5	3.0699	1.5073	0.5092	4.9036	0.1051	0.2652
61	Rogue	F	OES	HLW	148	608	136.7	253.5	314.4	1.723E+11	13.8	3.7672	1.5381	0.5390	5.7154	0.1083	0.3047
62	Rogue	F	NAO	ETW	133	472	131.5	247.3	268.9	1.474E+11	5.9	1.7445	1.0346	0.2664	2.7544	0.0678	0.1588
63	F-150	F	LM	ETW	261	637	88.4	210.8	105.1	3.925E+11	14.5	6.5346	2.7330	0.7429	8.3941	0.1812	0.5220
64	F-150	F	LM	HLW	291	626	110.2	264.1	115.7	4.277E+11	18.9	10.8371	3.8848	0.7797	13.199	0.2432	0.8083
65	F-150	F	NAO	ETW	242	610	102.1	227.3	53.6	2.004E+11	2.9	1.8582	0.9182	0.3070	2.6385	0.0639	0.1608
66	**Tunnel Blank 2**								0.4						0.0962		
67	F-150	F	OES	ETW	261	630	69.1	159.3	14.5	8.013E+10	4.2	0.5668	0.2393	0.2140	1.3995	0.0346	0.0778
68	Sienna	F	OES	HLW	198	577	124.5	259.6	275.8	1.514E+11	10.1	2.6269	1.2261	0.2320	3.9597	0.0760	0.2130
69	Sienna	F	NAO	ETW	156	482	115.1	248.2	803.5	4.448E+11	3.8	2.6351	1.3625	0.5110	4.0958	0.0977	0.2351
70	Sienna	F	NAO	HLW	184	573	126.7	274.6	484.0	2.656E+11	8.4	4.0160	1.7572	0.6438	6.2149	0.1252	0.3346
71	Camry	F	NAO	ETW	141	514	104.8	254.2	189.0	1.037E+11	7.2	1.9406	0.8306	0.2826	3.1981	0.0580	0.1592
72	Camry	F	LM	ETW	143	505	101.1	223.5	146.0	8.011E+10	4.8	2.6269	0.6129	0.1381	3.1771	0.0392	0.1761
73	Camry	F	OES	ETW	143	591	79.3	178.4	24.7	2.273E+10	5.2	0.5023	0.1566	0.0475	0.6961	0.0156	0.0539

Test Day #	Test Veh.	F / R	Pad	Tst Wt	Avg. Torq N·m	Avg. Press kPa	Avg. Rotor Temp °C	Peak Rotor Temp °C	PN 23 nm-2.1 µm CPC #/cc	Avg. CPC PN 23 nm - 2.1 µm #	Total Pad and Rotor Wear (g)[a]	100S4 Sg3 (PM2.5-10) Emission mg/mi	100S4 Sg4 (PM1-2.5) Emission mg/mi	100S4 Aft Filter (PM < 1) Emission mg/mi	Brake PM_{10} per PMS (mg/mi)	100S4 PM2.5 per s braking time (mg/s)	100S4 PM10 per s braking time (mg/s)
74	F-150	R	OES	ETW	92	414	73.9	144.6	203.4	1.117E+11	5.9	0.9210	0.5715	0.1228	1.6133	0.0362	0.0842
75	F-150	R	NAO	ETW	79	323	72.2	119.7	224.8	1.234E+11	6	2.0653	1.0736	0.3268	3.4768	0.0730	0.1807
76	F-150	R	LM	ETW	79	431	68.6	120.2	306.3	1.681E+11	4.4	1.4341	0.7892	0.2266	2.4870	0.0530	0.1277
77	F-150	R	OES	HLW	99	349	91.4	150.5	229.9	1.263E+11	4.8	2.0013	0.9708	0.2411	3.2885	0.0632	0.1675
78	F-150	R	LM	HLW	97	422	83.6	131.7	383.3	2.106E+11	2.4	2.2069	1.0535	0.3422	3.6268	0.0728	0.1879
79	Prius	R	OES	ETW	20	261	60.0	151.3	20.3	4.170E+10	0.9	0.2083	0.1915	0.0472	0.4232	0.0124	0.0233
80	Prius	R	NAO	ETW	21	242	66.6	168.4	20.0	4.092E+10	0.7	0.1649	0.1818	0.1551	0.3686	0.0176	0.0262
81	Rogue	R	OES	ETW	51	631	68.2	145.3	163.8	8.976E+10	2.8	0.7546	0.4059	0.1156	1.3110	0.0272	0.0665
82	Rogue	R	NAO	ETW	46	477	72.2	141.3	104.9	5.747E+10	2.3	0.5387	0.3816	0.0831	0.4514	0.0242	0.0523
83	Rogue	R	NAO	HLW	51	510	79.7	168.3	127.4	6.987E+10	3.6	0.6408	0.4449	0.0822	1.1996	0.0275	0.0609
84	Civic	F	OES	ETW	112	560	107.4	233.0	157.5	8.669E+10	3.3	0.9255	0.4161	0.0930	1.1391	0.0265	0.0748
85	Civic	F	NAO	ETW	103	532	105.9	245.6	409.3	2.254E+11	4.2	1.4231	0.7178	0.1923	2.2485	0.0475	0.1217
86	Sienna	R	OES	HLW	92	811	155.6	273.5	193.9	1.068E+11	4.2	1.5052	0.7826	0.1535	2.4259	0.0488	0.1273
87	Sienna	R	NAO	ETW	84	738	143.6	248.5	84.2	4.623E+10	1.2	0.6640	0.3804	0.0650	1.1487	0.0232	0.0578
88	Sienna	R	NAO	HLW	96	836	167.3	298.7	93.1	5.105E+10	8.5	0.7798	0.4349	0.1129	1.1979	0.0286	0.0692
89	F-150	F	OES	ETW	251	613	72.9	159.5	14.2	7.996E+10	3.5	0.5392	0.2495	0.2728	0.7214	0.0398	0.0810
90	F-150	F	OES	ETW	259	557	100.2	221.6	14.9	5.553E+10	2.2	0.7425	0.3616	0.2149	1.1561	0.0301	0.0688

[a] – Note that the total pad and rotor wear is measured as the difference between the components' weight before installation into the dynamometer and the weight after removal from the dynaomomter. As such, it includes mass lost during both the burnish cycle and the test cycle.

Appendix I

LINK Test Result Reports

This appendix references the attached LINK test result reports for each test day. Each filename references the test day from the matrix as well as abbreviations of the model, axle, friction material, LeafMark, testweight, and replicate count. The reports are in Excel format with multiple tabs containing a variety of test parameters, result tables, plots, and before and after photographs and measurements of the test components.

The final tab, “Test Data”, contains top-down data from the continuous measurements made during the test day. To reduce file space, each row represents a single event (ie either a deceleration (braking), a cruise, or an acceleration. Values are given as average or max/mins of the measurements taken during each event. The first column, CSV File, indicates the segment of the test day. In general, segment 2 is the burnish and 4 is the test cycle (this can be verified by cross-referencing the times given in the Cumulative Schedule Duration column). Note that, in these automated test reports, values given on a per-distance basis are based on the actual dyno distance traveled, not the CBDC represented distance as in the main report. For analysis of the data, any analysis is encouraged to use the total emissions and divide by the CBDC represented distance as described in the report.

- E.Test-6-F150-FA-OES-NAO-N-ETW-Refn.xlsx
- E.Test-7-F150-FA-OES-NAO-N-HLW-rA.xlsx
- E.Test 8-CAM-FA-OES-NAO-A-ETW-rA.xlsx
- E.Test 9-CIV-RA-OES-NAO-N-ETW-rA.xlsx
- E.Test 10-CAM-RA-OES-NAO-A-ETW-rA.xlsx
- E.Test-11-SIE-FA-OES-NAO-A-ETW-rA.xlsx
- E.Test-12-PRI-FA-OES-NAO-A-ETW-rA.xlsx
- E.Test-13-SIE-RA-OES-NAO-B-ETW-rA.xlsx
- E.Test-14-ROG-FA-OES-NAO-A-ETW-rA.xlsx
- E.Test-15-CAM-FA-OES-NAO-A-ETW-rB.xlsx
- E.Test 16-F150-RA-OES-NAO-A-ETW-rA.xlsx
- E.Test-18-ROG-RA-AM1-NAO-N-HLW-rA.xlsx
- E.Test-19-ROG-RA-OES-NAO-A-ETW-rA.xlsx
- E.Test-20-ROG-RA-AM1-NAO-N-ETW-rA.xlsx
- E.Test 21-CAM-RA-OES-NAO-A-ETW-rB.xlsx
- E.Test-22-CAM-RA-AM1-NAO-N-ETW-rB.xlsx
- E.Test-23-CAM-RA-AM2-LM-A-ETW-rB.xlsx
- E.Test-24-F150-FA-OES-NAO-N-ETW-rNA.xlsx
- E.Test-25-CIV-RA-OES-NAO-N-ETW-rB.xlsx
- E.Test-26-CIV-RA-AM1-NAO-N-ETW-rB.xlsx
- E.Test-27-PRI-RA-OES-NAO-A-ETW-rA.xlsx
- E.Test-28-PRI-RA-AM1-NAO-N-ETW-rA.xlsx
- E.Test-29-F150-RA-AM1-NAO-N-ETW-rA.xlsx
- E.Test-30-F150-RA-AM2-LM-A-ETW-rA.xlsx
- E.Test-31-F150-RA-OES-NAO-A-HLW-rA.xlsx
- E.Test-32-F150-RA-AM2-LM-A-HLW-rA.xlsx
- E.Test-33-SIE-FA-OES-NAO-A-ETW-rB.xlsx
- E.Test-34-SIE-FA-OES-NAO-A-HLW-rB.xlsx
- E.Test-35-SIE-FA-AM1-NAO-N-ETW-rB.xlsx

- E.Test-36-SIE-FA-AM1-NAO-N-HLW-rB.xlsx
- E.Test-37-ROG-FA-OES-NAO-A-HLW-rA.xlsx
- E.Test-38-ROG-FA-AM1-NAO-N-ETW-rA.xlsx
- E.Test-39-F150-FA-OES-NAO-N-HLW-rB.xlsx
- E.Test-40-F150-FA-AM2-LM-A-ETW-rB.xlsx
- E.Test-41-F150-FA-AM2-LM-A-HLW-rB.xlsx
- E.Test-42-F150-FA-AM1-NAO-N-ETW-rB.xlsx
- E.Test-43-F150-FA-OES-NAO-N-ETW-rNA.xlsx
- E.Test-44-F150-FA-OES-NAO-N-ETW-rNA.xlsx
- E.Test-45-CAM-FA-AM1-NAO-N-ETW-rA.xlsx
- E.Test-46-CAM-FA-AM2-LM-A-ETW-rA.xlsx
- E.Test-47-CAM-FA-OES-A-ETW-rWLTP A.xlsx
- E.Test-48-PRI-FA-OES-NAO-A-ETW-rB.xlsx
- E.Test-49-PRI-FA-AM1-NAO-N-ETW-rA.xlsx
- E.Test-50-PRI-FA-AM1-NAO-N-ETW-rB.xlsx
- E.Test-51-CIV-FA-OES-NAO-A-ETW-rA.xlsx
- E.Test-52-CIV-FA-AM1-NAO-N-ETW-rA.xlsx
- E.Test-53-SIE-RA-OES-NAO-B-ETW-rB.xlsx
- E.Test-54-SIE-RA-OES-NAO-B-HLW-rB.xlsx
- E.Test-55-SIE-RA-AM1-NAO-N-ETW-rB.xlsx
- E.Test-56-SIE-RA-AM1-NAO-N-HLW-rB.xlsx
- E.Test-57-CIV-RA-AM1-NAO-N-ETW-rA.xlsx
- E.Test-58-CAM-RA-AM1-NAO-N-ETW-rA.xlsx
- E.Test-59-CAM-RA-AM2-LM-A-ETW-rA.xlsx
- E.Test-60-ROG-FA-OES-NAO-A-ETW-rB.xlsx
- E.Test-61-ROG-FA-OES-NAO-A-HLW-rB.xlsx
- E.Test-62-ROG-FA-AM1-NAO-N-ETW-rB.xlsx
- E.Test-63-F150-FA-AM2-LM-A-ETW-rA.xlsx
- E.Test-64-F150-FA-AM2-LM-A-HLW-rA.xlsx
- E.Test-65-F150-FA-AM1-NAO-N-ETW-rA.xlsx
- E.Test-67-F150-FA-OES-NAO-N-ETW-WLTP rA.xlsx
- E.Test-68-SIE-FA-OES-NAO-A-HLW-rA.xlsx
- E.Test-69-SIE-FA-AM1-NAO-N-ETW-rA.xlsx
- E.Test-70-SIE-FA-AM1-NAO-N-HLW-rA.xlsx
- E.Test-71-CAM-FA-AM1-NAO-N-ETW-rB.xlsx
- E.Test-72-CAM-FA-AM2-LM-A-ETW-rB.xlsx
- E.Test-73-CAM-FA-OES-A-ETW-WLTP rB.xlsx
- E.Test-74-F150-RA-OES-NAO-A-ETW-rB.xlsx
- E.Test-75-F150-RA-AM1-NAO-N-ETW-rB.xlsx
- E.Test-76-F150-RA-AM2-LM-A-ETW-rB.xlsx
- E.Test-77-F150-RA-OES-NAO-A-HLW-rB.xlsx
- E.Test-78-F150-RA-AM2-LM-A-HLW-rB.xlsx
- E.Test-79-PRI-RA-OES-NAO-A-ETW-rB.xlsx
- E.Test-80-PRI-RA-AM1-NAO-N-ETW-rB.xlsx
- E.Test-81-ROG-RA-OES-NAO-A-ETW-rB.xlsx
- E.Test-82-ROG-RA-AM1-NAO-N-ETW-rB.xlsx

- E.Test-83-ROG-RA-AM1-NAO-N-HLW-rB.xlsx
- E.Test-84-CIV-FA-OES-NAO-A-ETW-rB.xlsx
- E.Test-85-CIV-FA-AM1-NAO-N-ETW-rB.xlsx
- E.Test-86-SIE-RA-OES-B-HLW-rA.xlsx
- E.Test 87-SIE-RA-AM1-NAO-N-ETW-rA.xlsx
- E.Test 88-SIE-RA-AM1-NAO-N-HLW-rA.xlsx
- E.Test-89-F150-FA-OES-N-ETW-WLTP rB.xlsx
- E.Test-90-F150-FA-OES-N-ETW-rNA.xlsx

The two tunnel blank tests are:

- TBlank.Test 2_Test day 17_ROG-RA-rA.xlsx
- TBlank.Test 3_Test day 66_ROG-RA-rB.xlsx

Appendix J

Teflon Filter Masses and Weight Gains

The Appendix 3 table includes the Teflon filter weights for each test. The table presents the test information such as matrix test day, vehicle and friction material, then initial and final filter masses along with the filter weight gain. Measured masses were corrected by LINK according to 40 CFR 1065.690.

Test Day	Vehicle	Axle	FM	Initial Mass, mg	Final mass, mg	Gain, mg
6	2015 Ford F-150	Front	OES-NAO	397.300	397.420	0.120
7	2015 Ford F-150	Front	OES-NAO	398.036	398.186	0.150
8	2011 Toyota Camry	Front	OES-NAO	140.149	141.174	1.026
9	2013 Honda Civic	Rear	OES-NAO	393.764	393.971	0.206
10	2011 Toyota Camry	Rear	OES-NAO	137.179	137.878	0.699
11	2013 Toyota Sienna	Front	OES-NAO	393.233	395.281	2.048
12	2016 Toyota Prius	Front	OES-NAO	397.415	397.649	0.234
13	2013 Toyota Sienna	Rear	OES-NAO	392.106	392.965	0.859
14	2016 Nissan Rogue	Front	OES-NAO	136.503	138.207	1.704
15	2011 Toyota Camry	Front	OES-NAO	393.155	394.453	1.298
16	2015 Ford F-150	Rear	OES-NAO	390.599	391.409	0.810
17	Tunnel Blank 1	Holder 1	N/A	391.932	391.952	0.020
17	Tunnel Blank 1	Holder 2	N/A	392.407	392.424	0.017
18	2016 Nissan Rogue	Rear	AM1-NAO	393.805	394.271	0.466
19	2016 Nissan Rogue	Rear	OES-NAO	134.383	135.112	0.729
20	2016 Nissan Rogue	Rear	AM1-NAO	139.931	140.506	0.575
21	2011 Toyota Camry	Rear	OES-NAO	393.603	394.331	0.728
22	2011 Toyota Camry	Rear	AM1-NAO	392.703	393.475	0.772
23	2011 Toyota Camry	Rear	AM2-LM	393.149	394.566	1.417
24	2015 Ford F-150	Front	OES-NAO	389.913	390.016	0.103
25	2013 Honda Civic	Rear	OES-NAO	139.579	139.781	0.202
26	2013 Honda Civic	Rear	AM1-NAO	394.218	395.017	0.800
27	2016 Toyota Prius	Rear	OES-NAO	393.438	393.525	0.087
28	2016 Toyota Prius	Rear	AM1-NAO	140.551	140.608	0.057
29	2015 Ford F-150	Rear	AM1-NAO	138.622	140.263	1.641
30	2015 Ford F-150	Rear	AM2-LM	138.622	140.263	1.641
31	2015 Ford F-150	Rear	OES-NAO	136.124	136.880	0.757
32	2015 Ford F-150	Rear	AM2-LM	140.479	141.382	0.903
33	2013 Toyota Sienna	Front	OES-NAO	140.272	141.922	1.650
34	2013 Toyota Sienna	Front	OES-NAO	395.212	397.267	2.055
35	2013 Toyota Sienna	Front	AM1-NAO	385.961	388.048	2.087
36	2013 Toyota Sienna	Front	AM1-NAO	390.25509	393.5353	3.280213
37	2016 Nissan Rogue	Front	OES-NAO	137.16998	140.54	3.369999
38	2016 Nissan Rogue	Front	AM1-NAO	139.26646	140.8154	1.548947
39	2015 Ford F-150	Front	OES-NAO	398.76226	398.8559	0.093603
40	2015 Ford F-150	Front	AM2-LM	386.14182	386.6455	0.503642
41	2015 Ford F-150	Front	AM2-LM	397.83607	398.7045	0.868463
42	2015 Ford F-150	Front	AM1-NAO	394.15255	394.2648	0.112251
43	2015 Ford F-150	Front	OES-NAO	140.57629	140.6887	0.112449
44	2015 Ford F-150	Front	OES-NAO	391.06811	391.1615	0.093414
45	2011 Toyota Camry	Front	AM1-NAO	138.90356	140.5453	1.641713
46	2011 Toyota Camry	Front	AM2-LM	136.4385	138.9856	2.547125
47	2011 Toyota Camry	Front	OES-NAO	397.24408	397.7454	0.501278

Test Day	Vehicle	Axle	FM	Initial Mass, mg	Final mass, mg	Gain, mg
48	2016 Toyota Prius	Front	OES-NAO	138.26622	138.4028	0.136554
49	2016 Toyota Prius	Front	AM1-NAO	139.52668	139.6785	0.151833
50	2016 Toyota Prius	Front	AM1-NAO	394.66786	394.9486	0.28079
51	2013 Honda Civic	Front	OES-NAO	138.64294	139.4748	0.831865
52	2013 Honda Civic	Front	AM1-NAO	138.72689	139.8098	1.082931
53	2013 Toyota Sienna	Rear	OES-NAO	139.70822	140.7141	1.005873
54	2013 Toyota Sienna	Rear	OES-NAO	397.6197	399.0959	1.476172
55	2013 Toyota Sienna	Rear	AM1-NAO	398.91986	399.5321	0.612234
56	2013 Toyota Sienna	Rear	AM1-NAO	393.55956	394.1107	0.551122
57	2013 Honda Civic	Rear	AM1-NAO	138.67537	139.2955	0.620158
58	2011 Toyota Camry	Rear	AM1-NAO	139.12557	139.8727	0.747152
59	2011 Toyota Camry	Rear	AM2-LM	140.84926	142.8771	2.027863
60	2016 Nissan Rogue	Front	OES-NAO	137.08673	140.11	3.023235
61	2016 Nissan Rogue	Front	OES-NAO	397.17737	400.5745	3.397165
62	2016 Nissan Rogue	Front	AM1-NAO	398.49649	400.1743	1.677852
63	2015 Ford F-150	Front	AM2-LM	137.55389	138.3013	0.747395
64	2015 Ford F-150	Front	AM2-LM	138.04894	139.2027	1.153721
65	2015 Ford F-150	Front	AM1-NAO	134.84165	135.078	0.236363
66	Tunnel Blank 2	Holder 1	N/A	137.5176	137.5451	0.027471
66	Tunnel Blank 2	Holder 2	N/A	399.15441	399.2404	0.085962
67	2015 Ford F-150	Rear	OES-NAO	395.69223	395.8723	0.180073
68	2013 Toyota Sienna	Front	OES-NAO	140.67803	143.1193	2.441265
69	2013 Toyota Sienna	Front	AM1-NAO	140.3819	142.9374	2.555467
70	2013 Toyota Sienna	Front	AM1-NAO	138.91632	142.7021	3.785822
71	2011 Toyota Camry	Front	AM1-NAO	391.42171	393.358	1.936318
72	2011 Toyota Camry	Front	AM2-LM	402.79979	404.6765	1.876715
73	2011 Toyota Camry	Front	OES-NAO	391.02543	391.6269	0.601518
74	2015 Ford F-150	Rear	OES-NAO	133.68903	134.6658	0.976815
75	2015 Ford F-150	Rear	AM1-NAO	401.15934	403.3029	2.143558
76	2015 Ford F-150	Rear	AM2-LM	400.94102	402.4835	1.542485
77	2015 Ford F-150	Rear	OES-NAO	394.76378	396.767	2.003203
78	2015 Ford F-150	Rear	AM2-LM	393.19452	395.4306	2.236035
79	2016 Toyota Prius	Rear	OES-NAO	137.48165	137.5553	0.073652
80	2016 Toyota Prius	REAR	AM1-NAO	138.53058	138.5905	0.059953
81	2016 Nissan Rogue	Rear	OES-NAO	395.58496	396.3594	0.774408
82	2016 Nissan Rogue	Rear	AM1-NAO	401.93869	402.2087	0.269963
83	2016 Nissan Rogue	Rear	AM1-NAO	394.0117	394.738	0.726318
84	2013 Honda Civic	Front	OES-NAO	393.52493	394.2314	0.70647
85	2013 Honda Civic	Front	AM1-NAO	393.7694	395.1889	1.41946
86	2013 Toyota Sienna	Rear	OES-NAO	138.36691	139.8178	1.450881
87	2013 Toyota Sienna	REAR	AM1-NAO	140.40394	141.1037	0.699745
88	2013 Toyota Sienna	Rear	AM1-NAO	136.94338	137.6687	0.725299
89	2015 Ford F-150	Front	OES-NAO	398.31912	398.4171	0.097973
90	2015 Ford F-150	Front	OES-NAO	139.29281	139.3964	0.103568

Appendix K

Vehicle-Level Particle Number Emission Rates by Speed Segment

This Appendix presents the CPC-measured vehicle-level particle number emission rates for each vehicle model. Bar charts are given for each model, categorized by pad material and grouped by average speed range. The values presented indicate the vehicle-level particle count emission rate on a per-distance basis.

Camry

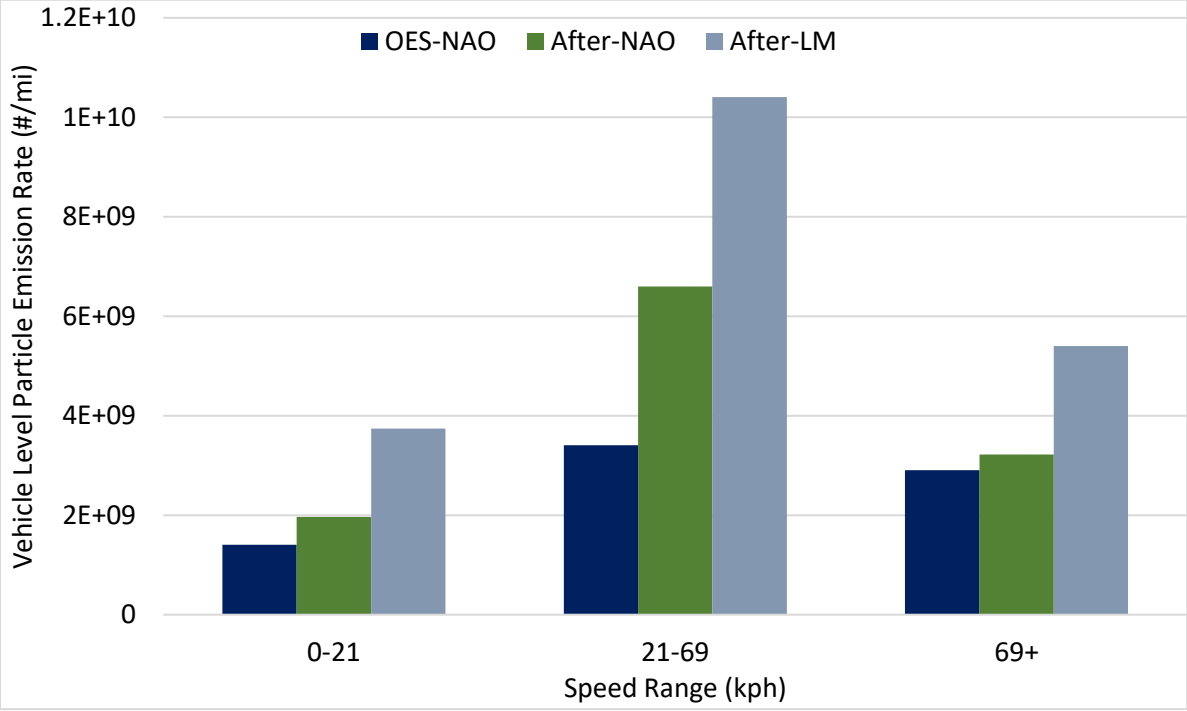

Civic

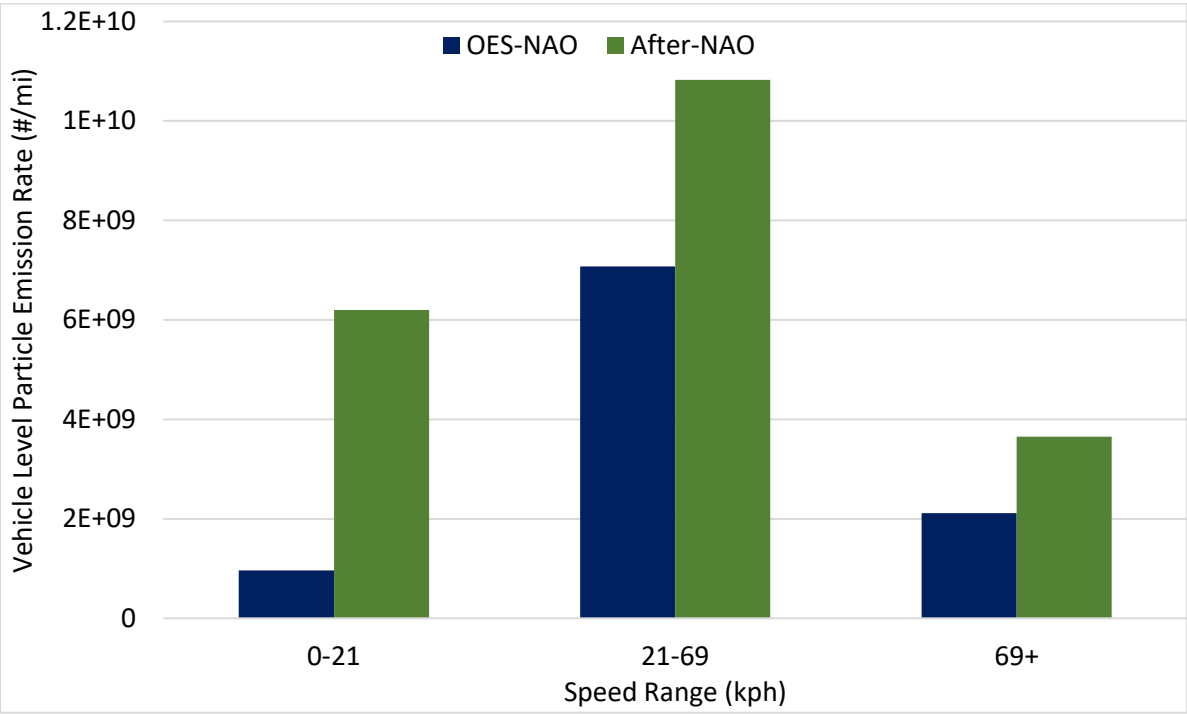

F-150

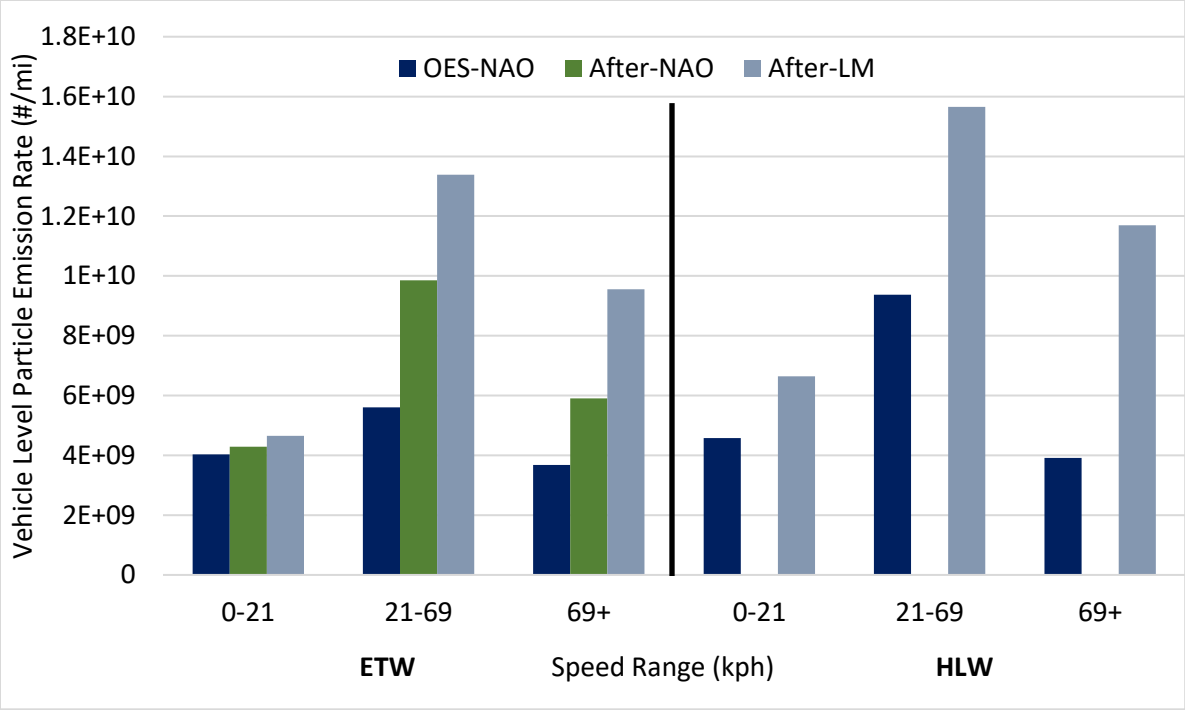
1.8E+10
1.6E+10
1.4E+10
1.2E+10
1E+10
8E+09
6E+09
4E+09
2E+09
0
Vehicle Level Particle Emission Rate (#/mi)
OES-NAO
After-NAO
After-LM
0-21
21-69
69+
0-21
21-69
69+
ETW
Speed Range (kph)
HLW

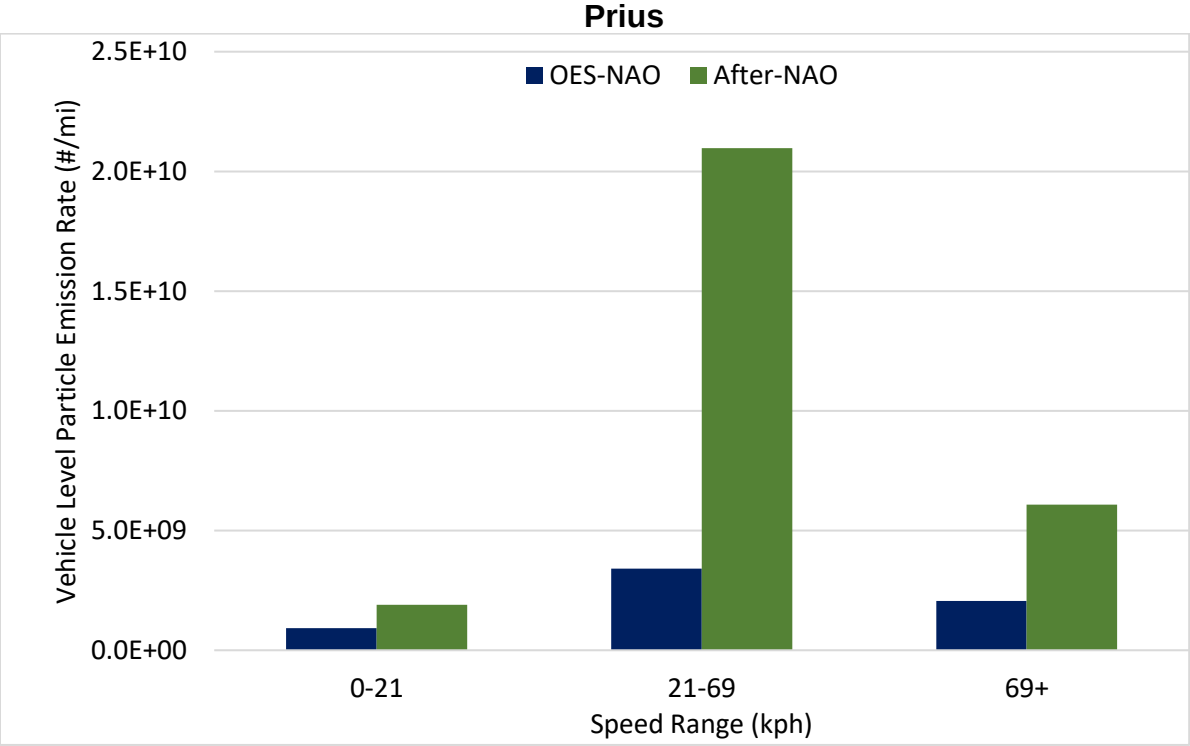
Prius
2.5E+10
2.0E+10
1.5E+10
1.0E+10
5.0E+09
0.0E+00
Vehicle Level Particle Emission Rate (#/mi)
OES-NAO
After-NAO
0-21
21-69
69+
Speed Range (kph)

Rogue

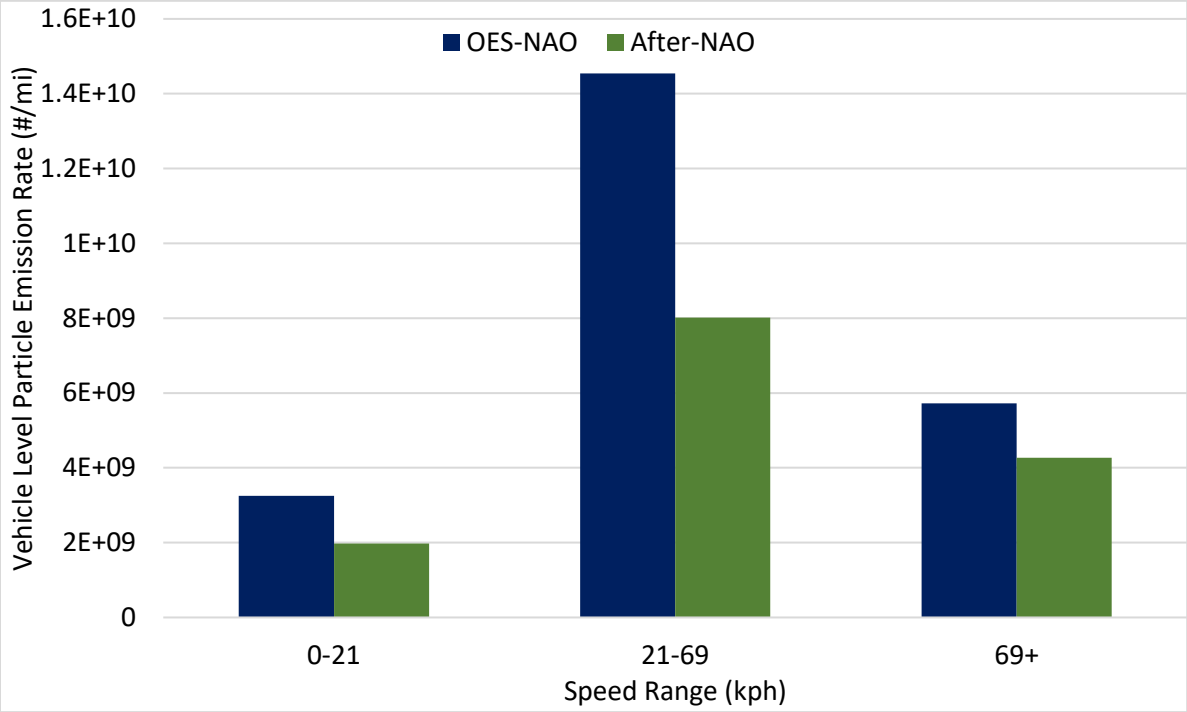

Sienna (outlying value presented as measured)

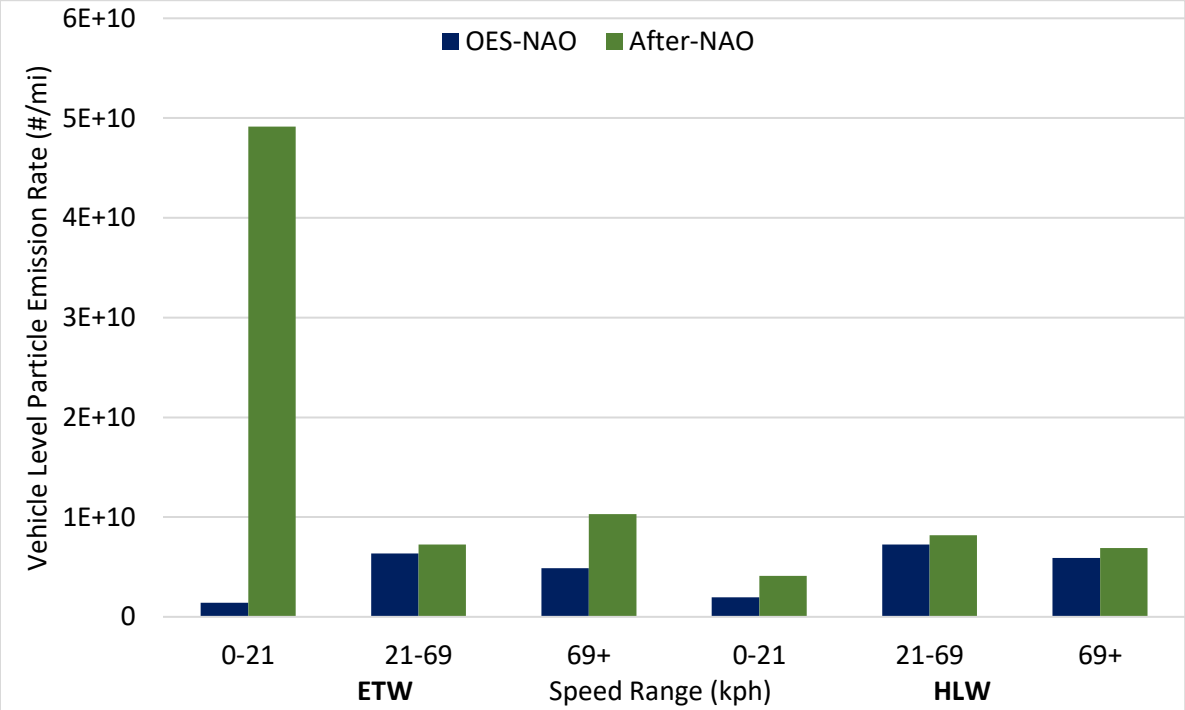

Appendix L

EEPS Particle Size Distributions

This appendix includes the particle size distributions measured by the EEPS ((5.6 – 560 nm)) during each test. Results are presented for the front and rear assemblies of each vehicle, and are color coded by the friction material and, where applicable, the test weight.

Camry Particle Size Distributions Measured by EEPS

Front

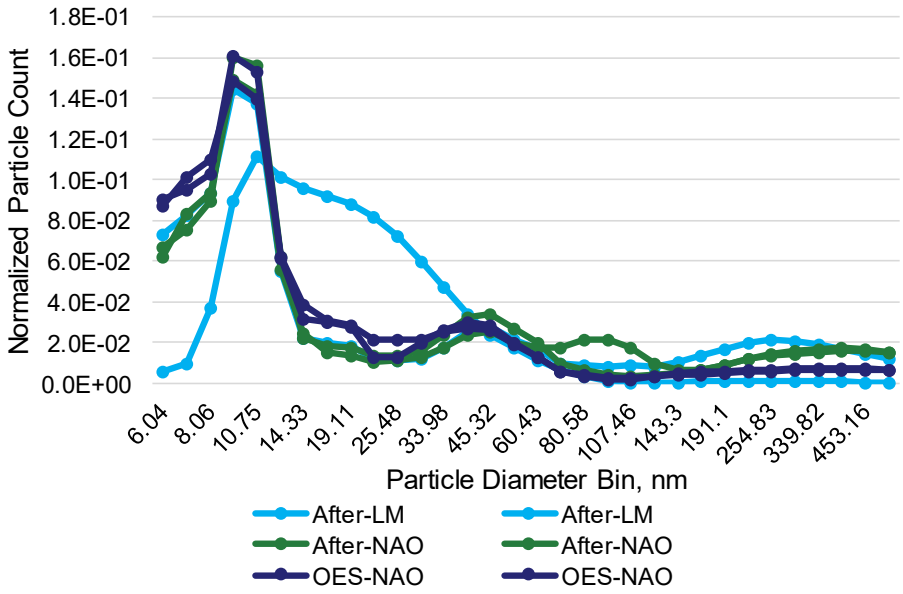

Rear

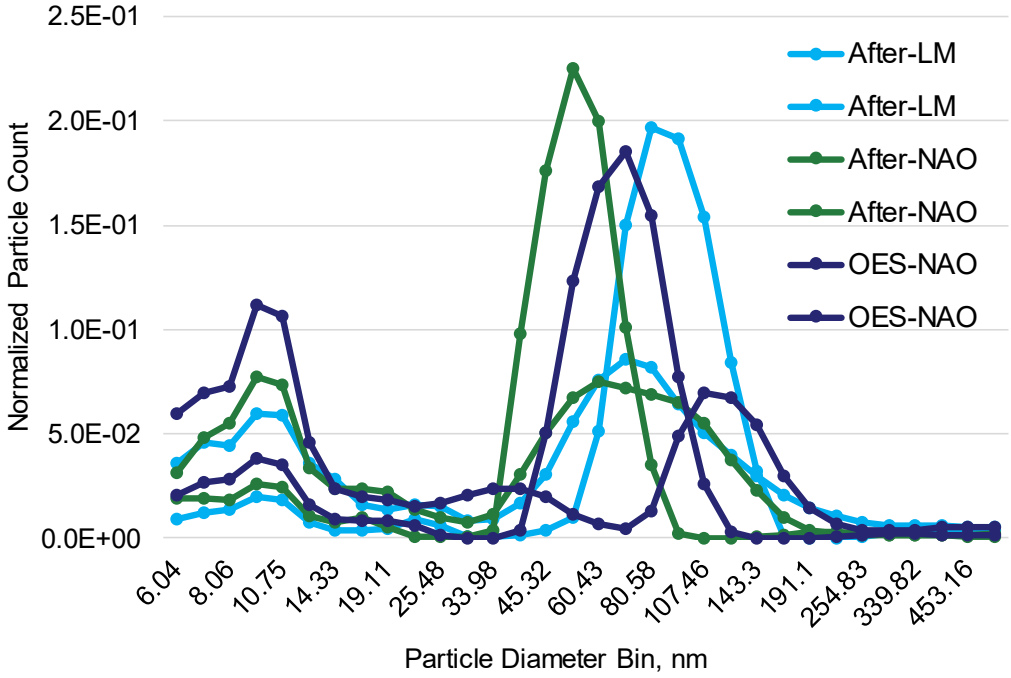

Civic Particle Size Distributions Measured by EEPS

Front

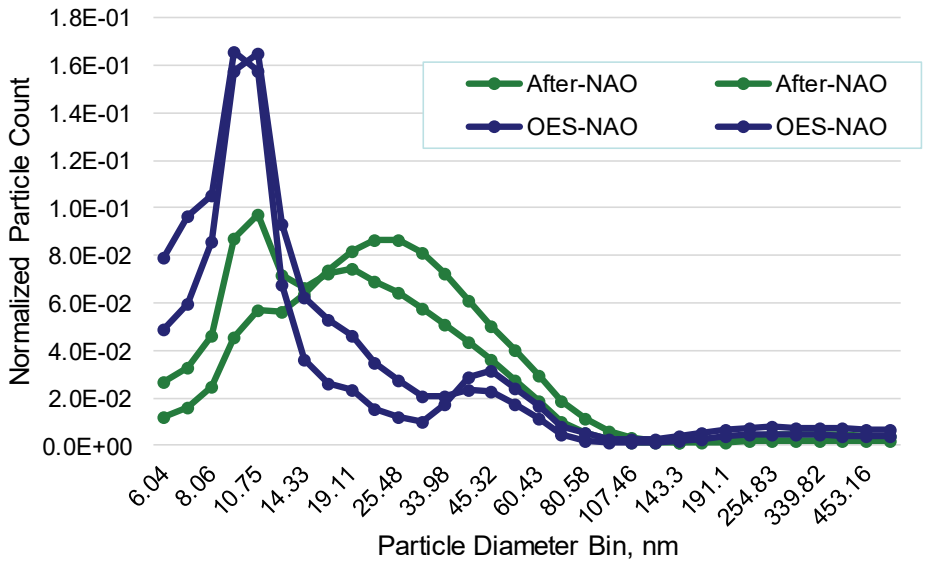

Rear

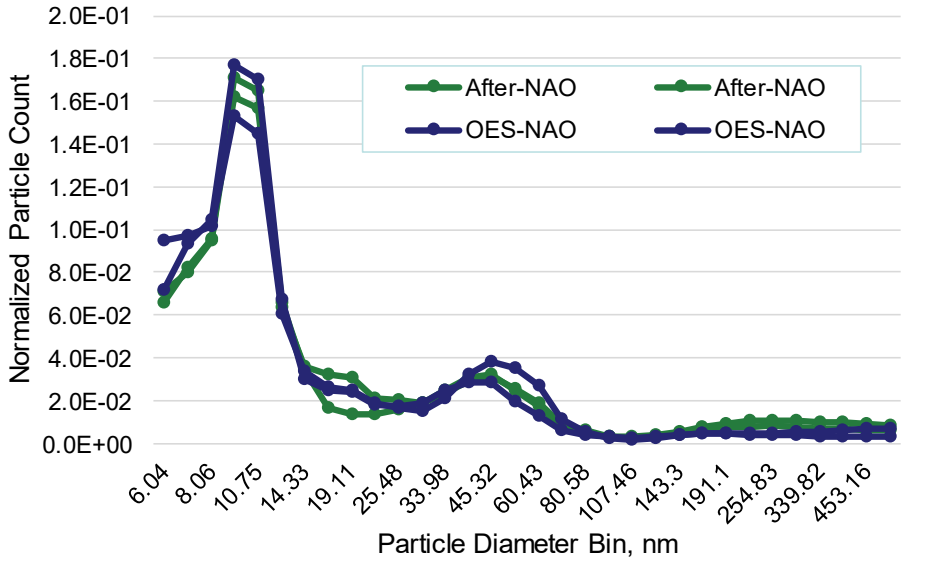

F-150 Particle Size Distributions Measured by EEPS

Front

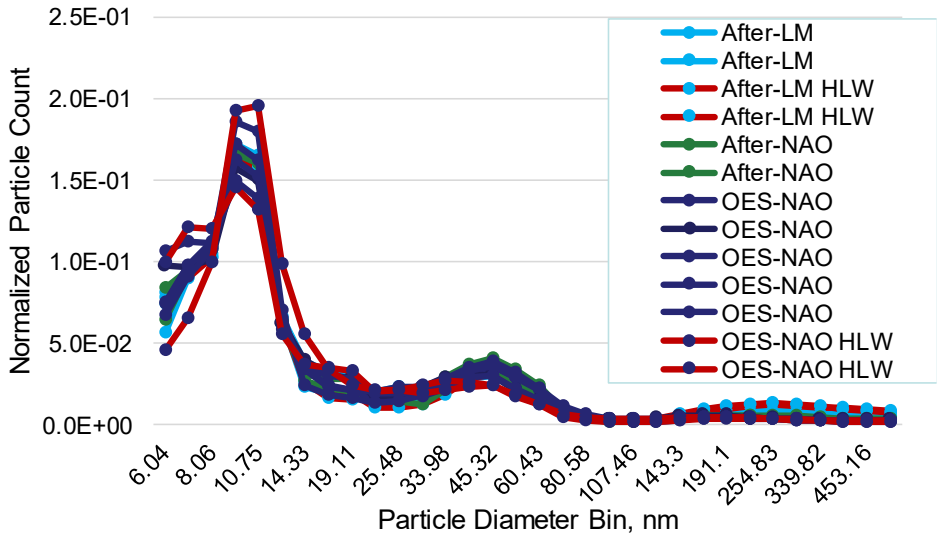

Rear

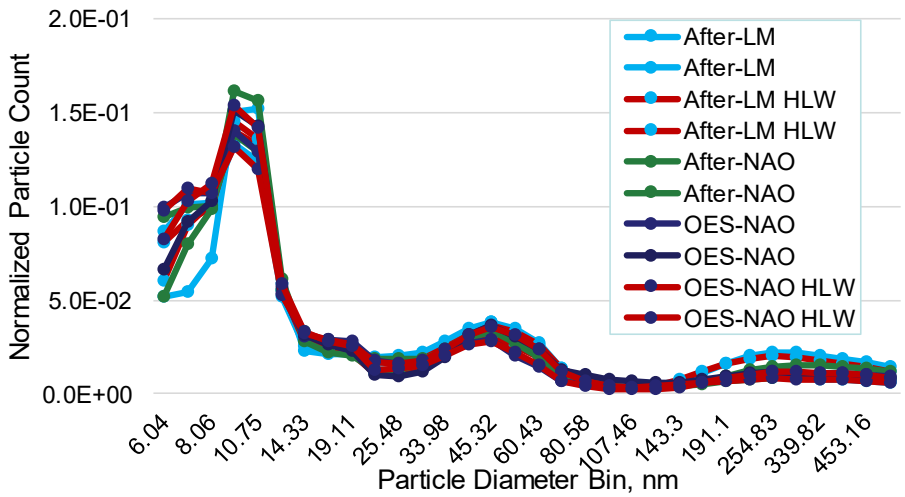

Prius Particle Size Distributions Measured by EEPS

Front

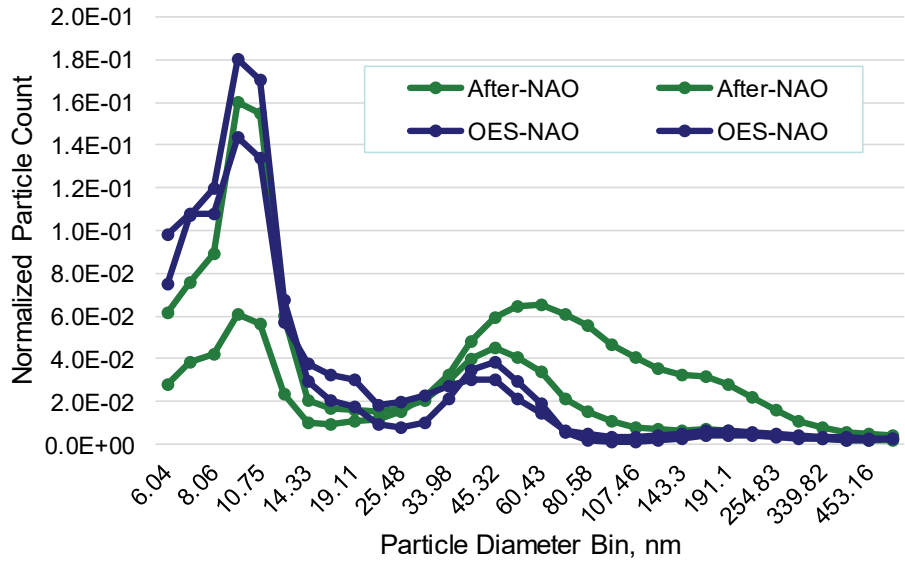

Rear

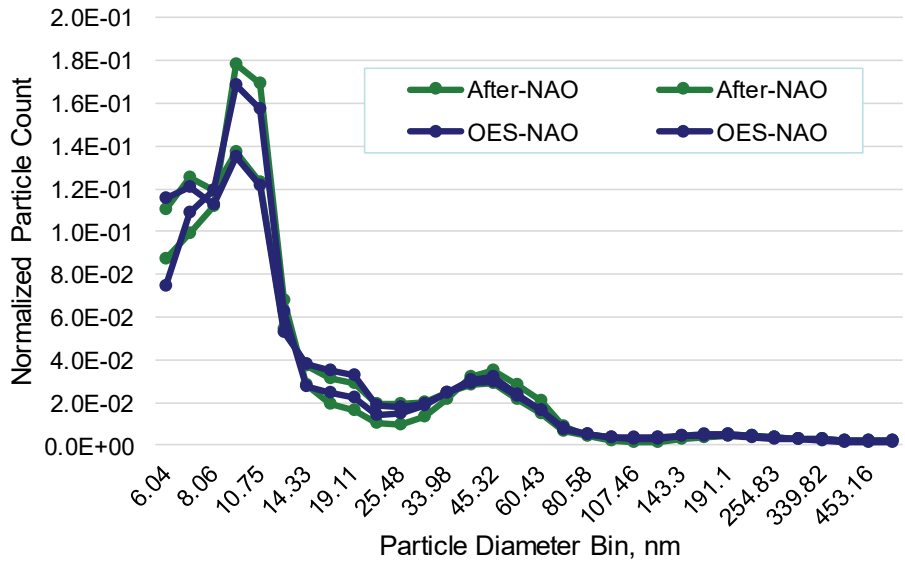

Rogue Particle Size Distributions Measured by EEPS

Front

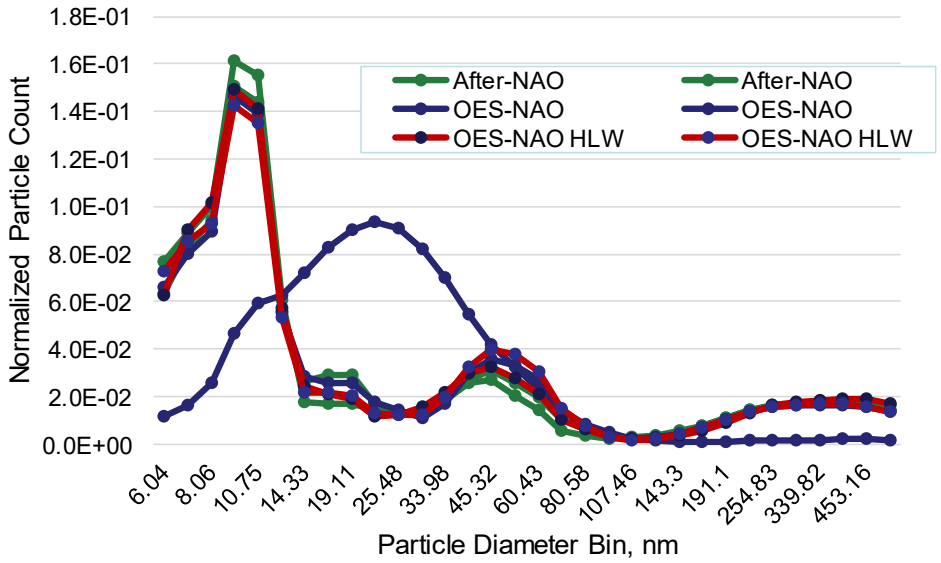

Rear

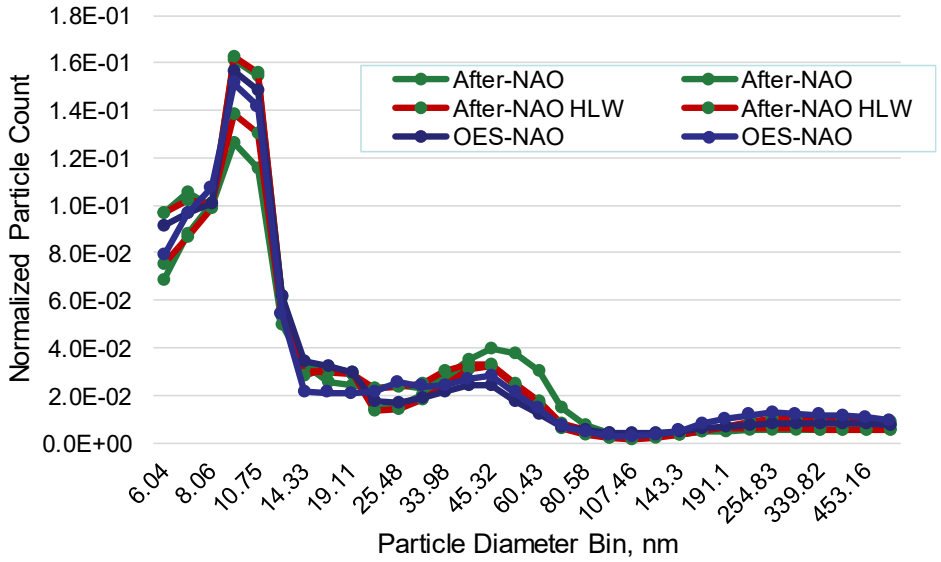

Sienna Particle Size Distributions Measured by EEPS

Front

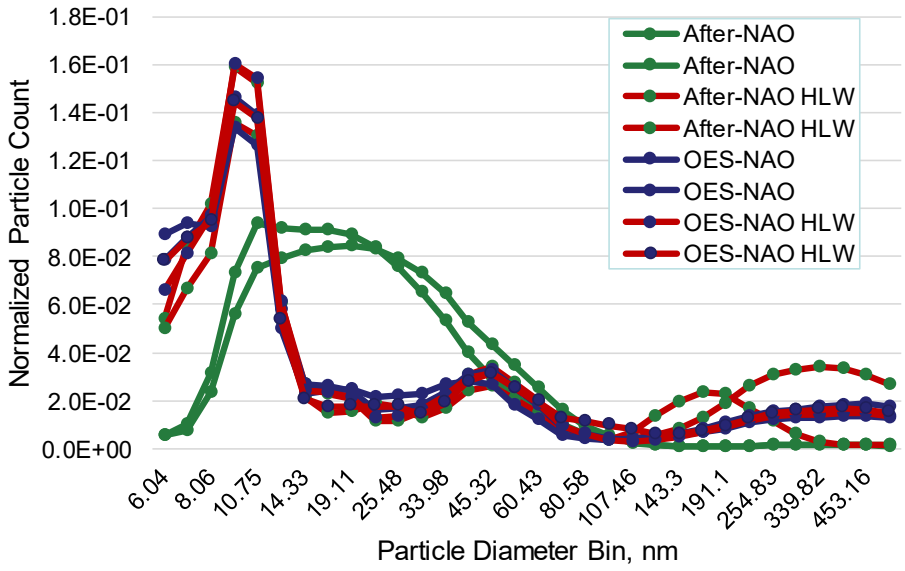

Rear

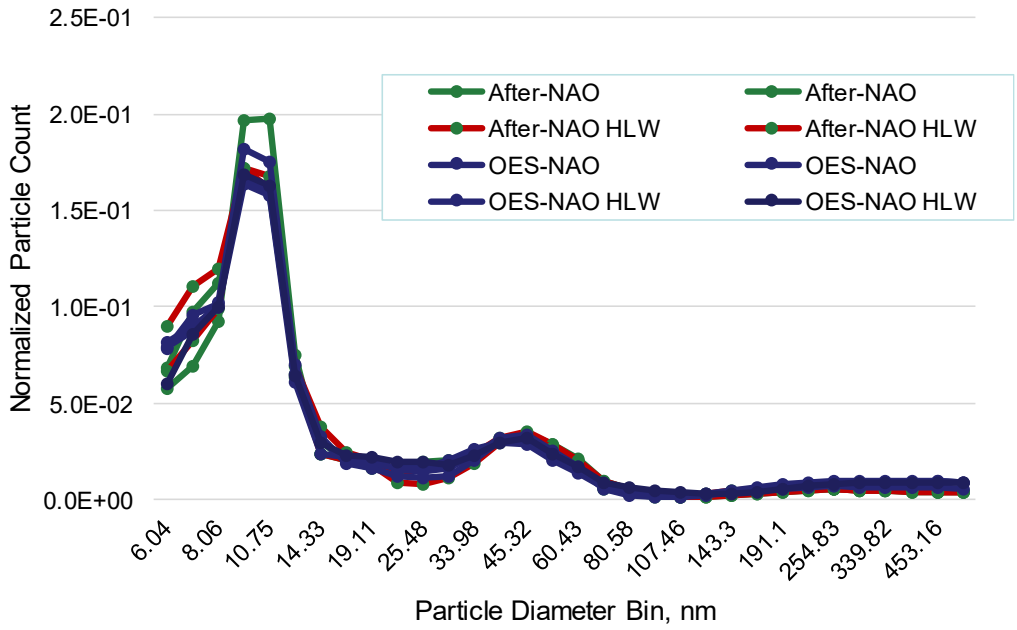

Tunnel Blank Particle Size Distributions Measured by EEPS

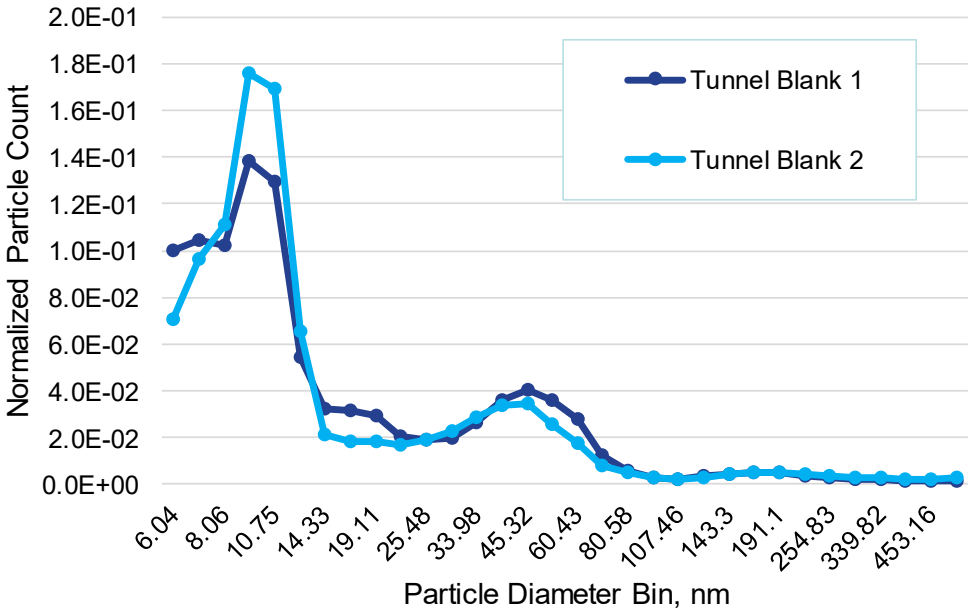

Appendix M

Zero Blank Results

The table in this Appendix presents the PTFE filter and 100S4 impactor weights and weight gains during the zero blank experiments.

Experiment	Measurement Location	Initial (mg)	Final (mg)	Weight Gain (mg)
Zero Blank 1	100S4 Stg1	78.648	78.638	-0.010
	100S4 Stg2	78.224	78.222	-0.002
	100S4 Stg3	78.251	78.253	0.002
	100S4 Stg4	78.303	78.304	0.001
	100S4 AF	120.988	120.979	-0.009
	PMS PM10	391.103	391.114	0.011
Zero Blank 2	100S4 Stg1	78.152	78.149	-0.003
	100S4 Stg2	78.149	78.146	-0.003
	100S4 Stg3	78.142	78.140	-0.002
	100S4 Stg4	78.361	78.360	-0.001
	100S4 AF	123.260	123.240	-0.020
	PMS PM10	136.924	136.943	0.019
Zero Blank 3	100S4 Stg1	77.825	77.827	0.002
	100S4 Stg2	77.863	77.862	-0.001
	100S4 Stg3	78.048	78.048	0.000
	100S4 Stg4	77.840	77.838	-0.002
	100S4 AF	122.583	122.581	-0.002
	PMS PM10	398.319	398.320	0.001
Zero Blank 4	100S4 Stg1	76.757	76.758	0.001
	100S4 Stg2	77.828	77.823	-0.004
	100S4 Stg3	78.090	78.088	-0.002
	100S4 Stg4	77.822	77.819	-0.002
	100S4 AF	121.674	121.667	-0.007
	PMS PM10	140.422	140.489	0.067
Zero Blank 5	100S4 Stg1	77.837	77.836	0.000
	100S4 Stg2	77.354	77.354	0.000
	100S4 Stg3	78.256	78.255	-0.001
	100S4 Stg4	77.661	77.660	-0.001
	100S4 AF	121.697	121.693	-0.004
	PMS PM10	383.604	383.621	0.017
Zero Blank 6	100S4 Stg1	76.758	76.761	0.003
	100S4 Stg2	77.823	77.830	0.007
	100S4 Stg3	78.088	78.089	0.001
	100S4 Stg4	77.819	77.823	0.004
	100S4 AF	121.667	121.673	0.006
	PMS PM10	140.489	140.404	-0.085